Determinants of Rotavirus Polymerase Localization and Activity

Allison O. McKell

Dissertation submitted to the faculty of the Virginia Polytechnic Institute and State University in partial fulfillment of the requirements for the degree of

Doctor of Philosophy
In
Biomedical and Veterinary Sciences

Sarah McDonald, Chair
Terence Dermody
Michael Friedlander
Xiang-Jin Meng
Lijuan Yuan

July 28, 2017
Blacksburg, Virginia

Keywords: rotavirus, polymerase, VP1, localization, viroplasms, GFP fusion proteins

Determinants of Rotavirus Polymerase Localization and Activity

Allison O. McKell

ACADEMIC ABSTRACT

Virally induced gastroenteritis is one of the leading causes of childhood disease and death worldwide. Rotavirus (RV) is a significant contributor to this global burden, affecting the young of humans and other animals. To protect itself from the intracellular immune response and to facilitate genome replication, RV forms inclusion bodies in the cell cytoplasm via the activities of viral non-structural proteins, NSP2 and NSP5. The RNA-dependent RNA polymerase (RdRp), VP1, localizes to these inclusion bodies, which are called 'viroplasms,' where it catalyzes genome replication. The mechanism by which this happens is poorly understood.

The work described in this dissertation focused on identifying region(s) and residue(s) of the polymerase essential for its intracellular localization and function. First, we developed an ectopic expression system that we then used to biochemically validate phenotypes associated with a temperature-sensitive simian strain SA11 mutant RV. We found that a single lesion in the N-terminal domain of SA11 VP1 negatively impacted its catalytic activity as well as its capacity to interact with NSP2 and/or NSP5 and to localize to viroplasms during infection. Follow up studies using VP1 genes from divergent strains (human strain Bristol and avian strain PO-13) and an N-terminal domain-only mutant provided more insight into polymerase localization determinants. Moreover, bioinformatic analyses bolstered the experimental results, and allowed us to generate more hypotheses for future research. In total, our work suggests that the VP1 N-terminal domain plays an important role in localizing the polymerase to viroplasms via NSP2 and/or NSP5 interactions and supporting its robust catalytic activity.

Determinants of Rotavirus Polymerase Localization and Activity

Allison O. McKell

GENERAL AUDIENCE ABSTRACT

Rotavirus (RV) is a viral pathogen that causes severe, watery diarrhea and vomiting in the young of humans and other animals. RV infections result in over 200,000 pediatric deaths around the world each year, especially in developing nations. Within the infected host cell, RV forms inclusion bodies, called viroplasms, where many stages of viral replication occur. The RV polymerase, known as VP1, must localize to viroplasms during infection where it replicates the virus' RNA genome.

The work described in this dissertation focused on identifying region(s) of VP1 essential for its viroplasmic localization and its function as a polymerase. We found that a single amino acid change in a region of the polymerase called the N-terminal domain negatively impacted its capacity to localize to viroplasms during infection as well as its enzymatic activity in a test tube. Follow up studies using VP1 proteins from divergent strains and a mutant containing only the N-terminal domain of VP1 provided more insight into polymerase localization determinants. In total, our work suggests that the VP1 N-terminal domain plays an important role in localizing the polymerase to viroplasms via interactions with other viral proteins and supporting its function as a polymerase.

DEDICATION

I would like to dedicate this dissertation to my husband, Jim, and my children, Teagan and Parker, for all of their love and support during my graduate training at Virginia Tech. I would also like to dedicate it to my mother, Debra Overstreet, and to my grandmother, Lurlene Walker Todd (*in memoriam*), for inspiring me to undertake this training in the first place.

ACKNOWLEDGEMENTS

The greatest and most heart-felt appreciation goes to my advisor and PhD committee chairperson, Dr. Sarah McDonald. She believed in me and provided me with endless encouragement, patience, and many hours of one-on-one training and mentorship. I could not have done this without her as my advisor and friend. Moreover, I would like to give thanks to the members of my doctoral advisory committee—Dr. Terence Dermody, Dr. Michael Friedlander, Dr. Xiang-Jin (X.J.) Meng, and Dr. Lijuan Yuan—for the dedication of their time and guidance to my graduate education and training.

I would also like to express gratitude to my collaborators, Dr. John Chappell, Dr. Michael Fox, and Dr. James Smyth (Virginia Tech Carilion Research Institute and School of Medicine) for the use of their confocal microscopy equipment and for sharing their expertise in the capturing and quantification of immunofluorescent images. In addition, I would like to thank Dr. Leslie LaConte (Virginia Tech Carilion Research Institute and School of Medicine) for contributing her specialized knowledge of protein structure and molecular modeling to my research as well as the invaluable hours of personal and profession mentoring she gave me. In a similar vein, I would like to thank my MPH advisor, Dr. Andrea Bertke, for her mentorship, encouragement, and infectious tenacity.

Special thanks to the following former and current members of the McDonald Laboratory: Dr. Crystal Boudreaux, Dr. Shu Zhang, Dr. Rebecca Mingo Seamon, Dr. Paul McDonald, Dr. Joshua Nichols, Dr. Donald Vile, Dr. Priya Srihari, Dr. Joseph Pechacek, Caroline Reist and Tyler Johnson. You were my partners, teachers, mentors, mentees, and most importantly, my friends. Thank you also to Dr. Roger Avery, former Senior Associate Dean for Research and Graduate Studies for believing in me, supporting me, and giving me this opportunity to pursue my graduate education. And thank you to Mrs. Becky Jones, (former BMVS Graduate Program Coordinator) for her advice and continuous support. I would also like to thank Dr. S. Ansar Ahmed, the current Senior Associate Dean for Research and Graduate Studies, and Ms. Susan Rosebrough and Ms. Demetria (Mimi) Harris (current BMVS Graduate Program Coordinators) for their support as I concluded my graduate work.

I also wish to thank my husband, Jim, for his constant encouragement over my graduate studies and training. He is my rock, and his support and patience have been priceless to me over

the years. Finally, I want to thank my many family members and friends for being some of my greatest cheerleaders.

This dissertation project was supported in part by National Institute of Allergy and Infectious Disease grant number from the National Institutes of Health (R01-AI116815 and R21-AI119588). The Biomedical and Veterinary Sciences Graduate Program of the Virginia-Maryland College of Veterinary Medicine and the Virginia Tech Carilion Medical Scholars fund also provided support for this work.

ATTRIBUTIONS

The work described within this dissertation would not have been possible without help from colleagues. A list and brief description of their contributions are included below:

Chapters 2, 3, and Appendix C:

Sarah M. McDonald, Ph.D. was an Assistant Professor at Virginia Tech and is the corresponding author on this manuscript. She helped with the development of these projects as well as the writing and editing of the manuscripts.

Chapter 2:

Leslie E. LaConte, Ph.D. (Department of Biological Sciences, Virginia Tech Carilion School of Medicine and Research Institute) is an Assistant Dean for Research at the Virginia Tech School of Medicine, an Assistant Professor at Virginia Tech, and is a co-author on this manuscript. She was instrumental for the performance and analysis of the molecular dynamics experiments. She also contributed to the writing and editing of the manuscript.

Appendix C:

Joshua C. Nichols, M.D. is an Emergency Medicine Physician in the Department of Emergency Medicine at Carilion Clinic and is a coauthor of the manuscript. He helped with the development and testing of the PCR-based genotyping method as well as with the editing of the manuscript.

TABLE OF CONTENTS

LIST OF FIGURES

Chapter 1:

Chapter 2:

Chapter 3:

Chapter 4:

LIST OF TABLES

GENERAL INTRODUCTION

Rotavirus (RV) is a double-stranded RNA (dsRNA) virus and member of the *Reoviridae* family that is responsible for a significant disease burden in animals and humans worldwide (9). This viral pathogen is a leading cause of viral gastroenteritis, which presents as severe, watery diarrhea that is sometimes accompanied by fever and vomiting (1). It predominantly affects the very young of host species, and in human children (ages 1 month to 5 years), more than 215,000 deaths each year are attributable to RV infection (9). Two live-attenuated vaccines are currently administered in infants and children to prevent more serious illness or death from natural infection (4). These vaccines have been mostly successful in lowering RV-related morbidity and mortality; however, some concerns remain about the safety of this type of RV vaccine, efficacy in certain regions of the world, and evolutionary pressures for RV to mutate and escape vaccine protection (4). It is important to continue to elucidate the overall biology of RVs in order to inform next-generation vaccines and therapies for the prevention and treatment of RV infections. This dissertation documents research that seeks to better understand which residue(s) and region(s) of the RV polymerase are important for its intracellular localization, protein interactions, and catalytic activity.

At the beginning of my graduate studies, no fully-recombinant reverse genetics system existed which meant that research into RV replication relied on other methodologies, including forward genetic approaches such as temperature-sensitive mutant viruses. In the case of the RV RNA-dependent RNA polymerase (RdRp), VP1, a temperature-sensitive mutant simian RV strain was created and mapped to gene 1 (3, 6). That mutant strain was shown to be defective in RNA synthesis, protein synthesis, and general viral protein localization (2, 7). It was later discovered through sequencing that there was only a single amino acid change in gene 1 located in the N-terminus; however, it was unknown whether that mutation was the singular cause of the previously characterized phenotypes (8). In addition, previous studies have deduced the full genomic sequence of VP1, and the atomic structure of the RV polymerase was determined by X-ray crystallography (5). During replication, in order to fulfill its function as a polymerase, VP1 must localize to the protected environment of cytoplasmic inclusions, called viroplasms, where it can synthesize dsRNA. When the work that forms this dissertation began, the precise

mechanisms behind RV genome replication and particle assembly were elusive. Specifically, the functional significance of VP1's accessory (i.e., non-catalytic) domains was not known.

The work presented in this dissertation primarily focused on elucidating cis-acting determinants within VP1's structure that affects its localization to viroplasms and its function as the viral polymerase. It seeks to answer the questions: What is the mechanism for VP1 localization to viroplasms? And what region(s) and residue(s) are important for that function of the polymerase? Answering these questions will lead to a better understanding of RV biology and replication generally. Not all viruses that replicate in a manner similar to RV or possess RdRps have as large of repository of tools and data available for their study. As such, it could also provide information that can be applied as a model for other viruses' replication cycles and polymerases. Chapter 2 of this dissertation details the further characterization of a temperature-sensitive (ts) mutant of simian RV, called SA11-tsC, and reveals the full genome sequence of this virus, which was previously unknown. Additionally, Chapter 2 describes experiments performed using the ts mutant that showed how a lesion in the N-terminal domain of VP1 affected its capacity to localize to replication sites and its catalytic activity. Work presented in Chapter 3 provides more information towards determining intramolecular aspects of VP1 that are necessary for its localization to viroplasms.

REFERENCES

1. **Carr, M.E., McKendrick, G.D., and Spyridakis, T.** 1976. The clinical features of infantile gastroenteritis due to rotavirus. Scandinavian Journal of Infectious Diseases, **8**(4):241-243.
2. **Chen, D., Gombold, J.L., and Ramig, R.F.** 1990. Intracellular RNA synthesis directed by temperature-sensitive mutants of simian rotavirus SA11. Virology, **178**:143-151.
3. **Gombold, J.L. and Ramig, R.F.** 1987. Assignment of simian rotavirus SA11 temperature-sensitive mutant groups A, C, F, and G to genome segments. Virology, **161**:463-473.
4. **Jonesteller, C.L., Burnett, E., Yen, C., Tate, J.E., and Parashar, U.D.** 2017. Effectiveness of rotavirus vaccination: a systematic review of the first decade of global post-licensure data, 2006-2016. Clinical Infectious Diseases, Epub ahead of print.
5. **Lu, X., McDonald, S.M., Tortorici, M.A., Tao, Y.J., Vasquez-Del Carpio, R., Nibert, M.L., Patton, J.T., and Harrison, S.C.** 2008. Mechanism for coordinated RNA packaging and genome replication by rotavirus polymerase VP1. Structure, **16**:1676-1688.
6. **Ramig, R.F.** 1982. Isolation and genetic characterization of temperature-sensitive mutants of simian rotavirus SA11. Virology, **120**:93-105.
7. **Ramig, R.F. and Petrie, B.L.** 1984. Characterization of temperature-sensitive mutants of simian rotavirus SA11: protein synthesis and morphogenesis. Journal of Virology, **49**:665-673.
8. **Small, C., Barro, M., Brown, T.L., and Patton, J.T.** 2007. Genome heterogeneity of SA11 rotavirus due to reassortment with "O" agent. Virology, **359**:415-424.
9. **Tate, J.E., Burton, A.H., Boschi-Pinto, C., Parashar, U.D., and World Health Organization-Coordinated Global Rotavirus Surveillance Network.** 2016. Global, regional, and national estimates of rotavirus mortality in children <5 years of age, 2000-2013. Clinical Infectious Diseases, **62**:S96-S105.

Chapter 1

Rotavirus - Literature Review

DISCOVERY AND CLASSIFICATION

Rotavirus (RV) received its name due to the virion's wheel-like ('rota' means 'wheel' in Latin) appearance when viewed via electron microscopy (65). It was first isolated in 1943 from children with diarrhea, but it was not until 1973, that a couple of research groups recognized what would come to be called RV as the infectious agent that caused gastroenteritis in infants and young children (20, 64). They performed electron microscopy on the duodenal mucosa of children with acute non-bacterial gastroenteritis and found the virus particles. At first RV was identified as an orbivirus, which includes such species as Bluetongue Virus (BTV) (20).

Early studies on RV determined that the virion is a non-enveloped, triple-layered particle that houses an eleven-segmented, double-stranded (ds) RNA genome within its core (81, 180). This dsRNA genome is what relegates RV to Group III within the Baltimore classification scheme, which is the same group as orbiviruses Similarly, the classification system devised by the International Committee on Taxonomy of Viruses (ICTV) places RV in the same family and subfamily as BTV (13). Within Group III, RV is also a member of the *Reoviridae* family and due to its lack of 'turrets' on the inner capsid, it falls under the *Sedoreovirinae* subfamily (13). These characteristics are also true for orbiviruses, so that initial designation for the first isolated RV particles was not entirely unfounded. However, later studies found RVs to be different from orbiviruses and thus a new genus was created (81). Interestingly, before the name 'rotavirus' was adopted, the virus was called 'infantile enteritis virus' with 'duovirus' also proposed as a final name due to the location of virus particles during infection (81). There are eight species of RVs (groups RVA-RVH), and most of the work described in this dissertation will focus on the model RV strain, SA11, which is a simian member of RVA (127, 141). RVAs are the most well studied species because they are responsible for the vast majority of human disease (126). SA11 RV was first isolated from a rectal swab of a velvet monkey in 1958 and later adapted to grow to high titers in monkey kidney cell culture (59, 114, 192).

GENOME AND STRUCTURE

The RVA genome is comprised of 18,550 bp of dsRNA that makes up eleven genome segments that each encodes a single viral protein with the exception of gene 11, which encodes two viral proteins in some strains (130). The viral structural proteins (VPs) encoded are: VP1, VP2, VP3, VP4, VP6, and VP7 (122). In addition to the structural proteins, the viral genome also encodes five to six nonstructural proteins (NSPs) that are important for the RV lifecycle. These proteins include: NSP1, NSP2, NSP3, NSP4, NSP5, and in some strains, NSP6 (122, 130). Each gene segment possesses 5' and 3' untranslated regions (UTRs), which include conserved sequences at either end that are important for translation and replication. Interestingly, the 3' ends lack polyladenylation signals and instead possess a 5'-UGUGACC-3' consensus sequence that is conserved across almost all eleven genes of RVA (157). For most RVA gene segments, there is a start codon, a long open reading frame (ORF), and stop codon; however, some strains have a secondary ORF for NSP6 expression in their gene segment 11 (130).

This RV genome is encapsidated within a non-enveloped, triple-layered particle (TLP) that is icosahedral in shape with a diameter of approximately 100 nm (Figure 1. and 2A.) (168). The core capsid layer is made up of 120 copies of viral protein 2 (VP2) and has a triangulation number of T=1 (105). RV cores contain the virus' genome, coiled tightly in an ordered fashion (131). They also contain 11 to 12 copies of VP1 and VP3 with VP1 located at the five-fold axes of the icosahedron (61). The middle and outer capsid layers are formed by VP6 and VP7, respectively, and they both exhibit T=13 symmetry (169). A structural study using cryo-electron microscopy has shown that VP7 holds onto the VP6 capsid layer via its N-terminal domain, which helps with the stability of the virion (43). Sixty 'spikes' are present on the outer capsid layer and are made of VP4. The spikes are approximately 40Å in length and protrude away from the VP7 layers (169). RV virions (i.e., TLPs) can be further reduced naturally and/or *in vitro* into double-layered particles (DLPs) that consist of VP1, VP3, dsRNA surrounded by VP2 and VP6 (Figure 2B.) or core particles that contain VP1, VP3, dsRNA, and VP2 but lack VP6 (Figure 2C.) (131).

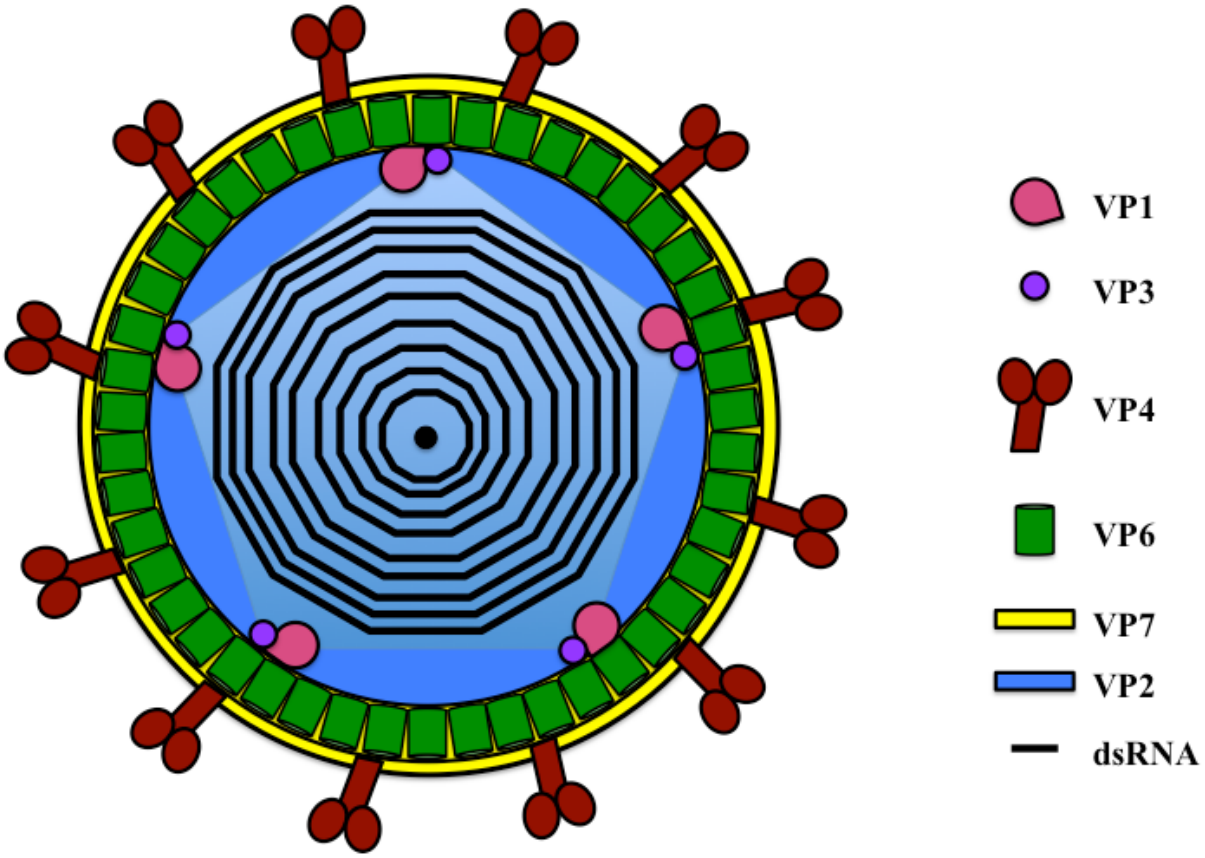

Figure 1. Schematic diagram of the RV virion. The viral structural proteins are color-coded and shown in the legend on the right. The outer capsid layer made up of VP7 (yellow) and is decorated with the spike and attachment protein, VP4 (red). Under that layer is the intermediate protein layer formed by VP6 (green) and the core capsid layer comprised of VP2 (blue). RV genomic dsRNA (black) is encapsidated within the core. The RNA-dependent RNA polymerase, VP1, (pink) and capping enzyme, VP3, (purple) form pairs at 11-12 of the core capsid's icosahedral vertices.

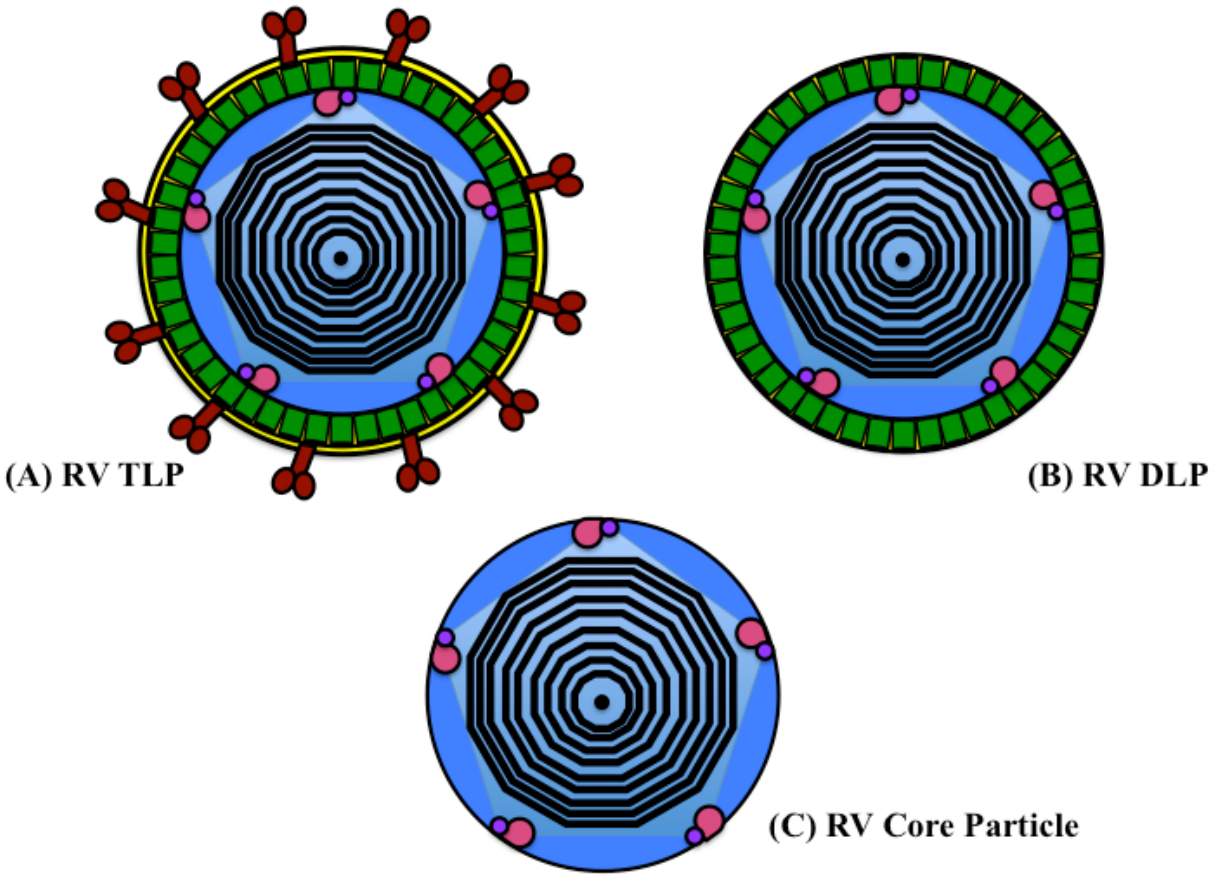

Figure 2. Schematic diagram of the RV TLP, DLP, and core particles. (A) The RV triple-layered particle (TLP) is the mature, infectious form of the virus and is composed of VP4, VP7, VP6, VP2, VP1, VP3, and RV genomic dsRNA. (B) The RV double-layered particle (DLP) is formed by loss of the outer capsid layer during endosomal escape and is made up of VP6, VP2, VP1, VP3, and RV genomic dsRNA. This particle is what transcribes +RNAs to for use as templates for translation of viral proteins and for encapsidation and –RNA synthesis of RV genomic RNA. (C) The RV core particle can be isolated *in vitro* and is made of VP2, VP1, VP3, and RV genomic dsRNA.

Structural Proteins

VP1

Gene 1 was first found to encode for what would come to be identified as the RV protein, VP1 (122, 193). One way the function(s) of VP1 were initially studied was through creation and characterization of temperature-sensitive (ts) mutants of the simian RV strain SA11. This work found that VP1 was critical to viral replication because the ts mutant that mapped to gene 1, SA11-tsC, possessed replication-deficient phenotypes when infection proceeded at the non-permissive temperature (68, 172). Cells infected with tsC were unable to synthesis protein, ssRNA, or dsRNA. They also produced empty viral capsids and viral proteins were mislocalized as seen through immunostaining and epifluorescence (41, 172). Later, it was shown that VP1 is the RV RNA-dependent RNA polymerase (RdRp) through radiolabeling and cross-linking using a nucleotide analog that inhibited viral RNA transcription (211).

VP1 is a globular, 125 kDa protein that consists of a centralized 'right-handed' polymerase domain (110). That domain is flanked by N- and C-terminal accessory domains—a feature that is unique to and found across the other members of *Reoviridae* (132). Another unique feature of RV (and other *Reoviridae* RdRps) is a priming loop, which is a loop between the fingers and palm subdomains that is predicted to rest in an inactive state presumably unless VP1 is engaged by its activation cofactor, VP2 (110, 160, 199). The exact function(s) for the accessory domains is not known; however, they have been implicated as being critical for replication in a study on the related BTV polymerase (224). The accessory domains are related to another interesting feature of VP1 and other *Reoviridae* RdRps, which is the formation of four tunnels that lead to the buried catalytic center of the polymerase domain (110, 199). These tunnels are used to direct the entry and exit of nucleotides, template RNA, and product RNA.

As a primer-independent polymerase, VP1 needs to bind single-stranded plus-sense RNA (+RNAs) in order to perform minus-strand synthesis and thereby replicate the RV genome. It has been shown to bind specifically to a conserved sequence (5'-UGUGACC-3') at the 3' end of plus-strand RNAs; however, VP1 bound to RNA is not enough to initiate genome replication (157). Research into residues of VP1 important for this +RNA binding, found several residues in the RNA entry tunnel that are important for correctly orienting the template RNA. Some of these residues bind to RNA specifically, while others bind non-specifically. It was hypothesized that the residues that bind specifically are responsible for aligning the RNA template in a manner

that 'oversho[ots] the register for initiation by a single nucleotide,' (110, 151). In addition to RNA, VP1 interacts with many RV proteins, including: VP2, VP3, NSP2, NSP5 and NSP6 (Table 1.) (11, 160, 221).

VP2

As mentioned previously, VP2 is the component of the core shell of RV, and it is encoded by gene segment 2 (103). It is a 102 kDa protein, and 120 copies join together in heterodimers to form a T=1 icosahedron. The heterodimers consist of one VP2-A and one VP2-B conformer that share many structural similarities; for example, they are both comma-shaped and possess three subdomains (apical, central, and dimerization). Between those subdomains lies a flexible region that has not been solved and could allow for the slight differences seen in the A and B conformations of VP2 (131). Five VP2-A's form a star-like pattern at the icosahedral vertex, and five VP2-B's are interspersed between them. These decamers join together to form the core shell. The VP2 core shell surrounds the RV genome as well as VP1 and VP3, which are located inside the core at the vertices. In early studies, VP2 was shown to bind to RNA and later that interface was found to reside in the N-terminal domain of the protein (23, 102). Interestingly, VP2 is also a cofactor for VP1, activating the protein in order for RNA synthesis to occur during transcription and replication (115, 160). Unsurprisingly, VP6, which forms the intermediate capsid layer, also interacts with VP2 via hydrophobic residues that likely enhance the stability of the DLP (40). Besides being the component of the core shell, VP2 is a critical binding partner of the viral RNA-dependent RNA polymerase, VP1. It serves to activate VP1 during RNA synthetic processes (transcription and replication), is implicated in VP1 recruitment to viroplasms, and likely plays an important role in the encapsidation of the VP1-VP3-RNA complex (22, 48, 49, 160, 231). NSP2 and NSP5 have also been shown to bind with VP2 (Table 1.) (19, 221). In one study, work in mammalian and insect cells demonstrated that VP2 and NSP5 can co-immunoprecipitate, that NSP5 can affect the intracellular distribution of VP2, and that VP2-NSP5 binding may compete with VP2-VP6 binding (19). VP2 interacts with VP6, VP1, VP3, NSP2, NSP5, and RNA (Table 1).

VP3

Gene 3 encodes, VP3, a 98 kDa viral structural protein that is responsible for the 5' capping of RV transcripts. As such, it binds RNA and performs guanylation, N-7-methylation, and 2'-O-methylation (107, 158). VP3 has also been shown to act as a methyl transferase (42). Work performed with a temperature sensitive mutant of simian SA11 (SA11-tsB) with a found that at non-permissive temperature (39˚C) transcription and capping were unaffected. Instead, infection that proceeded thusly resulted in high numbers of empty particles, which could show that VP3 is important for RNA assortment and packaging (212). While the full structure of VP3 remains unknown, recent work by Ogden and colleagues has used bioinformatics approaches to predict the domains of VP3 that are associated with its functions as a capping enzyme. Moreover, they tested their identification of the GTase domain biochemically to further support their structural predictions (152). Other work has shown that VP3 may participate in viral countering of the host cell immune response. The structure of the C-terminal domain of VP3 is a 2H phosphoesterase, which means that it can antagonize the OAS/RNase L pathway (150). This function would be beneficial for VP3 to help protect the polymerase complexes that form as early replication intermediates. Addition of the 5' cap is extremely important for viral mRNAs as it protects it from nucleases and facilitates translation on host ribosomes. In addition to binding RNA, VP3 has been shown to interact with the other viral core proteins, VP1 and VP2 (Table 1.) (231).

VP4

The outermost layer of the RV virion has 60 trimeric 'spikes' made of VP4 that extend through the VP7 outer capsid (169). It interacts with VP7 as well as the inner capsid protein, VP6, in a manner that may denote one function for VP4 is its actions as a scaffold (Table 1.). The portion of VP4 outside the virus particle forms a rod-like structure that has a 'bi-lobed head.' The interior portion is organized into a pedestal-like base (167, 228). VP4 (88 kDa) is encoded by gene 4 and is important for the attachment and entry of the RV particle into cells. In order to enter the intestinal epithelial cells, VP4 must first be proteolytically cleaved by trypsin (in cell culture) or trypsin-like (in infected individuals) proteases. This cleavage results in two fragments, VP5* (60 kDa) and VP8* (28 kDa) (60). Given its location on the exterior of the virion, it is also a target for the host immune response, as it is a prime target for neutralizing

antibodies. Studies using a simian rhesus RV strain (RRV) found that VP4 possessed sites for both homo- and heterotypic neutralization with most of those sites found on the VP8* cleavage product (113). Early studies using temperature-sensitive mutants deduced that VP4 is the viral hemagglutinin (94). As such, VP4 is an essential contributor to RV classification and the genotype of the VP4 will lead to the determination of the virus' P-genotype (126). Early studies into RV virulence factors implicated that VP4 may be important in this capacity in addition to its other roles (153).

VP6

VP6 is encoded by gene segment 6 and makes up the majority of the RV virion. It is the sole component of the intermediate capsid layer. That intermediate shell forms a T=13 icosahedron made up of 260 copies of VP6 trimers. Each VP6 monomer is 45 kDa and has two structural domains: a jelly-roll β-barrel and an α-helical pedestal (123, 131). The structure of VP6 is important for stabilization of the core particle through binding with VP2 and as a tether for the outer shell proteins, VP4 and VP7 (Table 1.). Indeed, studies using virus double-layered particles that were stripped of VP6 found that those cores were unable to transcribe. Transcription was rescued after VP6 was added back (179). Work on a temperature sensitive virus that has mutations in its VP6 gene found that the N-terminus of VP6 may be important for its viroplasmic localization (116). It is also found in high abundance in cells. Another important role for VP6 is for identification of RVs due to it being extremely antigenic, making it a prime target for laboratory tests. For RVAs, VP6 historically served as a way to differentiate between subgroup genotypes; however, nucleic acid sequence analysis has overtaken VP6 subgrouping (125-127).

VP7

The smallest structural protein of RV is encoded by gene segment 9 and has been identified as the glycoprotein, VP7, at 37 kDa (as a monomer). This protein forms the outer capsid shell with 260 trimers that rest upon the trimers formed by the intermediate capsid layer protein, VP6. The N-terminal 'arms' of VP7 are what attach the outer capsid proteins to the VP6 layer (Table 1.) (43). Given its location, it is no surprise that VP7 is important for eliciting neutralizing antibody response from the host. It causes both homo- and heterotypic

neutralization (112). When VP7 was knocked down through use of siRNAs, it did not affect any aspect of RV replication except for addition of the outer capsid (189). VP7 is also important for RV classification and imparts the virus' G-genotype (126).

Table 1-RV Protein Interactions

Protein 1	Residues	Location	Protein 2	Source
VP1	28-56	N-terminal	NSP2	Viskovsha et al., 2014
VP1	442-458	Polymerase-fingers	NSP2	Viskovsha et al., 2014
VP1	562-578	Polymerase-fingers	NSP2	Viskovsha et al., 2014
VP1	823-836	C-terminal	NSP2	Viskovsha et al., 2014
VP2	1 to 27	N-terminal	VP1	Patton et al., 1997
VP2	1 to 92	N-terminal	VP1	Zeng et al., 1998
VP2	100-880	Principal Domain	VP1	McDonald and Patton, 2011
VP2	1 to 92	N-terminal	VP3	Zeng et al., 1998
VP2	34-86	N-ternimal	NSP2	Viskovsha et al., 2014
VP2	514-518	Principal Domain	NSP2	Viskovsha et al., 2014
VP2	664-674	Principal Domain	NSP2	Viskovsha et al., 2014
VP2	838-845	Principal Domain	NSP2	Viskovsha et al., 2014
VP2	93-880	Principal Domain	NSP5	Berois et al., 2003
VP4	not specified	C-terminal-Foot	VP6	Settembre et al., 2011
VP4-VP5*	267, 375, 467	Body	VP7	Settembre et al., 2011
VP6	65, 70, 71	N-terminal	VP2	Charpilienne et al., 2002
VP6	264, 266, 270, 286	Domain H	VP4	Mathieu et al., 2001
VP6	296-302	Domain H	VP7	Mathieu et al., 2001
VP7	not specified	N-terminal	VP4	Settembre et al., 2011
VP7	170, 200, 210	Domain II	VP4-VP5*	Settembre et al., 2011
VP7	58-78	N-terminal	VP6	Chen et al., 2009
NSP2	22-32	N-terminal-Catalytic cleft	VP1	Viskovsha et al., 2014
NSP2	67-74	N-terminal-Catalytic cleft	VP1	Viskovsha et al., 2014
NSP2	91-104	N-terminal-Catalytic cleft	VP1	Viskovsha et al., 2014
NSP2	27-40	N-terminal	VP2	Viskovsha et al., 2014
NSP2	223-237	C-terminal	VP2	Viskovsha et al., 2014
NSP2	291-302	C-terminal	NSP5	Jiang et al., 2006
NSP2	64-68	N-terminal	NSP5	Jiang et al., 2006
NSP2	179-183	C-terminal	NSP5	Jiang et al., 2006
NSP2	232-251	C-terminal	NSP5	Jiang et al., 2006
NSP2	79-107	N-terminal	NSP6	Viskovsha et al., 2014
NSP2	271-287	C-terminal	NSP6	Viskovsha et al., 2014
NSP4	175	C-terminal	VP6	Taylor et al., 1992
NSP5	last 48	C-Terminal	VP1	Arnoldi et al., 2007
NSP5	1 to 33	N-terminal	NSP2	Afrikanova et al., 1998
NSP5	163-197	C-terminal	NSP6	Torres-Vega et al., 2000
NSP6	22-29	Central	NSP2	Viskovsha et al., 2014
NSP6	52-68	Central	NSP2	Viskovsha et al., 2014

Non-Structural Proteins

NSP1

One of the most important tasks for viral proteins is evasion of the host cell's immune response. The 59 kDa NSP1 is one of RV's main tools for direct immune response antagonism. Earlier studies into NSP1 found it was encoded by gene 5 and is the most genetically variable RV protein. Despite this variability, it does possess a conserved zinc-biding RING domain that consists of a specific pattern of cysteine and histidine residues that could make it an E3 ligase homologue (84, 26, 142). It acts by binding transcription factors for interferon and targeting them for proteasomal degradation. Specifically, work on NSP1 and interferon regulatory factor 3 (IRF3) has led to the hypothesis that NSP1 is an E3 ubiquitin ligase (17, 71, 72). In addition to stimulating the degradation of IRF3, NSP1 also induces the degradation of IRF5 and IRF7 through a similar mechanism. From this work, it was hypothesized that this degradation occurs via interactions with the IRFs and the NSP1 C-terminal (18). More recently, NSP1 has also been implicated in the degradation of β-TrCP, which is required to activate NFκB (70). Thus, NSP1 is essential for RV to evade the host cell's innate immune response. Despite this important function, NSP1 is not required for viral replication as shown by RVs that exist with truncated NSP1s, which are still replication competent (85). Moreover, when siRNAs against NSP1 were used, protein synthesis, RNA synthesis, and virus assembly were unaffected other than significantly lower levels of NSP1 expression (189).

NSP2

RV NSP2 (35 kDa), encoded by gene segment 8, is one of the viral proteins required for viroplasm formation (161). Structural studies have revealed an approximately 280 kDa octameric protein that is formed as a dimer of two NSP2 tetramers, and this octamer is the functional form of the protein (89, 97, 202). The octamer forms a circular shape that resembles a doughnut due to a 35Å hole found in the center of the protein, and within the clefts of the NSP2 monomers are histidine triad (HIT)-like motifs that are responsible for NSP2's ability to perform nucleotide hydrolysis (33, 89, 213).

NSP2 is a RV protein of particular interest given that extensive research reveals it to be an enzyme that performs numerous different functions during infection, which points to it as a central player in RV replication. Indeed, evidence of this can be seen by NSP2's necessity for

viroplasm formation. *In vitro* studies show that infected cells treated with siRNAs against NSP2 are prevented from synthesizing viral proteins, +RNA, and dsRNA (189). The studies also show that morphology is also affected in that viroplasm and progeny virion formation are negatively impacted. Additionally, when cells are infected with a temperature-sensitive mutant of SA11 RV that possesses an alanine to valine lesion at position 152 (A152V) in its NSP2 gene (SA11-tsE), viroplasms are unable to form at the non-permissive temperature (39˚C) (172, 191). Why NSP2 is important for viroplasms can be surmised from its functions. Work investigating this protein over the decades has found that it possesses the ability to bind to single-stranded RNAs (ssRNA), exhibits ATP-independent helicase activity, acts as an NTPase, and also performs as an NDP kinase (98, 101, 200, 201). All of these roles for NSP2 make it important to the processes of viroplasm formation and downstream RV genome replication and assembly. It is also important to note work that showed that these functions of NSP2 were abrogated when using the SA11-tsE mutant, which could not form octamers (202). This finding demonstrates that the functional form of NSP2 is octameric. More recent data have indicated that there may be two distinct forms of NSP2: a 'dispersed' NSP2 that resides in the host cell cytoplasm as well as viroplasms early in infection and a 'viroplasmic' NSP2 found in viroplasms more later in infection (51). The existence of these separate forms could explain why NSP2 possesses so many different functions and is implicated in many aspects relating to virus genome replication and assembly. Traditionally, NSP5 is a well-known binding partner of NSP2 (Table 1.), and the two expressed in the absence of any other viral proteins will form viroplasm-like structures in host cells (58, 62). However, other viral proteins—namely, VP1, VP2, and NSP6—have also been found to directly interact with NSP2 (Table 1.) (97, 221).

NSP3

RV gene 7 encodes NSP3, which is a 36 kDa viral non-structural protein that is considered a functional homologue of poly(A) binding protein (PABP) (216). It presents as a heart-shaped homodimer with two N-terminals that match in structure and two C-terminals that are organized differently, making it asymmetric (53). It recognizes a 3'-GACC consensus sequence in the untranslated region (UTR) of all RV mRNA, which it binds to using its N-terminal domain (164). It was shown that the specificity of this RNA-binding activity was due to the formation of a tunnel in the NSP3 homodimer caused by its asymmetry (53). The C-terminal

domain of NSP3 binds eIF4G (eukaryotic initiation factor 4G) along a site that is also where PABP binds; thus, inhibiting cell protein translation (162, 163). Indeed, for decades it was proposed that NSP3 abrogated host cell translation and was required for translation of RV mRNAs. However, recent work has shown that NSP3 may function more as a viral translation enhancer that allows it to out compete host cell mRNAs yet is not critical for viral protein translation in general (73, 143).

NSP4

Severe diarrhea is one of the main clinical symptoms of RV gastroenteritis. The viral non-structural protein, NSP4 (20 kDa, encoded by gene 10), has been identified as the viral enterotoxin and is implicated as a possible factor in viral virulence. Thus, it is thought to play a central role in the development of diarrhea (16, 233). Studies in human cells and mice models have suggested that NSP4 acts via stimulating the activation of phospholipase C, which causes an increase in the amount of intracellular calcium (56, 145, 206, 207). This is likely caused by disruption of the calcium homeostasis in the endoplasmic reticulum, and the intracellular calcium up regulation in turn leads to chloride secretion. How NSP4 accomplishes this is not definitively known, but clues to the mechanism have arisen from studies investigating its structure.

The structure of NSP4 has not been fully solved because it tends to aggregate in solution, but several studies have investigated specific domains. In one study, it was found that one of those NSP4 domains, which is known to disrupt membranes, also structurally resembled viroporins (86). And while viroporins tend to have roles in virus entry or exit, it was shown that NSP4's viroporin activity likely increases cytoplasmic calcium by working in the endoplasmic reticulum. This role could help many processes in replication including viroplasm formation and outer capsid assembly (86). It is well known that NSP4 accumulates in the rough endoplasmic reticulum where it is poised to help with nascent particle budding and outer capsid layer acquisition, acting as a receptor with the VP6 capsid layer of the DLP as the ligand (14, 140, 161). NSP4 is also implicated in the removal of the transient envelope that surrounds nascent, assembling virions as they exit the cell (205). Other roles for NSP4 were discovered by knocking down the protein in RV-infected cells through use of siRNAs. In one study, loss of NSP4 lead to a mislocalization of viral proteins found in viroplasms as well as increased

production of empty capsids. This result is interesting because it indicates a role for NSP4 in early replication as well as during progeny virus exit (190).

NSP5

The other RV protein critical for viroplasm formation is NSP5, an o-linked glycoprotein encoded by gene segment 11 of the RV genome (69, 225). NSP5 exists in 26, 28, 32, and 35 kDa isoforms that are related to phosphorylation, which could be in part due to an autophosphoylation mechanism (3). Viral proteins, NSP2 and VP2 (Table 1.), are known to interact with NSP5 and are also implicated in its phosphorylation (2, 11, 19, 165). The viral polymerase, VP1, and viral RNA are also binding partners with NSP5 (Table 1.) (11, 217). Cells that have been infected with RV and then treated with siRNAs against NSP5 result in a reduction of: viral protein synthesis, viroplasm formations, viral mRNA synthesis, genomic dsRNA synthesis, and progeny virions (32, 109). These observations underscore NSP5 as a critical player in RV replication. As mentioned previously, NSP5 is a binding partner of NSP2, and they are critical components for formation of viroplasms or viroplasm-like structures (VLSs) (58, 62). A more recent study found that NSP5 could also form VLSs when NSP5 was co-expressed with VP2 but not NSP2. In fact, the VP2-NSP5 VLSs were able to recruit more viroplasmically-associated viral proteins than the NSP2-NSP5 VLSs (48). It should be noted that results within this dissertation did not support those findings (138).

The structure of NSP5 was predicted from data obtained by analyzing purified recombinant protein. It was further shown that NSP5 forms a decameric structure that consists of pentamers of dimers. This particular quaternary organization is likely important for viroplasm formation (121). These results build off earlier studies that found that the C-terminal helical domain of NSP5 was important for the formation of VLSs (183). Interestingly, recent data has demonstrated that NSP5 may be the first viral metalloprotein that coordinates an iron-sulfur cluster (119). This discovery has important implications for the relationship between NSP5 and its binding partners, especially viral RNA. While it is not important for VLS (and likely viroplasm) formation, it is possible that the cluster plays a part in genome replication and/or assembly (119).

NSP6

Interestingly, NSP6 is the only RV protein that is only associated with some strains and not others. It is a small protein solely comprised of 92 amino acid residues. In addition, it is the only protein that is not encoded by its own gene segment and is instead encoded by a +1 alternative open reading frame (ORF) in RV gene 11, which also encodes NSP5 (130). Its function remains unknown; however, given that is it not found in all strains, it is likely not required for viral replication. Moreover, siRNA knockdown experiments that used a complementation strategy strongly suggested that loss of NSP6 likely did not affect virus replication (32). NSP6 is known to interact with other RV structural proteins, NSP2 and NSP5 (Table 1.) (209, 221).

Genetic Variation

RV is a ubiquitous pathogen that infects the young of most animals, including humans. RVs can increase their genetic diversity by error-prone genome replications (mutation) or by swapping genome segments during co-infection (reassortment) (135, 181, 195). Compared to mutation, reassortment can have more dramatic effects on genetic variation of the population, providing RVs the opportunity to adapt rapidly in the face of selective pressures. Indeed, in co-infections of cells, gene segments may 'swap out,' or reassort, with one another to form progeny virus whose genomes contain segments from both parental strains. Thus, the potential genetic variation amongst rotavirus can be significant. Indeed, naturally occurring reassortant rotaviruses have been isolated from a variety of species, and bioinformatic analyses of genome constellations from simian strains used in the laboratory have revealed likely historical reassortant events (128, 146).

Before the advent of polymerase chain reaction and sequencing, electropherotyping of viral genomes were used to differentiate strains since the migration patterns of the dsRNA would differ between non-related strains. Another early method to compare rotavirus genomes was the use of RNA hybridization assays that utilized radiolabeled probes (124, 181, 195). It was found that there are eight species of RV, RVA-RVH, with the majority of human disease caused by RVA. Most currently circulating strains of human RVA can be further categorized as either derived from a porcine background (strain Wa-like) or from a bovine background (strain DS-1-like) (125). Other strains, such as Au-1 that resembles feline RVs, are also associated with

infections in humans although these are typically smaller isolated events in immunocompromised individuals (99, 147, 148). Similarly, occasional crossover infections from other animal species have been reported, often in remote places where direct human contact with livestock and wildlife is common (118). Thus, it is important to maintain surveillance of the genetic diversity of circulating RVs and to continue to develop tools for detection of novel, potentially reassortant strains. One example of such surveillance is performed by members of the McDonald laboratory, who frequently collaborates with the Patton laboratory and other colleagues to analyze sequencing data from a variety of sources in order to monitor the molecular epidemiology of RVAs circulating in the United States and elsewhere (52, 134, 187, 235). These researchers have also contributed towards making surveillance more easily attainable in countries that may not have easy access to sequencing tools by developing a PCR-based method that can distinguish between the two major human RVA genotypes (139).

Even though the number of RV sequences from all groups has increased dramatically as sequencing has become more affordable and accessible, the majority of sequences deposited into NCBI's GenBank are for RVA strains. In order to better understand and classify the genetic diversity of RVAs, a group was formed to define what constitutes a novel strain based upon consensus genome cut-offs. This group also established standardized nomenclature for the gene segments as well as for deposition of sequences into NCBI's GenBank. Each RVA protein was assigned a letter and the constellation of a RVA genome would be as follows: Gx-P[x]-Ix-Rx-Cx-Mx-Ax-Nx-Tx-Ex-Hx, where 'x' is a number that corresponds to the protein's genotype. This protocol has led to the approval of more than 50 new genotypes (125, 126).

REPLICATION

Attachment and internalization

RV particles are introduced to the host via the fecal-oral transmission route (96). Virions are able to survive and pass through the upper gastrointestinal tract where they eventually encounter their target cells, the mature enterocytes of the small intestine villi (79). In this environment, the attachment protein, VP4, encounters host trypsin-like proteases that cleave it to yield VP5** and VP8* (60). The precise mechanism by which RV is able to enter these cells is complicated and not yet well understood. Multiple receptors on cells—including: sialic acids,

integrins, α2β1, α4β1, αvβ3, αxβ, hsc70, JAM-A, and gangliosides—have been implicated in RV attachment and entry (9, 45, 74, 208). In fact, it appears that the receptors used for RV entry may be strain-dependent. This is evident by RV strains that are sensitive or resistant to treatment with neuraminidase, which is an enzyme that removes sialic acid from glycoproteins. While some animal strains appear to require sialic acid residues on the cell, most human and animal strains do not (45). More recent evidence suggests that while some strains may not interact with sialic acid residues on the cell surface, they may still bind to sialic acid found on the interior of the cell (9). Additionally, some RV strains have been shown to be independent of integrin since blocking of integrin by antibodies did not affect RV binding. Instead, integrin was proposed to be important for other aspects of RV entry besides initial attachment (46). Very interestingly, recent work has suggested that RV may be similar to norovirus in that it may recognize histo-blood group antigen (HBGA) (82). This could indicate that susceptibility and response to infection by RV could be related to an individual's blood type. HBGAs are also interesting in that they are developmentally regulated in children, which could be why age-related differences in RV infection and vaccine protection are noted (as reviewed by 91 and 170). There are also some HBGAs that are shared with animals, which could explain cross-species infections. In fact, HBGAs may play an important role in host range restriction (as reviewed by 91 and 170). However, using the work reviewed above to inform how RV enters cell is complicated since most studies relied on non-polarized cell types, such as MA104 green monkey kidney cells. While some studies have sought to address this limitation (47), more work using polarized cell types or even primary cells from infected individuals could prove helpful in enlightening the complicated process of RV receptor binding and cell entry.

The aforementioned VP4 cleavage event is thought to enhance infectivity of the virion by stabilizing the spike protein. Analysis via cryo-electron microscopy and biochemical assays using radiolabeled proteins showed that VP4 changed from disordered to ordered conformation following treatment with trypsin (50). After the infectious RV virion attaches, how it is taken into the cell may be similarly strain-specific as the initial binding step (75). The results of some early experiments indicated that RV might introduce itself to the cell by direct entry (95). However, morphological studies indicated that RV enters the host cell cytoplasm via receptor-mediated endocytosis. Endocytosis can occur through several different mechanisms, and the specific one(s) relevant to RV are not clear. There may be multiple possible mechanisms for RV

endocytosis with different strains following different pathways. In fact, relatively recent studies in a line of monkey kidney cells (MA104) have found that characteristics of a strain's VP4 could determine the mechanism for endocytosis (54). Work by the López laboratory has shed some light onto RV entry. They initially found that RV intake was not dependent on clatherin or caveolin; however, cholesterol and dynamin were important (177). Conversely, later studies actually support the theory that most RV strains enter via a clathrin-dependent endocytosis mechanism (75). A model for endocytotic internalization was hypothesized through studies using a simian rhesus RV strain (RRV). The authors proposed that RV enters the cell through endocytosis in a manner that requires VP4 conformational changes which result in loss of VP8* signal but a retention of VP5** signal, as shown by immunofluorescent imaging. So VP4 attaches and becomes cleaved by trypsin-like proteases, changing conformation to reveal VP8* and VP5**. VP8* is lost as the virion is internalized and VP5** folds backward, and the particle enters the early endosome (227). Further studies using live-cell fluorescence imaging agreed with this model and found that this process occurs rather quickly—within 10 minutes in their assays (1). The stability of the outer capsid shell of the TLP is dependent on calcium. Thus, the lower calcium levels and changes in compartmental pH in the endosome are thought to cause VP7 to destabilize and disassemble. VP7 disassembly likely triggers a change in conformation of VP4 that rearranges VP5** in a manner that could lead to penetration of the endosomal membrane (210, 229). This endosomal escape allows a transcriptionally-active double-layered particle (DLP) to be deposited into the host cell cytoplasm.

Transcription and translation

Transcription of the RV genome occurs after the DLP is released into the host cell cytoplasm. There are two rounds of viral transcription—an early stage that occurs in the first couple of hours post-infection and a later stage that occurs 8-9 hours post-infection (189). The first stage produces lower levels of +RNAs, and the later stage produces exponentially more which is likely due to some new DLPs also serving as centers for transcription (15, 189). The loss of the outer capsid layer as virus particles are deposited into the cytoplasm is thought to cause conformational changes in VP6 and VP2 that lead to the activation of the polymerase, VP1. VP1 transcribes the minus-strand RNA of the dsRNA genome segments from within the protected environment of the DLP, and the resulting +RNA transcripts exude from the DLP

through pores formed by VP2 and VP6 at the five-fold axes (104, 159). In further support of this model, cryo-electronmicroscopy and X-ray structure data shows that VP1 is located just offset from these five-fold axes with the +RNA exit tunnel abutting an opening (61). Presumably, VP3 is located adjacent to VP1 in the core because RV transcripts have methylated 5' caps (m^7GpppGm) that they would need to receive before exiting the DLP (42). These viral +RNA transcripts are used as mRNA templates for viral protein synthesis on host cell ribosomes. Additionally, transcripts are recruited to early replication complexes where they are used as templates for viral genome replication later in infection.

In addition to the 5' cap structures, it is thought that RV +RNAs are protected from degradation and recruited to host ribosomes with help from NSP3, at least during early transcription. It accomplishes this by binding to the 3'-GACC sequence on those mRNAs as well as by competitively binding to eIF4G, effectively blocking host cell transcription (73, 162, 163). Thus, viral proteins are preferentially translated and accrue in the host cell. One of the results of this accrual is the formation of cytoplasmic inclusion bodies that serve as viral factories for RV replication.

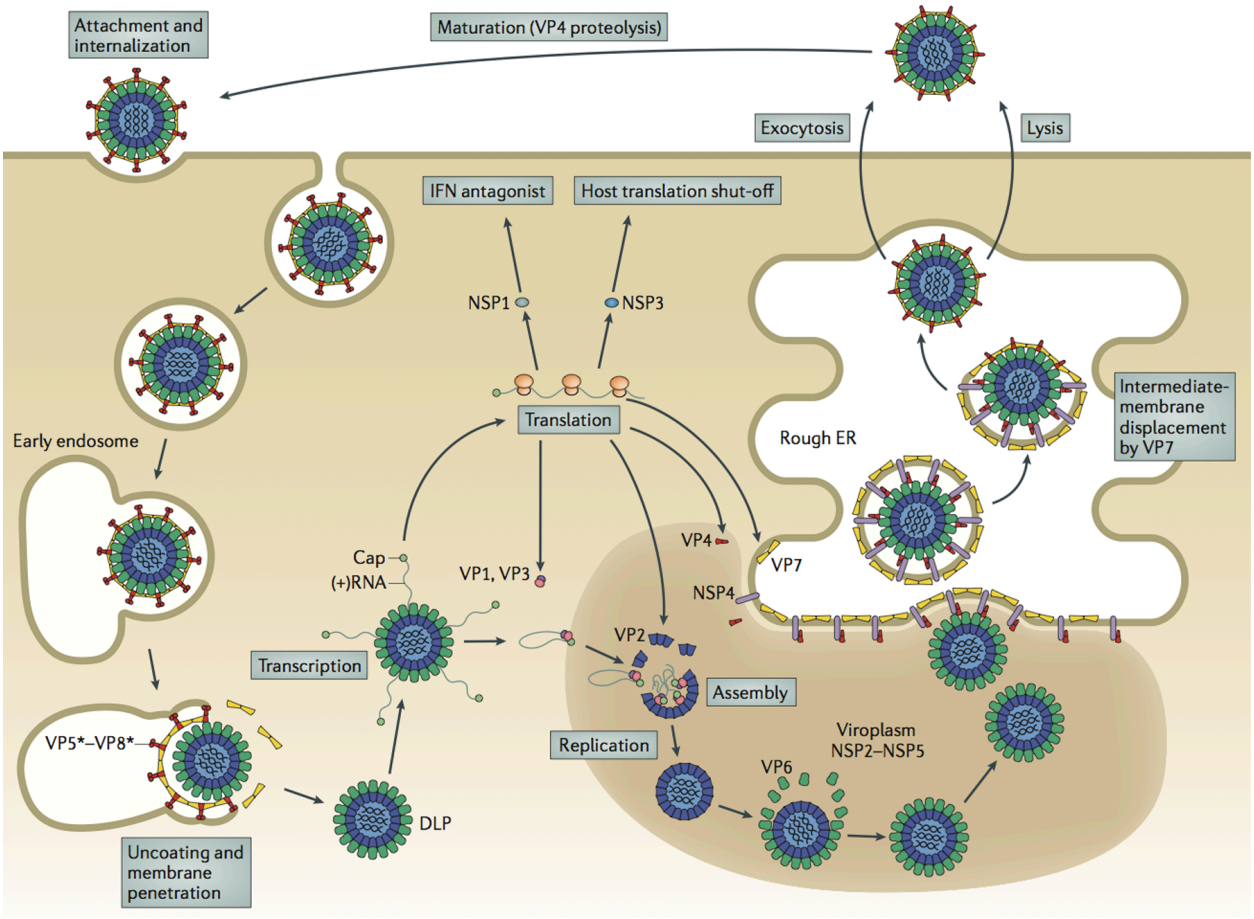

Figure 3- Schematic diagram of the RV life cycle. The RV virion attaches to the cell surface of small intestine villi enterocytes via the viral attachment protein, VP4. VP4 is cleaved by trypsin-like proteases into VP5** and VP8*, and along with the outer capsid and fusion protein, VP7, they bind with host cell receptors to enter via clatherin-dependent endo cytosis. Calcium levels drop within the endosomal compartment, triggering viral particle uncoating, and DLPs are deposited into the cell cytoplasm. The DLP is transcriptionally active, and the polymerases contained within the core transcribe the dsRNA genome, and +RNA transcripts exit the DLP through pores. They are translated on host cell ribosomes or later incorporated into polymerase complexes that locate to viroplasms, which are the sites of RV genome replication and early particle assembly. NSP 2 and NSP5 are the primary components of the viroplasm, and other nonstructural proteins, NSP1 and NSP3, serve to antagonize the host cell's innate immune response and impede host protein translation, respectively. In addition to polymerase complexes, VP2 and VP6 also accumulate in viroplasms. The polymerase complexes and dsRNA are assorted and encapsidated into newly-forming core particles that also acquire their VP6 layer before budding through the rough endoplasmic reticulum. NSP4 acts as a receptor and helps the new DLPs traverse the ER and accumulate the outer capsid glycoproteins. The progeny virion is coated transiently by a lipid bilayer that is lost as it exits via lysis or exosomal secretion. ***This image is from Trask et al., 2012, Nature Reviews in Mircobiology and is used with permission of an author (S.M.) and from the Nature Publishing Group.***

Viroplasms

Similar to many viruses, the genome replication and particle assembly mechanism of RV remains unclear despite a significant amount of research. The viral transcripts released from the DLP serve as mRNAs for the translation of RV proteins. As viral structural and nonstructural proteins are made and accumulate, one model for replication has some DLPs also functioning as nucleation centers for the formation of viral inclusion bodies in the host cell cytoplasm known as 'viroplasms' (189). However, more recent evidence found using fluorescently labeled RV particles does not support this hypothesis. Instead, this study suggested that viroplasms form after the accumulation of NSP2 and NSP5 reaches a certain critical level (35). Viroplasms are predominantly composed of viral nonstructural proteins NSP2 and NSP5. Indeed, *in vitro* studies in which NSP2 and NSP5 were expressed in cells showed that both proteins were required in order to form punctate structures similar to native viroplasms that are called 'viroplasm-like structures' (VLSs) (62). It is possible that early-stage viroplasms could be synonymous with the pre-core and/or core RIs given the composition of those entities: VP1/VP3/VP6/NSP2/NSP3/NSP5 or VP1/VP2/VP3/VP6/NSP2/NSP3/NSP5, respectively (66). As infection proceeds, the number of viroplasms decreases and their size increases (58). In addition to NSP2, VP2 may be important for viroplasm formation and recruitment of other viral proteins to viroplasms in conjunction with NSP5 (48). While VP2 may be a key player for bringing other viral proteins to viroplasms, whether it is essential for viroplasm formation is questionable based upon results from other studies. In one study, viroplasms were still formed despite the knocking down of VP2 using siRNAs. However, those viroplasms formed were smaller and fewer in number than those found in control cells (15). Data from another study that is included in this dissertation also found that when VP2 and NSP5 were transfected and expressed together in cells that viroplasm formation did not occur (138). This is in contrast to the results from similar experiments performed by Contin et al. (48).

Other viral and cellular factors are also important for viroplasm formation and processes that occur within the viroplasm. Chief amongst those proteins are the cell's cytoskeleton and cellular lipid complexes. Viroplasms were found to colocalize with microtubules, and inhibition of microtubule assembly also led to a negative impact on viroplasmic growth (31). One of the major components of the viroplasm, NSP2, was shown to directly interact with tubulin, and tubulin also colocalized with viroplasms and VLSs. It was also hypothesized that NSP2 helps to

disrupt cellular functions through triggering microtubule depolymerization (120). Other data studying the relationship between viroplasms and microtubules found that the microtubule network and an associated kinesin motor were important for the fusion of viroplasms. It also provided evidence that microtubules are important for viroplasm perinuclear localization since microtubule-depolarizing drugs interfered with fusion and localization whereas microtubule-stabilizing drugs did not (57). Viral interference and coopting of the cytoskeletal infrastructure would make sense as a method for inhibiting cellular mechanisms (virus detection, immune response, etc.) while promoting viral replication.

In addition to the cytoskeleton, cellular lipids are important for viroplasms. Cheung et al. (44) demonstrated that viroplasm proteins were able to colocalize with cell lipid droplet-associated proteins. Moreover, the same study found that one of these proteins, dsRNA, and NSP5 were isolated in the same fractions from RV-infected cells and were found close together in transfected cells analyzed via fluorescence resonance energy transfer (FRET). Another interesting finding was that drugs that were antagonistic towards cellular lipid complexes also disrupted viroplasm formation, hindering RV genome replication. As such, this work suggested that cellular lipids are important for those processes. The authors proposed a model where NSP2 and NSP5 would associate with each other and lipid droplet proteins during viroplasm formation. These viroplasm-lipid complexes could recruit VP1 and other pre-core RI components, and as cores and DLPs were assembled within the viroplasm, lipids may no longer be needed. Similar work applying a fatty acid synthesis inhibitor to RV-infected cells found significant decreases in DLPs and TLPs, which could indicate broader implications for cell lipids and their role in rotavirus replication (67).

Early viral particle assembly and packaging of viral RNA genome

Within the viroplasm, viral capsid proteins accumulate and ultimately assemble into new DLPs as the genome is replicated. One of the first studies to better describe this aspect RV replication used gradient centrifugation and non-denaturing electrophoresis to isolate different complexes from RV-infected cells. These complexes were thought to be different replication intermediates (RIs) and those containing VP2 were found to be replicatively active. The study identified precore RIs, core RIs, and single-shelled RIs that each contained different combinations of viral structural and nonstructural proteins (66). Interestingly, a follow up study

by the same group provided evidence that suggested that dsRNA synthesis proceeds from the smallest to largest genome segments. It also theorized that some of the +RNA template extends from the replicase particle in a manner that makes it sensitive to RNase degradation and thus unable to be used to synthesize full-length dsRNA (159). In order to better characterize RV replicase complexes and intermediates, Aponte and colleagues performed several experiments to investigate the role of NSP2 (8). They used photochemical cross-linking and immunoprecipitation to isolate radiolabeled protein-RNA complexes, which they used to perform a variety of downstream applications. From their results, they determined that active replicase complexes include VP1, VP2, VP6, and NSP2 and that NSP2 is an important component of those complexes due to its ability to bind and modify RNA (8). Experiments that used baculovirus-expressed VP1, VP2, VP3, and VP6 found that coexpression of these proteins caused the formation of single- or double-layered particles with VP1, VP3, or nothing inside (232). Only those particles containing VP1 could perform RNA synthesis. Later work, also performed *in vitro* using recombinant versions of several of the proteins implicated in replicase complexes/intermediates (VP1, VP2, and NSP2), demonstrated evidence that formation of RV replication intermediates/subviral particles is likely a temporally ordered process. This theory was formed due to how NSP2 binding to RNAs could prevent genome replication; thus, VP1 and VP2 must bind to RNA first (218). However, a more recent study used electron microscopy of subviral particle (SVP) preparations from infected cells to further elucidate RV replication intermediates. The authors found that NSP2 actually appeared to bind RNA transcripts that were newly emerged from DLPs and was hypothesized to act as a chaperone for RNA to replicase complexes. Moreover, small, 'pebble-like' complexes were also observed that could be enriched though use of antibodies against VP1 or VP3 and were RNase sensitive, which provided evidence of the 'polymerase complex' or could be pre-core RIs. Core-RIs were seen as permeable, electron-dense particles, and no +RNAs were seen extending from their surface, contradicting the early biochemical data (21).

How the RV genome is packaged into core particles is not well understood. Given that each viral particle contains only one copy of each of the eleven gene segments, it is likely that this process is complex. Several of the viral proteins involved in replication intermediates, unsurprisingly, possess RNA-binding properties (23, 26, 83, 98, 129, 157). It is also thought that packaging signals may be present in the UTRs of the plus-strand RNAs. Related to genome

replication, it is interesting to note that the synthesis of dsRNA was found to be equimolar—that is each segment of dsRNA exists in equal quantities despite size whereas transcription appears to be size-dependent (15, 156, 194). These differences could be due to the dissimilar goals of each of these processes. In transcription, multiple copies of +RNAs are made in order to act as templates. Given these multiple rounds of +RNA synthesis, it follows that there would be differing levels of transcripts due to size of the segments. Conversely, each nascent virion only needs one copy of each gene segment, so only a single round of negative-strand RNA synthesis would likely occur.

In a thorough review of these data, McDonald and Patton proposed two models for early assembly of the RV capsid and packaging of viral +RNAs (136). Each of these models is based upon data obtained from the study of other viral pathogens. First, they described a 'concerted assembly' model whereby RNA interactions drive assortment of the viral genome like that of influenza A virus. Transcripts are bound to polymerase complexes consisting of the polymerase, VP1, and capping enzyme, VP3. These +RNA-containing complexes somehow interact and assort with each other such that eleven genome segments are gathered together. VP2 then binds to VP1, causing conformational changes in the polymerase that initiate replication even as the core particle is formed. The second model they put forth is the 'capsid-filling' model, which involves +RNAs inserting themselves into a pre-formed core capsid. This model is based upon the mechanism through which some bacteriophages package themselves. For bacteriophages, such as Φ6, the +RNAs enter through pores at the vertices in a sequential manner that leads to an expansion of the capsid. The expansion of the core capsid could lead to conformational changes that activate the polymerase to perform negative-strand RNA synthesis. To date, most research into RV assortment and assembly support the first model. Moreover, recent work into the assembly and packaging of bluetongue virus (BTV) also supports the concerted assembly model. Using an *in vitro* RNA-RNA interaction assay, the investigators were able to show that the untranslated regions (UTRs) of gene segments, especially segment 10 (S10), were able to assort (196). The authors hypothesized that the UTRs drove the formation of secondary structures that aided in assortment of segments into complexes of RNA that are then encapsidated within a core shell. They could not determine whether this RNA complex occurred in tandem with core capsid assembly or whether the core formed around the assorted RNAs after the fact (196). This group further supported this work by abrogating these RNA-RNA interactions using short

complimentary oligonucleotide strands. These strands were able to competitively bind the UTRs and inhibit viral genome replication. Moreover, they found that segments 10 and 7 (S10 and S7) primarily drove the RNA-RNA interactions and that swapping the UTRs from one gene segment with another could not rescue replication. These data suggest that BTV assortment is a complex, sequential process with gene segment-specific packaging signals found on the UTRs of gene +RNAs (63). Even amongst *Reoviridae*, RV and BTV are closely related, so it would not be surprising if the packaging and assembly of RV followed a similar strategy as its cousin.

VP1-VP2 interactions during assembly and genome replication

One of the most important protein-protein interactions during early particle assembly and genome replication is that between the viral polymerase, VP1, and the core capsid protein, VP2. An early study of RV subviral particles used temperature-sensitive strains of RV to show that core formation with VP2 is important for activating VP1 replicase activity (115). Subviral particles from infections using SA11-tsF, which possesses a temperature-sensitive mutation mapped to gene 2, showed a dramatic reduction in dsRNA product at nonpermissive temperatures. In contrast, particles from SA11-tsG infection (VP6 temperature-sensitive mutant) demonstrated a much more modest reduction. These data further support the conclusions that VP2 is important for VP1 activation and also that viral progeny assembly is likely an ordered process where cores must first form and encapsidate the genome before replication occurs. The intermediate VP6 layer would be added after core formation has begun (115). This result is interesting since VP6 is necessary for RV transcription (179) and could suggest that the mechanisms for activation of and/or polymerization by VP1 are different between transcription and replication. These results were supported by work that recapitulated dsRNA synthesis *in* vitro that found VP1 and VP2 were necessary and sufficient for genome replication to occur (160). Further work using this *in vitro* replication system determined that the interaction interfaces of VP1 and VP2 are both conserved between groups as well as group-specific (133). These interfaces are so important that they could drive the genetic evolution of RV. The residues by which VP2 activates VP1 were found to be on the inner face of VP2 rather than in its N-terminal domain (137). In addition to important relationships for replicating the dsRNA genome of RV, VP1-VP2 interactions may be critical for packaging the genome as well. Research studying the formation of DLPs shows that VP2 and VP6 can form DLPs when expressed

together in the absence of other proteins. So presumably, VP1 interactions with VP2 are necessary for VP1, VP3, and RNA to be packaged into the newly forming viral particle (49). Research with virus-like particles (VLPs) that packaged VP1 and were replicatively active found that encapsidation did not occur when a VP2 truncation mutant was used to form the VLPs (231). Further analysis found that the N-terminal domain was likely important for VP1 and VP3 encapsidation. This hypothesis was supported by recent work using truncation and chimeric-swap mutants of VP2 to form virus-like particles (VLPs) *in vitro*. Specifically, the N-terminal domain was shown as necessary for VP1 encapsidation, and switching the N-terminal domain to that of a divergent strain did not prevent encapsidation. Since VP1 activation regions are also found in the N-terminus of VP2, it could be that there may be overlap in regions responsible for encapsidation (22).

Progeny virus egress

Progeny DLPs move towards the endoplasmic reticulum (ER) where NSP4 gathers adjacent to viroplasms (161). An affinity for NSP4 by VP6 leads to the particles being shuttled through the ER where NSP4 may help the DLP to gain VP4 and a transient membrane (envelope) (14, 140). As this passage continues, the temporary envelope is lost as VP7 assembles onto the particle, forming the outer shell and completing the nascent TLP (166). Studies using siRNAs against VP7 or depleting calcium in the ER resulted in aggregation of viral particles with envelopes and lacking their outer layers, which supports the model that VP7 dislocates the transient envelope (108). NSP4 provides an alternative possibility in the removal of the transient membrane. It was shown that this viral nonstructural protein destabilizes membranes, so that revelation coupled with the location of NSP4 along the path of the exiting virion make it possible that it may play a role in this process singularly or in conjunction with VP7 (205).

After obtaining VP4 and VP7 in the ER, newly made virions must exit the host cell. *In vitro* studies that utilize non-polarized cell types, RV particles appear to release via cell lysis. However, another study in polarized human intestinal cells found that virions are apically released through a previously unknown method of vesicular transport (5, 93).

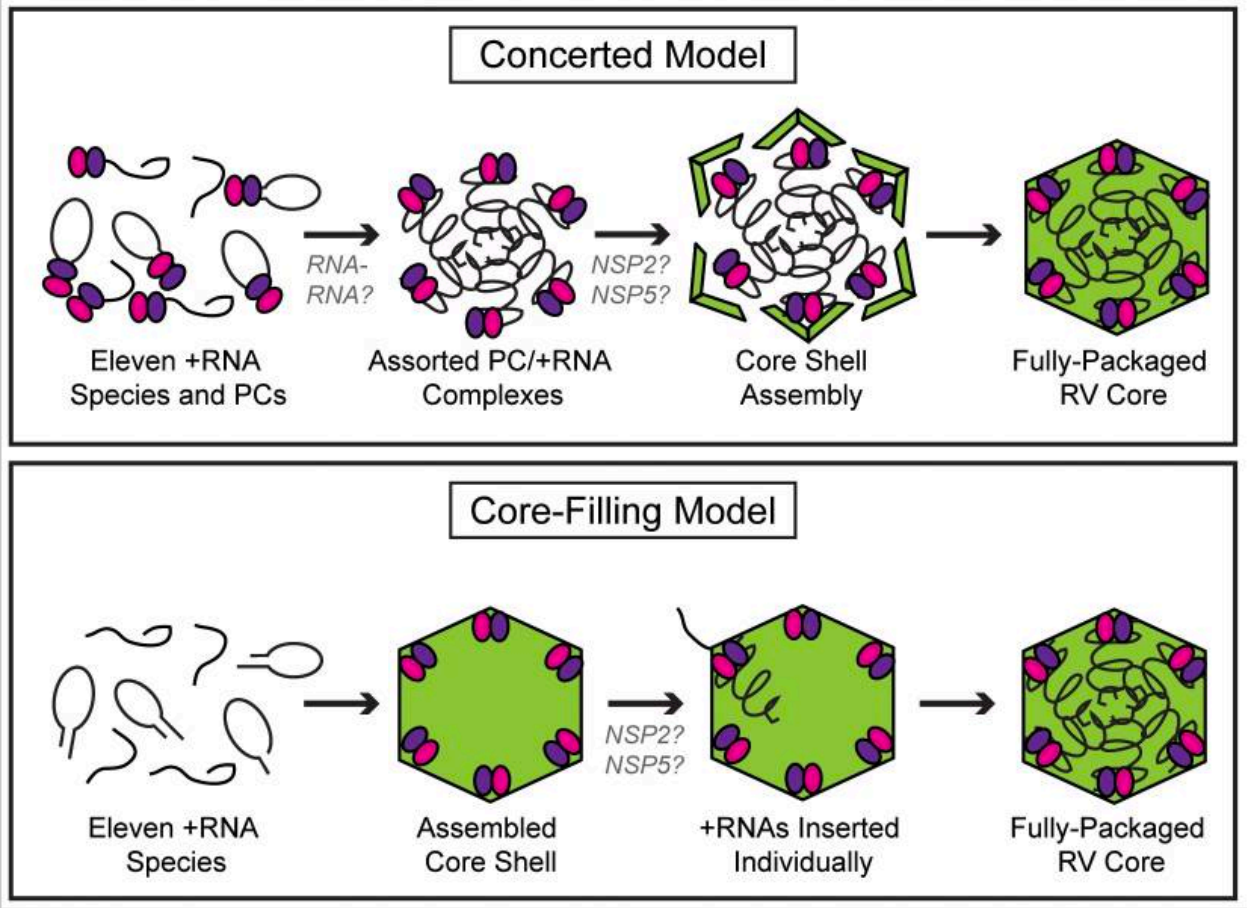

Figure 4-Schematic diagram of RV assortment and packaging models. In the concerted model of RV assortment and packaging (top), RV +RNAs are bound by VP1 and VP3 polymerase complexes (PCs). Specific RNA-RNA interactions allow the +RNA/PCs to assort and 'count to eleven such that one of each genome segment is included. Core capsid protein, VP2 binds to the PCs, leading to an expansion in particle diameter that decreases as the core shell is closed and the +RNAs fully packaged. VP2 activates VP1, and the +RNAs are used as template for –RNA synthesis and dsRNA genome replication. In the core-filling model of RV assortment and packaging (bottom), +RNAs gather near fully assembled core particles that already contain VP1 and VP3. The +RNAs are then sequentially inserted into the core particle, causing an increase in diameter. Once the particle is full, a conformational change is triggered leading to VP2 activation of VP1 and –RNA synthesis. ***This image is from McDonald and Patton, 2011, Trends in Microbiology. and is used with permission from an author (S.M.) and from Elsevier.***

PATHOGENESIS AND DISEASE

Cytopathology and mechanism of diarrhea

The disease manifested by RV infection presents in afflicted individuals as symptoms of severe gastroenteritis, such as diarrhea and vomiting, and research into the molecular biology of those symptoms is ongoing (34). Work in gnotobiotic piglets infected with calf-derived RV found that infection resulted in severe stunting of the microvilli as well as desquamation of cell in the stomach and lungs (79). For humans, within one to two days after infection by RV, villi enterocytes exhibit ischemia and atrophy. These effects and the recovery from them tend to correspond to the waxing and waning of diarrhea (154). These results in humans were also found in gnotobiotic piglets infected with a virulent human RV strain (223). However, the histological lesions present in the small intestine range from nearly no obvious lesions to more major changes like villus blunting (as reviewed in 171). Such damage to the small intestine enterocytes can lead to malabsorption of salts, carbohydrates, fats, proteins, and mucosal disaccharides that lead to these undigested entities landing in the colon. The bulk impedes proper water absorption and leads to osmotically-driven diarrhea (as reviewed in 171). The overall replication of RV likely causes this malabsorption mechanism for diarrhea. Another important mechanism of RV-induced diarrhea is via a secretory pathway that involves the RV nonstructural protein, NSP4. NSP4 important for viral replication, but it also plays a role as a viral enterotoxin (16, 233). NSP4 increases the intracellular calcium in RV infected cells by activating a phospholipase C cascade that releases calcium from the endoplasmic reticulum and induces chloride secretion (56, 145, 206, 207). Increased intracellular calcium leads to disruption of the villi cytoskeleton, impaired sodium transport, and necrosis (as reviewed in 171). Studies have suggested that NSP4 may be secreted from infected cells and bind to uninfected cells, further amplifying the localized effects of rotavirus infection on the intestinal tract (16, 27, 55, 234). This is possibly accomplished through a disruption of epithelial tight-junctions that causes a subsequent cellular leakage (197). Another method for RV-induced diarrhea was found via a study that blocked the enteric nervous system (ENS) using ENS inhibitory drugs on RV-infected mice (111). They found that a significant amount of fluid secretion is due to activation of the ENS (111). ENS activation may be accomplished via secreted NSP4 or other effectors (as reviewed in 171). Another possible role for secreted NSP4 is in causing vomiting via

stimulation of enterochromaffin (EC) cells to release serotonin. A study performed in human cell lines and a mouse model found that recombinant NSP4 and NSP4 from infected cells could lead to elevation of intracellular calcium in EC cells, which are located adjacent to the small intestinal villi (78). This increase in intracellular calcium in turn causes the release of serotonin (5-HT) that can activate vagal afferent nerve fibers that project into the medullary vomiting center of the central nervous system (78).

Innate Immune Response

During natural infection, RV infects the enterocytes of the small intestine villi, which are polarized cells (79). However, *in vitro* studies show that lab-adapted strains will also infect a wide variety of polarized and non-polarized cell types including: MA104, Cos-7, WiDR, Cao-2 cells and others. The tropism of RV is determined by the outer capsid proteins, VP4 and VP7. VP4, VP7, and NSP4 are considered virulence factors (153, 233). When RV particles enter host cells, they deposit transcriptionally active DLPs into the cytoplasm. Transcripts are synthesized within the DLP and are released via pores at the vertices. As they are released, they receive 5' caps (m^7GpppGm) from VP3; however, the capping process is not 100%, leading to both capped and uncapped viral RNAs in the cytoplasm (87). These non-self RNAs can trigger host innate immune responses, including RIG-I and MDA5 (25, 182). A cascade is triggered that ultimately activates type I interferon, which can suppress replication. RV counters this through NSP1 binding of interferon regulatory factors (IRFs) 3, 5, and 7 and targeting these for ubiquitin-driven proteasomal degradation (17, 18, 72). In addition to antagonizing the interferon pathway, RV also hampers the innate immune response through targeted degradation of β-TrCP, an NFκB activator protein. The study that initially demonstrated this method for rotavirus immune-evasion also showed that there may be redundant non-NSP1-related pathways that inhibit NFκB (70). Another method that cells employ to protect themselves from pathogenic threats is the 2'-5'oligoadenylate synthetase (OAS)/RNase L pathway (as reviewed in 188). The recognition of double-stranded RNAs leads to the activation of this pathway and ultimately the release of RNase L, which degrades RNA and inhibits the spread of infection. VP3 possesses a 2'-5'-phosphodiesterase domain on its C-terminus that prevents OAS/RNase activity (150). VP3's role in OAS/RNase L antagonism was confirmed by siRNA experiments (178). Moreover, while

the specific mechanism is not known, the same study found that OAS/RNase L was also inhibited during RV entry.

Adaptive Immune Response

Adaptive immunity to RV remains fairy poorly understood. It is known that once an individual experiences a RV infection, they are much less susceptible to the disease. Indeed, suffering from two infections can impart 100% protection, and this observation is what led to the use of live-attenuated RV vaccines (as reviewed in 7; 215). Much of the work into the development of adaptive immunity to RV has been performed in mouse models using the murine RV strain, EDIM, as a homotypic model or simian RRV as a heterotypic model. One of those heterotypic model studies found that antibody-secreting cells (ASC) secreted IgG, IgM, or IgA. In trying to further characterize the response in the context of VP4, they found that the response to VP4 was mostly IgA-based and in the gut (185). Even though VP4 is important for neutralization, this study also found that the bulk of ASCs were targeting VP2 and VP6 (185). A comprehensive study sought to tease out the nature of the immune response to several RV proteins previously implicated as antigenic. Again, through use of a mouse model, they infected animals with a homologous strain of rotavirus or heterologous one and then measured responses from the blood and feces. They found that responses were widely varied (88). More recently, exciting recent research into the antigenicity of VP6 found that IgAs could intracellularly neutralize RV by binding VP6 (4). The authors proposed that IgAs against VP6 enter the infected cell through transcytosis and bind to VP6 on the outside of DLPS near the transcriptional pores. Thus, these antibodies are able to neutralize infection by preventing transcription (4). In support of the data above, a systematic review of anti-rotavirus IgA found that there appears to be a correlation between serum IgA titers and RV vaccine efficacy with a certain critical level of IgAs needed for sustained protection following vaccination (155).

Since they can be successfully infected with human RV strains and their gastrointestinal physiology is very similar to that of humans, gnotobiotic piglets are also important models for studying RV immunity (as reviewed in 176). For example, work using these models have found that IF-gamma producing T cells may correlate with protective immunity (230). Interestingly, more recent studies using gnotobiotic piglet models have sought to investigate how gut and probiotic bacteria strains contribute to modulation of the immune system (222, 226).

Public Health Implications

Infection by RV leads to severe gastroenteritis that is particularly notable in the young. It typically presents fever accompanied by severe, watery diarrhea that lasts for upwards of a week and may or may not also include vomiting. Resulting dehydration from RV can be quite serious, especially in infants and small children (174). As such, RV is attributed to an estimated 215,000 deaths in those <5 years old globally each year (203). Most of these mortalities are found in areas that do not possess ready access to healthcare, including rehydration therapy for affected patients. In those countries that tend to have lower mortality from RV infections, loss in quality of life for patients and families is still a significant problem (6, 24, 117). In addition to loss of life or quality of life, RV infections pose substantial economic and societal costs (173, 198).

Vaccines

In 1998, a live-attenuated vaccine against RV, RotaShield (Wyeth) was licensed for use in the United States; however, it was pulled from the market due to safety concerns. There was evidence that indicated that infants who received this vaccine were at higher risk for intussusception, albeit at extremely low rates (36-38). Later, in 2006 and 2008, two new RV vaccines were approved and distributed in several countries. Both are orally administered, live-attenuated vaccines: RotaTeq (Merck) and Rotarix (GSK). RotaTeq is a pentavalent vaccine made up of five human-bovine reassortant virus strains that is administered to infants in a three-dose regimen (219). In contrast, Rotarix is a monovalent vaccine that only contains the most widely circulating human RV strain G1P[8] and is given to infants in two doses (175). Despite having fewer strains in it, Rotarix appears to provide cross-protection against multiple RVs. Indeed, a systematic review of available clinical trial data around the world provided evidence suggesting that the strain diversity included in vaccines do not alter their efficacy (214). The authors hypothesized that there could be other factors responsible for the differing efficacies seen between more and less affluent nations. For instance the oral method of vaccine delivery could be affected by factors unique to the respective geographical locations. Additionally, VP4 and VP7 may not be the gene segments that drive vaccine efficacy (29, 214). However, recent work in human intestinal B cells found that antibodies against VP4 and VP7, especially antibodies against VP5*, are likely drivers for heterotypic immunity to RV infections (149). This finding is

important towards better understanding the correlates of protection for RV and could be useful for the development of next-generation RV vaccines.

At first, Rotarix and RotaTeq did not present with any increased risk of intussusception like their predecessor (39, 76, 175, 219). However, further studies have indicated that a very small increased risk of intussusception does still exist amongst all current vaccines in countries across the globe, including in the United States (30, 77). Even though intussusception is an extremely serious adverse reaction, it is so rare that the benefits of avoiding RV infection via vaccination are considered to outweigh any potential risks. Another safety concern for rotavirus vaccines arose when it was found that porcine circovirus-1 (PCV1) DNA was found to contaminate Rotarix vaccine lots (220). This discovery led the United States Food and Drug Administration (FDA) to recommend a suspension of the use of Rotarix and to recommend physicians switch to using RotaTeq, which initially tested negative for PCV1 (100). However, subsequent tests by Merck also found that RotaTeq was likewise contaminated with PCV1 and additionally contained trace amounts of PCV2. The FDA's Vaccines and Related Biological Products Advisory Committee met to determine the risks to human health and found that there was no evidence that indicated PCV1 or PCV2 would cause human disease and that the benefits to vaccination outweighed the risk of not vaccinating (100). Thus, the vaccines were ultimately recommended for use; however, that use is conditional and the products are still monitored for safety.

More recently, these vaccines have also been distributed to many of those countries experiencing higher RV-related mortalities through programs associated with GAVI, the Vaccine Alliance. The projected benefits of this program were 2.46 million fewer pediatric deaths and the prevention of 83 million disability-adjusted life years (12). While the vaccine rollouts have been generally successful in lowering the cases of severe RV infection, the efficacy in areas of greater risk (Latin America, Africa, Southeastern Asia) has been questioned (10, 186). A recent systematic review found that the RV vaccines are quite effective; however, they also found evidence that supported the observation that the vaccines were not as effective in lower- and middle-income countries as compared to high-income countries (92). Some studies have noted that levels of protection may be lower in these regions and could be due to a number of factors, including co-morbidities with other pathogens, poor nutrition, differing gut microbiomes or differences in RV strain circulation amongst other factors (80). Also interesting is the inhibitory

effect breastfeeding can have when done in tandem with oral vaccination, and the factors in breastmilk that inhibit the rotavirus vaccines (lactoferrin, lactadherin, IgA, etc.) are more prevalent in mothers from developing rather than developed nations (144). In addition, limited refrigeration and transport infrastructure makes distribution and storage of live vaccines more costly and difficult (106). Despite these challenges in using live-attenuated vaccines for RV, there is no doubt that they have been successful in reducing the burden of RV-related disease and deaths (28).

SUMMARY

As this literature review captures, RV is an interesting and medically important pathogen that affects the young of most species. While current vaccines have enjoyed significant success, it is still necessary to work towards a better understanding of RV biology. Such research is essential in order to provide information that can be used for the development of novel therapies and next-generation vaccines. And although RV possesses many unique traits as amongst viruses, it remains at its heart an RNA virus. As such, it can ultimately serve as a model for other viral pathogens that do not yet enjoy the plethora of knowledge and tools already available from the decades of work on this virus. Indeed, there is still so much yet to learn from the study of RV, and the research shared below in this dissertation will hopefully help to fill in some of those gaps in knowledge.

REFERENCES

1. **Abdelhakim, A.H., Salgado, E.N., Fu, X., Pasham, M., Nicastro, D., Kirchhausen, T., and Harrison, S.C.** 2014. Structural correlates of rotavirus cell entry. PLoS Pathogens, **10**(9):e1004355.
2. **Afrikanova, I., Fabbretti, E., Miozzo, M.C., and Burrone, O.R.** 1998. Rotavirus NSP5 phosphorylation is up-regulated by interactions with NSP2. Journal of General Virology, **79**:2679-2686.
3. **Afrikanova, I., Miozzo, M.C., Giambiagi, S., and Burrone, O.** 1996. Phosphorylation generates different forms of rotavirus NSP5. Journal of General Virology, **77**:2059-2065.
4. **Aiyegbo, M.S., Sapparapu, G., Spiller, B.W., Eli, I.M., Williams, D.R., Kim, R., Lee, D.E., Liu, T., Li, S., Woods Jr., V.L., Nannemann, D.P., Meiler, J., Stewart, P.L., and Crowe Jr., J.E.** 2013. Human rotavirus VP6-specific antibodies mediate intracellular neutralization by binding to a quaternary structure in the transcriptional pore. PLoS One, **8**(5):e61101.
5. **Altenburg, B.C., Graham, D.Y., and Estes, M.K.** 1980. Ultrastructural study of rotavirus replication in cultured cells. Journal of General Virology, **46**:75-85.
6. **Alvarez Aldeán, J., Aristegui, J., López-Belmonte, J.L., Pedrós, M. and Sicilia, J.G.** 2014. Economic and psychosocial impact of rotavirus infection in Spain: a literature review. Vaccine, **32**:3740-3751.
7. **Angel, J., Franco, M.A., and Greenberg, H.B.** 2012. Rotavirus immune responses and correlates of protection. Current Opinion in Virology, **2**:419-425.
8. **Aponte, C., Poncet, D., and Cohen, J.** 1996. Recovery and characterization of a replicase complex in rotavirus-infected cells by using a monoclonal antibody against NSP2. Journal of Virology, **70**(2):985-991.
9. **Arias, C.F., Silva-Ayala, D., and López, S.** 2015. Rotavirus entry: a deep journey into the cell with several exits. Journal of Virology, **89**(2):890-893.
10. **Armah, G.E., Breiman, R.F., Tapia, M.D., Dallas, M.J., Neuzil, K.M., Binka, F.N., Sow, S.O., Ojwando, J., Ciarlet, M., and Steele, A.D.** Immunogenicity of the pentavalent rotavirus vaccine in African infants. Vaccine, **30**(Suppl 1):A86-93.
11. A**rnoldi, F., Campagna, M., Eichwald, C. Desselberger, U., and Burrone, O.R.** 2007. Interaction of rotavirus polymerase VP1 with nonstructural protein NSP5 is stronger than that with NSP2. Journal of Virology, **81**(5):2128-2137.
12. **Atherly, D.E., Lewis, K.D., Tate, J., Parashar, U.D., and Rheingans, R.D.** 2012. Projected health and economic impact of rotavirus vaccination in GAVI-eligible countries: 2011-2030. Vaccine, **30** (Suppl 1):A7-A14.
13. **Attoui, H., Mertens, P.P.C., Becnel, J., Belaganahalli, S., Bergoin, M., Brussaard, C.P., Chappell, J.D., Ciarlet, M., del Vas, M., Dermody, T.S., Dormitzer, P.R., Duncan, R., Fcang, Q., Graham, R., Guglielmi, K.M., Harding, R.M., Hillman, B., Makkay, A., Marzachì, C., Matthijnssens, J., Milne, R.G., Mohd Jaafar, F., Mori, H., Noordeloos, A.A., Omura, T., Patton, J.T., Rao, S., Maan, M., Stoltz, D., Suzuki, N., Upadhyaya, N.M., Wei, C., and Zhou, H. Reoviridae. In: King, A.M.Q., Adams, M.J., Carstens, E.B., and Lefkowitz, E.J., editors**. Virus Taxonomy: Ninth Report of the International Committee on Taxonomy of Viruses. Elsevier, Academic Press; Amsterdam, Holland: 2012. pp. 541-637.

14. **Au, K.S., Chen, W.K., Burns, J.W., and Estes, M.K.** 1989. Receptor activity of rotavirus nonstructural glycoprotein NS28. Virology, **194**:665-673.
15. **Ayala-Breton, C., Arias, M., Espinosa, R., Romero, P., Arias, C.F., and Lopez, S.** 2009. Analysis of the kinetics of transcription and replication of the rotavirus genome by RNA interference. Journal of Virology, **83**(17):8819-8831.
16. **Ball, J.M., Tian, P., Zeng, C.Q., Morris, A.P., and Estes, M.K.** 1996. Age-dependent diarrhea induced by a rotaviral nonstructural glycoprotein. Science, **272**:101-104.
17. **Barro, M., and Patton, J.T.** 2005. Rotavirus nonstructural protein 1 subverts innate immune response by inducing degradation of IFN regulatory factor 3. PNAS, **102**:4114-4119.
18. **Barro, M. and Patton, J.T.** 2007. Rotavirus NSP1 inhibits expression of type I interferon by antagonizing the function of interferon regulatory factors IRF3, IRF5, and IRF7. Journal of Virology, **81**(9):4473-4481.
19. **Berois, M., Sapin, C., Erk, I., Poncet, D., and Cohen, J.** 2003. Rotavirus nonstructural protein NSP5 interacts with major core protein VP2. Journal of Virology, **77**(3):1757-1763.
20. **Bishop, R.F., Davidson, G.P., Holmes, I.H., and Ruck, B.J.** 1973. Virus particles in epithelial cells of duodenal mucosa from children with acute non-bacterial gastroenteritis. The Lancet, **302**(7841): 1281-1283.
21. **Boudreaux, C.E., Kelly, D.F., and McDonald, S.M.** 2015. Electron microscopic analysis of rotavirus assembly-replication intermediates. Virology, **477**:32-41.
22. **Boudreaux, C.E., Vile, D.C., Gilmore, B.L., Tanner, J.R., Kelly, D.F., and McDonald, S.M.** 2013. Rotavirus core shell subdomains involved in polymerase encapsidation into virus-like particles. Journal of General Virology, **94**(Pt 8):1818-1826.
23. **Boyle, J.F. and Holmes, K.V.** 1986. RNA-binding proteins of bovine rotavirus. Journal of Virology, **58**(2):561-568.
24. **Brisson, M., Sénécal, M., Drolet, M., and Mansi, J.A.** 2010. Health-related quality of life lost to rotavirus-associated gastroenteritis in children and their parents: a Canadian prospective study. Pediatric Infectious Disease Journal, **29**:73-75.
25. **Broquet, A.H., Hirata, Y., McAllister, C.S., and Kagnoff, M.F.** 2011. RIG-I/MDA5/MAVS are required to signal a protective IFN response in rotavirus-infected intestinal epithelium. Journal of Immunology, **186**(3):1618-1626.
26. **Brottier, P., Nandi, P., Bremont, M., and Cohen, J.** 1992. Bovine rotavirus segment 5 protein expressed in the baculovirus system interacts with zinc and RNA. Journal of General Virology, **73**:1931-1938.
27. **Bugarcic, A., and Taylor, J.A.** 2006. Rotavirus nonstructural glycoprotein NSP4 is secreted from the apical surfaces of polarized epithelial cells. Journal of Virology, **80**(24):12343-12349.
28. **Burnett, E., Jonesteller, C.L., Tate, J.E., Yen, C., and Parashar, U.D.** 2017. Global impact of rotavirus vaccination on childhood hospitalizations and mortality from diarrhea. Journal of Infectious Diseases, **215**(11):1666-1672.
29. **Buttery, J.P., and Kirkwood, C.D.** 2014. What can rotavirus vaccines teach us about rotavirus? Lancet Infectious Diseases, **14**(9):786-788.
30. **Buttery, J.P., Standish, J., and Bines, J.E.** 2014. Intussusception and rotavirus vaccines: consensus on benefits outweighing recognized risk. Pediatric Infectious Disease Journal, **33**(7):772-773.

31. **Cabral-Romero, C. and Padilla-Noriega, L.** 2006. Association of rotavirus viroplasms with microtubules through NSP2 and NSP5. Mem. Inst. Oswaldo. Cruz., **101**:603-611.
32. **Campagna, M., Eichwald, C., Vascotto, F., and Burrone, O.R.** 2005. RNA interference of rotavirus segment 11 mRNA reveals the essential role of NSP5 in the virus replicative cycle. Journal of General Virology, **86**(Pt 5):1481-1487.
33. **Carpio, R.V., Gonzalez-Nilo, F.D., Jayaram, H., Spencer, E., Prasad, B.V., Patton, J.T., and Taraporewala, Z.F.** 2004. Role of the histidine triad-like motif in nucleotide hydrolysis by the rotavirus RNA-packaging protein NSP2. Journal of Biological Chemistry, **279**:10624-10633.
34. **Carr, M.E., McKendrick, G.D., and Spyridakis, T.** 1976. The clinical features of infantile gastroenteritis due to rotavirus. Scandinavian Journal of Infectious Diseases, **8**(4):241-243.
35. **Carreño-Torres, J.J., Gutiérrez, M., Arias, C.F., López, S., and Isa, P.** 2010 Characterization of viroplasm formation during the early stages of rotavirus infection. Virology Journal, **7:**350.
36. **Centers for Disease Control and Prevention (CDC).** 1999a. Intussusception among recipients of rotavirus vaccine—United States, 1998-1999. Mobidity Mortaliy Weekly Report, **48**(27):577-581.
37. **Centers for Disease Control and Prevention (CDC).** 1999b. Withdrawal of rotavirus vaccine recommendation. Morbidity Mortality Weekly Report, **48**(43):1007.
38. **Centers for Disease Control and Prevention (CDC).** 2004. Rotavirus vaccine after reports of intussusception—United States, 1999. Morbidity Mortality Weekly Report, **53**(34):786-789.
39. **Centers for Disease Control and Prevention (CDC).** 2007. Postmarketing monitoring of intussusception after RotaTeq vaccination—United States, February 1, 2006-February 15, 2007. Mordbidity Mortality Weekly Report, **56**(10):218-222.
40. **Charpilienne, A., Lepault, J., Rey, F., and Cohen, J.** 2002. Identification of rotavirus VP6 residues located at the interface with VP2 that are essential for capsid assembly and transcriptase activity. Journal of Virology, **76**(15):7822-7831.
41. **Chen, D., Gombold, J.L., and Ramig, R.F.** 1990. Intracellular RNA synthesis directed by temperature-sensitive mutants of simian rotavirus SA11. Virology, **178**:143-151.
42. **Chen, D., Luongo, C.L., Nibert, M.L., and Patton, J.T.** 1999. Rotavirus open cores catalyze 5'-capping and methylation of exogenous RNA: evidence that VP3 is a methyltransferase. Virology, **265**:120-130.
43. **Chen, J.Z., Settembre, E.C., Aoki, S.T., Zhang, X., Bellamy, A.R., Dormitzer, P.R., Harrison, S.C., and Grigorieff, N.** 2009. Molecular interactions in rotavirus assembly and uncoating seen by high-resolution cryo-EM. PNAS, **106**(26):10644-10648.
44. **Cheung, W., Gill, M., Esposito, A., Kaminski, C.F., Courousse, N., Chwetzoff, S., Trugnan, G., Keshavan, N., Lever, A., Desselberger, U.** 2010. Rotaviruses associate with cellular lipid droplet components to replicate in viroplasms, and compounds disrupting or blocking lipid droplets inhibit viroplasm formation and viral replication. Journal of Virology, **84**(13):6782-6798.
45. **Ciarlet, M., and Estes, M.K.** 1999. Human and most animal rotavirus strains do not require the presence of sialic acid on the cell surface for sufficient infectivity. Journal of General Virology, **80**(Pt.4):943-948.

46. **Ciarlet, M., Crawford, S.E., Cheng, E., Blutt, S.E., Rice, D.A., Bergelson, J.M., and Estes, M.K.** 2002. VLA-2 ($\alpha 2\beta 1$) integrin promotes rotavirus entry into cells but is not necessary for rotavirus attachment. Journal of Virology, **76**(3):1109-1123.
47. **Ciarlet, M., Crawford, S.E., and Estes, M.K.** 2001. Differential infection of polarized epithelial cell lines by sialic acid-dependent and sialic acid-independent rotavirus strains. Journal of Virology, **75**(23):11834-11850.
48. **Contin, R., Arnoldi, F., Campagna, M., and Burrone, O.R.** 2010. Rotavirus NSP5 orchestrates recruitment of viroplasmic proteins. Journal of General Virology, **91**:1782-1793.
49. **Crawford, S.E., Labbe, M., Cohen, J., Burroughs, M.H., Zhou, Y.J., and Estes, M.K.** 1994. Characterization of virus-like particles produced by the expression of rotavirus capsid proteins in insect cells. Journal of Virology, **68**:5945-5952.
50. **Crawford, S.E., Mukherjee, S.K., Estes, M.K., Lawton, J.A., Shaw, A.L., Ramig, R.F., and Prasad, B.V.** 2001. Trypsin cleavage stabilizes the rotavirus VP4 spike. Journal of Virology, **75**:6052-6061.
51. **Criglar J.M., Hu, L., Crawford, S.E., Hyser, J.M., Broughman, J.R., Prasad, B.V., and Estes, M.K.** 2014. A novel form of rotavirus NSP2 and phosphorylation-dependent NSP2-NSP5 interactions are associated with viroplasm assembly. Journal of Virology, **88**(2):786-798.
52. **Dennis, A.F., McDonald, S.M., Payne, D.C., Mijatovic-Rustempasic, S., Esona, M.D., Edwards, K.M., Chappell, J.D., and Patton, J.T.** 2014. Molecular epidemiology of contemporary G2P[4] human rotaviruses cocirculating in a single U.S. community: footprints of a globally transitioning genotype. Journal of Virology, **88**(7):3789-3801.
53. **Deo, R.C., Groft, C.M., Rajashankar, K.R., and Burley, S.K.** 2002 Recognition of the rotavirus mRNA 3' consensus by an asymmetric NSP3 homodimer. Cell, **108**(1):71-81.
54. **Díaz-Salinas, M. A., Romero, P., Espinosa, R., Hoshino, Y., Lopez, S., and Arias, C.F.** 2013. The spike protein VP4 defines the endocytic pathway used by rotavirus to enter MA104 cells. Journal of Virology, **87**(3):1658:1663.
55. **Didsbury, A., Wang, C., Verdon, D., Sewell, M.A., McIntosh, J.D., and Taylor, J.A.** 2011. Rotavirus NSP4 is secreted from infected cells as an oligomeric lipoprotein and binds to glycosaminoglycans on the surface of non-infected cells. Virology Journal, **8**:551.
56. **Dong, Y., Zeng, C.Q., Ball, J.M., Estes, M.K., and Morris, A.P.** 1997. The rotavirus enterotoxin NSP4 mobilizes intracellular calcium in human intestinal cells by stimulating phospholipase C-mediated inositol 1,4,5-triphosphate production. PNAS, **94**:3960-3965.
57. **Eichwald, C., Arnoldi, F., Laimbacher, A.S., Schraner, E.M., Fraefel, C., Wild, P., Burrone, O.R., and Ackermann, M.** 2012. Rotavirus viroplasm fusion and perinuclear localization are dynamic processes requiring stabilized microtubules. PLoS One **7**(10):e47947.
58. **Eichwald, C., Rodriguez, J.F., and Burrone, O.R.** 2004. Characterization of rotavirus NSP2/NSP5 interactions and the dynamics of viroplasm formation. Journal of General Virology, **85**:625-634.
59. **Estes, M.K., Graham, D.Y., Gerba, C.P., and Smith, E.M.** 1979. Simian rotavirus SA11 replication in cell cultures. Journal of Virology, **31**(3):810-815.
60. **Estes, M.K., Graham, D.Y., and Mason, B.B.** 1981. Proteolytic enhancement of rotavirus infectivity: molecular mechanisms. Journal of Virology, **39**(3):879-888.

61. **Estrozi, L.F., Settembre, E.C., Goret, G., McClain, B., Zhang, X., Chen, J.Z., Grigorieff, N., Harrison, S.C.** 2013. Location of the dsRNA-dependent polymerase, VP1 in rotavirus particles. Journal of Molecular Biology, **425**(1):124-132.
62. **Fabbretti, E., Afrikanova, I., Vascotto, F., and Burrone, O.R.** 1999. Two non-structural rotavirus proteins, NSP2 and NSP5, form viroplasm-like structures in vivo. Journal of General Virology, **80**:333-339.
63. **Fajardo Jr., T., Sung, P.-Y., and Roy, P.** 2015. Disruption of specific RNA-RNA interactions in a double-stranded RNA virus inhibits genome packaging and virus infectivity. PLoS Pathogens, **11**(12):e1005321.
64. **Flewett, T.H., Bryden, A.S., and Davies, H.** 1973. Virus particles in gastroenteritis (letter). Lancet, **2:**1497.
65. **Flewett, T.H., Bryden, A.S., and Davies, H.** 1974. Relationship between viruses from acute gastroenteritis of children and newborn calves. Lancet, **2**:61-63.
66. **Gallegos, C., and Patton, J.T.** 1989. Characterization of rotavirus replication intermediates: a model for the assembly of single-shelled particles. Virology, **172**(2):616-627.
67. **Gaunt, E.R., Cheung, W., Richards, J.E., Lever, A., and Desselberger, U.** 2013. Inhibition of rotavirus replication by downregulation of fatty acid synthesis. Journal of General Virology, **94**:1310-1317.
68. **Gombold, J.L, and Ramig, R.F.** 1987. Assignment of simian rotavirus SA11 temperature-sensitive mutant groups A, C, F, and G to genome segments. Virology, **161**:463-473.
69. **Gonzáles, S.A. and Burrone, O.R.** 1991. Rotaivurs NS26 is modified by addition of single O-linked residues of N-acetylglucosamine. Virology, **182**:8-16.
70. **Graff, J.W., Ettayebi, K., and Hardy, M.E.** 2009. Rotavirus NSP1 inihibits NFκB activation by inducing proteasome-dependent degradation of β-TrCP: a novel mechanism of IFN antagonism. PLoS Pathogens, **5**(1):e1000280.
71. **Graff, J.W., Ewen, J., Ettayebi, K., and Hardy, M.E.** 2007. Zinc-binding domain of rotavirus NSP1 is required for proteasome-dependent degradation of IRF3 and autoregulatory NSP1 stability. Journal of General Virology, **88**(Pt 2):613-620.
72. **Graff, J.W., Mitzel, D.N., Weisend, C.M., Flenniken, M.L., and Hardy, M.E.** 2002. Interferon regulatory factor 3 is a cellular partner of rotavirus NSP1. Journal of Virology, **76**(18):945-950.
73. **Gratia, M., Sarot, E., Vende, P., Charpilienne, A., Baron, C.H., Duarte, M., Pyronnet, S., and Didier, P.** 2015. Rotavirus NSP3 is a translational surrogate of the poly(A) binding protein-poly(a) complex. Journal of Virology, 89(17):8773-8782.
74. **Guerrero, C.A., Bouyssounade, D., Zarate, S., Isa, P., Lopez, T., Espinosa, R., Romero, P., Mendez, E., Lopez, S., and Arias, C.F.** 2002. Heat shock cognate protein 70 is involved in rotavirus cell entry. Journal of Virology, **76**:4096-4102.
75. **Gutiérrez, M., Isa, P., Sánchez-San Martin, C., Pérez-Vargas, J., Espinosa, R., Arias, C.F., and Lopez, S.** 2010. Different rotavirus strains enter MA104 cells through different endocytic pathways: the role of clathrin-mediated endocytosis. Journal of Virology, **84**(18):9161-9169.
76. **Haber, P., Patel, M., Izurieta, H.S., Baggs, J., Gargiullo, P., Weintraub, E., Cortese, M., Braun, M.M., Belongia, E.A., Miller, E., Ball, R., Iskander, J., and Parashar,**

U.D. 2008. Postlicensure monitoring of intussusception after RotaTeq vaccination in the United States, February 1, 2006, to September 25, 2007. Pediatrics, **121**(6):1206-1212.
77. **Haber, P., Patel, M., Pan, Y., Baggs, J., Haber, M., Museru, O., Yue, X., Lewis, P., Destefano, F., and Parashar, U.D.** 2013. Intussusception after rotavirus vaccines reported to US VAERS, 2006-2012. Pediatrics, **131**(6):1042-1049.
78. **Hagbom, M., Istrate, C., Engblom, D., Karlsson, T., Rodriguez-Diaz, J., Buesa, J., Taylor, J.A., Loitto, V.-M., Magnusson, K.-E., Ahlman, H., Lundgren, O., and Svensson, L.** 2011. Rotavirus stimulates release of serotonin (5-HT) from human enterochromaffin cells and activates brain structures involved in nausea and vomiting. PLoS Pathogens, **7**(7):e1002115.
79. **Hall, G.A., Bridger, J.C., Chandler, R.L., and Woode, G.N.** 1976. Gnotobiotic piglets experimentally infected with neonatal calf diarrhea reovirus-like agent (Rotavirus). Veterinary Pathology, **13**(3):197-210.
80. **Harris, V.C., Armah, G., Fuentes, S., Korpela, K.E., Parashar, U., Victor, J.C., Tate, J., de Weerth, C., Giaquinto, C., Wiersinga. W.J., Lewis, K.D., and de Vos, W.M.** 2017. Significant correlation between the infant gut microbiome and rotavirus vaccine response in rural Ghana. Journal of Infectious Diseases, **215**(1):34-41.
81. **Holmes, I.H., Ruck, B.J., Bishop, R.F., and Davidson, G.P.** 1975. Infantile Enteritis Virus: morphogenesis and morphology. Journal of Virology, **16**(4):937-943.
82. **Hu, L., Crawford, S.E., Czako, R., Cortes-Penfield, N.W., Smith, D.F., Le Pendu, J., Estes, M.K., and Prasad, B.V.V.** 2012. Cell attachment protein VP8* of a human rotavirus specifically interacts with A-type histo-blood group antigen. Nature, **485**(7397):256-259.
83. **Hua, J., Chen, X., and Patton, J.T.** 1994. Deletion mapping of the rotavirus metalloproteinNS53 (NSP1): the conserved cysteine-rich region is essential for virus-specific RNA binding. Journal of Virology, **68**(6):3990-4000.
84. **Hua, J., Mansell, E.A., and Patton, J.T.** 1993. Comparative analysis of the rotavirus NS53 gene: conservation of basic and cysteine-rich regions in the protein and possible stem-loop structures in the RNA. Virology, **196**(1):372-378.
85. **Hua, J. and Patton, J.T.** 1994. The carboxyl-half of the rotavirus nonstructural protein NS53 (NSP1) is not required for virus replication. Virology, **198**(2):567-576.
86. **Hyser, J.M., Collinson-Pautz, M.R., Utama, B., and Estes, M.K.** 2010. Rotavirus disrupts calcium homeostasis by NSP4 viroporin activity. mBio, **1**(5):e00265-10.
87. **Imai, M., Akatani, K., Ikegami, N., and Furuchi, Y.** 1983. Capped and conserved terminal structures in human rotavirus genome double-stranded RNA segments. Journal of Virology, **47**(1):125-136.
88. **Ishida, S.I., Feng, N., Gilbert, J.M., Tang, B., and Greenberg, H.B.** 1997. Immune response to individual rotavirus proteins following heterologous and homologous rotavirus infection in mice. Journal of Infectious Diseases, **175**(6):1317-1323.
89. **Jayaram, H., Taraporewala, Z., Patton, J.T., and Prasad, B.V.** 2002. Rotavirus protein involved in genome replication and packaging exhibits a HIT-like fold. Nature, **417**:311-315.
90. **Jiang, X., Jayaram, H., Kumar, M., Ludtke, S.J., Estes, M.K., Prasad, B.V.V.** 2006. Cryoelectron microscopy structures of rotavirus NSP2-NSP5 and NSP2-RNA complexes: implications for genome replication. Journal of Virology, **80**(21):10829-10835.

91. **Jiang, X., Liu, Y., and Tan, M.** 2017. Histo-blood group antigens as receptors for rotavirus, new understanding on rotavirus epidemiology and vaccine strategy. Emerging Microbes & Infection, **6**(4):e22.
92. **Jonesteller, C.L., Burnett, E., Yen, C., Tate, J.E., and Parashar, U.D.** 2017. Effectiveness of rotavirus vaccination: a systematic review of the first decade of global post-licensure data, 2006-2016. Clinical Infectious Diseases, Epub ahead of print.
93. **Jourdan, N., Maurice, M., Delautier, D.** 1997. Rotavirus is released from the apical surface of cultured human intestinal cells through nonconventional vesicular transport that bypasses the Golgi apparatus. Journal of Virology, **71**:8268-8278.
94. **Kalica, A.R., Flores, J., and Greenberg, H.B.** 1983. Identification of the rotaviral gene that codes for hemagglutination and protease-enhanced plaque formation. Virology, **125**(1):194-205.
95. **Kaljot, K.T., Shaw, R.D., Rubin, D.H., and Greenberg, H.B.** 1988. Infectious rotavirus enters cells by direct cell membrane penetration, not by endocytosis. Journal of Virology, **62**:1136-1144.
96. **Kapikian, A.Z., Wyatt, R.G., and Levine, M.M.** 1983. Oral administration of human rotavirus to volunteers: induction of illness and correlates of resistance. Journal of Infectious Diseases, **147**:95-106.
97. **Kattoura, M.D., Chen, X., and Patton, J.T.** 1994. The rotavirus RNA-binding protein NS35 (NSP2) forms 10S multimers and interacts with the viral RNA polymerase. Virology, **202**(2):803-813.
98. **Kattoura, M.D., Clapp, L.L., and Patton, J.T.** 1992. The rotavirus nonstructural protein, NS35, possesses RNA-binding activity *in vitro* and *in vivo*. Virology, **191**(2):698-708.
99. **Kitaoka, S., Nakagomi, T., Fukuhara, N., Hoshino, Y., Suzuki, H., Nakagomi, O., Kapikian, A.Z., Ebina, T., Konno, T., and Ishida, N.** 1987. Serologic characteristics of a human rotavirus isolate, AU-1, which has a "long" RNA pattern and subgroup I specificity. Journal of Medical Virology, **23**(4):351-357.
100. **Kuehn, B.M.** 2010. FDA: Benefits of rotavirus vaccination outweigh potential contamination risk. Journal of the American Medical Association, **304**(1):30-31.
101. **Kumar, M., Jayaram, H., Vasquez-Del Carpio, R., Jiang, X., Taraporewala, Z.F., Jacobson, R.H., Patton, J.T., and Prasad, B.V.** 2007. Crystallographic and biochemical analysis of rotavirus NSP2 reveals a nucleoside diphosphate kinase-like activity. Journal of Virology, **81**(22):12272-12284.
102. **Labbé, M., Baudoux, P., Charpilienne, A., Poncet, D., and Cohen, J.** 1994. Identification of the nucleic acid binding domain of the rotavirus VP2 protein. Journal of General Virology, **75**:3423-3430.
103. **Labbé, M., Charpilienne, A., Crawford, S.E., Estes, M.K., and Cohen, J.** 1991. Expression of rotavirus VP2 produces empty corelike particles. Journal of Virology, **65**(6):2946-2952.
104. **Lawton, J.A., Estes, M.K., and Prasad, B.V.** 1997a. Three-dimensional visualization of mRNA release from actively transcribing rotavirus particles. Nature Structural Biology, **4**:118-121.
105. **Lawton, J.A., Zeng, C.Q.Y., Mukherjee, S.K., Cohen, J., Estes, M.K., and Prasad B.V.V.** 1997b. Three-dimensional structural analysis of recombinant rotavirus-like

particles with intact and amino-terminal deleted VP2: implications for the architecture of the VP2 capsid layer. Journal of Virology, **71**:7353-7360.
106. **Lee, B.Y., Wedlock, P.T., Haidari, L.A., Elder, K., Potet, J., Manning, R., Connor, D.L., Spiker, M.L., Bonner, K., and Rangarajan, A.** 2017. Economic impact of thermostable vaccines. Vaccine, **35**(23):3135-3142.
107. **Liu, M., Mattion, N.M., and Estes, M.K.** 1992. Rotavirus VP3 expressed in insect cells possesses guanylyltransferase activity. Virology, **188**(1):77-84.
108. **López, T., Camacho, M., Zayas, M., Nájera, R., Sánchez, R., Arias, C.F., and López, S.** 2005a. Silencing the morphogenesis of rotavirus. Journal of Virology, **79**(1):184-192.
109. **López, T., Rojas, M., Ayala-Bretón, C., López, S., and Arias, C.F.** 2005b. Reduced expression of the rotavirus NSP5 gene has a pleiotropic effect on virus replication. Journal of General Virology, **86**:1609-1617.
110. **Lu, X., McDonald, S.M., Tortorici, M.A., Tao, Y.J., Vasquez-Del Carpio, R., Nibert, M.L., Patton, J.T., and Harrison, S.C.** 2008. Mechanism for coordinated RNA packaging and genome replication by rotavirus polymerase VP1. Structure, **16**:1676-1688.
111. **Lundgren, O., Peregrin, A.T., Persson, K., Kordasti, S., Uhnoo, I., and Svensson, L.** 2000. Role of the enteric nervous system in the fluid and electrolyte secretion of rotavirus diarrhea. Science, **287**(5452):491-495.
112. **Mackow, E.R., Shaw, R.D., Matsui, S.M., Vo, P.T., Benfield, D.A., and Greenberg, H.B.** 1988a. Characterization of homotypic and heterotypic VP7 neutralization sites of rhesus rotavirus. Virology, **165**(2):511-517.
113. **Mackow, E.R., Shaw, R.D., Matsul, S.M., Vo, P.T., Dang, M.N., and Greenberg, H.B.** 1988b. The rhesus rotavirus gene encoding protein VP3: location of amino acids involved in homologous and heterologous rotavirus neutralization and identification of a putative fusion region. PNAS, **85**(3):645-649.
114. **Malherbe, H.H. and Strickland-Cholmley, M.** 1967. Simian virus S.A. 11 and the related O agent. Archiv für die gesampte Virusforschung, **22**:235-245.
115. **Mansell, E.A. and Patton, J.T.** 1990. Rotavirus RNA replication: VP2, but not VP6, is necessary for viral replicase activity. Journal of Virology, **64**(10):4988-4996.
116. **Mansell, E.A., Ramig, R.F., and Patton, J.T.** 1994. Temperature-sensitive lesions in the capsid proteins of the rotavirus mutants tsF and tsG that affect virion assembly. Virology, **204**(1):69-81.
117. **Marlow, R., Finn, A., and Trotter, C.** 2015. Quality of life impacts from rotavirus gastroenteritis on children and their families in the UK. Vaccine, **33**(39): 5212-5216.
118. **Martella, V., Bányai, K., Matthijnssens, J., Buonavoglia, C., and Ciarlet, M.** 2010. Zoonotic aspects of rotaviruses. Veterinary Microbiology, **140** (3-4):246-255.
119. **Martin, D., Charpilienne, A., Parent, A., Boussac, A., D'Autreaux, B., Poupon, J., and Poncet, D.** 2017. The rotavirus nonstructural protein NSP5 coordinates a [2Fe-2S] iron-sulfur cluster that modulates interaction to RNA. FASEB Journal, **27**(3):1074-1083.
120. **Martin, D., Duarte, M., Lepault, J., and Poncet, D.** 2010. Sequestration of free tubulin molecules by the viral protein NSP2 induces microtubules depolymerization during rotavirus infection. Journal of Virology, **84**(5):2522-2532.
121. **Martin, D., Ouldali, M., Ménétrey, J., and Poncet, D.** 2011. Structural organization of the rotavirus nonstructural protein NSP5. Journal of Molecular Biology, **413**:209-221.

122. **Mason, B.B., Graham, D.Y., and Estes, M.K.** 1983. Biochemical mapping of the simian rotavirus SA11 genome. Journal of Virology, **46**(2):413-423.
123. **Mathieu, M., Petitpas, I., Navaza, J., Lepault, J., Kohli, E., Pothier, P., Prasad, B.V.V., Cohen, J., and Rey, F.A.** 2001. Atomic structure of the major capsid protein of rotavirus: implications for the architecture of the virion. EMBO Journal, **20**(7):1485-1497.
124. **Matsuno, S. and Nakajima, K.** 1982. RNA of rotavirus: comparison of RNAs of human and animal rotaviruses. Journal of Virology, **41**(2):710-714.
125. **Matthijnssens, J., Ciarlet, M., Heiman, E., Arijs, I., Delbeke, T., McDonald, S.M., Palombo, E.A., Iturriza-Gómara, M., Maes, P., Patton, J.P., Rahman, M., and Van Ranst, M.** 2008. Full genome-based classification of rotaviruses reveals a common origin between human Wa-like and porcine rotavirus strains and human DS-1-like and bovine rotavirus strains. Journal of Virology, **82**(7):3204-3219.
126. **Matthijnssens, J., Ciarlet, M., McDonald, S.M., Attoui, H., Bányai, K., Brister, J.R., Buesa, J., Esona, M.D., Estes, M.K., Gentsch, J.R., Iturriza-Gómara, M., Johne, R., Kirkwood, C.D., Martella, V., Mertens, P.P., Nakagomi, O., Parreño, V., Rahman, M., Ruggeri, F.M., Saif, L.J., Santos, N., Steyer, A., Taniguchi, K., Patton, J.T., Desselberger, U., and Van Ranst, M.** 2011. Uniformity of rotavirus strain nomenclature proposed by the Rotavirus Classification Working Group (RCWG). Arch Virology, **156**(8):1397-1413.
127. **Matthijnssens, J., Otto, P.H., Ciarlet, M., Desselberger, U., Van Ranst, M., and Johne, R.** 2012. VP6-sequence-based cutoff values as a criterion for rotavirus species demarcation. Archives of Virology, **157**:1177-1182.
128. **Matthijnssens, J., Taraporewala, Z.F., Yang, H., Rao, S., Yuan, L., Cao, D., Hoshino, Y., Mertens, P.P., Carner, G.R., McNeal, M., Sestak, K., Van Ranst, M., and Patton, J.T.** 2010. Simian rotaviruses possess divergent gene constellations that originated from interspecies transmission and reassortment. Journal of Virology, **84**(4):2013-2026.
129. **Mattion, N.M., Cohen, J., Aponte, C., Estes, M.K.** 1992. Characterization of an oligomerization domain and RNA-binding properties on rotavirus nonstructural protein NS34. Virology, **190**(1):68-83.
130. **Mattion, N.M., Mitchell, D.B., Both, G.W., and Estes, M.K.** 1991. Expression of rotavirus proteins encoded by alternative open reading frames of genome segment 11. Virology, **181**:295-304.
131. **McClain, B., Settembre, E., Temple, B.R., Bellamy, A.R., and Harrison S.C.** 2010. X-ray crystal structure of the rotavirus inner capsid particle at 3.8 Å resolution. Journal of Molecular Biology, **397**:587-599.
132. **McDonald, S.M.** 2013. RNA synthetic mechanisms employed by diverse families of RNA viruses. WIREs RNA, **4**:351-367.
133. **McDonald, S.M., Aguayo, D., Gonzalez-Nilo, F.D., and Patton, J.T.** 2009. Shared and group-specific features of the rotavirus RNA polymerase reveal potential determinants of gene reassortment. Journal of Virology, **83**:6135-6148.
134. **McDonald, S.M., McKell, A.O., Rippinger, C.M., McAllen, J.K., Akopov, A., Kirkness, E.F., Payne, D.C., Edwards, K.M., Chappell, J.D., and Patton, J.T.** 2012. Diversity and relationships of cocirculating modern human rotaviruses revealed using large-scale comparative genomics. Journal of Virology, **86**(17):9148-9162.

135. **McDonald, S.M., Nelson, M.I., Turner, P.E., and Patton, J.T.** 2016. Reassortment in segmented RNA viruses: mechanisms and outcomes. Nature Reviews Microbiology, **14**(7):448-460.
136. **McDonald, S.M., and Patton, J.T.** 2011a. Assortment and packaging of the segmented rotavirus genome. Trends in Microbiology, **19**(3):136-144.
137. **McDonald, S.M. and Patton, J.T.** 2011b. Rotavirus VP2 core shell regions critical for viral polymerase activation. Journal of Virology, **85**:3095-3105.
138. **McKell, A.O., LaConte, L.E., and McDonald, S.M.** 2017. Temperature-sensitive lesion in the n-terminal domain or the rotavirus polymerase affects its intracellular localization and enzymatic activity. Journal of Virology, **91**(7):e00062-17.
139. **McKell, A.O., Nichols, J.C., and McDonald, S.M.** 2013. PCR-based approach to distinguish group A human rotavirus genotype 1 vs. genotype 2 genes. Journal of Virological Methods, **194**(1-2):197-205.
140. **Meyer, J.C., Bergmann, C.C., and Bellamy, A.R.** 1989. Interaction of rotavirus cores with the nonstructural glycoprotein NS28. Virology, **171**:98-107.
141. **Mitchell, D.B. and Both, G.W.** 1990a. Completion of the genomic sequence of the simian rotavirus SA11: nucleotide sequences of segments 1, 2, and 3. Virology, **177**:324-331.
142. **Mitchell, D.B. and Both, G.W.** 1990b. Conservation of a potential metal binding motif despite extensive sequence diversity in the rotavirus nonstructural protein NS53. Virology, **174**(2):618-621.
143. **Montero, H., Arias, C.F., and Lopez, S.** 2006. Rotavirus nonstructural protein NSP3 is not required for viral protein synthesis. Journal of Virology, **80**(18):9031-9038.
144. **Moon, S.S., Tate, J.E., Ray, P., Dennehy, P.H., Archary, D., Coutsoudis, A., Bland, R., Newell, M.L., Glass, R.I., Parashar, U., and Jiang, B.** Differential profiles and inhibitory effect on rotavirus vaccines of nonantibody components in breast milk from mothers in developing and developed countries. Pediatric Infectious Disease Journal, **32**(8):863-870.
145. **Morris, A.P., Scott, J.K., Ball, J.M., Zeng, C.Q., O'Neal, W.K., and Estes, M.K.** 1999. NSP4 elicits age-dependent diarrhea and Ca(2+)mediated I(-)influx into intestinal crypts of CF mice. American Journal of Physiology, **277**(2 Pt 1):G431-444.
146. **Nakagomi, O., Kaga, E., Gerna, G., Sarasini, A., and Nakagomi, T.** 1992. Subgroup I serotype 3 human rotavirus strains with long RNA patterns as a result of naturally occurring reassortment between members of the bovine and AU-1 genogroups. Archives of Virology, **126**(1-4):337-342.
147. **Nakagomi, O., Nakagomi, T., Hoshino, Y., Flores, J., and Kapikian, A.Z.** 1987. Genetic analysis of a human rotavirus that belongs to subgroup I but has an RNA pattern typical of subgroup II human rotaviruses. Journal of Clinical Microbiology, **25**(7):1159-1164.
148. **Nakagomi, T. and Nakagomi, O.** 1989. RNA-RNA hybridization identifies a human rotavirus that is genetically related to feline rotavirus. Journal of Virology, **63**(3):1431-1434.
149. **Nair, N., Feng, N., Blum, L.K., Sanyal, M., Ding, S., Jiang, B., Sen, A., Morton, J.M., He, X.S., Robinson, W.H., and Greenberg, H.B.** VP4- and VP7-specific antibodies mediate heterotypic immunity to rotavirus in humans. Science Translational Medicine, **9**(395):eaam5435.

150. **Ogden, K.M., Hu, L., Jha, B.K., Sankaran, B., Weiss, S.R., Silverman, R.H., Patton, J.T., and Prasad, B.V.V.** 2015. Structural basis for 2'-5'-oligoadenylate binding and enzyme activity of a viral RNase L antagonist. Journal of Virology, **89**(13):6633-6645.
151. **Ogden, K.M., Ramanathan, H.N., and Patton, J.T.** 2011. Residues of the rotavirus RNA-dependent RNA polymerase template entry tunnel that mediate RNA recognition and genome replication. Journal of Virology, **85**(5):1958-1969.
152. **Ogden, K.M., Snyder, M.J., Dennis, A.F., and Patton, J.T.** 2014. Predicted structure and domain organization of rotavirus capping enzyme and innate immune antagonist VP3. Journal of Virology, **88**(16):9072-9085.
153. **Offit, P.A., Shaw, R.D., and Greenberg, H.B.** 1986. Passive protection against rotavirus-induced diarrhea by monoclonal antibodies to surface proteins VP3 and VP7. Journal of Virology, **58**(2):700-703.
154. **Osbourne, M.P., Haddon, S.J., Worton, K.J., Spencer, A.J., Starkey, W.G., Thornber, D., and Stephen, J.** 1991. Rotavirus-induced changes in the microcirculation of intestinal villi of neonatal mice in relation to the induction and persistence of diarrhea. Journal of Pediatric Gastroenterology and Nutrition, **12**(1):111-120.
155. **Patel, M., Glass, R.I., Jiang, B., Santosham, M., Lopman, B., and Parashar, U.** 2013. A systematic review of anti-rotavirus serum IgA antibody titer as a potential correlate of rotavirus vaccine efficacy. Journal of Infectious Diseases, **208**(2):284-294.
156. **Patton, J.T.** 1990. Evidence for equimolar synthesis of double-stranded RNA and minus-strand RNA in rotavirus-infected cells. Virus Research, **17**:199-208.
157. **Patton, J.T.** 1996. Rotavirus VP1 alone specifically binds to the 3' end of viral mRNA, but the interaction is not sufficient to initiate minus-strand synthesis. Journal of Virology, **70**:7940-7947.
158. **Patton, J.T. and Chen, D.** 1999. RNA-binding and capping activities of proteins in rotavirus open cores. Journal of Virology, **73**(2):1382-1391.
159. **Patton, J.T. and Gallegos, C.** 1990. Rotavirus RNA replication: single-stranded RNA extends from the replicase particle. Journal of General Virology, **71**(Pt 5):1087-1094.
160. **Patton, J.T., Jones, M.T., Kalbach, A.N., He, Y.W., and Xiaobo, J.** 1997. Rotavirus RNA polymerase requires the core shell protein to synthesize the double-stranded RNA genome. Journal of Virology, **71**:9618-9626.
161. **Petrie, B.L., Greenberg, H.B., Graham, D.Y., and Estes, M.K.** 1984. Ultrastructural localization of rotavirus antigens using colloidal gold. Virus Research, **1**:133-152.
162. **Piron, M., Delaunay, T., Grosclaude, J., and Poncet, D.** 1999. Identification of the RNA-binding, dimerization, and eIF4GI-binding domains of rotavirus nonstructural protein NSP3. Journal of Virology, **73**(7):5411-5421.
163. **Piron, M., Vende, P., Cohen, J., and Poncet, D.** 1998. Rotavirus RNA-binding protein NSP3 interacts with eIF4GI and evicts the poly(A) binding protein from eIF4F. EMBO Journal, **17**(19):5811-5821.
164. **Poncet, D., Aponte, C., and Cohen, J.** 1993. Rotavirus protein NSP3 (NS34) is bound to the 3' end consensus sequence of viral mRNAs in infected cells. Journal of Virology, **67**(6):3159-3165.
165. **Poncet, D., Lindenbaum, P., Haridon, R.L., and Cohen, J.** 1997. *In vivo* and *in vitro* phosphorylation of rotavirus NSP5 correlates with its localization in viroplasms. Journal of Virology, **71**:34-41.

166. **Poruchynsky, M.S., Maass, D.R., and Atkinson, P.H.** 1991. Calcium depletion blocks the maturation of rotavirus by altering the oligomerization of virus-encoded proteins in the ER. Journal of Cell Biology, **114**:651-656.
167. **Prasad, B.V., Burns, J.W., Marietta, E., Estes, M.K., and Chiu, W.** 1990. Localization of VP4 neutralization sites in rotavirus by three-dimensional cryo-electron microscopy. Nature, **343**(6257):476-479.
168. **Prasad, B.V., Rothnagel, R., Zeng, C.Q., Jakana, J., Lawton, J.A., Chiu, W., and Estes, M.K.** 1996. Visualization of ordered genomic RNA and localization of transcriptional complexes in rotavirus. Nature, **382**(6590):471-473.
169. **Prasad, B.V., Wang, G.J., Clerx, J.P., and Chiu, W.** 1988. Three-dimensional structure of rotavirus. Journal of Molecular Biology, **199**(2):269-275.
170. **Ramani, S., Hu, L., Prasad, B.V.V., and Estes, M.K.** 2016. Diversity in rotavirus-host glycan interactions: A "sweet" spectrum. Cellular and Molecular Gastroenterology and Hepatology, **2**(3):263-273.
171. **Ramig, R.F.** 2004. Pathogenesis of intestinal and systemic rotavirus infection. Journal of Virology, **78**(19):10213-10220.
172. **Ramig, R.F. and Petrie, B.L.** 1984. Characterization of temperature-sensitive mutants of simian rotavirus SA11: protein synthesis and morphogenesis. Journal of Virology, **49**:665-673.
173. **Rheingans, R.D., Antil, L., Dreibelbis, R., Podewils, L.J., Bresee, J.S., Parashar, U.D.** 2009. Economic costs of rotavirus gastroenteritis and cost-effectiveness of vaccines in developing countries. Journal of Infectious Diseases, **200** (Suppl 1):S16-27.
174. **Rodriguez, W.J., Kim, H.W., Arrobio, J.O.** 1977. Clinical features of acute gastroenteritis associated with human reovirus-like agent in infants and young children. Journal of Pediatrics, **91**:188-193.
175. **Ruiz-Palacios, G.M., Pérez-Schael, I., Velázquez, F.R., Abate, H., Breuer, T., Clemens, S.C., Cheuvart, B., Espinoza, F., Gillard, P., Innis, B.L., Cervantes, Y., Linhares, A.C., López, P., Macías-Parra, M., Ortega-Barría, E., Richardson, V., Rivera-Medina, D.M., Rivera, L., Salinas, B., Pavía-Ruz, N., Salmerón, J., Rüttimann, R., Tinoco, R.F., Vesikari, T., Bouckenooghe, A., Clemens, R., De Vos, B., O'Ryan, M.; Human Rotavirus Vaccine Study Group.** 2006. Safety and efficacy of an attenuated vaccine against severe rotavirus gastroenteritis. New England Journal of Medicine, **354**(1):11-22.
176. **Saif, L.J., Ward, L.A., Yuan, L., Rosen, B.I., and To, T.L.** 1996. The gnotobiotic piglet as a model for studies of disease pathogenesis and immunity to human rotaviruses. Archives of Virology, **12** (Suppl):153-61.
177. **Sánchez-San Martín, C., López, T., Arias, C.F., and López, S.** 2004. Characterization of rotavirus cell entry. Journal of Virology, **78**(5):2310-2318.
178. **Sánchez-Tacuba, L., Rojas, M., Arias, C.F., and López, S.** 2015. Rotavirus controls activation of the 2'-5'oligoadenylate synthetase/RNase L pathway using at least two distinct mechanisms. Journal of Virology, **89**(23):12145-12153.
179. **Sandrino, A.M., Jashes, M., Faúndez, G., and Spencer, E.** 1986. Role of the inner protein capsid on in vitro human rotavirus transcription. Journal of Virology, **60**(2):797-802.
180. **Schnagl, R.D. and Holmes, I.H.** 1976. Characteristics of the genome of Human Infantile Enteritis Virus (Rotavirus). Journal of Virology, **19**(1):267-270.

181. **Schroeder, B.A., Street, J.E., Kalmakoff, J., and Bellamy, A.R.** 1982. Sequence relationships between the genome segments of human and animal rotavirus strains. Journal of Virology, **43**(2):379-385.
182. **Sen, A., Pruijssers, A.J., Dermody, T.S., Garcia-Sastre, A., and Greenberg, H. B.** 2011. The early interferon response to rotavirus is regulated by PKR and depends on MAVS/IPS-1, RIG-I, MDA-5, and IRF3. Journal of Virology, **85**:37137-3732.
183. **Sen, A., Sen, N., and Mackow, E.R.** 2007. The formation of viroplasm-like structures by the rotavirus NSP5 protein is calcium regulated and directed by a c-terminal helical domain. Journal of Virology, **81**(21):11758-11767.
184. **Settembre E.C., Chen, J.Z., Dormitzer, P.R., Grigorieff, N., and Harrison, S.C.** Atomic model of an infectious rotavirus particle. EMBO Journal, **30**(2):408-416.
185. **Shaw, R.D., Groene, W.S., Mackow, E.R., Merchant, A.A., and Cheng, E.H.** 1991. VP4-specific intestinal antibody response to rotavirus in a murine model of heterotypic infection. Journal of Virology, **65**(6):3052-3059.
186. **Shin, S., Anh, D.D., Zaman, K., Yunus, M., Mai le, T.P., Thiem, V.D., Azim, T., Victor, J.C., Dallas, M.J., Steele, A.D., Neuzil, K.M., and Ciarlet, M.** Immunogenicity of the pentavalent rotavirus vaccine among infants in two developing countries in Asia, Bangladesh and Vietnam. Vaccine, **30**(Suppl 1):A106-113.
187. **Silva, F.D., Gregori, F., and McDonald S.M.** 2016. Distinguishing the genotype 1 genes and proteins of human Wa-like rotaviruses vs. porcine rotaviruses. Infection, Genetics, and Evolution, **43**:6-14.
188. **Silverman, R.H.** 2007. Viral encounters with 2', 5'-oligoadenylate synthetase and RNase L during the interferon antiviral response. Journal of Virology, **81**:12720-12729.
189. **Silvestri, L.S., Taraporewala, Z.F., and Patton, J.T.** 2004. Rotavirus replication: plus-sense templates for double-stranded RNA synthesis are made in viroplasms. Journal of Virology, **78**:7763-7774.
190. **Silvestri, L.S., Tortorici, M.A., Vasquez-Del Carpio, R., and Patton, J.T.** 2005. Rotavirus glycoprotein NSP4 is a modulator of viral transcription in the infected cell. Journal of Virology, **79**(24):15165-15174.
191. **Small, C., Barro, M., Brown, T.L., and Patton, J.T.** 2007. Genome heterogeneity of SA11 rotavirus due to reassortment with "o" agent. Virology, **359**(2):415-424.
192. **Smith, E.M., Estes, M.K., Graham, D.Y., and Gerba, C.P.** 1979. A plaque assay for the simian rotavirus SA11. Journal of General Virology, **43**:513-519.
193. **Smith, M.L., Lazdins, I., and Holmes, I.H.** 1980. Coding assignments of double-stranded RNA segments of SA 11 rotavirus establish by in vitro translation. Journal of Virology, **33(**3):976-982.
194. **Stacy-Phipps, S., and Patton, J.T.** 1987. Synthesis of plus- and minus-strand RNA in rotavirus-infected cells. Journal of Virology, **61**:3479-3484.
195. **Street, J.E., Croxson, M.C., Chadderton, W.F., and Bellamy, A.R.** 1982. Sequence diversity of human rotavirus strains investigated by northern blot hybridization analysis. Journal of Virology, **43**(2):369-378.
196. **Sung, P.-Y. and Roy, P.** 2014. Sequential packaging of RNA genomic segments during the assembly of Bluetongue virus. Nucleic Acids Research, **42**(22):13824-13838.
197. **Tafazoli, F., Zeng, C.Q., Estes, M.K., Magnusson, K.E., and Svensson, L.** 2001. NSP4 enterotoxin of rotavirus induces paracellular leakage in polarized epithelial cells. Journal of Virology, **75**(3):1540-1546.

198. **Tam, C.C. and O'Brien, S.J.** 2016. Economic cost of campylobacter, norovirus, and rotavirus disease in the United Kingdom. PLoS One, **11**(2): e0138526.
199. **Tao, Y., Farsetta, D.L., Nibert, M.L., and Harrison, S.C.** 2002. RNA synthesis in a cage—structural studies of reovirus polymerase lambda3. Cell, **111**(5):733-745.
200. **Taraporewala, Z., Chen, D., and Patton, J.T.** 1999. Multimers formed by the rotavirus nonstructural protein NSP2 bind to RNA and have nucleoside triphosphatase activity. Journal of Virology, **73**(12):9934-9943.
201. **Taraporewala, Z, and Patton, J.T.** 2001. Identification and characterization of the helix-destabilizing activity of rotavirus nonstructural protein NSP2. Journal of Virology, **75**(10):4519-4527.
202. **Taraporewala, Z.F., Schuck, P., Ramig, R.F., Silvestri, L., and Patton, J.T.** 2002. Analysis of a temperature-sensitive mutant rotavirus indicates that NSP2 octamers are the functional form of the protein. Journal of Virology, **76**(14):7082-7093.
203. **Tate, J.E., Burton, A.H., Boschi-Pinto, C., Parashar, U.D., and World Health Organization-Coordinated Global Rotavirus Surveillance Network.** 2016. Global, regional, and national estimates of rotavirus mortality in children <5 years of age, 2000-2013. Clinical Infectious Diseases, **62**:S96-S105.
204. **Taylor, J.A., Meyer, J.C., Legge, M.A., O'Brien, J.A., Street, J.E., Lord, V.J., Bergmann, C.C., and Bellamy, A.R.** 1992. Transient expression and mutational analysis of the rotavirus intracellular receptor: The C-terminal methionine residue is essential for ligand binding. Journal of Virology, **66**(6):3566-3572.
205. **Tian, P., Ball, J.M., Zeng, C.Q., and Estes, M.K.** 1996. The rotavirus nonstructural glycoprotein NSP4 possesses membrane destabilization activity. Journal of Virology, **70**(10):6973-6981.
206. **Tian, P., Estes, M.K., Hu, Y., Ball, J.M., Zeng, C.Q., Schilling, W.P.** 1995. The rotavirus nonstructural glycoprotein NSP4 mobilizes Ca2+ from the endoplasmic reticulum. Journal of Virology, **69**(9):5763-5772.
207. **Tian, P., Hu, Y., Schilling, W.P., Lindsay, D.A., Eiden, J., and Estes, M.K.** 1994. The nonstructural glycoprotein of rotavirus affects intracellular calcium levels. Journal of Virology, **68**(1):251-257.
208. **Torres-Flores, J.M., Silva-Ayala, D., Espinoza, M.A., Lopez, S., and Arias, C.F.** 2015. The tight junction protein JAM-A functions as coreceptor for rotavirus entry into MA104 cells. Virology, **475**:172-178.
209. **Torres-Vega, M.A., González, R.A., Duarte, M., Poncet, D., López, S., and Arias, C.F.** 2000. The C-terminal domain of NSP5 is essential for its multimerization, hyperphosphorylation and interaction with NSP6. Journal of General Virology, **81**:821-830.
210. **Trask, S.D., Kim, I.S., Harrison, S.C., and Dormitzer, P.R.** 2010. A rotavirus spike protein conformational intermediate binds lipid bilayers. Journal of Virology, **84**(4):1764-1770.
211. **Valenzuela, S., Pizarro, J., Sandino, A.M., Vásquez, M., Fernández, J., Hernández, O., Patton, J., and Spencer, E.** 1991. Photoaffinity labeling of rotavirus VP1 with 8-azido-ATP: identification of the viral RNA polymerase. Journal of Virology, **65**(7):3964-3967.

212. **Vasquez, M., Sandino, A.M., Pizarro, J.M., Fernandez, J., Valenzuela, S., and Spencer, E.** 1993. Function of rotavirus VP3 polypeptide in viral morphogenesis. Journal of General Virology, **74**(Pt 5):937-941.
213. **Vasquez-Del Carpio, R., Gonzalez-Nilo, F.D., Riadi, G., Taraporewala, Z.F., and Patton, J.T.** 2006. Histidine triad-like motif of the rotavirus NSP2 octamer mediates both RTPase and NTPase activities. Journal of Molecular Biology, **362**(3):539-554.
214. **Velasquez, D.E., Parashar, U.D., and Jiang, B.** 2014. Strain diversity plays no major role in the varying efficacy of rotavirus vaccines: an overview. Infection, Genetics and Evolution, **28**:561-571.
215. **Velazquez, F.R., Matson, D.O., Calva, J.J., Guerrero, L., Morrow, A.L., Carter-Campbell, S., Glass, R.I., Estes, M.K., Pickering, L.K., and Ruiz-Palacois, G.M.** 1996. Rotavirus infections in infants as protection against subsequent infections. New England Journal of Medicine, **335**:1022-1028.
216. **Vende, P., Piron, M., Castagné, N., and Poncet, D.** 2000. Efficient translation of rotavirus mRNA requires simultaneous interaction of NSP3 with the eukaryotic translation initiation factor eIF4G and the mRNA 3' end. Journal of Virology, **74**(15):7064-7071.
217. **Vende, P., Taraporewala, Z., Poncet, D., and Patton, J.T.** 2002. RNA-binding activity of the rotavirus phosphoprotein NSP5 includes affinity for double-stranded RNA. Journal of Virology, **10**:5291-5299.
218. **Vende, P., Tortorici, M.A., Taraporewala, Z.F., and Patton, J.T.** 2003. Rotavirus NSP2 interferes with the core lattice protein VP2 in initiation of minus-strand synthesis. Virology, **313**(1):261-273.
219. **Vesikari, T., Matson, D.O., Dennehy, P., Van Damme, P., Santosham, M., Rodriguez, Z., Dallas, M.J., Heyse, J.F., Goveia, M.G., Black, S.B., Shinefield, H.R., Christie, C.D., Ylitalo, S., Itzler, R.F., Coia, M.L., Onorato, M.T., Adeyi, B.A., Marshall, G.S., Gothefors, L., Campens, D., Karvonen, A., Watt, J.P., O'Brien, K.L., DiNubile, M.J., Clark, H.F., Boslego, J.W., Offit, P.A., Heaton, P.M.; Rotavirus Efficacy and Safety Trial (REST) Study Team.** 2006. Safety and efficacy of a pentavalent human-bovine (WC3) reassortant rotavirus vaccine. New England Journal of Medicine, **354**(1):23-33.
220. **Victoria, J.G., Wang, C., Jones, M.S., Jaing, C., McLoughlin, K., Gardener, S., and Delwart, E.L.** 2010. Viral nucleic acids in live-attenuated vaccines: detection of minority variants and an adventitious virus. Journal of Virology, **84**(12):6033-6040.
221. **Viskovsha, M., Anish, R., Hu, L., Chow, D.C., Hurwitz, A.M., Brown, N.G., Palzkill, T., Estes, M.K., and Prasad, B.V.** 2014. Probing the sites of rotaviral proteins involved in replication. Journal of Virology, **88** (21):12866-12881.
222. **Wang, H., Gao, K., Wen, K., Allen, I.C., Li, G., Zhang, W., Kocher, J., Yang, X., Giri-Rachman, E., Li, G.H., Clarke-Deener, S., and Yuan, L.** 2016. Lactobacillus rhamnosus GG modulates innate signaling pathway and cytokine responses to rotavirus vaccine in intestinal mononuclear cells of gnotobiotic pigs transplanted with human gut microbiota. BMC Microbiology, **16**(1):109.
223. **Ward, L.A., Rosen, B.I., Yuan, L., and Saif, L.J.** 1996. Pathogenesis of an attenuated and a virulent strain of group A human rotavirus in neonatal gnotobiotic pigs. Journal of General Virology, **77**(Pt. 7):1431-1441.

224. **Wehrfritz, J.M., Boyce, M., Mirza, S., and Roy, P.** 2007. Reconstitution of bluetongue virus polymerase activity from isolated domains based on a three-dimensional structural model. Biopolymers, **86**:83-94.
225. **Welch, S.-K., W., Crawford, S.E., and Estes, M.K.** 1989. Rotavirus SA11 genome segment 11 protein is a nonstructural phosphoprotein. Journal of Virology, **63**:3974-3982.
226. **Wen, K., Li, G., Bui, T., Liu, F., Li, Y., Kocher, J., Lin, L., Yang, X., and Yuan, L.** 2012. High dose and low dose *Lactobacilli acidophilus* exerted differential immune modulating effects on T cell immune responses induced by an oral human rotavirus vaccine in gnotobiotic pigs. Vaccine, **30**(6):1198-1207.
227. **Wolf, M., Vo, P.T., and Greenberg, H.B.** 2011. Rhesus rotavirus entry into a polarized epithelium is endocytosis dependent and involves sequential VP4 conformational changes. Journal of Virology, **85**(6):2495-2503.
228. **Yeager, M., Berriman, J.A., Baker, T.S., and Bellamy, A.R.** 1994. Three-dimensional structure of the rotavirus haemagglutinin VP4 by cryo-electron microscopy and difference map analysis. EMBO Journal, **13**(5):1011-1018.
229. **Yoder, J.D, Trask, S.D., Vo, T.P., Binka, M., Feng, N., Harrison, S.C., Greenberg, H.B., and Dormitzer, P.R.** 2009. VP5* rearranges when rotavirus uncoats. Journal of Virology, **83**(21)11372-11377.
230. **Yuan, L., Wen, K., Azevedo, M.S.P., Gonzalez, A.M., Zhang, W., and Saif, L.J.** 2008. Virus-specific intestinal IFN-(gamma) producing T cell responses induced by human rotavirus infection and vaccines are correlated with protection against rotavirus diarrhea in gnotobiotic pigs. Vaccine, **26**(26):3322-3331.
231. **Zeng, C.Q., Estes, M.K., Charpilienne, A., and Cohen, J.** 1998. The N terminus of rotavirus VP2 is necessary for encapsidation of VP1 and VP3. Journal of Virology, **72**:201-208.
232. **Zeng, C.Q., Wentz, M.J., Cohen, J., Estes, M.K., and Ramig, R.F.** 1996. Characterization and replicase activity of double-layered and single-layered rotavirus-like particles expressed from baculovirus recombinants. Journal of Virology, **70**;2736-2742.
233. **Zhang, M., Zeng, C.Q., Dong, Y., Ball, J.M., Saif, L.J., Morris, A.P., and Estes, M.K.** 1998. Mutations in rotavirus nonstructural glycoprotein NSP4 are associated with altered virus virulence. Journal of Virology, **72**(5):3666-3672.
234. **Zhang, M., Zeng, C.Q., Morris, A.P., and Estes, M.K.** 2000. A functional NSP4 enterotoxin peptide secreted from rotavirus-infected cells. Journal of Virology, **74**(24):11663-11670.
235. **Zhang, S., McDonald, P.W., Thompson, T.A., Dennis, A.F., Akopov, A., Kirkness, E.F., Patton, J.T., and McDonald, S.M.** 2014. Analysis of human rotaviruses from a single location over an 18-year time span suggests that protein coadaption influences gene constellations. Journal of Virology, **88**(17):9842-9863.

CHAPTER 2

Temperature-sensitive Lesion in the N-terminal Domain of the Rotavirus Polymerase Affects its Intracellular Localization and Enzymatic Activity

Allison O. McKell[1,2], Leslie E. W. LaConte[1], and Sarah M. McDonald[1,2#]

[1]Virginia Tech Carilion School of Medicine and Research Institute, Roanoke, VA;
[2]Department of Biomedical Sciences and Pathobiology, Virginia-Maryland College of Veterinary Medicine, Blacksburg, VA

Journal of Virology 2017 April; 91(7):e00062-17. *Used with permission of the American Society for Microbiology, 2017*

ABSTRACT

Temperature-sensitive (*ts*) mutants of simian rotavirus (RV) strain SA11 have been previously created to investigate the functions of viral proteins during replication. One mutant, SA11-*ts*C, has a mutation that maps to the gene encoding the VP1 polymerase and shows diminished growth and RNA synthesis at 39°C compared to that at 31°C. In the present study, we sequenced all 11 genes of SA11-*ts*C, confirming the presence of an L138P mutation in the VP1 N-terminal domain and identifying 52 additional mutations in four other viral proteins (VP4, VP7, NSP1, and NSP2). To investigate whether the L138P mutation induces a *ts* phenotype in VP1 outside of the SA11-*ts*C genetic context, we employed ectopic expression systems. Specifically, we tested whether the L138P mutation affects the ability of VP1 to localize to viroplasms, which are the sites of RV RNA synthesis, by expressing the mutant as a GFP-fusion protein ($VP1_{L138P}$-GFP) (i) in WT SA11-infected cells or (ii) in uninfected cells along with the viroplasm-forming proteins NSP2 and NSP5. We found that $VP1_{L138P}$-GFP localized to viroplasms and interacted with NSP2 and/or NSP5 at 31°C but not at 39°C. Next,

we tested the enzymatic activity of a recombinant mutant polymerase ($rVP1_{L138P}$) *in vitro* and found that it synthesized less RNA at 39°C than at 31°C, as well as less RNA than the control at all temperatures. Together, these results provide a mechanistic basis for the *ts* phenotype of SA11-*ts*C and raise important questions about the role of leucine 138 in supporting key protein interactions and the catalytic function of the VP1 polymerase.

IMPORTANCE

RVs cause diarrhea in the young of many animal species, including humans. Despite their medical and economic importance, gaps in knowledge exist about how these viruses replicate inside host cells. Previously, a mutant simian RV (SA11-*ts*C) that replicates worse at higher temperatures was identified. This virus has an amino acid mutation in VP1, which is the enzyme responsible for copying the viral RNA genome. The mutation is located in a poorly understood region of the polymerase called the N-terminal domain. In this study, we determined that the mutation reduces the ability of VP1 to properly localize within infected cells at high temperatures as well as reduced the ability of the enzyme to copy viral RNA in a test tube. The results of this study explain the temperature sensitivity of SA11-*ts*C and shed new light on functional protein-protein interaction sites of VP1.

INTRODUCTION

Rotaviruses (RVs) are segmented, double-stranded RNA (dsRNA) viruses and gastrointestinal pathogens of many animal species (1). In unvaccinated children, RVs cause severe watery diarrhea and vomiting, killing an estimated 215,000 children each year (2). The RV virion is a nonenveloped, icosahedral particle with three concentric protein layers (3, 4). The outermost layer is composed of two proteins (VP4 and VP7), whereas the middle layer and inner core shell are each made of a single protein (VP6 and VP2, respectively). Within the viral core resides the 11 dsRNA genome segments (i.e., genes) and several copies each of the viral RNA polymerase (VP1) and RNA capping enzyme (VP3). Altogether, the genome codes for six

structural proteins (VP1 to VP4, VP6, and VP7) as well as five or six nonstructural proteins (NSP1 to NSP5 and NSP6 in some strains) that play various roles during intracellular viral replication.

Studies of RV protein function have been hampered by the lack of efficient reverse genetic approaches that allow for the targeted engineering of viral mutants. However, several temperature-sensitive (*ts*) mutant viruses have been created using forward genetic approaches (5-8). In particular, one panel of *ts* mutants was generated via chemical mutagenesis of prototypic laboratory strain SA11 (H96 derivative, hereafter referred to as SA11-H96) (7). Reassortment analyses were used to map *ts* lesions of several mutants to individual genes, i.e., SA11-*ts*A (VP4), SA11-*ts*B (VP3), SA11-*ts*C (VP1), SA11-*ts*E (NSP2), SA11-*ts*F (VP2), SA11-*ts*G and (VP6) (9). SA11-*ts*C mapped to the gene encoding the VP1 polymerase, and this mutant shows diminished viral growth, RNA synthesis, protein synthesis, and virion morphogenesis at 39°C compared to that at 31°C (10-12). By using a general anti-RV antiserum and epifluorescence microscopy, it was also shown that viral proteins were more diffusely distributed in the cytosol of SA11-*ts*C-infected cells than in that of the other *ts* mutants from this panel, which showed a more punctate localization pattern (10). The phenotype of SA11-*ts*C is less severe at 31°C, yet the virus still exhibits reduced RNA synthesis and diffuse protein localization even at the lower, more permissive temperature (10, 12). Sequencing of the VP1-coding gene from SA11-*ts*C identified a single leucine-to-proline change at position 138 (L138P) (13). It remains unknown whether the L138P lesion causes the VP1 protein to have a *ts* phenotype outside the genetic context of the virus. Moreover, the sequences of the other 10 genes of SA11-*ts*C have not yet been deduced, preventing an understanding of how additional mutations may contribute to its replication defect.

VP1 is a compact, globular 125-kDa protein and is organized as three distinct domains: (i) an N-terminal domain (residues 1-332), (ii) a central polymerase domain, with canonical fingers, palm, and thumb subdomains (residues 333-778), and (iii) a C-terminal 'bracelet' domain (residues 779-1089) (Fig. 1) (14). Together, the N- and C-terminal domains enclose the central polymerase domain to create a cage-like enzyme with a buried active site. The N-terminal domain is not directly involved in catalysis, and such a domain is missing from all other viral RNA polymerases outside of the *Reoviridae* family (15). This region of VP1 helps form a template RNA entry tunnel, and it may also aid in polymerase regulation by serving as a binding

platform for other viral proteins. VP1 is known to engage at least three other viral proteins (VP2, NSP2, and NSP5) during the RV lifecycle, though the interaction interfaces are poorly defined (16-19). Binding of VP1 by NSP2 and/or NSP5 localizes the polymerase to viroplasms, sites of genome replication and early particle assembly in the cell cytosol (20-21). Within the viroplasm, binding of VP1 by the core shell protein VP2 triggers the polymerase to initiate genome replication (i.e., dsRNA synthesis) in the context of subviral assembly intermediates (18, 19, 22). Because the VP1 protein of SA11-*ts*C has an L138P mutation in the N-terminal domain, we wondered whether it affected the capacity of the polymerase to localize to viroplasms, interact with other viral proteins, and synthesize viral dsRNA in a temperature-dependent manner.

In this study, we sequenced all 11 genes of SA11-*ts*C, confirming the presence of the L138P mutation in the VP1 N-terminal domain and also identifying an additional 52 changes in four other viral proteins (VP4, VP7, NSP1, and NSP2). By employing VP1 ectopic expression systems, we show that the L138P mutation alone abrogates NSP2 and/or NSP5 interactions at high temperatures and prevents efficient localization of the polymerase to viroplasms. We further show that the L138P mutation alone reduces the enzymatic activity of the polymerase *in vitro* in a temperature-dependent manner. Altogether, our findings increase a mechanistic understanding of the basis for the *ts* phenotype of SA11-*ts*C phenotype and raise interesting questions about the importance of leucine 138 and its involvement in polymerase regulation.

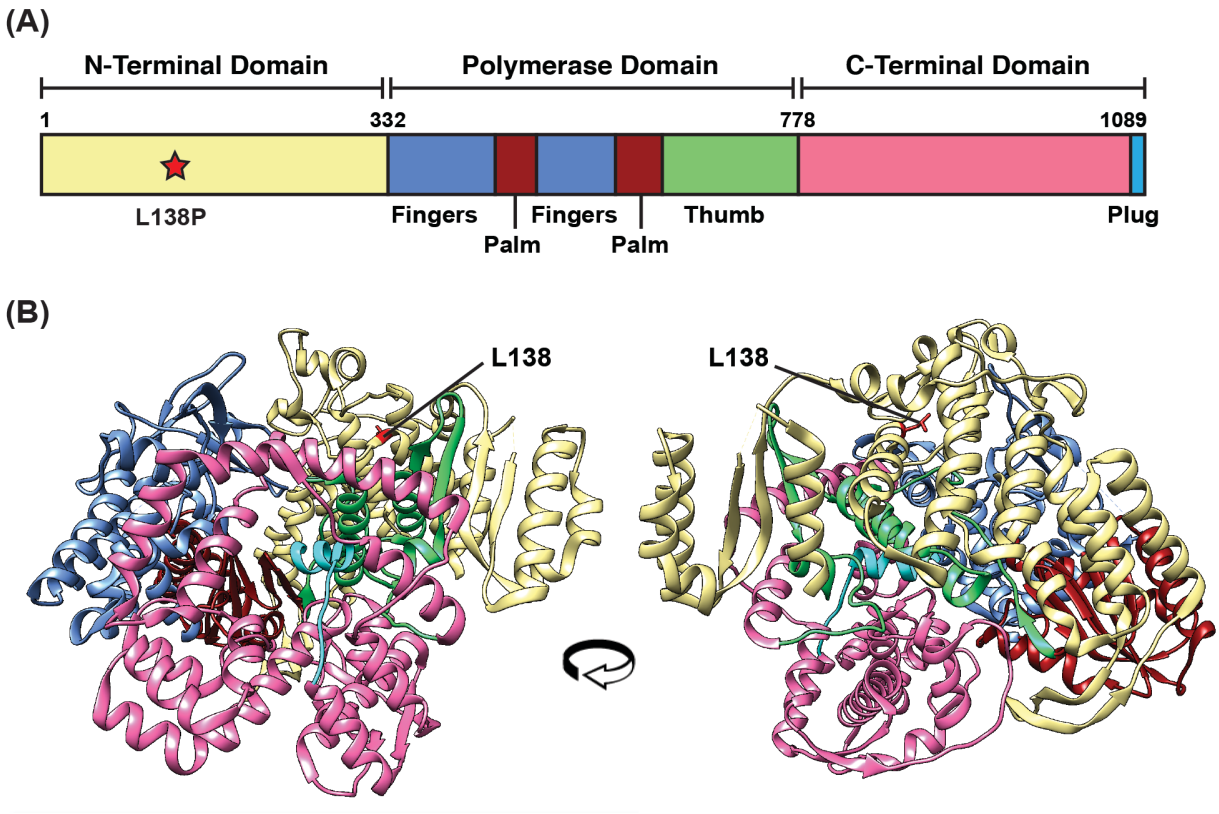

Figure 1-VP1 domain organization and location of the L138P mutation. (A) Linear schematic of VP1 (not drawn to scale). The N-terminal (yellow) and C-terminal (pink) domains flank the central polymerase domain, which contains canonical with fingers (blue), palm (dark red), and thumb (green) subdomains. The extreme C-terminus of the protein forms a plug subdomain (cyan). The amino acid residues making up each domain are listed at the top of the schematic, and the location of the L138P mutation in SA11-*ts*C is shown as a red star. (B) Atomic structure of VP1 (PDB accession no. 2R7R) in ribbon representation. Domains and subdomains are colored as in panel A, and L138 is colored red and labeled. The left side is the traditional front view of VP1, and on the right side is the protein rotated approximately 100° to the left so that L138 can be better visualized.

MATERIALS AND METHODS

Monkey kidney cells and RVs. Monkey kidney cell lines (MA104 and Cos-7) were obtained from American Type Cell Culture and maintained as described by Arnold et al. (30) in either Medium 199 (Life Technologies) or DMEM (Life Technologies) that was supplemented to contain 10% heat-inactivated fetal bovine serum, 100 U/ml penicillin, 100 μg/ml streptomycin, and 0.5 μg/ml Amphotericin B (30). Wildtype (WT) SA11-4F and SA11-*ts*C (clone 606) were generously provided by John Patton (University of Maryland, College Park) with permission from Frank Ramig (Baylor University). Infections with WT SA11-4F or SA11-*ts*C were performed as described previously (30). Guinea pig polyclonal antisera against VP2 (αVP2-SM) was generated against baculovirus-expressed, recombinant protein (SA11-4F strain) by Pocono Rabbit Farm and Laboratory, Inc. (Canadensis, PA). Guinea pig polyclonal sera against NSP2 (αNSP2-53962) and NSP5 (αNSP5-53964) was generously provided by John Patton (University of Maryland, College Park). AOM performed this work.

Sequencing the 11 genes of SA11-*ts*C. Plaque-purified SA11-*ts*C was used to infect MA104 cells in a 75-cm^2 culture flask (~1 x 10^7 cells) at 31°C for 72 h. Total RNA was extracted from the clarified cell supernatant using Trizol® LS Reagent (Life Technologies) as per the manufacturer's protocol. Reverse transcription-polymerase chain reaction (RT-PCR) was performed using the Super Script® One-Step RT-PCR System with Platinum® *Taq* DNA Polymerase (Life Technologies). Primers were designed based upon the published gene sequences of SA11-H96 (GenBank accession numbers: DQ838610, DQ838615, DQ838620, DQ838625, DQ838630, DQ838635, DQ838637, DQ838640, DQ838645, DQ838650, and DQ841262). For the NSP2-coding gene, primers were also designed based on the O agent strain (GenBank accession number DQ838599). In general, the primers were designed to amplify <1-kb regions of each viral gene. All primer sequences used in this study for RT-PCR and sequencing are available from the authors by request. The RT-PCR reactions were performed according to the manufacturer's instructions with the exception that the RNA template was denatured at 95°C for 10 min in 50% dimethyl sulfoxide (DMSO) prior to being used. The amplified cDNA products were gel purified and cleaned using the QIAquick® gel extraction kit

(Qiagen) as per the manufacturer's protocol prior to being sent to the Biocomplexity Institute of Virginia Tech (Virginia Tech, Blacksburg, VA) for Sanger sequencing.

Contigs were assembled *de novo* from the raw sequence data using Geneious© Pro v6.8.1 (Biomatters, Inc.). For each of the 11 SA11-*ts*C genome segments, the entire open-reading frame (ORF) was sequenced; for some genes, portions of 5' and 3' untranslated regions were also sequenced. The ORF sequences were deposited into GenBank using accession numbers KX548930-KX548939 and KX766185. Basic Local Alignment Search Tool (BLAST) was used to determine the likely parental origin for each of the 11 SA11-*ts*C genes (http://blast.ncbi.nlm.nih.gov/Blast.cgi). To identify nucleotide and amino acid differences, the deduced SA11-*ts*C gene sequences were aligned to those of the following strains: SA11-H96 (GenBank accession numbers DQ838610, DQ838615, DQ838620, DQ838625, DQ838630, DQ838635, DQ838637, DQ838640, DQ838645, DQ838650, and DQ841262) and O agent (NSP2-coding gene only; GenBank accession number DQ838599). AOM performed this work.

Localization of WT and mutant VP1 as GFP-fusion proteins in mock or infected cells. The ORF sequences of WT or mutant L138P VP1 were cloned into the pEGFP-N1 vector (Clonetech) to express the polymerases with enhanced GFP fused to their C-termini ($VP1_{WT}$-GFP or $VP1_{L138P}$-GFP, respectively). The WT SA11-4F VP1 ORF was amplified from the pENTR-SA11 VP1 vector using PCR (18). Primer-generated restrictions sites (5' *Sac I* and 3' *Kpn I*) were used to subclone the WT SA11-4F VP1 ORF into the pEGFP-N1 vector, thereby creating pEGFP-SA11-$VP1_{WT}$, which expresses $VP1_{WT}$-GFP. Outward PCR and site-directed mutagenesis was then used to engineer the L138P mutation into the SA11-4F VP1 ORF using pEGFP-SA11-$VP1_{WT}$ as template, thereby creating pEGFP-SA11-$VP1_{L138P}$, which expresses $VP1_{L138P}$-GFP. Both expression vectors were sequenced to verify the integrity of the VP1 ORF, maintenance of the translational frame with GFP, and the absence of second-site mutations.

To express $VP1_{WT}$-GFP, $VP1_{L138P}$-GFP, or the unfused GFP control, Cos-7 cells grown on glass coverslips in 12-well plates (~0.5 x 10^6 cells/well) were transfected with 1 µg of plasmid DNA (pEGFP-SA11-$VP1_{WT}$, pEGFP-SA11-$VP1_{L138P}$, or the pEGFP-N1 empty vector, respectively) using Trans-IT®-LT1 (Mirus) according to the manufacturer's instructions. The transfected cells were incubated for 48 h at 31°C, 37°C, or 39°C, depending upon the experiment, to allow for protein expression. Thereafter, the transfected cells were either mock

infected or infected with SA11-4F at a multiplicity of infection (MOI) of 10 plaque-forming units (pfu) per cell. Infections proceeded at 31°C, 37°C, or 39°C, depending upon the experiment. At 8-12 h post-infection (p.i.), the cells on coverslips were washed once with Dulbecco's phosphate-buffered saline (DPBS) prior to being fixed and permeabilized by incubation in 100% methanol for 5 min at room temperature. The coverslips were then stored in DPBS at 4°C for <3 d prior to immunostaining. AOM performed this work.

Localization of WT and mutant VP1 GFP-fusion proteins to viroplasm-like structures. The NSP2 ORFs of strains SA11-4F and SA11-*ts*C were amplified from viral RNA by RT-PCR and subcloned into the pCI mammalian expression vector (Promega) using restriction sites 5' *Xho I* and 3' *Xba I*, yielding pCI-NSP2$_{SA11}$ and pCI-NSP2$_{Oagent}$. The NSP5 ORF of strain SA11-4F was similarly subcloned into pCI except using restriction sites 5' *Xho I* and 3' *Not I*, yielding pCI-NSP5. Expression vectors were sequenced to verify the integrity of the cloned ORFs. Cos-7 cells on glass coverslips were co-transfected with pCI vector pCI-NSP5 along with either pCI-NSP2$_{SA11}$ or pCI-NSP2$_{Oagent}$, to express NSP5 along with either NSP2$_{SA11}$ or NSP2$_{Oagent}$. To test whether VP1$_{WT}$-GFP or VP1$_{L138P}$-GFP could localize to viroplasm-like structures, the respective expression vectors (i.e., pEGFP-SA11-VP1$_{WT}$, pEGFP-SA11-VP1$_{L138P}$) or that expressing unfused GFP (i.e., pEGFP-N1) were included in the transfection mixture. In all experiments, Cos-7 cells grown on glass coverslips in 12-well plates (~0.5 x 10^6 cells/well) were transfected with a total of 1 µg plasmid DNA using Trans-IT®-LT1 (Mirus) according to the manufacturer's instructions. The transfected cells were incubated for 48 h at 31°C or 39°C, depending upon the experiment, to allow for protein expression. The cells on coverslips were washed once with DPBS prior to being fixed and permeabilized by incubation in 100% methanol for 5 min at room temperature. The coverslips were then stored in DPBS at 4°C for <3 d prior to immunostaining. AOM performed this work.

Immunostaining and confocal microscopy. Coverslips were blocked overnight at 4°C with rocking using a solution of 5% bovine serum albumin (BSA) in DPBST (1.6 mM KH_2PO_4, 2.7 mM KCl, 8.1 mM N_2HPO_4, 137.1 mM NaCl, and 0.1% Triton X100). Following 3×10-min washes with DPBST, primary guinea pig antisera was added at a 1:1,000 dilution in a solution of 2.5% BSA in DPBST for 1 h at room temperature with rocking. Following 3×10-min washes

with DPBST, the Alexa Fluor® 546 goat anti-guinea pig IgG (Life Technologies) secondary antibody was added at a 1:10,000 dilution in 2.5% BSA in DPBST for 30 min at room temperature with rocking. Following 3×10-min washes with DPBST, the stained coverslips were inverted and mounted onto glass microscope slides using the ProLong® Diamond Antifade Mountant with DAPI (Life Technologies). The slides cured for >24 h at room temperature, protected from light, prior to imaging.

Imaging was performed using a Zeiss LSM 880 inverted laser-scanning confocal microscope using the 63× oil immersion objective and the 405-nm, 488-nm, 561-nm laser lines. The following settings were used for all images: pinhole=1 AU, digital offset=0, and digital gain=1.0. Amplitude and master gain were optimized for each image to prevent pixel saturation. Quantification of unmodified images were performed using ImageJ (31). Specifically, binary masks of images were used to independently calculate green signal and red signal in each cell. The percent of total green signal that colocalized with red signal for each cell was determined by subtracting the masks. Averages were obtained using four to six cells per condition tested. Two-sample t-tests of the mean were performed for each data set using Smith's Statistical Package, version 2.80. *P* values of <0.01 were considered statistically significant. Representative confocal micrographs of each condition were minimally modified for Hue/Saturation and Brightness/Contrast using Adobe Photoshop (Ver. 13.0). AOM performed this work.

Expression and purification of WT and mutant recombinant VP1 proteins. The BaculoDirect expression system (Life Technologies) was used according to the manufacturer's protocol to create His-tagged recombinant VP1 containing the L138P lesion ($rVP1_{L138P}$). Briefly, outward PCR and site-directed mutagenesis was used to engineer the L138P mutation into the SA11-4F VP1 ORF of the pENTR-SA11 VP1 vector (18). The entire $VP1_{L138P}$ ORF was then transferred into the BaculoDirect C-Term linear DNA by recombination with LR clonase II. *Spodoptera frugiperda* (Sf9) in were maintained at 28°C in complete Grace's medium (Life Technologies) supplemented to contain 10% heat-inactivated fetal bovine serum, 100 U/ml penicillin, 100 µg/ml streptomycin, 0.5 µg/ml Amphotericin B and 1% Pluronic® F-68 (Life Technologies). The recombinant baculovirus DNA was transfected into Sf9 cells using the Cellfectin reagent (Life Technologies), and recombinant baculovirus was harvested from medium containing 100 µM ganciclovir. Baculoviruses expressing His-tagged, WT SA11-4F

VP1 ($rVP1_{WT}$), catalytically-inactive His-tagged SA11-4F VP1 ($rVP1_{D632A}$), and WT SA11-4F VP2 (rVP2) were described previously (18, 32). Protein expression and purification was performed as described previously by McDonald et al. 2011 (18). Purified proteins were assessed for quality and relative quantity by electrophoresis versus protein standards in sodium dodecyl sulfate (SDS)-polyacrylamide gels and GelCode™ Blue staining (Thermo Scientific). The Precision Plus Protein™ Kaleidoscope™ Prestained Protein Standards (BioRad) were used as molecular weight markers. Proteins were stored at 4°C in low salt buffer (2 mM Tris-HCl [pH 7.5], 0.5 mM EDTA, 0.5 mM dithiothreitol) containing 1× complete protease inhibitors (Roche). rVP1 proteins were used within 3 d of their purification. AOM performed this work.

***In vitro* dsRNA synthesis.** The activity of $rVP1_{WT}$, $rVP1_{L138P}$, and $rVP1_{D632A}$ was determined using an *in vitro* dsRNA synthesis assay (18, 26). Each 20-µl reaction contained 2 pmol of rVP1, 20 pmol of rVP2, 4 pmol of SA11 gene 8 +RNA, 50 mM Tris-HCl (pH 7.5), 1µl 30% PEG-8000, 20 mM MgAc, 1.6 mM MnAc, 2.5 mM DTT, 1.25 mM each of ATP/CTP/UTP, 5 mM GTP, 1 µl RNasin® (Promega), and 1 µCi of [α-^{32}P] UTP (3,000 Ci/mmol, Perkin Elmer). Reactions proceeded at 31°C, 37°C, or 39°C for indicated times. The [^{32}P]-labeled dsRNA products of the reaction were electrophoresed in 12% SDS-polyacrylamide gels. The gels were dried onto filter paper and dsRNA bands were visualized and quantitated using a GE Healthcare Storm™ 860 phosphorimager. One-sample or two-sample t-tests of the mean were performed for each replicase assay data set using Smith's Statistical Package, version 2.80. *P* values of <0.01 were considered statistically significant. AOM performed this work.

***In silico* molecular dynamics simulations.** Molecular dynamics simulations were performed using GROMACS v5.1.3 on modified atomic models of strain SA11-4F VP1 (PDB#2R7Q) (14, 34). Specifically, to create WT VP1 for simulations, we needed to model a flexible loop (residues 346 to 358) that is missing in the SA11-4F structure. This loop was modeled using the Modeller loop-modeling tool embedded in the program UCSF Chimera v1.11 (35, 36). The model with the most favorable zDOPE score was chosen for further computations, and the resulting structure is consistent with that of a previous study that used strain Bristol VP1 (24). To create the L138P VP1 structure for simulations, Chimera's Rotamers tool was used to replace the native leucine residue at position 138 in the WT VP1 structure with a proline residue.

The proline rotamer from the Dunbrack backbone-dependent rotamer library with the highest probability was chosen for the L138P VP1 model. The PDB files of both structures are available upon request. Prior to performing the simulations, the complete WT VP1 and L138P VP1 structures were explicitly solvated with a three-point water model (TIP3P) in rhombic dodecahedron water box (solute-box distance of 1.0 nm) under periodic boundary conditions, with charges neutralized by chloride ions. The AMBER99SB-ILDN force field was used for all simulations (37). Starting structures were energy minimized until convergence at Fmax<1000 kJ/mol/nm. A 100-ps position-restrained NVT equilibration simulation was run for water relaxation at 312K using a modified Berendsen (velocity rescaling) thermostat, followed by a 100 ps NPT equilibration simulation using the Parrinello-Rahman barostat for pressure coupling. After equilibration, an unrestrained 20 ns NPT molecular dynamics simulation was run at 312K. Three trajectories initiated with different random seeds were run for each protein structure. The root mean square fluctuation (RMSF) of all α-carbons from each of the three trajectories was calculated using the gmx rmsf command in GROMACS. B-factors for each residue were calculated from the RMSF values using the equation: B-factor = $(8\Pi^2/3) \times (\text{RMSF})^2$. LEWL performed this work.

RESULTS

Sequencing of the 11 genes of SA11-*ts*C. Previous studies have determined the VP1-coding gene sequence for SA11-*ts*C, revealing an L138P lesion in the N-terminal domain of the polymerase (13). However, the sequences of the other 10 genes of SA11-*ts*C had not yet been determined, limiting our understanding of additional mutations that may contribute to the replication-defective, *ts* phenotype of this virus. Therefore, we employed reverse transcription (RT)-PCR and the Sanger approach to determine the sequences of all 11 SA11-*ts*C gene open reading frames (ORFs). To identify changes that may contribute to the SA11-*ts*C phenotype, we aligned the deduced ORF nucleotide and amino acid sequences to those of the parental strain SA11-H96 (7) (Table 1). Altogether, we identified 219 nucleotide and 53 amino acid differences when comparing SA11-*ts*C to SA11-H96; the vast majority of these differences were in the NSP2-coding gene. BLAST analyses revealed that the SA11-*ts*C NSP2-coding gene is identical

to that of O agent, an RV strain isolated in 1965 from a slaughterhouse (23). Indeed, an amino acid sequence alignment shows that SA11-*ts*C NSP2 shows no amino acid changes compared to O agent NSP2 but that this protein differs at 45 residues compared to the parental SA11-H96 strain (Fig. 2). BLAST analyses of the other 10 SA11-*ts*C genes verified that they are most closely related to the parental strain SA11-H96. This result suggests that SA11-*ts*C is a monoreassortant with 10 genes derived from SA11-H96 and an NSP2-coding gene derived from O agent.

Not counting the reassorted NSP2-coding gene, there are a total of 16 nucleotide and 8 amino acid differences when comparing SA11-*ts*C versus SA11-H96 (Table 1). The VP1-coding gene of SA11-*ts*C had only the single previously-reported nucleotide change, which results in the L138P lesion in the N-terminal domain of the polymerase (13). The VP4-coding gene had eight nucleotide changes, five of which caused amino acid changes in the protein (T72M, P157S, A187G, Y332S, and V366M). The VP7-coding gene had two nucleotide changes, one of which (T60A) caused an amino acid change in the protein. Likewise, two nucleotide changes were identified for the NSP1-coding gene, one of which (K39N) caused an amino acid change in the protein. Three nucleotide changes were identified for the VP3- and VP6-coding genes, but none of them resulted in changes in the viral proteins. No nucleotide changes were found in the VP2-, NSP3-, NSP4-, and NSP5/6-coding genes.

These results demonstrate that, in addition to the VP1 L138P lesion, SA11-*ts*C virus has multiple differences from the parental strain in its genome, including 52 amino acid changes in four other viral proteins (Table 1). Because we currently lack reverse genetic technologies to recapitulate the VP1 L138P mutation in an isogenic SA11-H96 background, it is not possible to determine its contribution toward the *ts* phenotype in the context of an infectious virus. Therefore, in this study, we sought to investigate the effect of the L138P lesion alone on the temperature-dependent localization and enzymatic activity of the VP1 protein using ectopic expression systems.

Table 1: Nucleotide (nt) and amino acid (aa) changes in SA11-*ts* C genes

Gene	Reference	nt Change	aa Change
VP1	SA11-H96	U431C	**L138P**
VP2	SA11-H96	nc	nc
VP3	SA11-H96	A886G	nc
		U1998A	nc
VP4	SA11-H96	C224U	**T72M**
		A318G	nc
		C478U	**P157S**
		C569G	**A187G**
		U603C	nc
		G792A	nc
		A1004C	**Y332S**
		G1105A	**V366M**
VP6	SA11-H96	U305C	nc
VP7	SA11-H96	C192U	nc
		A226G	**T60A**
NSP1	SA11-H96	G147C	**K39N**
		U648C	nc
NSP2	SA11-H96	203Δs	**45Δs**
	O agent	nc	nc
NSP3	SA11-H96	nc	nc
NSP4	SA11-H96	nc	nc
NSP5/6	SA11-H96	nc	nc

Abbrev: no change (nc)

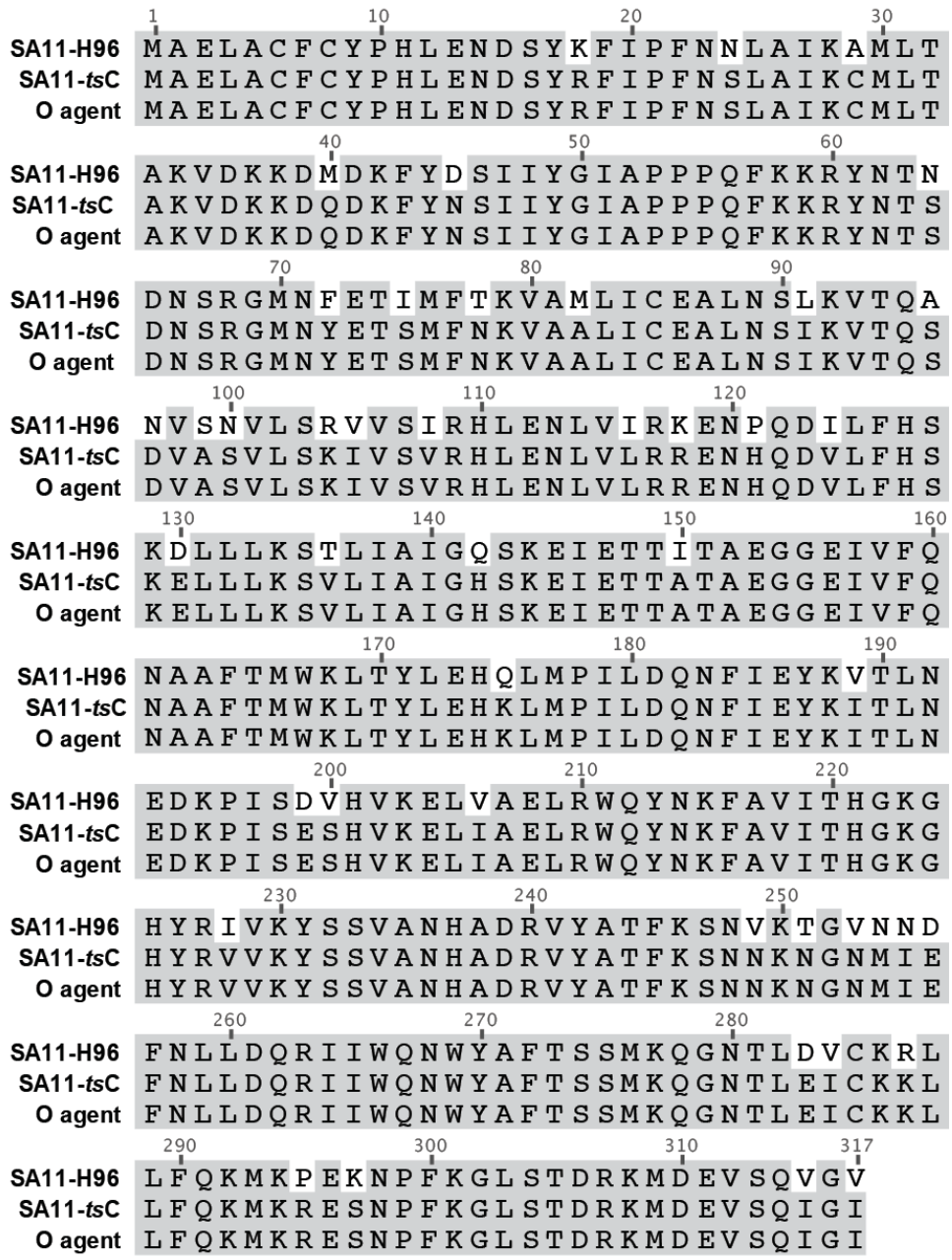

Figure 2-NSP2 amino acid sequence alignment. The primary NSP2 amino acid sequences of strains SA11-H96, SA11-*ts*C, and O agent are shown. Amino acid positions are listed at the top of the sequence alignment, and conserved residues are shown in grey.

The L138P lesion abrogates the ability of VP1 to efficiently localize to viroplasms in a temperature-dependent manner. To test the effect of the L138P lesion on the ability of VP1 to localize to viroplasms at various temperatures, we first needed to establish an ectopic expression system that would allow us to track the mutant polymerase in wild-type (WT) virus-infected cells. Therefore, we engineered WT or mutant VP1 proteins with green fluorescent protein (GFP) fused to their C-termini ($VP1_{L138P}$-GFP and $VP1_{WT}$-GFP, respectively) and determined their localization relative to that of unfused GFP by using immunofluorescence confocal microscopy. For these experiments, Cos-7 cells were used because they are permissive for RV infection and show high plasmid DNA transfection efficiencies. Strain SA11-4F was used as WT RV because it infects Cos-7 cells significantly better than does SA11-H96 as a result of changes in its VP4 attachment protein (13). However, we note that the VP1 proteins of SA11-4F and SA11-H96 are 100% identical, eliminating any concerns about potential strain-specific differences in VP1-protein interactions.

To verify that $VP1_{WT}$-GFP localized to viroplasms in infected cells and that unfused GFP did not, these control proteins were expressed in Cos-7 cells on glass coverslips for 48 h at 37°C (Fig. 3). The cells were then either mock-infected or infected with SA11-4F and incubated for 8 h at 37°C. The confocal micrographs showed that both unfused GFP and $VP1_{WT}$-GFP were diffusely distributed throughout the cytosol of mock-infected cells (Fig. 3A and 3B). The localization pattern of unfused GFP was the same in infected cells compared to mock-infected cells, with the vast majority of the protein localizing in the cytosol and no visible enrichment in viroplasms, which were stained with antiserum against VP2 or NSP2 (Fig. 3A and data not shown). In contrast, nearly all of the visible $VP1_{WT}$-GFP colocalized with viroplasms, and very little diffuse protein was seen in the cytosol (Fig. 3B). These results suggest that ectopically expressed WT VP1 is capable of being recruited to/retained within viroplasms and that the C-terminal GFP tag does not interfere with any interactions that mediate its viroplasmic localization.

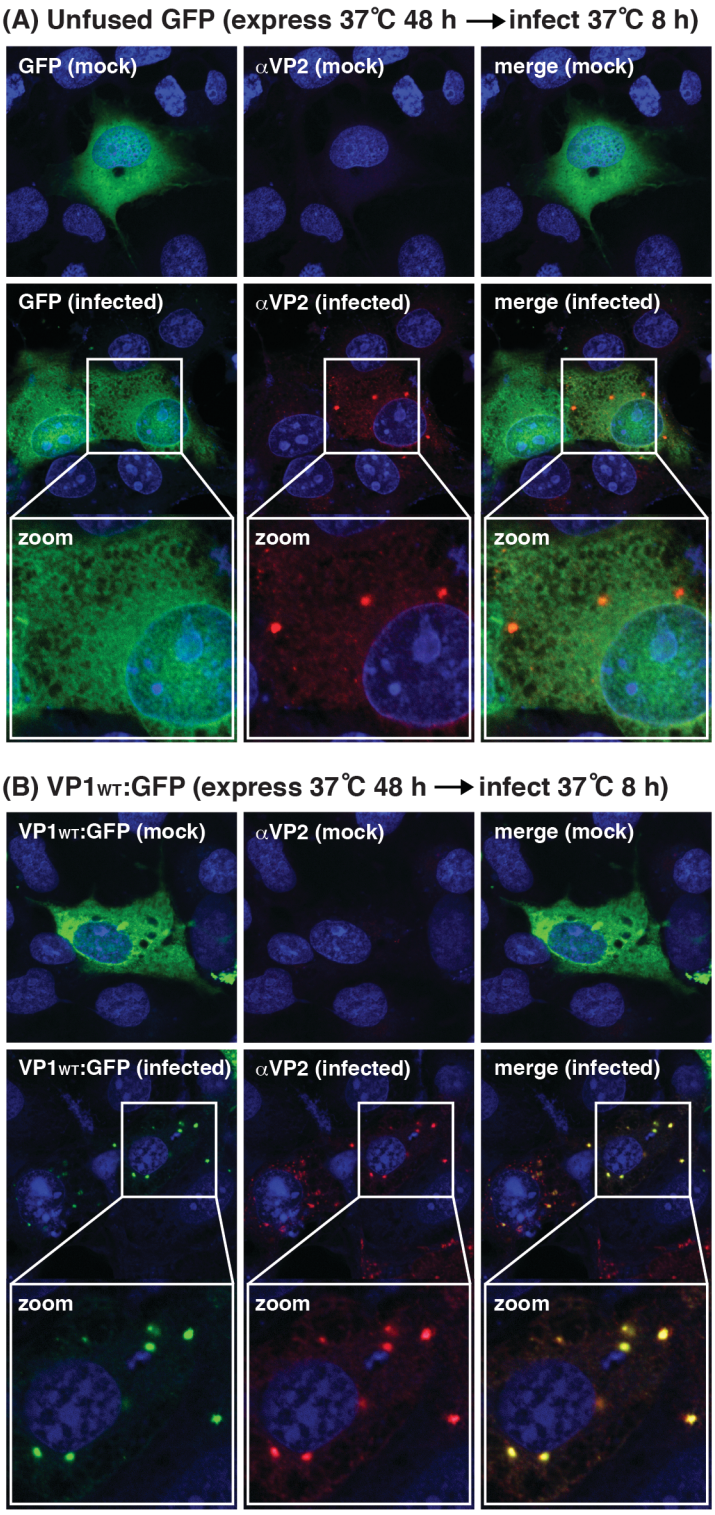

Figure 3-Ectopically expressed WT VP1 localizes to viroplasms as a GFP-fusion protein. Cos-7 cells on glass coverslips were transfected with plasmids expressing either unfused GFP (A) or the WT VP1 fusion protein, $VP1_{WT}$-GFP (B). Following their incubation at 37°C for 48 h, the cells were either mock-infected or infected with SA11-4F (MOI of 10) at 37°C for 8 h. Immunofluorescence confocal microscopy was used to determine the localization of GFP (green) relative to viroplasms (anti-VP2; red) and nuclei (DAPI; blue). Colocalization of GFP and VP2 is yellow in the merged images.

To determine the effect of the L138P lesion on VP1 localization, $VP1_{L138P}$-GFP, $VP1_{WT}$-GFP, or unfused GFP were expressed in Cos-7 cells on glass coverslips at 31°C, 37°C, or 39°C for 48 h (Fig. 4). Thereafter, cells were either mock infected (data not shown) or infected for 12 h at 31°C or 8 h at 39°C. The percentage of expressed $VP1_{WT}$-GFP, $VP1_{L138P}$-GFP, or GFP that colocalized with viroplasms (i.e., anti-VP2 staining) was quantified for several individual cells and averaged (Fig. 5). The expression levels of $VP1_{WT}$-GFP, $VP1_{L138P}$-GFP, and GFP were equivalent at all of the temperatures tested, as determined by average signal intensities and Western blot analyses (data not shown). The results show that, when the infections proceeded at 31°C, the average percent colocalization of $VP1_{L138P}$-GFP with viroplasms was similar to that of $VP1_{WT}$-GFP (Fig. 4A and C and Fig. 5). However, when the infections proceeded at 39°C, the average percent colocalization of $VP1_{L138P}$-GFP with viroplasms was significantly less than that of $VP1_{WT}$-GFP (Fig. 4D, B and F and Fig. 5). Specifically, there was no visible enrichment of $VP1_{L138P}$-GFP in viroplasms at this high temperature, and instead, the mutant protein was largely diffuse (Fig. 4D and F and Fig. 5). In fact, the average percentage of $VP1_{L138P}$-GFP that localized to viroplasms at 39°C was indistinguishable from that of unfused GFP (Fig. 5). Together, these results suggest that the L138P lesion abrogates the ability of VP1 to efficiently be recruited to/retained within viroplasms in a temperature-dependent manner. Interestingly, we noticed that while the ability of $VP1_{L138P}$-GFP to localize to viroplasms was dependent upon the infection temperature, it was independent of the temperature at which the protein was expressed (Fig. 4C to 4F and Fig. 5). For example, even following its expression at 31°C, the average percent colocalization of $VP1_{L138P}$-GFP with viroplasms was still significantly reduced relative to that of $VP1_{WT}$-GFP after 8 h of infection at 39°C (Fig. 4F and Fig. 5). This observation suggests that the increased infection temperature of 39°C can cause defects in $VP1_{L138P}$-GFP, even following its expression (and presumably its proper folding) at the lower temperature of 31°C.

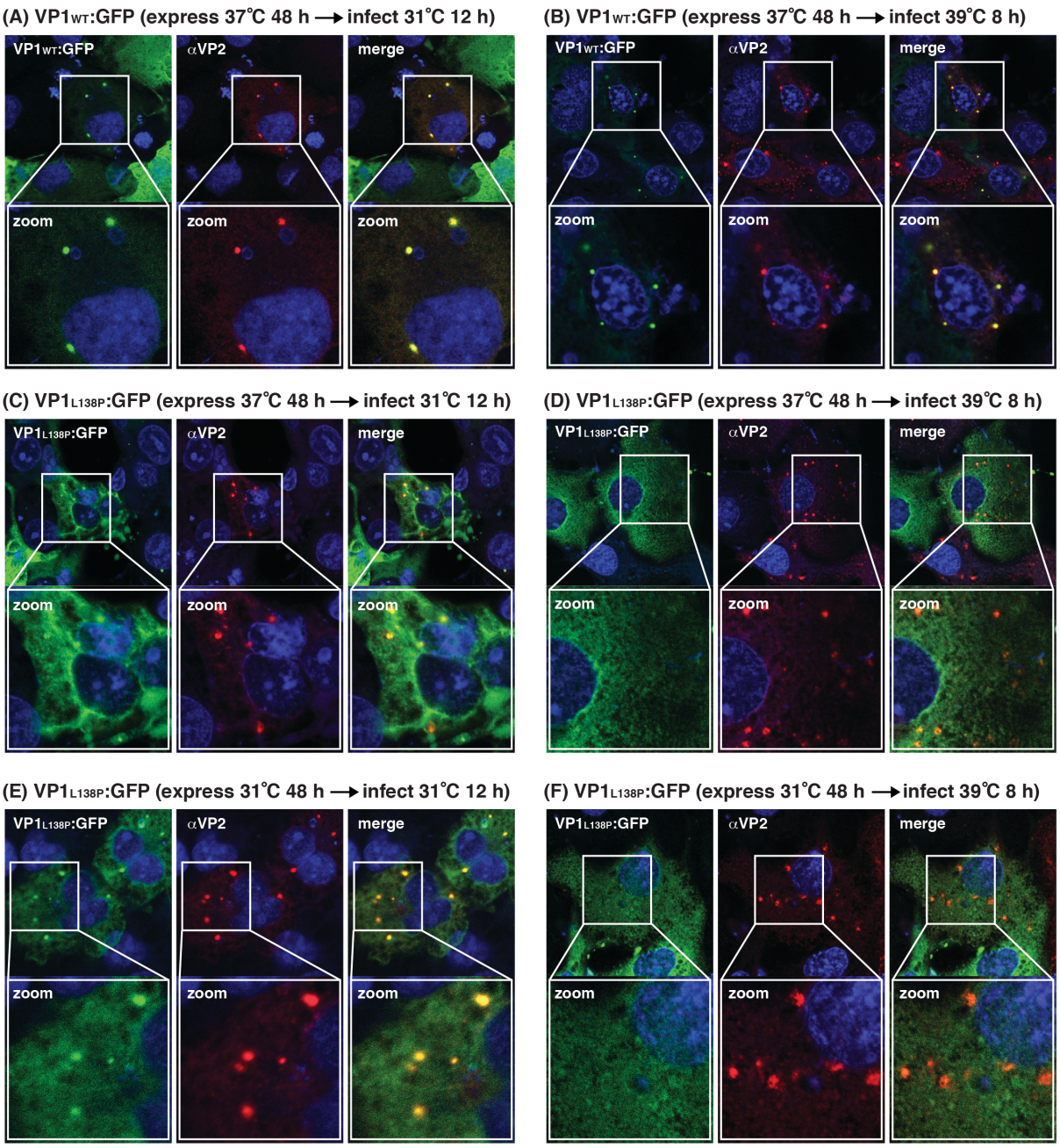

Figure 4-Localization of $VP1_{L138P}$-GFP in infected cells at various temperatures. Cos-7 cells on glass coverslips were transfected with plasmids expressing either $VP1_{WT}$-GFP (A, B) or $VP1_{L138P}$-GFP (C to F). Following their incubation for 48 h at the temperature indicated, the cells were infected with SA11-4F (MOI of 10) at either 31°C for 12 h or 39°C for 8 h. Immunofluorescence confocal microscopy was used to determine the localization of GFP (green) relative to viroplasms (anti-VP2; red) and nuclei (DAPI; blue). Colocalization of GFP and VP2 is yellow in the merged images.

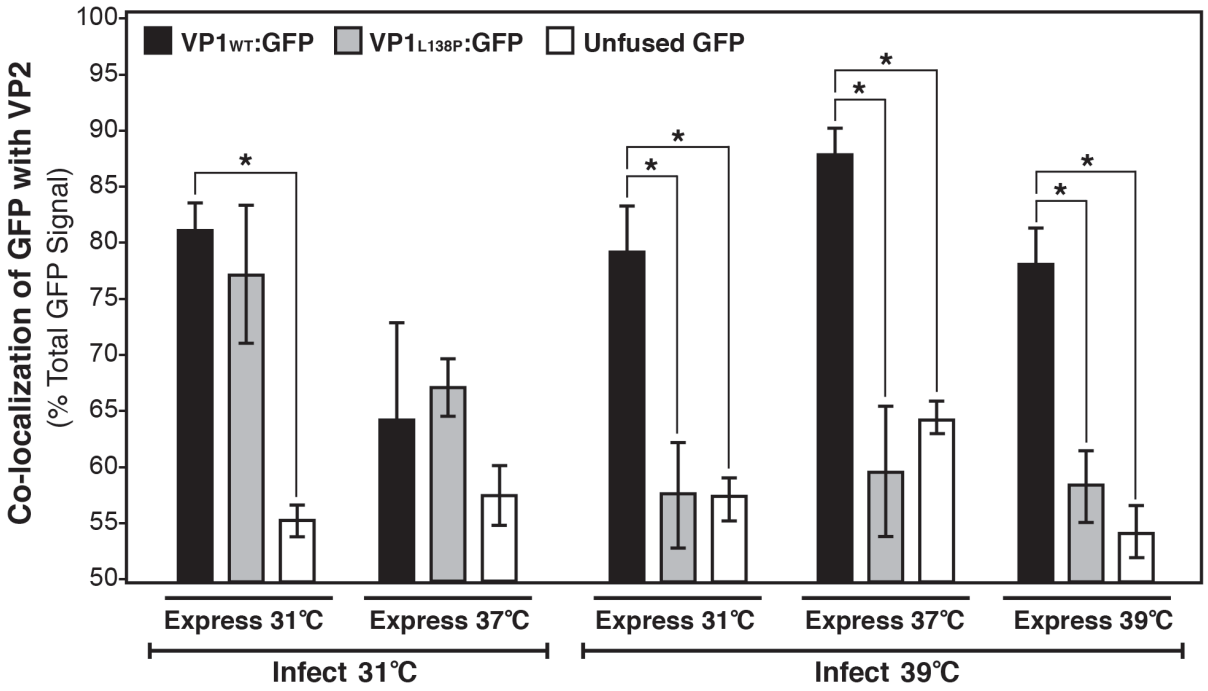

Figure 5-Quantitation of percent colocalization of GFP proteins with VP2. Confocal micrographs of infected, Cos-7 cells expressing $VP1_{WT}$-GFP (black bars), $VP1_{L138P}$-GFP (grey bars), or unfused GFP (white bars) were quantified for percent colocalization with viroplasms (i.e., anti-VP2 staining) at various temperatures with ImageJ software. Approximately four to six cells were quantified for each condition, and averages are shown. Error bars represent the standard deviation from the mean. Asterisks (*) indicate *P* values of <0.01.

The L138P lesion abrogates VP1 interactions with NSP2 and/or NSP5 in a temperature-dependent manner. It has been previously demonstrated that when NSP2 and NSP5 are co-expressed in uninfected cells, they interact to form discrete structures resembling viroplasms (i.e., viroplasm-like structures) (20). It has also been shown that ectopically expressed WT VP1 is recruited to/retained within these inclusions via its interaction(s) with NSP2 and/or NSP5 (21). Therefore, we sought to investigate whether the defect in $VP1_{L138P}$-GFP viroplasmic localization at 39°C was due to lack of interactions with NSP2 and/or NSP5 by testing its ability to localize to viroplasm-like structures. For these experiments, Cos-7 cells on glass coverslips were transfected with plasmids expressing $VP1_{WT}$-GFP or $VP1_{L138P}$-GFP along with WT NSP5 of strain SA11-4F and either WT NSP2 of strain SA11-4F (i.e., $NSP2_{SA11}$) or WT NSP2 of strain SA11-tsC (i.e., $NSP2_{Oagent}$) (Fig. 6). Following incubation of the cells at 31°C or 39°C for 48 h, protein localization was determined using immunostaining and confocal microscopy. Antiserum against NSP2 served as a marker for punctate viroplasm-like structures in cells expressing $NSP2_{SA11}$ (Fig. 6A to D). Antiserum against NSP5 served as marker for punctate viroplasm-like structures in cells expressing the genetically divergent $NSP2_{Oagent}$ (Fig. 6E and F). No punctate structures were detected in cells expressing VP1 and NSP2, but lacking NSP5 (data not shown). The percent of expressed $VP1_{WT}$-GFP or $VP1_{L138P}$-GFP that colocalized with NSP2 or NSP5 in viroplasm-like structures was quantified for several individual cells at both temperatures and averaged (Fig. 7).

Our results show that $VP1_{WT}$-GFP was enriched in punctate inclusions and colocalized with NSP2 or NSP5 (i.e., viroplasm-like structures) at both 31°C or 39°C (Fig. 6A and B and 7). For $VP1_{L138P}$-GFP, however, we observed a temperature-dependent difference in the viroplasm-like structure localization. Specifically, at 31°C the average percent colocalization of $VP1_{L138P}$-GFP with viroplasm-like structures was the same as that of $VP1_{WT}$-GFP (Fig. 6C and E and 7). In contrast, at 39°C, much less $VP1_{L138P}$-GFP than $VP1_{WT}$-GFP colocalized with viroplasm-like structures (Fig. 6D and F and 7). Importantly, the localization of pattern of $VP1_{L138P}$-GFP was the same irrespective of which strain's NSP2 was used (i.e., $NSP2_{SA11}$ or $NSP2_{Oagent}$). These results suggest that the L138P lesion causes a temperature-dependent defect in VP1 that prevents it from binding to NSP2 and/or NSP5, which in turn prevents it from being recruited to/retained within viroplasms.

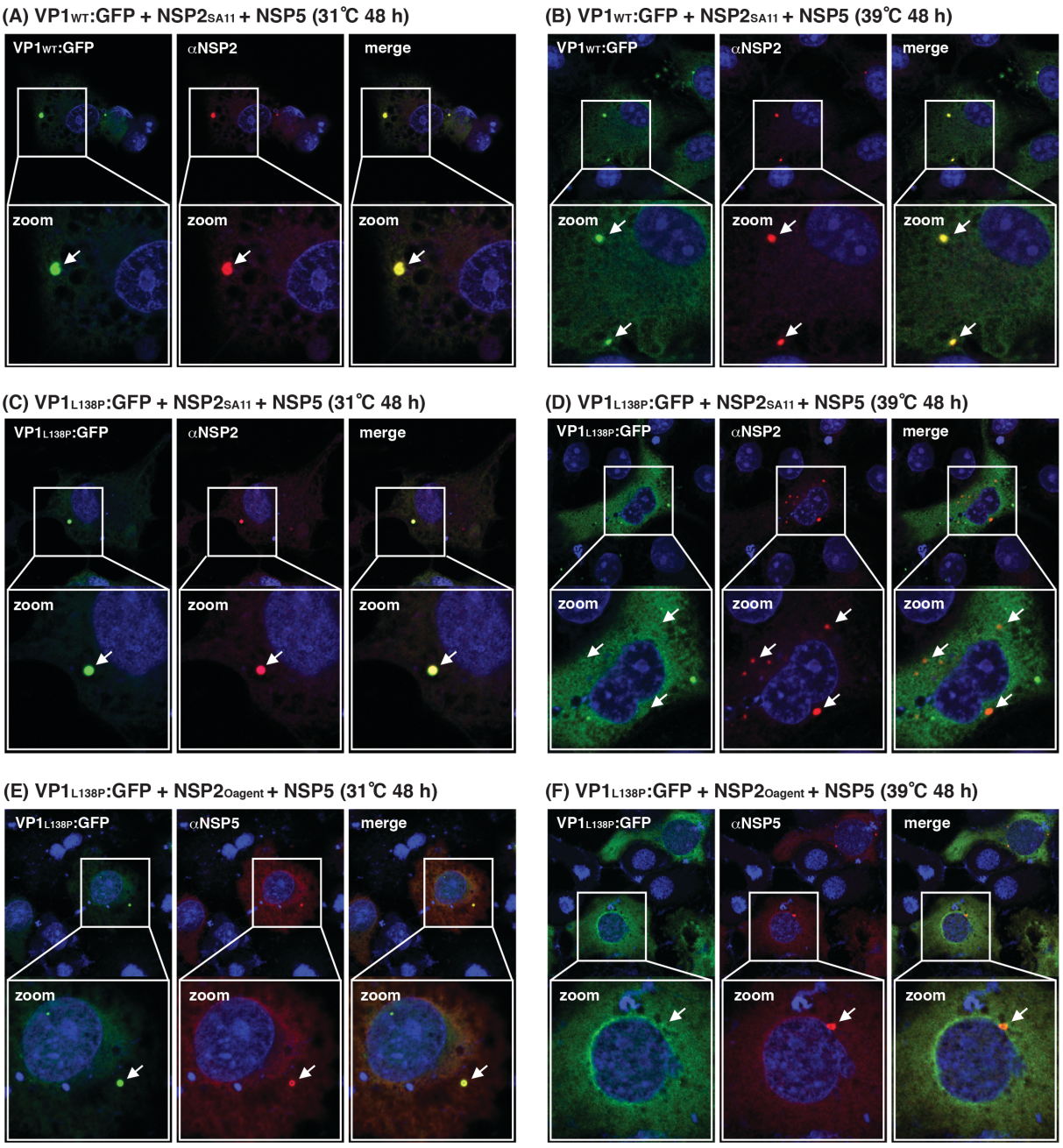

Figure 6-Localization of $VP1_{L138P}$-GFP to viroplasm-like structures at various temperatures. Cos-7 cells on glass coverslips were transfected with plasmids expressing $VP1_{WT}$-GFP, $NSP2_{SA11}$, and NSP5 (A, B); $VP1_{L138P}$-GFP, $NSP2_{SA11}$, and NSP5 (C, D); and $VP1_{L138P}$-GFP, $NSP2_{Oagent}$, and NSP5 (E, F). The temperature and timing of protein expression are indicated. Immunofluorescence confocal microscopy was used to determine the localization of GFP (green) relative to viroplasm like structures (anti-NSP2 or anti-NSP5; punctate red) and nuclei (DAPI; blue). Colocalization of GFP and NSP2/NSP5 is yellow in the merged images. The locations of punctate viroplasm-like structures formed of NSP2 and NSP5 are indicated by arrows in the zoomed images.

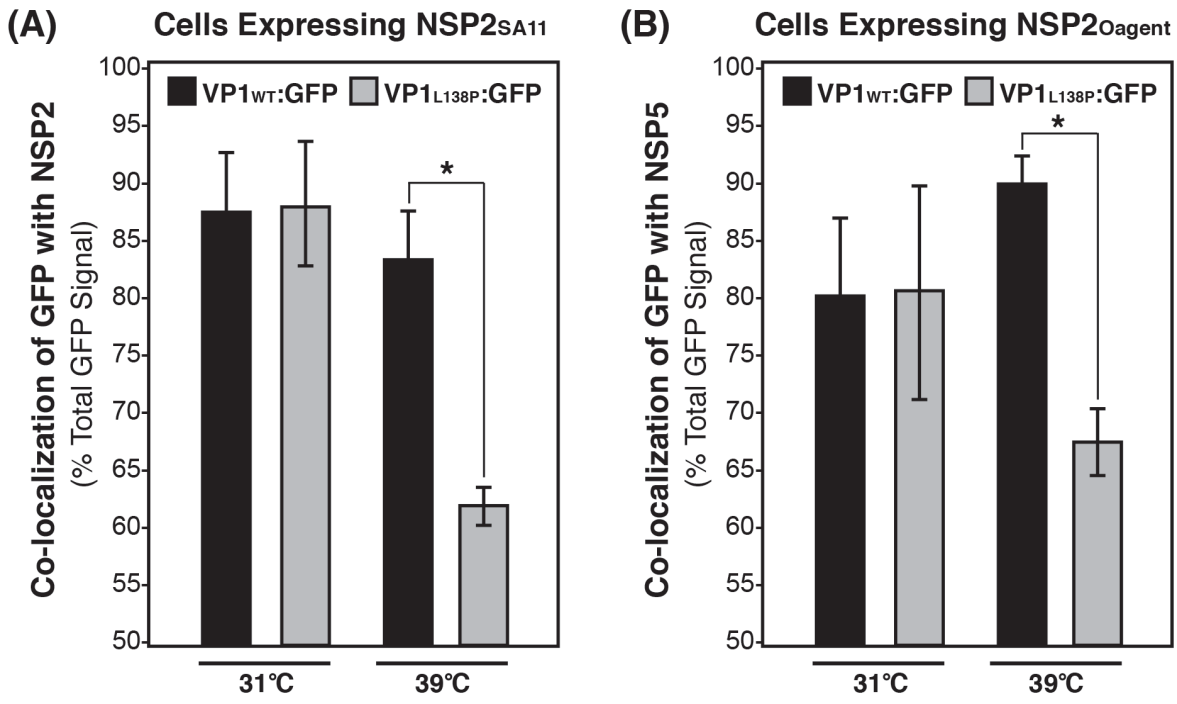

Figure 7-Quantitation of percent colocalization of GFP proteins with viroplasm-like structures. Confocal micrographs of Cos-7 cells expressing either $VP1_{WT}$-GFP (black bars) or $VP1_{L138P}$-GFP (grey bars) along with NSP2 and NSP5 were quantified with ImageJ software for percent colocalization with NSP2 in cells expressing $NSP2_{SA11}$ (A) or NSP5 in cells expressing $NSP2_{Oagent}$ (B). Approximately four to six cells were quantified for each condition, and averages are shown. Error bars represent standard deviation from the mean. Asterisks (*) indicate *P* values of <0.01.

The L138P lesion diminishes VP1 enzymatic activity in a temperature-dependent manner. We next sought to determine if the L138P lesion affects the enzymatic activity of the polymerase. To test this, we expressed and purified the recombinant mutant protein ($rVP1_{L138P}$) and assayed it for the ability to support VP2-dependent dsRNA synthesis *in vitro* at 31°C, 37°C, or 39°C as compared to that of the WT control protein ($rVP1_{WT}$) or a catalytically-inactive mutant ($rVP1_{D632A}$) (Fig. 8). We found that the solubility of $rVP1_{L138P}$ was indistinguishable from $rVP1_{WT}$, even following heating at 39°C for 3 h, suggesting that the recombinant mutant polymerase was not grossly misfolded (Fig. 8A and data not shown). The amount of dsRNA synthesized by $rVP1_{L138P}$ after a 180-min incubation was significantly diminished relative to that of the control at all of the temperatures tested (Fig. 8B and C). In particular, at 31°C, 37°C, 39°C, the levels of RNA produced by $rVP1_{L138P}$ were ~73%, ~63% and ~50%, respectively, of $rVP1_{WT}$ (Fig. 8C). However, the mutant was more sensitive to higher temperatures, as the percentage of dsRNA made by $rVP1_{L138P}$ at 39°C versus 31°C was ~65% of that made at 31˚C while that made by $rVP1_{WT}$ was ~93%, (Fig. 8C). To determine if the temperature-induced defect is reversible, $rVP1_{L138P}$ was incubated at 39°C for 60 min and then assayed for dsRNA synthesis at 31°C for 180 min (Fig. 8D). The results showed that $rVP1_{L138P}$ synthesized less dsRNA synthesis following a high-to-low temperature shift than when it was maintained at 31°C during the entire reaction (Fig. 8D). However, the levels of dsRNA were higher than when $rVP1_{L138P}$ was maintained at 39°C during the entire reaction (Fig. 8D). This result suggests that the temperature-induced defect in $rVP1_{L138P}$ defect was partially reversible or that it was reversible for some fraction of the protein population. Time-course analyses indicated no obvious kinetic delay for $rVP1_{L138P}$ at 39°C, as the levels of dsRNA plateau by 60 min and never reach those of $rVP1_{WT}$ even following longer incubation (Fig. 8E and 8F). These results suggest that the L138P lesion in VP1 reduces its activity in a temperature-dependent manner, possibly because of local structural alterations in the protein.

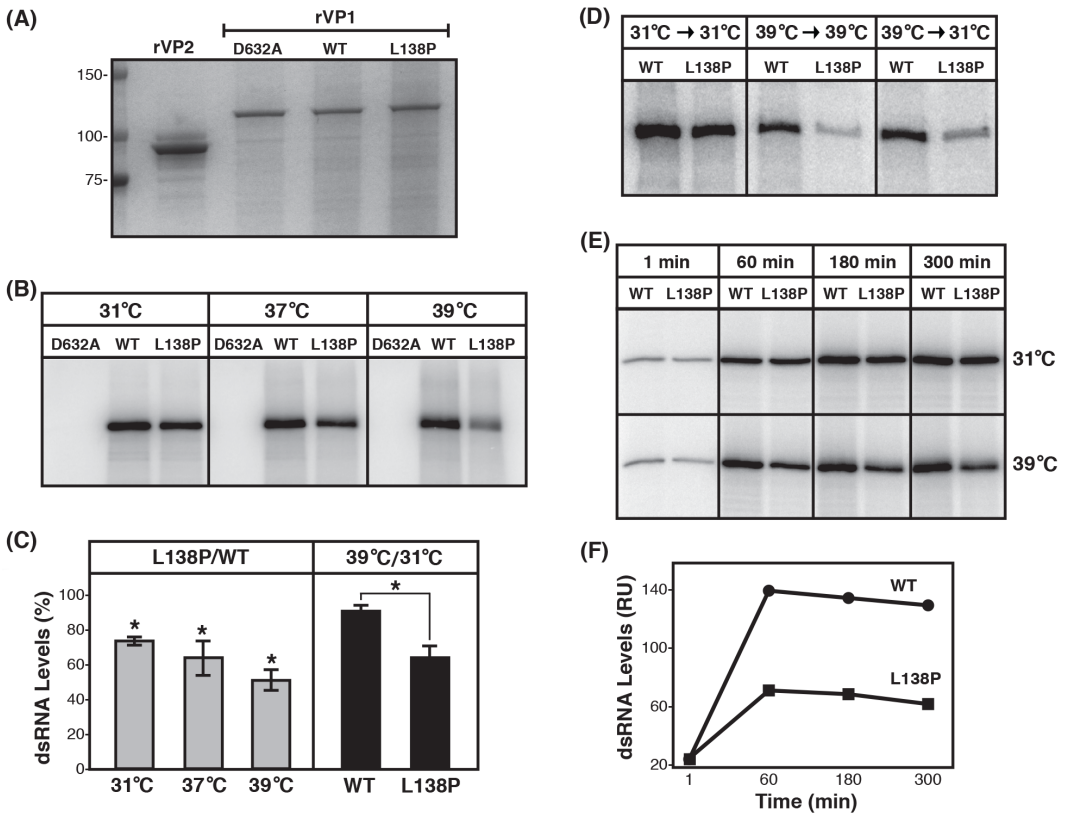

Figure 8-*In vitro* dsRNA synthesis by recombinant VP1 proteins. (A) Purified, recombinant polymerase proteins (rVP1) or core shell protein (rVP2) was electrophoresed in a SDS-polyacrylamide gel and stained with GelCode Blue. Molecular mass standards (in kilodaltons) are shown to the left. WT and catalytically-inactive (D632A mutant) proteins served as positive and negative controls, respectively, for the activity of the mutant (L138P) protein. (B) dsRNA synthesis by rVP1 proteins at various temperatures. Radiolabeled dsRNA product made by each rVP1 during 180-min reactions at 31°C, 37°C or 39°C were electrophoresed in SDS-polyacrylamide gels and detected with a phosphorimager. (C) Quantification of dsRNA levels. The left portion of the graph shows the percentage of dsRNA made by $rVP1_{L138P}$ relative to that made by $rVP1_{WT}$ (L138P/WT). The right portion of the graph shows the dsRNA level made by each protein at 39°C as a percentage of that made at 31˚C (39°C/31°C). Asterisks (*) indicate *P* values of <0.01. (D) dsRNA synthesis by rVP1 proteins following a temperature shift. rVP1 proteins were incubated at either 31°C or 39°C for 60 min prior to being assayed for dsRNA synthesis at 31°C or 39°C for 180 min. dsRNA products were electrophoresed in SDS-polyacrylamide gels and detected with a phosphorimager. (E) Time course of dsRNA synthesis. Radiolabeled dsRNA product made by each rVP1 at indicated times and temperatures were electrophoresed in SDS-polyacrylamide gels and detected with a phosphorimager. (F) Quantification of time course. Radiolabeled dsRNA from three independent experiments was quantified (relative units [RU]). The graph shows the results of a single, representative experiment.

Molecular dynamics simulations of WT and mutant VP1 at high temperature. To gain insight into the possible temperature-induced structural changes resulting from the VP1 L138P lesion, unrestrained molecular dynamics simulations were performed. Structures of WT and L138P mutant VP1 were each simulated for 20 ns at 312K to approximate the conditions under which the mutant shows reduced viroplasmic localization and enzymatic activity (i.e., 39°C). Over the last 5-10 ns of the simulation, both WT and L138P mutant VP1 had similar backbone root mean square deviations compared to the simulation starting structures (data not shown), suggesting that the mutation does not induce a globally destabilizing effect in VP1 at a high temperature. To identify putative locally destabilizing impacts of the L138P mutation, root mean square fluctuations (RMSFs) of the α-carbons (WT VP1 versus L138P mutant VP1) were used to calculate B-factors for each residue. We found small but significant differences in B-factors at positions proximal to 138 (residues S137, L/P138, S140, and L141) (Fig. 9A and B). More dramatic differences were detected for a modeled flexible loop (residues 346 to 358) of the polymerase domain, specifically for residues K348, E350, Y351, and D356 (Fig. 9A and C) (14, 24). Thus, *in silico* analyses predict subtle, temperature-dependent changes in the region proximal to the L138P lesion of the VP1 N-terminal domain, as well as in a distal loop element of the polymerase domain.

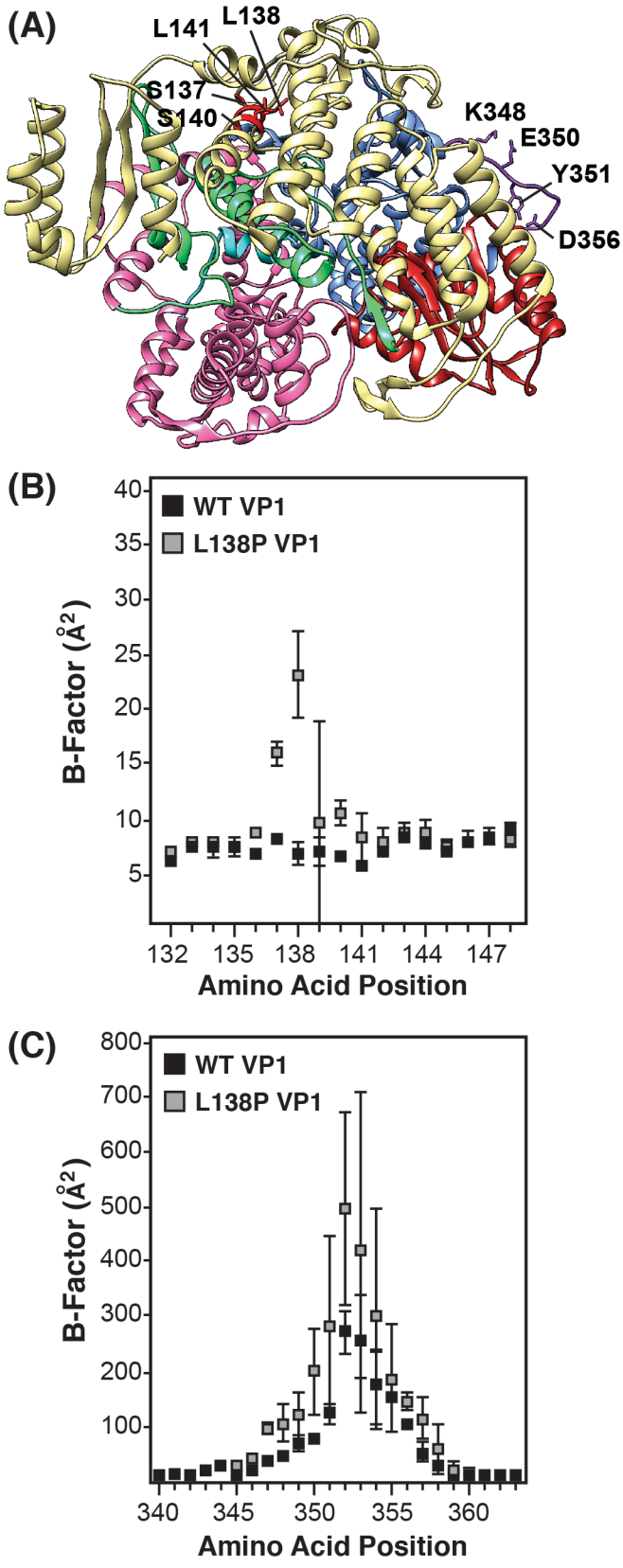

Figure 9-Molecular dynamics simulations of VP1 protein structures. (A) Structure of WT VP1 with modeled loop (residues 346 to 358). The view of WT VP1 is from the back, similar to that shown in Fig. 1B (right). Domains and subdomains are colored as in Fig. 1, except that the modeled loop is purple and the region proximal to L138 is bright red. Residues with significantly different B-factors are shown as stick models and labeled. Average B-factors are shown for the region proximal to position 138 (B) and the modeled loop region (C). In both panels B and C, residue position numbers are shown on the *x* axis, WT VP1 B-factors are plotted as black boxes, and L138P mutant VP1 B-factors are plotted as grey boxes. Error bars represent standard deviation from the mean following three independent simulations.

DISCUSSION

Mutant viruses with *ts* phenotypes have been widely used to interrogate viral protein function and to engineer live-attenuated vaccines (25). Because their mutations are conditionally lethal only at specific temperatures, *ts* mutants are particularly useful when studying viral proteins that are essential for replication or those that mediate multiple, distinct steps of the replication cycle. For RV, several different panels of *ts* mutants have been generated and characterized to varying degrees over the years (5-8). The most well-studied of these were created by using the prototypic simian RV strain SA11-H96 in the early 1980's by Dr. Frank Ramig (7). These so-called 'Baylor mutants' show diminished replication when infections proceed at the non-permissive temperature of 39°C rather than the more permissive temperature of 31°C. By genetically crossing individual mutant clones with rhesus RV and screening for *ts* progeny, Ramig and colleagues mapped the *ts* lesions to individual viral genes (SA11-*ts*A, VP4; SA11-*ts*B, VP3; SA11-*ts*C, VP1; SA11-*ts*E, NSP2; SA11-*ts*F, VP2; and SA11-*ts*G, VP6) (9). However, prior to this study, SA11-*ts*E was the only Baylor mutant whose *ts* phenotype had been biochemically validated at the protein level (26). Here, we provide similar biochemical validation for SA11-*ts*C and show that an L138P mutation in the VP1 protein is a true *ts* lesion that abrogates polymerase localization and enzymatic activity at 39°C.

SA11-*ts*C shows defects in growth, RNA synthesis, protein synthesis, virion morphogenesis and protein localization at 39°C compared to 31°C (10-12). Yet, even when incubated at the lower temperature of 31°C, the mutant still does not replicate as efficiently as WT virus (12). This observation suggests that SA11-*ts*C also has a general replication defect in addition to a *ts* phenotype, and it is possible that the L138P mutation in VP1 is responsible for both effects. In support of this idea, we found that the *in vitro* enzymatic activity of the recombinant mutant $rVP1_{L138P}$ at 31°C was ~27% lower than that of the WT control $rVP1_{WT}$. While modest, such a reduction *in vitro* could translate into larger defects in the infected cell, where multiple rounds of robust RNA synthesis are required for successful infection. Alternatively, it could be the combination of mutations in the SA11-*ts*C genome that account for its poor growth at low temperatures. For instance, we discovered that the SA11-*ts*C NSP2 gene exhibits 203 nucleotide changes (45 amino acid changes) compared to SA11-H96 but that it is 100% identical to the NSP2 gene of O agent strain, which is a putative bovine RV that was

isolated from slaughterhouse remnants (23). SA11-*ts*C likely acquired this NSP2 gene at some point by reassortment with O agent following an unintentional culture contamination. We do not have O agent in our laboratory, suggesting that the contamination occurred during earlier SA11-*ts*C genesis or propagation, similar to what has been reported for other SA11 strains (13). In addition to the reassorted NSP2 gene, we also identified several non-coding changes throughout the genome, as well as five coding changes in VP4 (viral attachment protein), and one coding change each in VP7 (viral outer capsid protein) and NSP1 (viral innate immune antagonist). The five changes in VP4 (T72M, P157S, A187G, Y332S, and V366M) are found in other SA11 derivatives and are reported to correlate with differences in viral plaque size (27). For VP7, the single T60A change is reported in at least one other SA11 sequence in GenBank, but the consequence of this change is not known. The single K39N change for NSP1 is unique to SA11-*ts*C and is not reported for another other group A RV whose sequence is available. It is possible that these mutations together contribute to the general replication defect of SA11-*ts*C. However, reverse genetics would be required to formally test this notion and determine the effect of each mutation on viral replication. Nevertheless, the results of this study shed new light on the mechanistic basis for the phenotype of SA11-*ts*C.

Two distinct classes of *ts* mutant proteins (thermolabile and folding) have been described on the basis of how they behave following low-to-high temperature shift experiments (28). In particular, thermolabile mutants show functional defects at high temperatures, even when they are synthesized at lower, permissive temperatures. In contrast, folding mutants do not show defects when shifted to higher, non-permissive temperatures if they are synthesized at lower, permissive temperatures. Our results suggest that the L138P lesion causes VP1 to behave as a thermolabile mutant as opposed to a folding mutant. For instance, even when $VP1_{L138P}$-GFP was expressed at 31°C, a temperature that allows for proper folding, the mutant protein was still defective in the ability to localize to viroplasms during the 39°C infections. Likewise, *in vitro* dsRNA synthesis by $rVP1_{L138P}$ was diminished at 39°C despite the expression of the protein at room temperature in insect cells. For thermolabile mutants, higher temperatures induce structural alterations of the protein, thereby abrogating its interactions and functions (28). Of course, the extent of the structural alterations (i.e., global versus local) impacts the conclusions that can be drawn from the loss-of-function phenotype. For RV VP1, we think that the L138P lesion causes local alterations at high temperatures as opposed to global changes in the overall

protein fold. In support of this notion, we showed that when $VP1_{L138P}$-GFP was expressed at the high temperature of 37°C, the mutant protein was able to localize to viroplasms with the same efficiency as $VP1_{WT}$-GFP when shifted to 31°C during infection. This result suggests that the ability to target to viroplasms at the lower temperature was restored in some fraction of the mutant VP1 protein population. Likewise, following incubation at 39°C, we found no differences in the solubility of recombinant mutant $rVP1_{L138P}$, and we showed that its activity was partially restored when shifted to 31°C. Because VP1 is a large, globular protein, it is unlikely that we would detect any reversibility of protein function at a low temperature if there were gross structural alterations. Even more, molecular dynamics simulations did not predict a global destabilization of the L138P mutant protein at high temperatures. Instead, the *in silico* analyses showed only subtle temperature-dependent structural changes in a region proximal to the *ts* lesion (i.e., around position 138) and in a flexible loop (residues 346 to 358) that is located in the polymerase domain (14, 24).

If it is the case that the mutation induces only local changes, then the results presented here may shed new light on the functional regions of VP1. The leucine at position 138 is conserved for all group A RVs, and it resides in the N-terminal domain of the protein. In the atomic structure of SA11-4F VP1, the N-terminal domain wraps around one side of the polymerase domain and creates a continuous surface between the finger and thumb subdomains, effectively closing the enzyme (14). While it is not directly involved in catalysis, the N-terminal domain is essential for VP1 activity because it helps create a channel for the entry of single-stranded RNA templates into the catalytic interior and is involved in sequence-specific recognition of viral RNAs (14, 29). The large surface-exposed area of the N-terminal domain may also provide a platform for the binding of regulatory cofactor proteins (e.g., VP2, NSP2, and NSP5), in turn orchestrating VP1 localization and function (15, 17). A leucine at position 138 in the N-terminal domain may be critical for maintaining such intra- and inter-molecular protein interactions. *In silico* simulations of VP1 structural dynamics also revealed that the L138P mutation increases the movement of a highly flexible loop in the polymerase domain (residues 346 to 358), which may impede VP1-protein interaction and/or polymerase activity. Ongoing and future experiments in our laboratory are employing biochemical approaches (e.g., protease accessibility mapping, surface plasmon resonance, gel shift assays, etc.) to further investigate the effect of the L138P mutation on VP1 folding, structural dynamics, protein-protein, and protein-

RNA interactions. We are also keen to elucidate the role, if any, the flexible loop plays in VP1 localization and activity.

In addition to enhancing a mechanistic understanding for the *ts* phenotype of SA11-*ts*C, this study also describes the development of a novel system to study VP1 localization determinants. More specifically, we show that VP1 can target to viroplasms when it is ectopically expressed as a GFP fusion protein. The WT control $VP1_{WT}$-GFP was highly enriched in viroplasms in infected cells at all temperatures tested, suggesting (i) that the fusion protein does not drastically impede viroplasm formation or viral replication and (ii) that the GFP tag does not prevent interactions required for VP1 recruitment to or retention within viroplasms. It was previously shown by Contin et al. that SA11 VP1 with an N-terminal SV5 tag localizes to viroplasm-like structures formed of NSP2 and NSP5, as well as to structures formed of VP2 and NSP5 (21). We did not detect viroplasm-like structure formation using VP2 and NSP5 (data not shown), perhaps because of several experimental differences between our study and the previous one (i.e., differences in RV strain, cell type, fixation method, and protein expression conditions). Nevertheless, our results confirm and extend the finding that ectopically expressed VP1 localizes to inclusions made of NSP2 and NSP5 (21). An advantage of tagging VP1 with GFP, as opposed to SV5, is that it affords an opportunity to perform live-cell imaging. Future experiments in our laboratory will employ $VP1_{WT}$-GFP, $VP1_{L138P}$-GFP, and other engineered mutants to study the temporal dynamics of VP1 viroplasmic localization (timing of recruitment and retention), to identify *cis*-acting residues within VP1 critical for viroplasmic targeting, and to define the *trans*-acting factors (i.e., NSP2, NSP5, VP2, cellular protein, etc.) that regulate polymerase recruitment to and retention within viroplasms. We also seek to determine whether ectopically expressed VP1 can substitute for the virally-expressed protein, as such a *trans*-complementation assay would allow us to probe functional domains of the RV polymerase in the context of the infected cell.

In summary, the results of this study clarify the genetic identity of SA11-*ts*C and validate the contribution of the L138P lesion to the *ts* phenotype of this mutant virus. These results also raise new questions about the importance of leucine 138 in VP1 and describe a novel assay system to investigate VP1 localization determinants. This work is significant because it informs an understanding of RV replication, which may in turn stimulate the development of novel therapeutics to prevent or treat viral disease.

ACKNOWLEDGEMENTS

We thank members of the McDonald laboratory for intellectual and technical support on this. We also thank John Patton (University of Maryland, College Park) for the generous donation of viruses and antisera. Finally, we express our gratitude to John Chappell, Michael Fox, and Jamie Smyth (Virginia Tech Carilion) for assistance with confocal microscopy and image quantitation.

This work was supported through start-up funding from the Virginia Tech Carilion Research Institute and through grants from the National Institutes of Health (R01-AI116815 and R21-AI119588). AOM was also supported by the Biomedical and Veterinary Sciences Graduate Program of the Virginia-Maryland College of Veterinary Medicine and the Virginia Tech Carilion Medical Scholars fund.

REFERENCES

1. **Estes, MK, Kapikian, AZ.** 2007. Rotaviruses and Their Replication, In: Knipe, DM, Howley, PM (Eds). *Fields Virology*. 5th Edition. Lippincott Williams and Wilkens; Philadelphia, p. 1917-1974.
2. **Tate JE, Burton AH, Boschi-Pinto C, Parashar UD, World Health Organization-Coordinated Global Rotavirus Surveillance N**. 2016. Global, Regional, and National Estimates of Rotavirus Mortality in Children <5 Years of Age, 2000-2013. Clin. Infect. Dis. **62**:S96-S105.
3. **Li Z, Baker ML, Jiang W, Estes MK, Prasad BV.** 2009. Rotavirus architecture at subnanometer resolution. J. Virol. **83**:1754-1766.
4. **Settembre EC, Chen JZ, Dormitzer PR, Grigorieff N, Harrison SC.** 2011. Atomic model of an infectious rotavirus particle. EMBO J. **30**:408-416.
5. **Greenberg HB, Kalica AR, Wyatt RG, Jones RW, Kapikian AZ, Chanock RM.** 1981. Rescue of noncultivatable human rotavirus by gene reassortment during mixed infection with ts mutants of a cultivatable bovine rotavirus. Proc. Natl. Acad. Sci. USA **78**:420-424.
6. **Faulkner-Valle GP, Clayton AV, McCrae MA.** 1982. Molecular biology of rotaviruses. III. Isolation and characterization of temperature-sensitive mutants of bovine rotavirus. J. Virol. **42**:669-677.
7. **Ramig RF.** 1982. Isolation and genetic characterization of temperature-sensitive mutants of simian rotavirus SA11. Virology **120**:93-105.
8. **Criglar J, Greenberg HB, Estes MK, Ramig RF.** 2011. Reconciliation of rotavirus temperature-sensitive mutant collections and assignment of reassortment groups D, J, and K to genome segments. J. Virol. **85**:5048-5060.
9. **Ramig RF.** 1983. Isolation and genetic characterization of temperature-sensitive mutants that define five additional recombination groups in simian rotavirus SA11. Virology **130**:464-473.
10. **Ramig RF, Petrie BL.** 1984. Characterization of temperature-sensitive mutants of simian rotavirus SA11: protein synthesis and morphogenesis. J. Virol. **49**:665-673.
11. **Gombold JL, Ramig RF.** 1987. Assignment of simian rotavirus SA11 temperature-sensitive mutant groups A, C, F, and G to genome segments. Virology **161**:463-473.
12. **Chen D, Gombold JL, Ramig RF.** 1990. Intracellular RNA synthesis directed by temperature-sensitive mutants of simian rotavirus SA11. Virology **178**:143-151.
13. **Small C, Barro M, Brown TL, Patton JT.** 2007. Genome heterogeneity of SA11 rotavirus due to reassortment with "O" agent. Virology **359**:415-424.
14. **Lu X, McDonald SM, Tortorici MA, Tao YJ, Vasquez-Del Carpio R, Nibert ML, Patton JT, Harrison SC.** 2008. Mechanism for coordinated RNA packaging and genome replication by rotavirus polymerase VP1. Structure **16**:1678-1688.
15. **McDonald SM, Tao YJ, Patton JT.** 2009. The ins and outs of four-tunneled Reoviridae RNA-dependent RNA polymerases. Curr. Opin. Struct. Biol. **19**:775-782.
16. **Arnoldi F, Campagna M, Eichwald C, Desselberger U, Burrone OR.** 2007. Interaction of rotavirus polymerase VP1 with nonstructural protein NSP5 is stronger than that with NSP2. J. Virol. **81**:2128-2137.

17. **Viskovska M, Anish R, Hu L, Chow DC, Hurwitz AM, Brown NG, Palzkill T, Estes MK, Prasad BV.** 2014. Probing the sites of interactions of rotaviral proteins involved in replication. J. Virol. **88**:12866-12881.
18. **McDonald SM, Patton JT.** 2011. Rotavirus VP2 core shell regions critical for viral polymerase activation. J. Virol. **85**:3095-3105.
19. **Trask SD, McDonald SM, Patton JT.** 2012. Structural insights into the coupling of virion assembly and rotavirus replication. Nat. Rev. Microbiol. **10**:165-177.
20. **Fabbretti E, Afrikanova I, Vascotto F, Burrone OR.** 1999. Two non-structural rotavirus proteins, NSP2 and NSP5, form viroplasm-like structures in vivo. J. Gen. Virol. **80**:333-339.
21. **Contin R, Arnoldi F, Campagna M, Burrone OR.** 2010. Rotavirus NSP5 orchestrates recruitment of viroplasmic proteins. J. Gen. Virol. **91**:1782-1793.
22. **Guglielmi KM, McDonald SM, Patton JT.** 2010. Mechanism of intraparticle synthesis of the rotavirus double-stranded RNA genome. J. Biol. Chem. **285**:18123-18128.
23. **Malherbe HH, Strickland-Cholmley M.** 1967. Simian virus SA11 and the related O agent. Arch Gesamte Virusforsch **22**:235-245.
24. **McDonald SM, Aguayo D, Gonzalez-Nilo FD, Patton JT.** 2009. Shared and group-specific features of the rotavirus RNA polymerase reveal potential determinants of gene reassortment restriction. J. Virol. **83**:6135-6148.
25. **Fenner F.** 1969. Conditional lethal mutants of animal viruses. Curr. Top. Microbiol. Immunol. **48**:1-28.
26. **Taraporewala ZF, Schuck P, Ramig RF, Silvestri L, Patton JT.** 2002. Analysis of a temperature-sensitive mutant rotavirus indicates that NSP2 octamers are the functional form of the protein. J. Virol. **76**:7082-7093.
27. **Taniguchi K, Nishikawa K, Kobayashi N, Urasawa T, Wu H, Gorziglia M, Urasawa S.** 1994. Differences in plaque size and VP4 sequence found in SA11 virus clones having simian authentic VP4. Virology **198**:325-330.
28. **Sadler JR, Novick A.** 1965. The properties of repressor and the kinetics of its action. J. Mol. Biol. **12**:305-327.
29. **Ogden KM, Ramanathan HN, Patton JT.** 2011. Residues of the rotavirus RNA-dependent RNA polymerase template entry tunnel that mediate RNA recognition and genome replication. J. Virol. **85**:1958-1969.
30. **Arnold M, Patton JT, McDonald SM.** 2009. Culturing, storage, and quantification of rotaviruses. Curr. Protoc. Microbiol. Chapter 15:Unit 15C 13.
31. **Schneider CA, Rasband WS, Eliceiri KW.** 2012. NIH Image to ImageJ: 25 years of image analysis. Nat. Methods **9**:671-675.
32. **Ogden KM, Ramanathan HN, Patton JT.** 2012. Mutational analysis of residues involved in nucleotide and divalent cation stabilization in the rotavirus RNA-dependent RNA polymerase catalytic pocket. Virology **431**:12-20.
33. **Tortorici MA, Broering TJ, Nibert ML, Patton JT.** 2003. Template recognition and formation of initiation complexes by the replicase of a segmented double-stranded RNA virus. J. Biol. Chem. **278**:32673-32682.
34. **Abraham MJ, Murtola T, Schulz R, Páll S, Smith JC, Hess B, Lindahl E.** 2015. GROMACS: High performance molecular simulations through multi-level parallelism from laptops to supercomputers. SoftwareX **1–2**:19–25

35. **Sali A, Blundell TL.** 1993. Comparative protein modelling by satisfaction of spatial restraints. J. Mol. Biol. **234**:779-815.
36. **Pettersen EF, Goddard TD, Huang CC, Couch GS, Greenblatt DM, Meng EC, Ferrin TE.** 2004. UCSF Chimera--a visualization system for exploratory research and analysis. J. Comput. Chem. **25**:1605-1612.
37. **Lindorff-Larsen K, Piana S, Palmo K, Maragakis P, Klepeis JL, Dror RO, DE.** 2010. Improved side-chain torsion potentials for the Amber ff99SB protein force field. Proteins. **78**: 1950–1958.

Chapter 3

Characterization of the Strain-Specificity of VP1 Localization and the Non-sufficiency of the N-terminal Domain

ABSTRACT

Viroplasms are inclusions formed in rotavirus (RV)-infected cells that are made up of viral proteins and are the sites of genome replication and early particle assembly. In order for genome replication to occur, the RV RNA-dependent RNA polymerase (RdRp), VP1, needs to localize to these viral factories. The method through which VP1 is recruited to/retained within viroplasms remains unknown. It could be that there are *cis*-acting element(s) within the structure of VP1 that act as targeting signals and that viral cofactors are acting in-*trans* to chaperone the polymerase to viroplasms. Previous work has suggested that the VP1 N-terminal domain (NTD) contains determinants of its viroplasmic localization. In this study, we engineered three new VP1-EGFP fusion proteins to test: SA11 VP1 NTD-only, PO-13 VP1, and Bristol VP1. These fusion proteins were expressed within cells on glass cover slips that were then infected with wild-type simian SA11 RV. The coverslips were stained using immunohistochemistry and imaged by confocal microscopy. We found that none of the three EGFP fusion proteins were able to colocalize with viroplasms. These results demonstrated that the VP1 NTD is not sufficient for the polymerase to localize to viroplasms. In addition, the failure of PO-13 (avian RV strain) and Bristol (human group C RV strain [RVC]) to localize with SA11 infection-induced viroplasms suggests that polymerase localization could be dependent on species-specific differences. These immunofluorescent experiments were augmented by structural analysis performed on SA11 VP1 using the PoPMuSiC-2.1 algorithm, which yielded interesting insights that can also drive the development of VP1 structure-function hypotheses. Indeed, further work will be needed to more fully define determinants of VP1 localization to viroplasms.

INTRODUCTION

RV is a non-enveloped, triple-layered, double-stranded RNA virus in the family *Reoviridae* (19). It causes severe, watery diarrhea that can lead to death due to rapid dehydration (16). The RV particle is formed by three co-centric, icosahedral layers that surround an eleven-segmented, double-stranded RNA genome (19). These segments code for six structural (VP1, VP2, VP3, VP4, VP6, and VP7) and five to six nonstructural (NSP1, NSP2, NSP3, NSP4, NSP5, and NSP6) viral proteins (10). Additionally, the RV polymerase, VP1, and capping enzyme, VP3, are also found within the core of the virion (19).

Central to RV genome replication and early particle assembly are the formation of viral inclusions in the host cell cytoplasm called 'viroplasms' (5, 6, 12). These inclusions are dense and protein-rich, making it difficult to discern the processes that occur within them. Thus, RV replication remains poorly understood. One important step in replication is for the viral polymerase, VP1, to travel to the viroplasm where it can synthesize dsRNA in a protected environment (12). Some insights into the intramolecular components of VP1 that may be important for this localization have been reported.

VP1 is the viral RdRp and is encoded by RV gene segment 1 (10, 20). The structure of VP1 is globular and cage-like, formed by three domains: the N-terminal domain (NTD), the polymerase domain, and the C-terminal domain (CTD) (9). The central polymerase domain forms a canonical right-handed polymerase structure with fingers, palm, and thumb subdomains (9). Buried at the heart of the structure lies the enzyme's active site where catalysis of RNA polymerization occurs (9). Members of the Reoviridae family all possess 'accessory domains' at the N-terminus and C-terminus in addition to their canonical polymerase domains (11). These extra domains serve to physically form the RV RdRp, including its unique four-tunneled architecture (9). The CTD forms a 'bracelet,' and it also contains an α-helical 'plug' subdomain (9). The NTD wraps around the polymerase and anchors the fingers and thumb subdomains (9). In addition to forming the tunnels, the NTD and CTD likely serve other functions as has been demonstrated by work on the Bluetongue virus (BTV) polymerase (21). Moreover, a temperature-sensitive mutant of SA11 VP1 (SA11-tsC) has replication-related phenotypes (7). This virus' VP1 gene possesses a single amino acid change—leucine to proline at residue 138 (L138P)—and is RNA and protein synthetic deficient at non-permissive temperature (39˚)(2, 15,

18). Cells infected by this virus and incubated at 39˚C also exhibit viral protein mislocalization and produce larger-than-normal amounts of empty capsids (15). Recent work described in detail in this dissertation used an ectopic expression system to deduce whether this L138P mutation caused the SA11 VP1 protein to share the SA11-tsC phenotypes (14). It was found that the lesion did lead to VP1 to be unable to localize/remain retained within infected-cell viroplasms, and it negatively impacted VP1's enzymatic capacity in a temperature-dependent manner (14). Interestingly, this mutation resides in the NTD of the polymerase, and the resulting abrogation of VP1 viroplasmic localization strongly suggests that the NTD may play role in this function. Further, this study implicated that the mutation may be affecting VP1 localization by interfering with interactions with viral nonstructural proteins, NSP2 and/or NSP5, which are critical for viroplasm formation (5, 6, 14).

In this study we sought to further probe residues and/or regions of VP1 that may be important for the polymerase to localize to viroplasms during infection. We created three additional EGFP fusion proteins that included an SA11 NTD-only mutant as well as the VP1s of strains divergent from simian strain SA11 RV (PO-13 and Bristol). The EGFP fusion proteins were expressed in cells that were then infected with RV strain SA11. The cells were then stained using antibodies that detect SA11 viroplasmic proteins and imaged using confocal microscopy. We found that none of the three new EGFP fusion proteins were able to colocalize with SA11 proteins in infected cell viroplasms. The wildtype control SA11 VP1-EGFP fusion protein, in contrast, localized to viroplasms. In addition to the localization experiments, we also performed bioinformatics analyses on the protein sequence and structure of SA11 VP1. That data further supported the results from previous modeling experiments and provided more evidence that the VP1 NTD is a functionally important component of the polymerase.

MATERIALS AND METHODS

Monkey kidney cells and RVs. Monkey kidney cell lines (MA104 and Cos-7) were obtained from American Type Cell Culture and maintained as described by Arnold et al. (1), in either Medium 199 (Life Technologies) or DMEM (Life Technologies) that was supplemented to contain 10% heat-inactivated fetal bovine serum, 100 U/ml penicillin, 100 μg/ml streptomycin,

and 0.5 μg/ml Amphotericin B (1). Wildtype (WT) SA11-4F was generously provided by Dr. John Patton (University of Maryland, College Park). Infections with WT SA11-4F were performed as described previously (1). Guinea pig polyclonal antisera against VP2 (αVP2-SM) was generated against baculovirus-expressed, recombinant protein (SA11-4F strain) by Pocono Rabbit Farm and Laboratory, Inc. (Canadensis, PA). Guinea pig polyclonal sera against NSP2 (αNSP2-53962) and NSP5 (αNSP5-53964) was generously provided by Dr. John Patton (University of Maryland, College Park). AOM performed this work.

Localization of WT and mutant VP1s as GFP-fusion proteins in mock or infected cells. The N-terminal domain (NTD) sequence of WT SA11 VP1 as well as the ORF sequences of WT PO-13 VP1 and WT Bristol VP1 were cloned into the pEGFP-N1 vector (Clonetech) to express the polymerases with enhanced GFP fused to their C-termini (SA11 $VP1_{NTD}$-GFP, PO-13 $VP1_{WT}$-GFP, Bristol $VP1_{WT}$-GFP respectively). The WT SA11-4F VP1 NTD-coding region (nucleotides 1-996 and amino acid residues 1-332) was amplified from the pENTR-SA11 VP1 vector using PCR. Similarly, the PO-13 VP1 ORF and Bristol VP1 ORF were amplified from the codon-optimized pENTR-PO-13 VP1 and pENTR-Bristol VP1 vectors, respectively, using PCR (137). Primer-generated restrictions sites (5' *Sac I* and 3' *Kpn I* for SA11 VP1 NTD and Bristol VP1; 5' *Nhe I* and 3' *Bam HI* for SA11 VP1 NTD) were used to subclone the WT SA11-4F VP1 NTD, WT PO-13 VP1, and WT Bristol VP1 into the pEGFP-N1 vector, thereby creating pEGFP-SA11-$VP1_{NTD}$, pEGFP-PO-13-$VP1_{WT}$, pEGFP-Bristol-$VP1_{WT}$, which expresses SA11 $VP1_{NTD}$-GFP, PO-13 $VP1_{WT}$-GFP, Bristol $VP1_{WT}$-GFP, respectively. All expression vectors were sequenced to verify the integrity of the VP1 NTD or ORF, maintenance of the translational frame with GFP, and the absence of second-site mutations.

To express SA11 $VP1_{NTD}$-GFP, PO-13 $VP1_{WT}$-GFP, Bristol $VP1_{WT}$-GFP, SA11 $VP1_{WT}$-GFP, or the unfused GFP control, Cos-7 cells grown on glass coverslips in 12-well plates (~0.5 x 10^6 cells/well) were transfected with 1 μg of plasmid DNA (pEGFP-SA11-$VP1_{NTD}$, pEGFP-PO-13-$VP1_{WT}$, pEGFP-Bristol-$VP1_{WT}$, or the pEGFP-N1 empty vector, respectively) using Trans-IT®-LT1 (Mirus) according to the manufacturer's instructions. The transfected cells were incubated for 48 h at 37°C to allow for protein expression. The transfected cells were then either mock infected or infected with SA11-4F at a multiplicity of infection (MOI) of 10 plaque-forming units (pfu) per cell. Infections proceeded at 37°C. At 8 h post-infection (p.i.), the cells

on coverslips were washed once with Dulbecco's phosphate-buffered saline (DPBS) prior to being fixed and permeabilized by incubation in 100% methanol for 5 min at room temperature. The coverslips were then stored in DPBS at 4°C for <3 d prior to immunostaining. AOM performed this work.

Immunostaining and confocal microscopy. Coverslips were blocked overnight at 4°C with rocking using a solution of 5% bovine serum albumin (BSA) in DPBST (1.6 mM KH_2PO_4, 2.7 mM KCl, 8.1 mM N_2HPO_4, 137.1 mM NaCl, and 0.1% Triton X100). Following 3×10-min washes with DPBST, primary guinea pig antisera was added at a 1:1,000 dilution in a solution of 2.5% BSA in DPBST for 1 h at room temperature with rocking. Following 3×10-min washes with DPBST, the Alexa Fluor® 546 goat anti-guinea pig IgG (Life Technologies) secondary antibody was added at a 1:10,000 dilution in 2.5% BSA in DPBST for 30 min at room temperature with rocking. Following 3×10-min washes with DPBST, the stained coverslips were inverted and mounted onto glass microscope slides using the ProLong® Diamond Antifade Mountant with DAPI (Life Technologies). The slides cured for >24 h at room temperature, protected from light, prior to imaging.

Imaging was performed using a Zeiss LSM 880 inverted laser-scanning confocal microscope using the 63× oil immersion objective and the 405-nm, 488-nm, 561-nm laser lines. The following settings were used for all images: pinhole=1 AU, digital offset=0, and digital gain=1.0. Amplitude and master gain were optimized for each image to prevent pixel saturation. Quantification of unmodified images were performed using ImageJ (17). Specifically, binary masks of images were used to independently calculate green signal and red signal in each cell. The percent of total green signal that colocalized with red signal for each cell was determined by subtracting the masks. Averages were obtained using 4-6 cells per condition tested. Two-sample t-tests of the mean were performed for each data set using Smith's Statistical Package, version 2.80. *P* values of <0.01 were considered statistically significant. Representative confocal micrographs of each condition were minimally modified for Hue/Saturation and Brightness/Contrast using Adobe Photoshop (Ver. 13.0). AOM performed this work.

Protein Alignments and PoPMuSiC Protein Structure Modeling and Analysis. Nucleotide sequences for the VP1 genes of multiple RV strains (SA11, PO-13, Bristol, ETD,

Wa, DS-1, Au-1) were imported into Geneious© Pro v6.8.1 (Biomatters, Inc.) from GenBank (X16830, [codon-optimized from AB009629], NC_007547, GQ479947, DQ490539, DQ870505, and DQ490533, respectively). Each of the nucleotide sequences was trimmed to remove the untranslated regions (UTRs), leaving the open-reading frame (ORF) for analysis. The trimmed nucleotide sequences were then converted to amino acid sequences. To identify amino acid differences, the protein sequences were aligned using the ClustalW plugin.

The SA11 VP1 crystal structure was imported into the PoPMuSiC-2.1 algorithm (http://dezyme.com/) (4) from the Protein DataBank (Protein Data Bank no. 2R7Q). PoPMuSiC was applied to search for amino acid substitutions that could possibly affect the thermostability of the polymerase. AOM performed this work.

RESULTS AND DISCUSSION

Construction of SA11 VP1 NTD-EGFP, PO-13 VP1-EGFP, and Bristol VP1-EGFP plasmids: After an initial study using a temperature-sensitive mutant of SA11 VP1, we sought to further identify residue(s) and/or regions of VP1 that are important for polymerase localization and/or retention to virosplasms in rotavirus-infected cells. The N-terminus of SA11 VP1 was excised from the full-length SA11 VP1 gene to form an insert using PCR that also added 5' and 3' restriction enzyme sites. Then, a similar cloning strategy as described in McKell et al. (14) was used to insert it into the pEGFP-N1 vector. In addition, this strategy was employed to insert the VP1 genes of strains PO-13 (group A avian rotavirus) and Bristol (group C human rotavirus) into pEGFP-N1. Each of these sequences was successfully engineered into pEGFP-N1 as verified by Sanger sequencing. Moreover, the constructs could be transfected into monkey kidney cells. Imaging of cells transfected with any of the three plasmids showed green fluorescent signal that indicated the EGFP was properly expressed and remained in-frame. Thus, the SA11 VP1 N-terminus, PO-13 VP1, and Bristol VP1 were successfully cloned into pEGFP-N1.

The SA11 VP1 NTD is not sufficient to mediate polymerase viroplasmic localization during infection: In order to discern whether the NTD alone was sufficient to VP1 localization

to infected cell viroplasms, amino acids 1-332 of the SA11 NTD was expressed as a GFP fusion protein (i.e., SA11 $VP1_{NTD}$-GFP) for 48 hours at 37˚C in Cos-7 cells grown on glass coverslips. After the initial incubation, transfected cells were then infected with wild-type SA11 RV for 8 hours, and the cover slips were then fixed and permeabilized using methanol. Coverslips were stained using an antibody against a viral protein also found in the viroplasm (VP2) and were imaged using confocal microscopy. The pattern of colocalization for SA11 $VP1_{NTD}$-GFP showed no discernable difference from the GFP-only control. Green signal from GFP was dispersed throughout the cell with no concentration evident around the red-stained (Alexa 546) viroplasmic puncta (Figure 1A.). In contrast, the full-length SA11 VP1 control protein (SA11 $VP1_{WT}$-GFP) colocalized with VP2 staining. This result suggests that the SA11 VP1 NTD is not sufficient to localize to viroplasms and indicates a role for other parts of VP1 for this function. While this result is not necessarily surprising, it is interesting since our previous work has demonstrated that the SA11 VP1 NTD is necessary for the protein to localize to the viroplams of infected cells (14). Indeed, as described in work in Chapter 2, a single amino acid change located in the NTD of VP1 is enough to significantly reduce its ability to localize to viroplasms (14). It is possible that truncating VP1 to the NTD-only insert could have led to protein misfolding, abrogating localization signals or hindering interactions with potential cofactor proteins. In order to work around this limitation and to test the strain/sequence specificity of VP1 localization, other fusion proteins were engineered using the VP1's of rotavirus strains genetically divergent from SA11 (see below).

Neither PO-13 VP1 nor Bristol VP1 localize to SA11 RV viroplasms when expressed as GFP fusion proteins: We next sought to determine whether the VP1's of genetically divergent RV strains would localize to viroplasms in SA11-infected cells. The VP1 gene from an avian group A RV (RVA) strain, PO-13, and a human group C RV strain (RVC), Bristol, were expressed as fusion proteins to GFP (PO-13 $VP1_{WT}$-GFP or Bristol $VP1_{WT}$-GFP, respectively) in Cos-7 cells on glass coverslips for 48 hours at 37˚C. The cells were then infected with wildtype simian RV strain SA11 for 8 hours. Coverslips were fixed and permeabilized using methanol, and then they were stained with antibodies against SA11 VP2, which is a viral protein also found in viroplasms. Confocal microscopy was used to obtain images of cells that both expressed the fusion protein and were infected with SA11.

The results show that both PO-13 $VP1_{WT}$-GFP or Bristol $VP1_{WT}$-GFP were successfully expressed in the Cos-7 cells. PO-13 $VP1_{WT}$-GFP did not localize to viroplasms of Cos-7 cells infected with wildtype SA11 RV. Again, the GFP signal was dispersed throughout the cell similar to the EGFP-only control rather than colocalized with viroplasmic puncta (Figures 1B. and 1C.). SA11 is a RVA, so in theory PO-13 VP1 could be homologous enough to SA11 VP1 target to viroplasms in SA11-infected cells. However, while PO-13 is RVA, it is still a strain from a different species (avian vs. simian), and its VP1 gene is 24-23% genetically divergent from the mammalian RVA VP1s based upon amino acid sequences (8). It is possible that PO-13 VP1 could localize to SA11-induced viroplasms if the infection occurred in an avian rather than a simian cell type if host-cell factors contribute to VP1 viroplasmic localization. Indeed, it could be that in addition to *cis*-acting elements of VP1 that aid in its localization that host cell factors play a role also. However, it is more likely that VP1 localization to viroplasms could be rescued by using cognate NSP2 and NSP5 proteins. Similar to PO-13 VP1, Bristol $VP1_{WT}$-GFP also did not colocalize with SA11 viroplasms. This result is less surprising, as Bristol is from an entirely different group (C), and RVC VP1 genes have been found to be 45.2% divergent from that of RVAs based on amino acid sequences (3). Since Bristol is a human strain, it was possible that it would localize when PO-13 did not due to SA11 and Cos-7 being simian-related and thus more closely related from a species standpoint. Similar to PO-13, it is more probable that using cognate NSP2 and NSP5's would rescue Bristol VP1 localization. While it is disappointing that neither of these VP1s were able to target to viroplasms, there is still important information to be gleaned from analyzing these results in conjunction with protein sequence alignments.

Figure 1

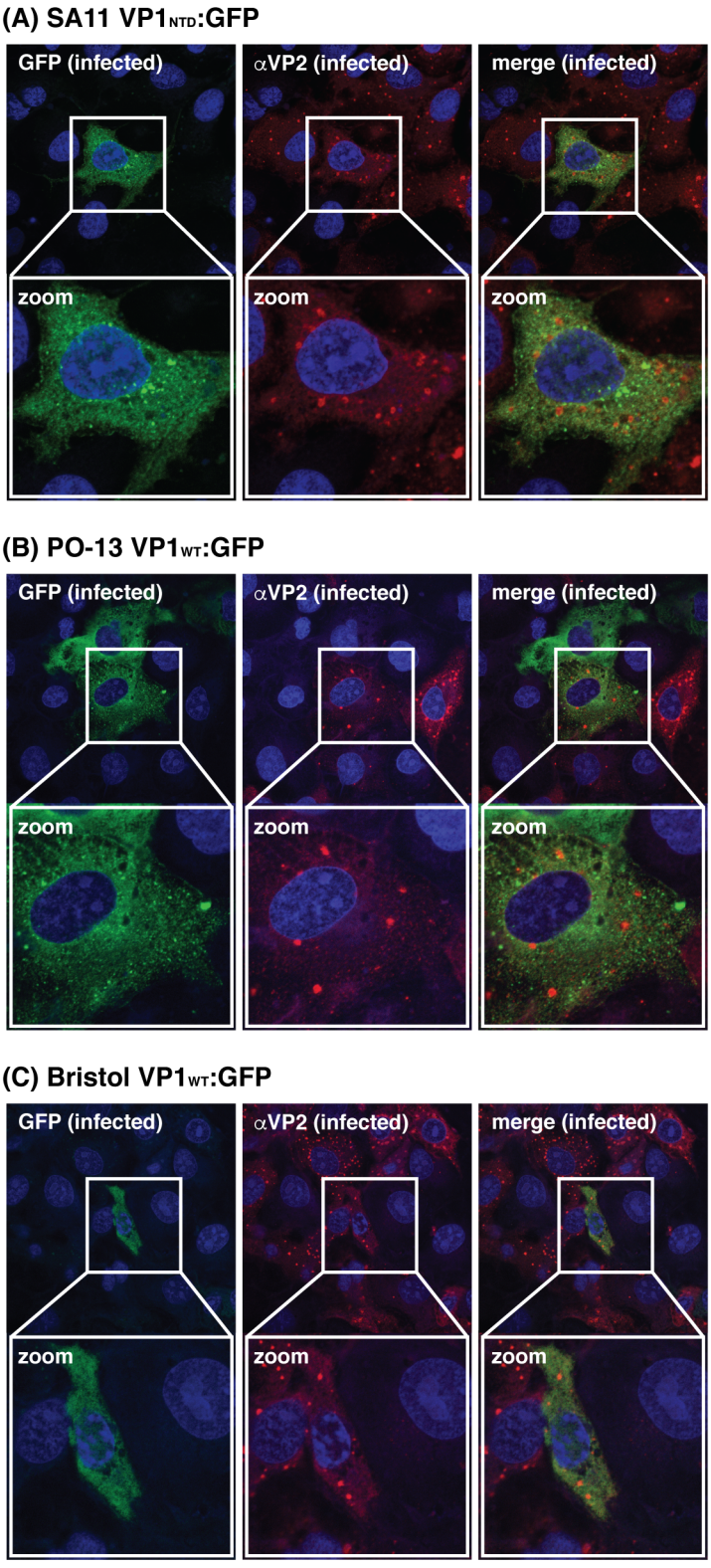

Figure 1-Ectopically-expressed SA11 VP1 NTD, PO-13 VP1, and Bristol VP1 do not localize to viroplasms as GFP-fusion proteins. Cos-7 cells on glass coverslips were transfected with plasmids expressing either (A) the WT SA11 VP1 NTD fusion protein, SA11 $VP1_{NTD}$-GFP, (B) the WT PO-13 VP1 fusion protein, PO-13 $VP1_{WT}$-GFP, or (C) the WT Bristol fusion protein, Bristol $VP1_{WT}$-GFP. Following their incubation at 37°C for 48 h, the cells were either mock-infected or infected with SA11-4F (MOI=10) at 37°C for 8 h. Immunofluorescence confocal microscopy was used to determine the localization of GFP (green) relative to viroplasms (αVP2; red) and nuclei (DAPI; blue). Co-localization of GFP and VP2 is shown as yellow in the merged images.

Bioinformatic analysis of the protein sequence of SA11 VP1 provides interesting insights: We next used bioinformatics approaches to further identify possible residue(s) of interest for VP1 localization to viroplasms. First, we performed amino acid sequence alignments of VP1s from strains SA11, PO-13, and Bristol in order to map potential areas of interest that could account for the differences seen between these strains in the localization experiments. The amino acid sequences between RV polymerases tend to be fairly conserved between strains. Thus, portions of the sequence alignments that are either very conserved or variable between strains or groups of RVs can point to areas of functional importance on the structure of VP1. The leucine at position 138 of VP1 is a residue that is conserved amongst most RV strains, especially all RVAs (14, Small et al., 2007). For those strains that possess a different residue, it is isoleucine (Figure 2.; full VP1 ORF alignment in Appendix A). Isoleucine is similar to leucine in that it also has a hydrophobic side chain and is comparably bulky, which would likely preserve the polymerase's conformation.

In addition to sequence alignments, the Protein DataBank structure file of the RV VP1 apoenzyme (Protein Data Bank accession no. 2R7Q) was uploaded into the PoPMuSiC-2.1 algorithm. This server uses a compilation of statistical calculations to predict changes in thermodynamic stability. According to its developers, it's also useful "to detect structural weaknesses, i.e., clusters of non-optimal residues, which represent particularly interesting sites for introducing targeted mutations," (4). Data from PoPMuSiC-2.1 is presented in a text (.txt) format as well as a linear graphic that shows the average stability of each amino acid residue in a protein sequence.

The first residue examined was the SA11 tsC leucine to proline mutation at residue 138 on the VP1 gene. Proline mutations are known to be destabilizing, especially on α-helices, which is where reside 138 is located. That information coupled with the compelling results described in Chapter 2 of this dissertation regarding that mutation's deleterious effect on the polymerase's catalytic activity and viroplasmic localization, led me to hypothesize that the L138P mutation would be shown as extremely destabilizing to the polymerase. Interestingly, based on the values of the folding free energy change (ΔΔG) predicted by the PoPMuSiC-2.1 algorithm, changing the wild-type leucine to a proline did have a predicted destabilizing effect. However, this effect was fairly modest compared with changes observed when swapping out different amino acids at site 138. For example, all of the amino acids with charged side chains

were more destabilizing to the polymerase's structure than proline (Table 1). This finding is congruous with the molecular dynamics data from Chapter 2. While we expected the L138P mutation to cause global misfolding of the protein, it did not. Further, a comparison between the VP1 domains revealed that there were more potential mutations of interest in the N-terminal and central polymerase domain than in the C-terminal domain. The top ten areas predicted to have the most stabilizing mutations possible were found in the polymerase and N-terminal domains (Appendix B, Table 2). This result indicates that the polymerase and N-terminal domains are areas of less stability in the protein. In the case of the polymerase domain this could underscore its functional importance to the enzyme. The less stable residues could indicate inherent flexibility that would be important for RNA to move through the catalytic site and for polymerization to occur. The less stable nature of the NTD could also be due to flexibility, which could be related to its location near the fingers subdomain of the polymerase domain. Alternatively, it could be relevant for the polymerase's interactions with cofactor proteins for activation, localization, etc.

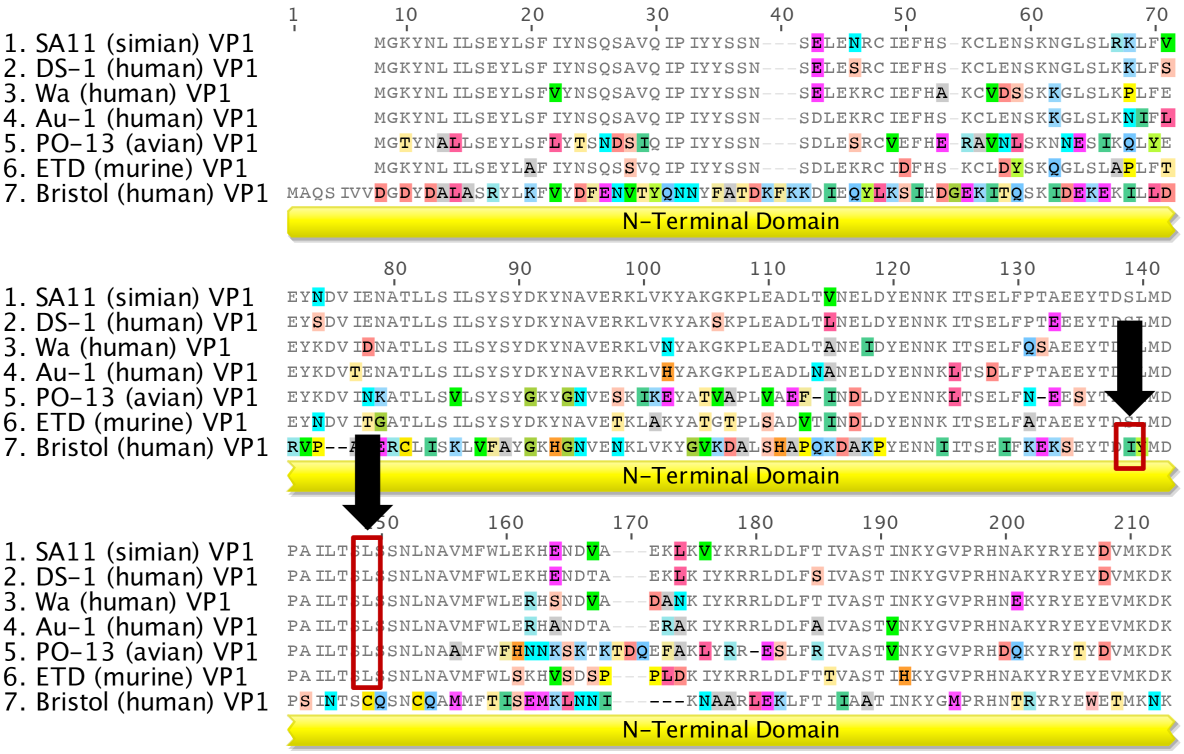

Figure 2-Amino acid sequence alignment of SA11-4F VP1, DS-1 VP1, Wa VP1, PO-13 VP1, ETD VP1 and Bristol VP1. The primary sequence alignment of these strains is shown. Dashes denote gaps in the protein sequence, and shading denotes conservation of amino acid identity. The NTD of RVA VP1 are shown below the sequence and is colored yellow. Leucine 138 is denoted with an arrow and outlined with a red box. The corresponding isoleucine in RVC strain Bristol is similarly highlighted. The differences in residue number are due to gaps from Bristol amino acid inserts. See Appendix A for a full-length VP1 amino acid sequence alignment.

Table 1-ΔΔG for SA11 VP1 point mutations at amino acid residue 138

Residue #	Wild Type	Mutant	ΔΔG
138	Leucine	Alanine	2.5
138	Leucine	Cysteine	2.08
138	Leucine	Aspartic Acid	3.32
138	Leucine	Glutamic Acid	3.15
138	Leucine	Phenyalanine	0.87
138	Leucine	Glycine	3.77
138	Leucine	Histidine	1.94
138	Leucine	Isoleucine	0.76
138	Leucine	Lysine	3.1
138	Leucine	Methionine	1.06
138	Leucine	Asparagine	2.93
138	Leucine	Proline	1.86
138	Leucine	Glutamine	2.56
138	Leucine	Arginine	2.16
138	Leucine	Serine	2.79
138	Leucine	Threonine	2.29
138	Leucine	Valine	0.98
138	Leucine	Tryptophan	0.87
138	Leucine	Tyrosine	0.88

Table 2-Top ten most potentially stabilizing residues for SA11 VP1

Residue	∑(-ΔΔG)	Location
378	-20.11	Pol
633	-11.37	Pol
533	-9.99	Pol
774	-9.59	Pol
764	-7.55	Pol
304	-7.48	N-term
683	-7.23	Pol
338	-7.1	Pol
141	-6.97	N-term
329	-6.78	N-term

REFERENCES

1. **Arnold, M., Patton, J.T., and McDonald, S.M.** 2009. Culturing, storage, and quantification of rotaviruses. Current Protocols in Microbiology. Chapter 15:Unit 15C 13.
2. **Chen, D., Gombold, J.L., and Ramig, R.F.** 1990. Intracellular RNA synthesis directed by temperature-sensitive mutants of simian rotavirus SA11. Virology, **178**:143-151.
3. **Chen, Z., Lambden, P.R., Lau, J., Caul, E.O., and Clarke, I.N.** 2002. Human group C rotavirus: completion of the genome sequence and gene coding assignments of a non-cultivatable rotavirus. Virus Research, **83**(1-2): 179-187.
4. **Dehouck, Y., Kwasigroch, J.M., Gillis, D., and Rooman, M.** 2011. PoPMuSiC: a web server for the estimation of protein stability changes upon mutation and sequence optimality. BMC Bioinformatics, **12**:151.
5. **Eichwald, C., Rodriguez, J.F., and Burrone, O.R.** 2004. Characterization of rotavirus NSP2/NSP5 interactions and the dynamics of viroplasm formation. Journal of General Virology, **85**:625-634.
6. **Fabbretti, E., Afrikanova, I., Vascotto, F., and Burrone, O.R.** 1999. Two non-structural rotavirus proteins, NSP2 and NSP5, form viroplasm-like structures in vivo. Journal of General Virology, **80**:333-339.
7. **Gombold, J.L, and Ramig, R.F.** 1987. Assignment of simian rotavirus SA11 temperature-sensitive mutant groups A, C, F, and G to genome segments. Virology, **161**:463-473.
8. **Ito, H., Sugiyama, M., Masubuchi, K, Mori, Y., and Minamoto, N.** 2001. Complete nucleotide sequence of a group A avian rotavirus genome and a comparison with its counterparts of mammalian rotaviruses. Virus Research, **75**(2): 123-138.
9. **Lu, X., McDonald, S.M., Tortorici, M.A., Tao, Y.J., Vasquez-Del Carpio, R., Nibert, M.L., Patton, J.T., and Harrison, S.C.** 2008. Mechanism for coordinated RNA packaging and genome replication by rotavirus polymerase VP1. Structure, **16**:1676-1688.
10. **Mason, B.B., Graham, D.Y., and Estes, M.K.** 1983. Biochemical mapping of the simian rotavirus SA11 genome. Journal of Virology, **46**(2):413-423.
11. **McDonald, S.M.** 2013. RNA synthetic mechanisms employed by diverse families of RNA viruses. WIREs RNA, **4**:351-367.
12. **McDonald, S.M., and Patton, J.T.** 2011a. Assortment and packaging of the segmented rotavirus genome. Trends in Microbiology, **19**(3):136-144.
13. **McDonald S.M. and Patton J.T.** 2011b. Rotavirus VP2 core shell regions critical for viral polymerase activation. Journal of Virology, **85**:3095-3105.
14. **McKell, A. O., LaConte, L.E., and McDonald, S.M.** 2017. A temperature-sensitive lesion in the N-terminal domain of the rotavirus polymerase affects its intracellular localization and enzymatic activity. Journal of Virology, **91**(7):e00062-17.
15. **Ramig, R.F. and Petrie, B.L.** 1984. Characterization of temperature-sensitive mutants of simian rotavirus SA11: protein synthesis and morphogenesis. Journal of Virology, **49**:665-673.

16. **Rodriguez, W.J., Kim, H.W., Arrobio, J.O.** 1977. Clinical features of acute gastroenteritis associated with human reovirus-like agent in infants and young children. Journal of Pediatrics, **91**:188-193.
17. **Schneider, C.A., Rasband, W.S., and Eliceiri, K.W.** 2012. NIH Image to ImageJ: 25 years of image analysis. Nature Methods, **9**:671-675.
18. **Small, C., Barro, M., Brown, T.L., and Patton, J.T.** 2007. Genome heterogeneity of SA11 rotavirus due to reassortment with "o" agent. Virology, **359**(2):415-424.
19. **Trask, S.D., McDonald, S.M., and Patton, J.T.** 2012. Structural insights into the coupling of virion assembly and rotavirus replication. Nature Reviews in Microbiology, **10**(3):165-177.
20. **Valenzuela, S., Pizarro, J., Sandino, A.M., Vásquez, M., Fernández, J., Hernández, O., Patton, J., and Spencer, E.** 1991. Photoaffinity labeling of rotavirus VP1 with 8-azido-ATP: identification of the viral RNA polymerase. Journal of Virology, **65**(7):3964-3967.
21. **Wehrfritz, J.M., Boyce, M., Mirza, S., and Roy, P.** 2007. Reconstitution of bluetongue virus polymerase activity from isolated domains based on a three-dimensional structural model. Biopolymers, **86**:83-94.

Chapter 4

SUMMARY, PERSPECTIVES, AND FUTURE DIRECTIONS

For decades, rotavirus (RV) has been a huge public health burden, causing immense morbidity and mortality around the world (14). Thus, researchers have tirelessly worked to understand the many facets of RV biology and its lifecycle. Despite many advances—including the virion structure (and many viral proteins) being solved and the development of vaccines—the mechanisms by which the virus replicates its genome and the early stages of capsid assembly remain elusive. The bulk of the experiments described in this dissertation seek to shed light on these processes using the cell culture-adapted simian RV, SA11, and ectopic expression systems. This work seeks to characterize a mutant RV polymerase, VP1, as well as to determine residues that are necessary for VP1's localization to viroplasms, the sites of virus replication. Results from this portion of the dissertation biochemically-validated that a L138P mutation in SA11 VP1 causes RNA synthesis and localization defects in a temperature-dependent manner and suggested a possible role for the N-terminal domain (NTD) of VP1 in its localization to viroplasms. In addition, this study further supports the hypothesis that VP1 interacts with viroplasm-forming proteins, NSP2 and NSP5, and it posits that one or both of those proteins could be a cofactor responsible for VP1 sequestration in the viroplasm. I hypothesize that a region of the N-terminal of VP1 allows it to interact with NSP2, which then helps it to traffic to or be retained within the viroplasm where it performs genome replication. This chapter will summarize how the findings from this dissertation contribute knowledge towards better understanding the RV polymerase and genome replication. It will also discuss the current state of the field and introduce questions raised by this work that merit further exploration by future studies.

Characterization and biochemical validation of a temperature-sensitive lesion in RV VP1 summary, conclusions, and future directions: Before the advent of a reverse genetics system, RV was studied using forward genetic approaches. One such approach was chemically induced mutagenesis that culminated in the creation of a panel of temperature-sensitive simian strain SA11 RVs (11). A temperature-sensitive mutant of SA11 RV, tsC, contains a single

leucine to proline lesion at position 138 (L138P) in its VP1 NTD (5, 12). In Chapter 2, we biochemically validated that this mutation causes a temperature-sensitive defect in SA11 VP1 (10). This result strongly suggests that L138P is responsible for tsC's temperature-sensitive phenotypes, specifically in polymerase location to viroplasms and catalytic activity. Molecular modeling of the temperature-sensitive lesion found that VP1 is not completely misfolded (10). Additionally, the localization work that used colocalization with VLSs as a read-out demonstrated that NSP2 and/or NSP5 could be important co-factors for ensuring that the polymerase is located in the viroplasms (10). This result makes sense given that NSP2 and NSP5 are both known components of replicase complexes and bind VP1 (1, 15). Our work was unable to determine whether only one or both proteins act as cofactors for VP1 localization to viroplasms; however, further studies using a mix of proteins from different strains could tease out that answer.

Now that a fully reverse genetics system is available for RV (6), the results of the study presented in Chapter 2 can be validated using recombinant viruses. In this way, the L138P mutation of SA11 tsC's VP1 gene can be recapitulated on an isogenic background and an appropriate control virus can be used. This approach would perform a similar function as the ectopic expression system by removing the confounding variables of mutations in other gene segments (as well as account for the O agent gene 8 reassortment). However, where reverse genetics becomes more powerful is that it removes the need for transfection followed by infection, so all VP1 translated is the mutant VP1, thus eliminating any possible competition from wild-type VP1 that could alter results. It also removes any possible interference with cofactors or possible conformational changes induced by the GFP tag in the expression system. Another interesting avenue of future investigation would be the use of live cell imaging and super resolution confocal microscopy. Using the GFP-tagged VP1 proteins in live cell imaging experiments would allow insight as to whether the mislocalization phenotype observed for the VP1 L138P mutant is a defect in the polymerase's ability to navigate to viroplasms or a defect in its ability to remain in viroplasms as infections proceed. Additionally, live cell imaging could provide data about the temporal progression of VP1 during infection. Super resolution microscopy is an especially useful tool that could elucidate the binding partners of the polymerase during replication and packaging.

The results from the work described in Chapter 2 point towards the NTD of VP1 as being important for RV replication. The NTD L138P lesion caused a modest reduction in dsRNA synthesis *in vitro*, which is likely due to subtle change in conformation and stability (10). Localization was affected more significantly, which could mean that the NTD facilitates interactions with cofactor proteins, like NSP2 and NSP5. This could happen via a sequence-specific binding signal or the physical conformation of the NTD gripping other proteins. Even though previous evidence has suggested a more central role for NSP5, other work supports the hypothesis that NSP2 acts as a chaperone and/or scaffold (15).

VP1 localization to viroplasms summary, conclusions, and future directions. The RV genome is comprised of double-stranded RNA, which is particularly vulnerable to cell defenses such as the RIG-I complex (2). Thus, it is important for the viral genome to be replicated in a protected environment. For RV, that means that its RNA-dependent RNA polymerase, VP1, must travel to viral inclusion bodies called 'viroplasms' that form in the host cell cytoplasm (9). Viroplasms are composed of and contain a myriad of viral and host proteins. The nonstructural proteins, NSP2 and NSP5, have been shown to be necessary and sufficient for the formation of viroplasms (3, 4). As mentioned previously, expression of those two proteins in the absence of infection produces viroplasm-like structures (VLSs) (4). In both Chapters 2 and 3, VP1 localization patterns were studied via ectopic expression of the protein in cells that were subsequently infected or not. Chapter 2 describes experiments performed using GFP-tagged VP1s, wild-type and mutant. That research and its implications are presented in greater detail in the previous section. The results in Chapter 3 takes the foundation laid in Chapter 2 and sets up a platform and strategy to further investigate the *cis*-acting features of VP1 that are responsible for its localization to viroplasms. I repeated the GFP-tagged transfection experiments using the SA11 NTD only, PO-13 VP1, and Bristol VP1, finding that none of these constructs target to viroplasms in SA11 RV-infected cells.

Since these experiments were performed in the context of SA11-infected monkey kidney cells, there could be too many confounders for PO-13 VP1 or Bristol VP1 to localize to viroplasms. Instead, another way to study the possible differences in localization could be to perform 'mix and match' experiments using the VLS system. In this manner, VP1s, NSP2s, and NSP5s from different strains could be simultaneously transfected into cells and imaged. For

example, PO-13$_{WT}$ VP1-GFP and its cognate PO-13 NSP2 and PO-13 NSP5 could be transfected into the monkey kidney cells. Ideally, VLSs would form and the tagged PO-13 VP1 would colocalize with those viroplasms. If that holds true for PO-13 or other strains' VP1s with their cognate proteins, then differences in functionality and sequence could be compared to elucidate areas of interest on the polymerase's structure important for localization. It could be that there are strain-dependent differences, or there could be a universal localization signal motif; however, that is less likely given the results reported in Chapter 3.

Bioinformatic analysis of VP1 summary, conclusions, and future directions. While biochemical analyses are important for probing protein functionality, another powerful tool is bioinformatics. Genomic sequences can yield insights about proteins from identifying conserved motifs to comparisons between homologous and non-homologous species. Viral polymerases are often structurally conserved, even across different virus families (8). This phenomenon of conservation is further carried through by the high percentage of sequence homology between RV VP1s from different strains. In Chapter 3 of this dissertation nucleotide and protein alignments were performed between divergent RV strains, including SA11, PO-13, Bristol, Wa, and DS-1. Additionally, the crystal structure for the VP1 apoenzyme was input into the PoPMuSiC-2.1 algorithm to predict how point mutations could affect the stability of the protein. The analysis of these data was centered on the L138P mutation as well as the NTD generally. We found that the leucine at 138 was conserved across most strains' VP1s and lies in an area are more conservation that abuts more variable regions. PoPMuSiC analysis showed that the proline mutation for tsC was not the most destabilizing residue by far, which was somewhat surprising given the how that amino acid can significantly disrupt α-helices. This provided support for the results from Chapter 2 that indicated that the L138P change did not catastrophically affect the entirety of VP1's structure (10). Interestingly, the residues whose mutations led to the largest increase in stabilization were found in the polymerase and NTDs.

This information can be useful for further studies by directing the strategy for the engineering of plasmid constructs or mutant viruses. The insight from the protein alignments identifies sections of proteins that could be swapped out in chimera experiments in order to better narrow down regions and residues important for certain polymerase functions such as

localization. Similarly, the PoPMuSiC results are useful for developing candidate residues for mutation and for generating hypotheses involving proteins' structures.

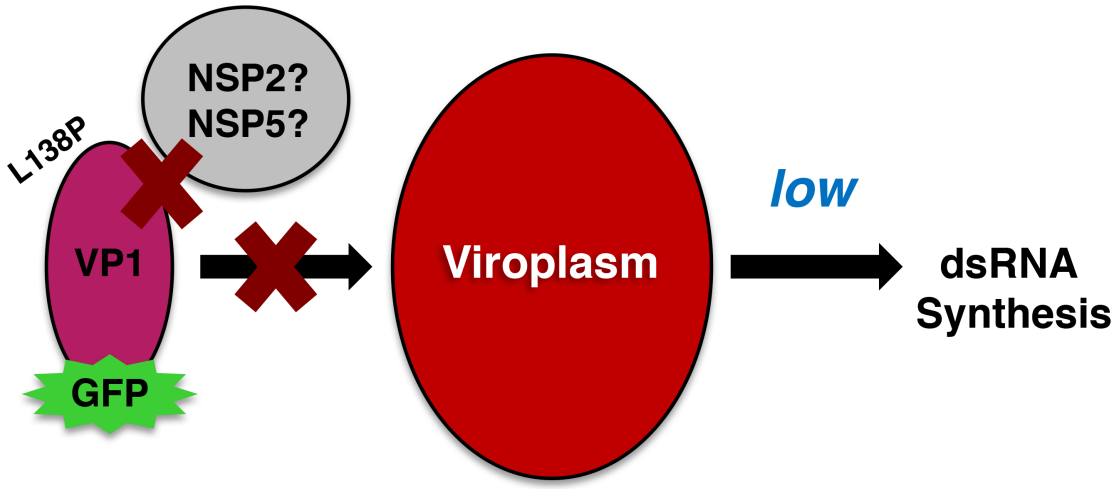

Figure 1-Summary model for mechanism of L138P VP1 defects at 39˚C. This figure provides a visual synopsis of the mechanism for the localization and dsRNA synthesis defects found in SA11 $VP1_{L138P}$. Based off the data in Chapter 2, it is likely that the mutant VP1 is unable to localize to viroplasms, which is where it needs to be to perform dsRNA synthesis. This inability to target is probably due to interrupted interactions with possible cofactor proteins, NSP2 and NSP5, that also are the primary viral components of viroplasms. Data from Chapter 3 suggests that localization and/or interactions with cofactor proteins may be strain-specific. In addition to mislocalization, the mutant VP1 is also unable to catalyze dsRNA at the same levels as wildtype VP1 at high temperatures (39˚C) *in vitro*. Thus, these two defective processes could explain the phenotypes observed in the RV, SA11 tsC, but work would need to be performed using viruses to validate that hypothesis.

Significance and application of research. Even though the development and introduction of vaccines against RV has significantly curtailed the number of related fatalities, RV remains an important public health concern (14). Since RNA viruses are so disposed towards point mutations, and since segmented viruses possess the ability to exchange entire gene segments, it remains important to better understand the biology behind RV replication (9). Studies that endeavor to do this may provide insights that could be important for the developments of second-generation vaccines or alternative anti-viral therapies. In particular, the work described in this dissertation sheds more light onto the RV RNA-dependent RNA polymerase (RdRp), VP1. All RNA viruses (except retroviruses) possess RdRps, and the structures of many of these polymerases are fairly conserved even between different viruses (8). These virus polymerases make excellent antiviral drug targets since there are no homologous proteins in host cells (8). Thus, if RV VP1 could be inhibited functionally by preventing interactions with cofactors and/or preventing its localization to viroplasms, then viral replication could be interrupted which could in turn halt the progression of infection and disease. Development of antiviral therapeutics directed specifically against RV is unlikely given the availability and effectiveness of current vaccines. However, if vaccine contamination or other safety issues become threaten the use of those vaccines, it is possible that alternatives could be sought out. Even in that scenario, the amount of resources needed to create, test, and market a new drug is immense. Thus, it would be questionable whether engineering a RV antiviral drug (or another agent) would be cost-effective. It is more likely that what is learned about the RV polymerase and its localization and catalytic activity could be applied more broadly to other viruses that pose significant health threats but do not yet have vaccines or treatments available.

Indeed, elucidating how the RV polymerase localizes to viroplasms, and thus also clarifying a portion of the steps involved in the early stages of viral replication could be useful when investigating other viruses and/or proteins. For instance, VP1 is similar to other RNA virus RdRps in that it possesses a canonical right-handed polymerase domain (7, 8). Despite dissimilar amino acid sequences, the ultimate structural organization of RNA virus polymerases closely resembles each other (8). However, it differs from those polymerases due to the addition of N-terminal and C-terminal accessory domains as well as the priming loop. These 'extra' domains are feature unique to RV and other members of *Reoviridae*. From a structural standpoint, they help to form the distinctive four tunnels of *Reoviridae* polymerases, but the

exact functional role(s) for these extra domains is not known (7, 13). Work from another related virus, bluetongue virus indicates that these domains are required for RNA synthesis (16). The results of this dissertation suggest that the N-terminal domain of VP1 is not sufficient for the polymerase to localize to viroplasms during RV infection but that it is certainly an important component for that function of the polymerase. We also provided further support that NSP2 and/or NSP5 are important cofactors for VP1, especially in the context of its viroplasmic localization. Moreover, the results of experiments using different strains' VP1 genes provide evidence that support a hypothesis that the VP1 viroplasmic determinants may be strain-specific and thus located in variable regions of the polymerase's sequence.

While the work shared in this dissertation contributes to what is known about the RV polymerase, it also continues the scientific tradition of generating more questions. What specific part(s) of the VP1 NTD are important for its localization during replication? Would this take the form of structural conformations or localization signals within the sequence? Are there strain-specific differences? What viral and/or cellular proteins act as cofactors for VP1's localization? It is my hope that my results and the methods and reagents developed for this thesis will help inform work in the future that will further investigate RV replication and viral polymerase biology. Indeed, a better understanding of these processes is key towards preventing the devastation viral diseases continue to cause in our world.

REFERENCES

1. A**rnoldi, F., Campagna, M., Eichwald, C. Desselberger, U., and Burrone, O.R.** 2007. Interaction of rotavirus polymerase VP1 with nonstructural protein NSP5 is stronger than that with NSP2. Journal of Virology, **81**(5):2128-2137.
2. **Broquet, A.H., Hirata, Y., McAllister, C.S., and Kagnoff, M.F.** 2011. RIG-I/MDA5/MAVS are required to signal a protective IFN response in rotavirus-infected intestinal epithelium. Journal of Immunology, **186**(3):1618-1626.
3. **Eichwald, C., Rodriguez, J.F., and Burrone, O.R.** 2004. Characterization of rotavirus NSP2/NSP5 interactions and the dynamics of viroplasm formation. Journal of General Virology, **85**:625-634.
4. **Fabbretti, E., Afrikanova, I., Vascotto, F., and Burrone, O.R.** 1999. Two non-structural rotavirus proteins, NSP2 and NSP5, form viroplasm-like structures in vivo. Journal of General Virology, **80**:333-339.
5. **Gombold, J.L, and Ramig, R.F.** 1987. Assignment of simian rotavirus SA11 temperature-sensitive mutant groups A, C, F, and G to genome segments. Virology, **161**:463-473.
6. **Kanai, Y., Komoto, S., Kawagishi, T., Nouda, R., Nagasawa, N., Onishi, M., Matsuura, Y., Taniguchi, K., and Kobayashi, T.** 2017. Entirely plasmid-based reverse genetics system for rotaviruses. PNAS, **114**(9):2349-2354.
7. **Lu, X., McDonald, S.M., Tortorici, M.A., Tao, Y.J., Vasquez-Del Carpio, R., Nibert, M.L., Patton, J.T., and Harrison, S.C.** 2008. Mechanism for coordinated RNA packaging and genome replication by rotavirus polymerase VP1. Structure, **16**:1676-1688.
8. **McDonald, S.M.** 2013. RNA synthetic mechanisms employed by diverse families of RNA viruses. WIREs RNA, **4**:351-367.
9. **McDonald, S.M., and Patton, J.T.** 2011. Assortment and packaging of the segmented rotavirus genome. Trends in Microbiology, **19**(3):136-144.
10. **McKell, A. O., LaConte, L.E., and McDonald, S.M.** 2017. A temperature-sensitive lesion in the N-terminal domain of the rotavirus polymerase affects its intracellular localization and enzymatic activity. Journal of Virology, **91**(7):e00062-17.
11. **Ramig, R.F. and Petrie, B.L.** 1984. Characterization of temperature-sensitive mutants of simian rotavirus SA11: protein synthesis and morphogenesis. Journal of Virology, **49**:665-673.
12. **Small, C., Barro, M., Brown, T.L., and Patton, J.T.** 2007. Genome heterogeneity of SA11 rotavirus due to reassortment with "o" agent. Virology, **359**(2):415-424.
13. **Tao, Y., Farsetta, D.L., Nibert, M.L., and Harrison, S.C.** 2002. RNA synthesis in a cage—structural studies of reovirus polymerase lambda3. Cell, **111**(5):733-745.
14. **Tate, J.E., Burton, A.H., Boschi-Pinto, C., Parashar, U.D., and World Health Organization-Coordinated Global Rotavirus Surveillance Network.** 2016. Global, regional, and national estimates of rotavirus mortality in children <5 years of age, 2000-2013. Clinical Infectious Diseases, **62**:S96-S105.

15. **Viskovsha, M., Anish, R., Hu, L., Chow, D.C., Hurwitz, A.M., Brown, N.G., Palzkill, T., Estes, M.K., and Prasad, B.V.** 2014. Probing the sites of rotaviral proteins involved in replication. Journal of Virology, **88** (21):12866-12881.
16. **Wehrfritz, J.M., Boyce, M., Mirza, S., and Roy, P.** 2007. Reconstitution of bluetongue virus polymerase activity from isolated domains based on a three-dimensional structural model. Biopolymers, **86**:83-94.

APPENDIX A

Amino acid sequence alignment of SA11-4F VP1, DS-1 VP1, Wa VP1, PO-13 VP1, ETD VP1 and Bristol VP1. The primary sequence alignment of these strains is shown. Dashes denote gaps in the protein sequence, and shading denotes conservation of amino acid identity. The domains and subdomains of RVA VP1 are shown above the sequence and are colored as follows: NTD (yellow), polymerase domain-fingers (blue), polymerase domain-palm (red), polymerase domain-thumb (green), CTD (pink), and plug (cyan).

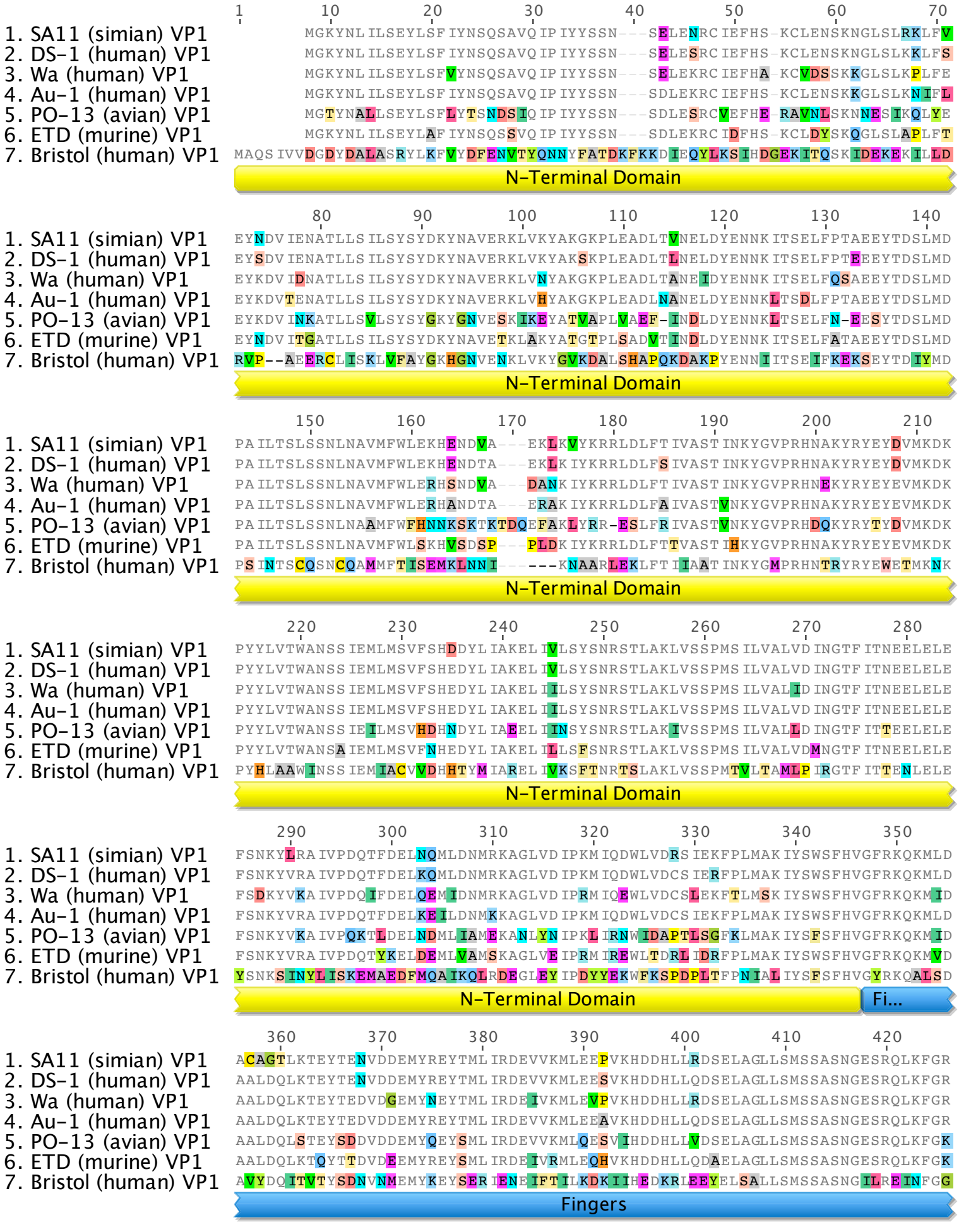
1. SA11 (simian) VP1
2. DS-1 (human) VP1
3. Wa (human) VP1
4. Au-1 (human) VP1
5. PO-13 (avian) VP1
6. ETD (murine) VP1
7. Bristol (human) VP1
N-Terminal Domain
Fingers

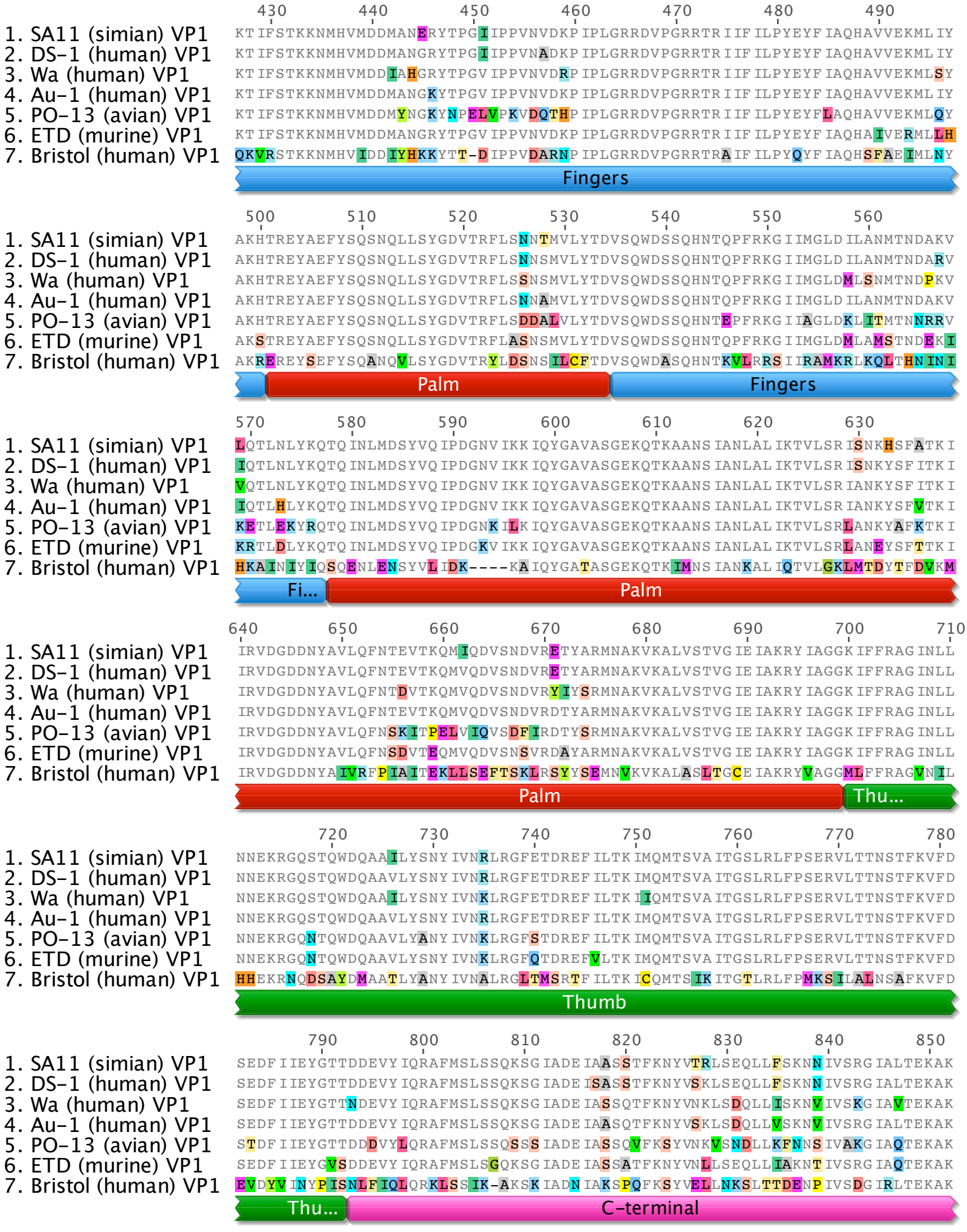
430 440 450 460 470 480 490
1. SA11 (simian) VP1 KTIFSTKKNMHVMDDMANERYTPGIIPPVNVDKPIPLGRRDVPGRRTRIIFILPYEYFIAQHAVVEKMLIY
2. DS-1 (human) VP1 KTIFSTKKNMHVMDDMANGRYTPGIIPPVNADKPIPLGRRDVPGRRTRIIFILPYEYFIAQHAVVEKMLIY
3. Wa (human) VP1 KTIFSTKKNMHVMDDIAHGRYTPGVIPPVNVDRPIPLGRRDVPGRRTRIIFILPYEYFIAQHAVVEKMLSY
4. Au-1 (human) VP1 KTIFSTKKNMHVMDDMANGKYTPGVIPPVNVDKPIPLGRRDVPGRRTRIIFILPYEYFIAQHAVVEKMLIY
5. PO-13 (avian) VP1 KTIFSTKKNMHVMDDMYNGKYNPELVPKVDQTHPIPLGRRDVPGRRTRIIFILPYEYFLAQHAVVEKMLQY
6. ETD (murine) VP1 KTIFSTKKNMHVMDDMANGRYTPGVIPPVNVDKPIPLGRRDVPGRRTRIIFILPYEYFIAQHAIVERMLLH
7. Bristol (human) VP1 QKVRSTKKNMHVIDDIYHKKYTT-DIPPVDARNPIPLGRRDVPGRRTRAIFILPYQYFIAQHSFAEIMLNY
Fingers
500 510 520 530 540 550 560
1. SA11 (simian) VP1 AKHTREYAEFYSQSNQLLSYGDVTRFLSNNTMVLYTDVSQWDSSQHNTQPFRKGIIMGLDILANMTNDAKV
2. DS-1 (human) VP1 AKHTREYAEFYSQSNQLLSYGDVTRFLSNNSMVLYTDVSQWDSSQHNTQPFRKGIIMGLDILANMTNDARV
3. Wa (human) VP1 AKHTREYAEFYSQSNQLLSYGDVTRFLSSNSMVLYTDVSQWDSSQHNTQPFRKGIIMGLDMLSNMTNDPKV
4. Au-1 (human) VP1 AKHTREYAEFYSQSNQLLSYGDVTRFLSNNAMVLYTDVSQWDSSQHNTQPFRKGIIMGLDILANMTNDAKV
5. PO-13 (avian) VP1 AKHTREYAEFYSQSNQLLSYGDVTRFLSDDALVLYTDVSQWDSSQHNTEPFRKGIIAGLDKLITMTNNRRV
6. ETD (murine) VP1 AKSTREYAEFYSQSNQLLSYGDVTRFLASNSMVLYTDVSQWDSSQHNTQPFRKGIIMGLDMLAMSTNDEKI
7. Bristol (human) VP1 AKREREYSEFYSQANQVLSYGDVTRYLDSNSILCFTDVSQWDASQHNTKVLRRSIIRAMKRLKQLTHNINI
Palm
Fingers
570 580 590 600 610 620 630
1. SA11 (simian) VP1 LQTLNLYKQTQINLMDSYVQIPDGNVIKKIQYGAVASGEKQTKAANSIANLALIKTVLSRISNKHSFATKI
2. DS-1 (human) VP1 IQTLNLYKQTQINLMDSYVQIPDGNVIKKIQYGAVASGEKQTKAANSIANLALIKTVLSRISNKYSFITKI
3. Wa (human) VP1 VQTLNLYKQTQINLMDSYVQIPDGNVIKKIQYGAVASGEKQTKAANSIANLALIKTVLSRIANKYSFITKI
4. Au-1 (human) VP1 IQTLHLYKQTQINLMDSYVQIPDGNVIKKIQYGAVASGEKQTKAANSIANLALIKTVLSRIANKYSFVTKI
5. PO-13 (avian) VP1 KETLEKYRQTQINLMDSYVQIPDGNKILKIQYGAVASGEKQTKAANSIANLALIKTVLSRLANKYAFKTKI
6. ETD (murine) VP1 KRTLDLYKQTQINLMDSYVQIPDGKVIKKIQYGAVASGEKQTKAANSIANLALIKTVLSRLANEYSFTTKI
7. Bristol (human) VP1 HKAINIYIQSQENLENSYVLIDK----KAIQYGATASGEKQTKIMNSIANKALIQTVLGKLMTDYTFDVKM
Fi...
Palm
640 650 660 670 680 690 700 710
1. SA11 (simian) VP1 IRVDGDDNYAVLQFNTEVTKQMIQDVSNDVRETYARMNAKVKALVSTVGIEIAKRYIAGGKIFFRAGINLL
2. DS-1 (human) VP1 IRVDGDDNYAVLQFNTEVTKQMVQDVSNDVRETYARMNAKVKALVSTVGIEIAKRYIAGGKIFFRAGINLL
3. Wa (human) VP1 IRVDGDDNYAVLQFNTDVTKQMVQDVSNDVRYIYSRMNAKVKALVSTVGIEIAKRYIAGGKIFFRAGINLL
4. Au-1 (human) VP1 IRVDGDDNYAVLQFNTEVTKQMVQDVSNDVRDTYARMNAKVKALVSTVGIEIAKRYIAGGKIFFRAGINLL
5. PO-13 (avian) VP1 IRVDGDDNYAVLQFNSKITPELVIQVSDFIRDTYSRMNAKVKALVSTVGIEIAKRYIAGGKIFFRAGINLL
6. ETD (murine) VP1 IRVDGDDNYAVLQFNSDVTEQMVQDVSNSVRDAYARMNAKVKALVSTVGIEIAKRYIAGGKIFFRAGINLL
7. Bristol (human) VP1 IRVDGDDNYAIVRFPIAITEKLLSFFTSKLRSYYSEMNVKVKALASLTGCEIAKRYVAGGMLFFRAGVNIL
Palm
Thu...
720 730 740 750 760 770 780
1. SA11 (simian) VP1 NNEKRGQSTQWDQAAILYSNYIVNRLRGFETDREFILTKIMQMTSVAITGSLRLFPSERVLTTNSTFKVFD
2. DS-1 (human) VP1 NNEKRGQSTQWDQAAVLYSNYIVNRLRGFETDREFILTKIMQMTSVAITGSLRLFPSERVLTTNSTFKVFD
3. Wa (human) VP1 NNEKRGQSTQWDQAAILYSNYIVNKLRGFETDREFILTKIIQMTSVAITGSLRLFPSERVLTTNSTFKVFD
4. Au-1 (human) VP1 NNEKRGQSTQWDQAAVLYSNYIVNRLRGFETDREFILTKIMQMTSVAITGSLRLFPSERVLTTNSTFKVFD
5. PO-13 (avian) VP1 NNEKRGQNTQWDQAAVLYANYIVNKLRGFSTDREFILTKIMQMTSVAITGSLRLFPSERVLTTNSTFKVFD
6. ETD (murine) VP1 NNEKRGQNTQWDQAAVLYSNYIVNKLRGFQTDREFVLTKIMQMTSVAITGSLRLFPSERVLTTNSTFKVFD
7. Bristol (human) VP1 HHEKRNQDSAYDMAATLYANYIVNALRGLTMSRTFILTKICQMTSIKITGTLRLFPMKSILALNSAFKVFD
Thumb
790 800 810 820 830 840 850
1. SA11 (simian) VP1 SEDFIIEYGTTDDEVYIQRAFMSLSSQKSGIADEIAASSTFKNYVTRLSEQLLFSKNNIVSRGIALTEKAK
2. DS-1 (human) VP1 SEDFIIEYGTTDDEVYIQRAFMSLSSQKSGIADEISASSTFKNYVSKLSEQLLFSKNNIVSRGIALTEKAK
3. Wa (human) VP1 SEDFIIEYGTTNDEVYIQRAFMSLSSQKSGIADEIASSQTFKNYVNKLSDQLLISKNVIVSKGIAVTEKAK
4. Au-1 (human) VP1 SEDFIIEYGTTDDEVYIQRAFMSLSSQKSGIADEIAASQTFKNYVSKLSDQLLVSKNVIVSRGIALTEKAK
5. PO-13 (avian) VP1 STDFIIEYGTTDDDVYLQRAFMSLSSQSSSIADEIASSQVFKSYVNKVSNDLLKFNNSIVAKGIAQTEKAK
6. ETD (murine) VP1 SEDFIIEYGVSDDEVYIQRAFMSLSGQKSGIADEIASSATFKNYVNLLSEQLLIAKNTIVSRGIAQTEKAK
7. Bristol (human) VP1 EVDYVINYPISNLFIQLQRKLSSIK-AKSKIADNIAKSPQFKSYVELLNKSLTTDENPIVSDGIRLTEKAK
Thu...
C-terminal

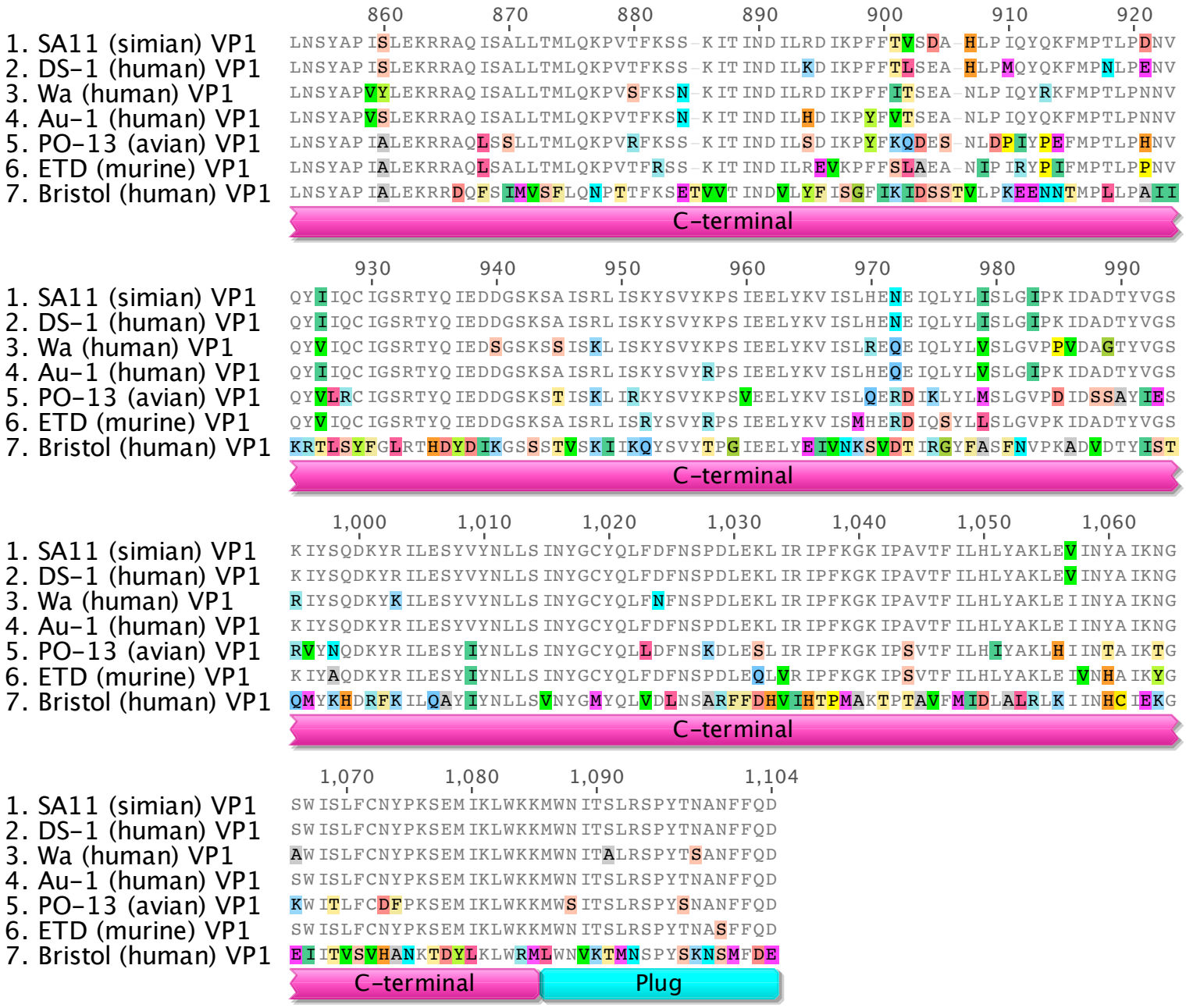
860 870 880 890 900 910 920
1. SA11 (simian) VP1 LNSYAPISLEKRRAQISALLTMLQKPVTFKSS-KITINDILRDIKPFFTVSDA-HLPIQYQKFMPTLPDNV
2. DS-1 (human) VP1 LNSYAPISLEKRRAQISALLTMLQKPVTFKSS-KITINDILKDIKPFFTLSEA-HLPMQYQKFMPNLPENV
3. Wa (human) VP1 LNSYAPVYLEKRRAQISALLTMLQKPVSFKSN-KITINDILRDIKPFFITSEA-NLPIQYRKFMPTLPNNV
4. Au-1 (human) VP1 LNSYAPVSLEKRRAQISALLTMLQKPVTFKSN-KITINDILHDIKPYFVTSEA-NLPIQYQKFMPTLPNNV
5. PO-13 (avian) VP1 LNSYAPIALEKRRAQLSSLLTMLQKPVRFKSS-KITINDILSDIKPYFKQDES-NLDPIYPEFMPTLPHNV
6. ETD (murine) VP1 LNSYAPIALEKRRAQLSALLTMLQKPVTFRSS-KITINDILREVKPFFSLAEA-NIPIRYPIFMPTLPPNV
7. Bristol (human) VP1 LNSYAPIALEKRRDQFSIMVSFLQNPTTFKSETVVTINDVLYFISGFIKIDSSTVLPKEENNTMPLLPAII
C-terminal
930 940 950 960 970 980 990
1. SA11 (simian) VP1 QYIIQCIGSRTYQIEDDGSKSAISRLISKYSVYKPSIEELYKVISLHENEIQLYLISLGIPKIDADTYVGS
2. DS-1 (human) VP1 QYIIQCIGSRTYQIEDDGSKSAISRLISKYSVYKPSIEELYKVISLHENEIQLYLISLGIPKIDADTYVGS
3. Wa (human) VP1 QYVIQCIGSRTYQIEDSGSKSSISKLISKYSVYKPSIEELYKVISLREQEIQLYLVSLGVPPVDAGTYVGS
4. Au-1 (human) VP1 QYIIQCIGSRTYQIEDDGSKSAISRLISKYSVYRPSIEELYKVISLHEQEIQLYLVSLGIPKIDADTYVGS
5. PO-13 (avian) VP1 QYVLRCIGSRTYQIEDDGSKSTISKLIRKYSVYKPSVEELYKVISLQERDIKLYLMSLGVPDIDSSAYIES
6. ETD (murine) VP1 QYVIQCIGSRTYQIEDDGSKSAISRLISRYSVYRPSIEELYKVISMHERDIQSYLLSLGVPKIDADTYVGS
7. Bristol (human) VP1 KRTLSYFGLRTHDYDIKGSSSTVSKIIKQYSVYTPGIEELYEIVNKSVDTIRGYFASFNVPKADVDTYIST
C-terminal
1,000 1,010 1,020 1,030 1,040 1,050 1,060
1. SA11 (simian) VP1 KIYSQDKYRILESYVYNLLSINYGCYQLFDFNSPDLEKLIRIPFKGKIPAVTFILHLYAKLEVINYAIKNG
2. DS-1 (human) VP1 KIYSQDKYRILESYVYNLLSINYGCYQLFDFNSPDLEKLIRIPFKGKIPAVTFILHLYAKLEVINYAIKNG
3. Wa (human) VP1 RIYSQDKYKILESYVYNLLSINYGCYQLFNFNSPDLEKLIRIPFKGKIPAVTFILHLYAKLEIINYAIKNG
4. Au-1 (human) VP1 KIYSQDKYRILESYVYNLLSINYGCYQLFDFNSPDLEKLIRIPFKGKIPAVTFILHLYAKLEIINYAIKNG
5. PO-13 (avian) VP1 RVYNQDKYRILESYIYNLLSINYGCYQLLDFNSKDLESLIRIPFKGKIPSVTFILHIYAKLHIINTAIKTG
6. ETD (murine) VP1 KIYAQDKYRILESYIYNLLSINYGCYQLFDFNSPDLEQLVRIPFKGKIPSVTFILHLYAKLEIVNHAIKYG
7. Bristol (human) VP1 QMYKHDRFKILQAYIYNLLSVNYGMYQLVDLNSARFFDHVIHTPMAKTPTAVFMIDLALRLKIINHCIEKG
C-terminal
1,070 1,080 1,090 1,104
1. SA11 (simian) VP1 SWISLFCNYPKSEMIKLWKKMWNITSLRSPYTNANFFQD
2. DS-1 (human) VP1 SWISLFCNYPKSEMIKLWKKMWNITSLRSPYTNANFFQD
3. Wa (human) VP1 AWISLFCNYPKSEMIKLWKKMWNITALRSPYTSANFFQD
4. Au-1 (human) VP1 SWISLFCNYPKSEMIKLWKKMWNITSLRSPYTNANFFQD
5. PO-13 (avian) VP1 KWITLFCDFPKSEMIKLWKKMWSITSLRSPYSNANFFQD
6. ETD (murine) VP1 SWISLFCNYPKSEMIKLWKKMWNITSLRSPYTNASFFQD
7. Bristol (human) VP1 EIITVSVHANKTDYLKLWRMLWNVKTMNSPYSKNSMFDE
C-terminal
Plug

APPENDIX B

Histogram representing the sum of the ΔΔGs for the stabilizing mutations in SA11-4F RV as a function of sequence position. The amino acid sequences are indicated above the histogram with secondary structure denoted and differentiated by color. Three turn α helices (G) are in bright red, four-turn α helices (H) are in brick red, ß-strands (E) are in lavender, coils (C) are in light green, bends (S) are in dark green, hydrogen bonded turns are in salmon (T), and ß-bridges (B) are in cyan. Larger negative integers indicate more stability possible.

Sequence optimality (sum of negative ddG per sequence position) - 2R7Q.pdb - Systematic - 17-12-2015

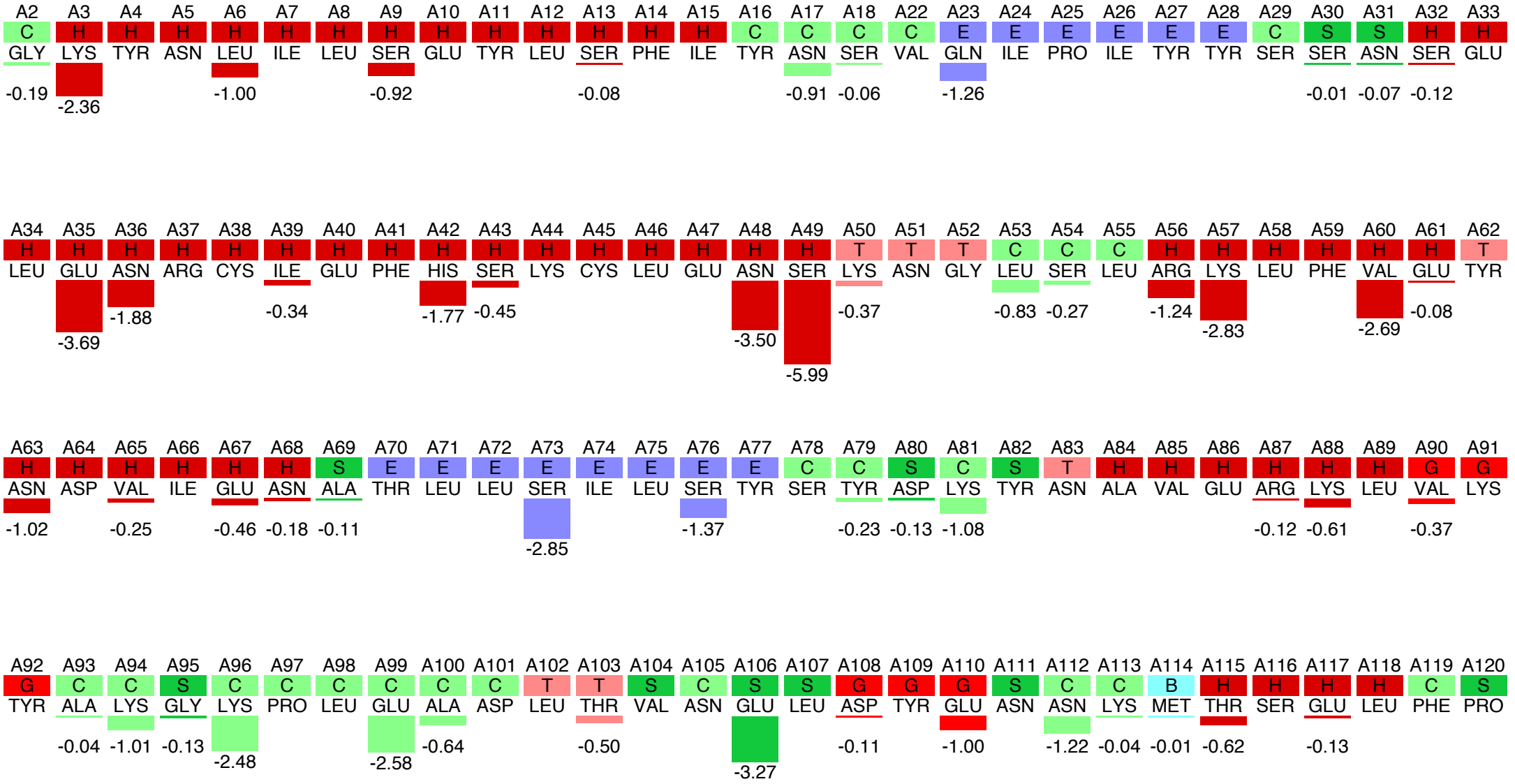

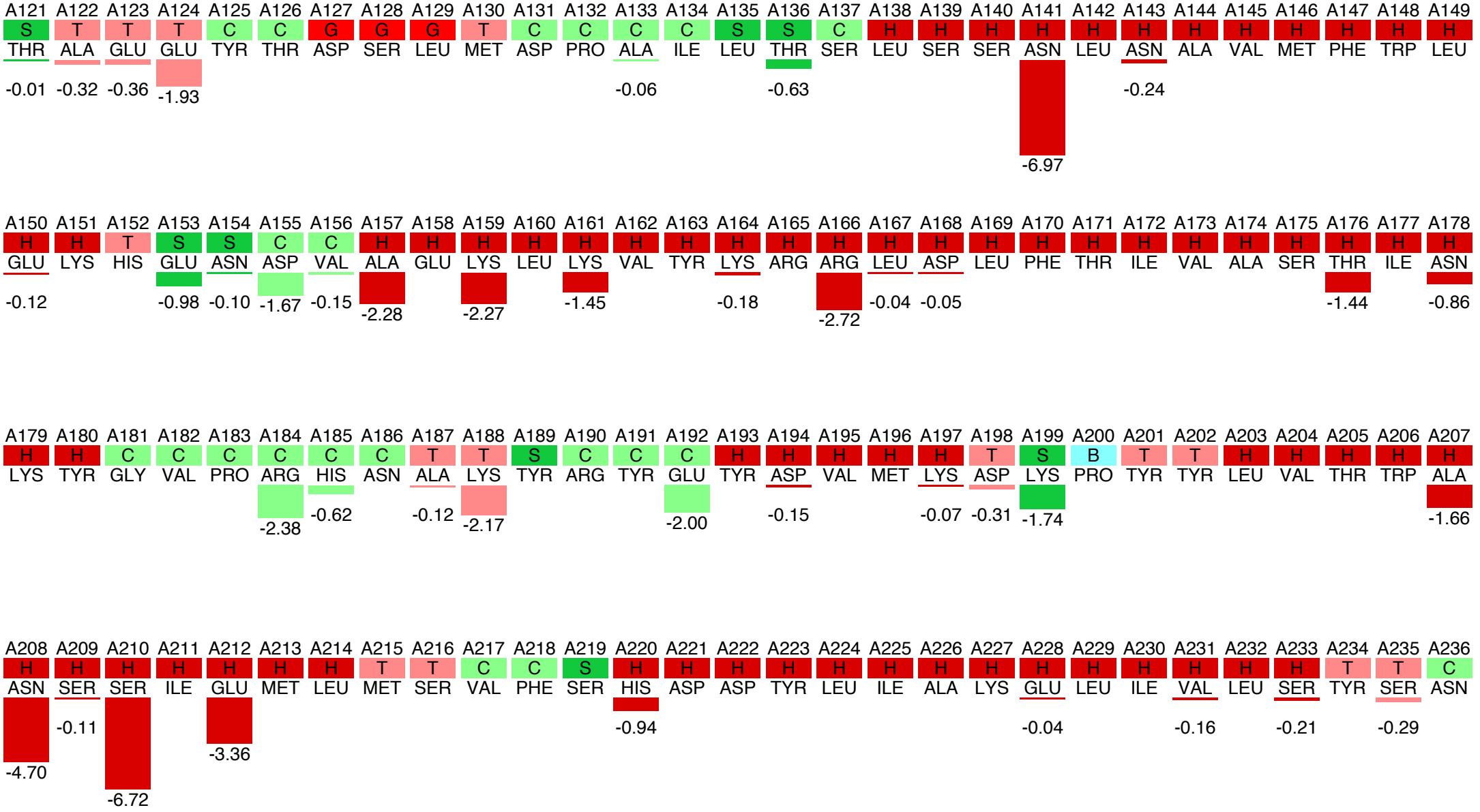
A121 S THR -0.01
A122 T ALA -0.32
A123 T GLU -0.36
A124 T GLU -1.93
A125 C TYR
A126 C THR
A127 G ASP
A128 G SER
A129 G LEU
A130 T MET
A131 C ASP
A132 C PRO
A133 C ALA -0.06
A134 C ILE
A135 S LEU
A136 S THR -0.63
A137 C SER
A138 H LEU
A139 H SER
A140 H SER
A141 H ASN -6.97
A142 H LEU
A143 H ASN -0.24
A144 H ALA
A145 H VAL
A146 H MET
A147 H PHE
A148 H TRP
A149 H LEU
A150 H GLU -0.12
A151 H LYS
A152 T HIS
A153 S GLU -0.98
A154 S ASN -0.10
A155 C ASP -1.67
A156 C VAL -0.15
A157 H ALA -2.28
A158 H GLU
A159 H LYS -2.27
A160 H LEU
A161 H LYS -1.45
A162 H VAL
A163 H TYR
A164 H LYS -0.18
A165 H ARG
A166 H ARG -2.72
A167 H LEU -0.04
A168 H ASP -0.05
A169 H LEU
A170 H PHE
A171 H THR
A172 H ILE
A173 H VAL
A174 H ALA
A175 H SER
A176 H THR -1.44
A177 H ILE
A178 H ASN -0.86
A179 H LYS
A180 H TYR
A181 C GLY
A182 C VAL
A183 C PRO
A184 C ARG -2.38
A185 C HIS -0.62
A186 C ASN
A187 T ALA -0.12
A188 T LYS -2.17
A189 S TYR
A190 C ARG
A191 C TYR
A192 C GLU -2.00
A193 H TYR
A194 H ASP -0.15
A195 H VAL
A196 H MET
A197 H LYS -0.07
A198 T ASP -0.31
A199 S LYS -1.74
A200 B PRO
A201 T TYR
A202 T TYR
A203 H LEU
A204 H VAL
A205 H THR
A206 H TRP
A207 H ALA -1.66
A208 H ASN -4.70
A209 H SER -0.11
A210 H SER -6.72
A211 H ILE
A212 H GLU -3.36
A213 H MET
A214 H LEU
A215 T MET
A216 T SER
A217 C VAL
A218 C PHE
A219 S SER
A220 H HIS -0.94
A221 H ASP
A222 H ASP
A223 H TYR
A224 H LEU
A225 H ILE
A226 H ALA
A227 H LYS
A228 H GLU -0.04
A229 H LEU
A230 H ILE
A231 H VAL -0.16
A232 H LEU
A233 H SER -0.21
A234 T TYR
A235 T SER -0.29
A236 C ASN

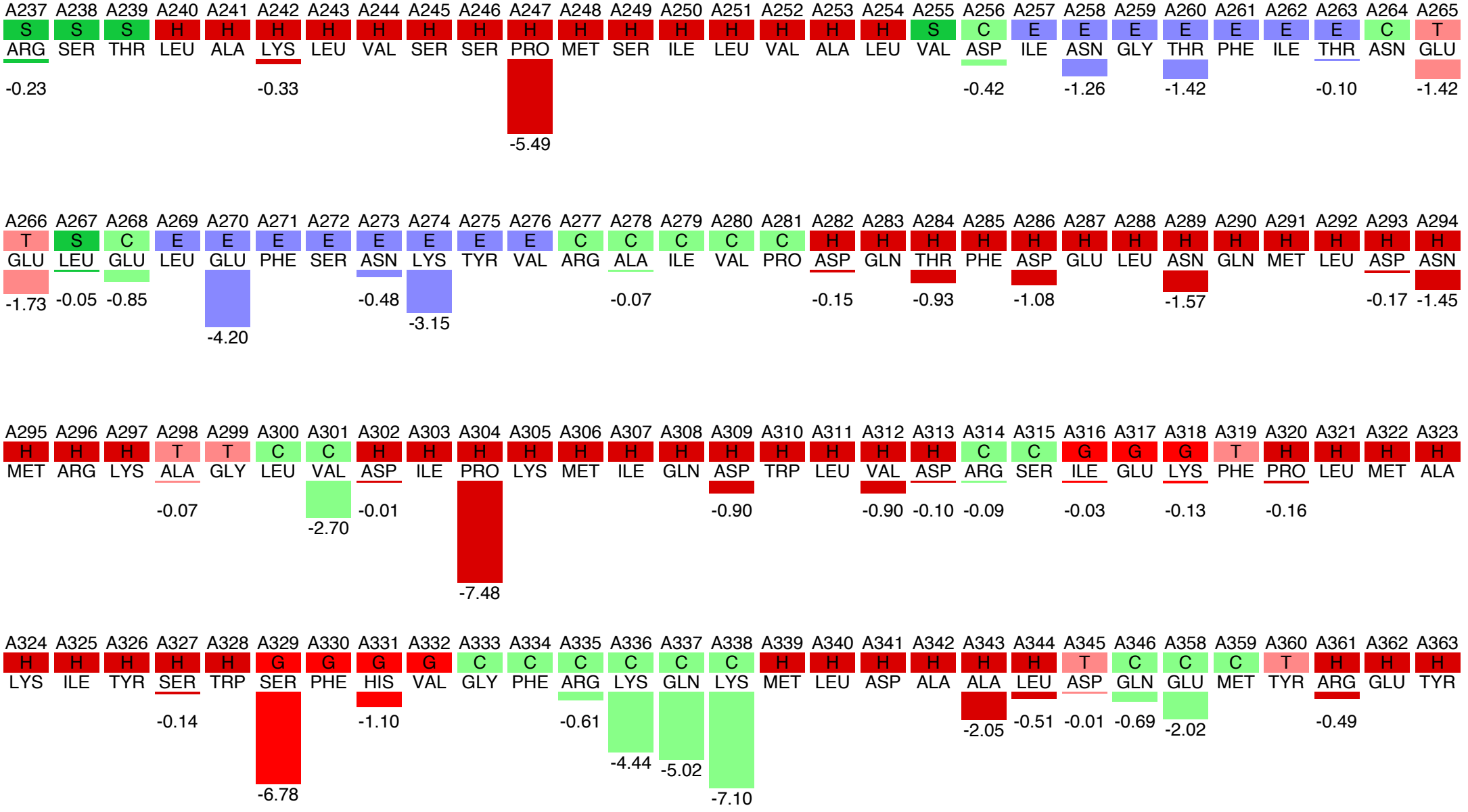
A237 S ARG -0.23
A238 S SER
A239 S THR
A240 H LEU
A241 H ALA
A242 H LYS -0.33
A243 H LEU
A244 H VAL
A245 H SER
A246 H SER
A247 H PRO -5.49
A248 H MET
A249 H SER
A250 H ILE
A251 H LEU
A252 H VAL
A253 H ALA
A254 H LEU
A255 S VAL
A256 C ASP -0.42
A257 E ILE
A258 E ASN -1.26
A259 E GLY
A260 E THR -1.42
A261 E PHE
A262 E ILE
A263 E THR -0.10
A264 C ASN
A265 T GLU -1.42
A266 T GLU -1.73
A267 S LEU -0.05
A268 C GLU -0.85
A269 E LEU
A270 E GLU -4.20
A271 E PHE
A272 E SER
A273 E ASN -0.48
A274 E LYS -3.15
A275 E TYR
A276 E VAL
A277 C ARG
A278 C ALA -0.07
A279 C ILE
A280 C VAL
A281 C PRO
A282 H ASP -0.15
A283 H GLN
A284 H THR -0.93
A285 H PHE
A286 H ASP -1.08
A287 H GLU
A288 H LEU
A289 H ASN -1.57
A290 H GLN
A291 H MET
A292 H LEU
A293 H ASP -0.17
A294 H ASN -1.45
A295 H MET
A296 H ARG
A297 H LYS
A298 T ALA -0.07
A299 T GLY
A300 C LEU
A301 C VAL -2.70
A302 H ASP -0.01
A303 H ILE
A304 H PRO -7.48
A305 H LYS
A306 H MET
A307 H ILE
A308 H GLN
A309 H ASP -0.90
A310 H TRP
A311 H LEU
A312 H VAL -0.90
A313 H ASP -0.10
A314 C ARG -0.09
A315 C SER
A316 G ILE -0.03
A317 G GLU
A318 G LYS -0.13
A319 T PHE
A320 H PRO -0.16
A321 H LEU
A322 H MET
A323 H ALA
A324 H LYS
A325 H ILE
A326 H TYR
A327 H SER -0.14
A328 H TRP
A329 G SER -6.78
A330 G PHE
A331 G HIS -1.10
A332 G VAL
A333 C GLY
A334 C PHE
A335 C ARG -0.61
A336 C LYS -4.44
A337 C GLN -5.02
A338 C LYS -7.10
A339 H MET
A340 H LEU
A341 H ASP
A342 H ALA
A343 H ALA -2.05
A344 H LEU -0.51
A345 T ASP -0.01
A346 C GLN -0.69
A358 C GLU -2.02
A359 C MET
A360 T TYR
A361 H ARG -0.49
A362 H GLU
A363 H TYR

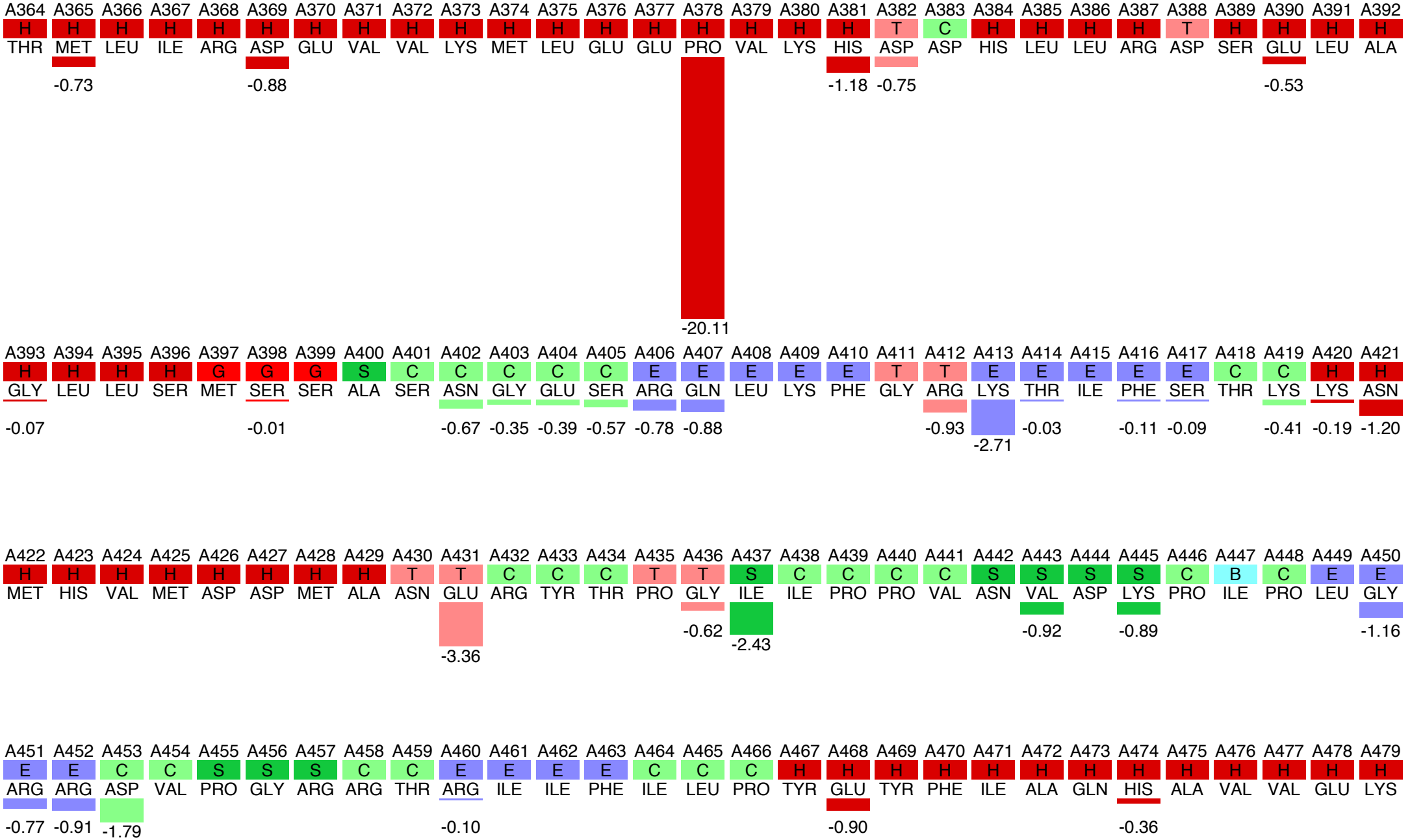
A364 H THR
A365 H MET -0.73
A366 H LEU
A367 H ILE
A368 H ARG
A369 H ASP -0.88
A370 H GLU
A371 H VAL
A372 H VAL
A373 H LYS
A374 H MET
A375 H LEU
A376 H GLU
A377 H GLU
A378 H PRO -20.11
A379 H VAL
A380 H LYS
A381 H HIS -1.18
A382 T ASP -0.75
A383 C ASP
A384 H HIS
A385 H LEU
A386 H LEU
A387 H ARG
A388 T ASP
A389 H SER
A390 H GLU -0.53
A391 H LEU
A392 H ALA
A393 H GLY -0.07
A394 H LEU
A395 H LEU
A396 H SER
A397 G MET
A398 G SER -0.01
A399 G SER
A400 S ALA
A401 C SER
A402 C ASN -0.67
A403 C GLY -0.35
A404 C GLU -0.39
A405 C SER -0.57
A406 E ARG -0.78
A407 E GLN -0.88
A408 E LEU
A409 E LYS
A410 E PHE
A411 T GLY
A412 T ARG -0.93
A413 E LYS -2.71
A414 E THR -0.03
A415 E ILE
A416 E PHE -0.11
A417 E SER -0.09
A418 C THR
A419 C LYS -0.41
A420 H LYS -0.19
A421 H ASN -1.20
A422 H MET
A423 H HIS
A424 H VAL
A425 H MET
A426 H ASP
A427 H ASP
A428 H MET
A429 H ALA
A430 T ASN
A431 T GLU -3.36
A432 C ARG
A433 C TYR
A434 C THR
A435 T PRO
A436 T GLY -0.62
A437 S ILE -2.43
A438 C ILE
A439 C PRO
A440 C PRO
A441 C VAL
A442 S ASN
A443 S VAL -0.92
A444 S ASP
A445 S LYS -0.89
A446 C PRO
A447 B ILE
A448 C PRO
A449 E LEU
A450 E GLY -1.16
A451 E ARG -0.77
A452 E ARG -0.91
A453 C ASP -1.79
A454 C VAL
A455 S PRO
A456 S GLY
A457 S ARG
A458 C ARG
A459 C THR
A460 E ARG -0.10
A461 E ILE
A462 E ILE
A463 E PHE
A464 C ILE
A465 C LEU
A466 C PRO
A467 H TYR
A468 H GLU -0.90
A469 H TYR
A470 H PHE
A471 H ILE
A472 H ALA
A473 H GLN
A474 H HIS -0.36
A475 H ALA
A476 H VAL
A477 H VAL
A478 H GLU
A479 H LYS

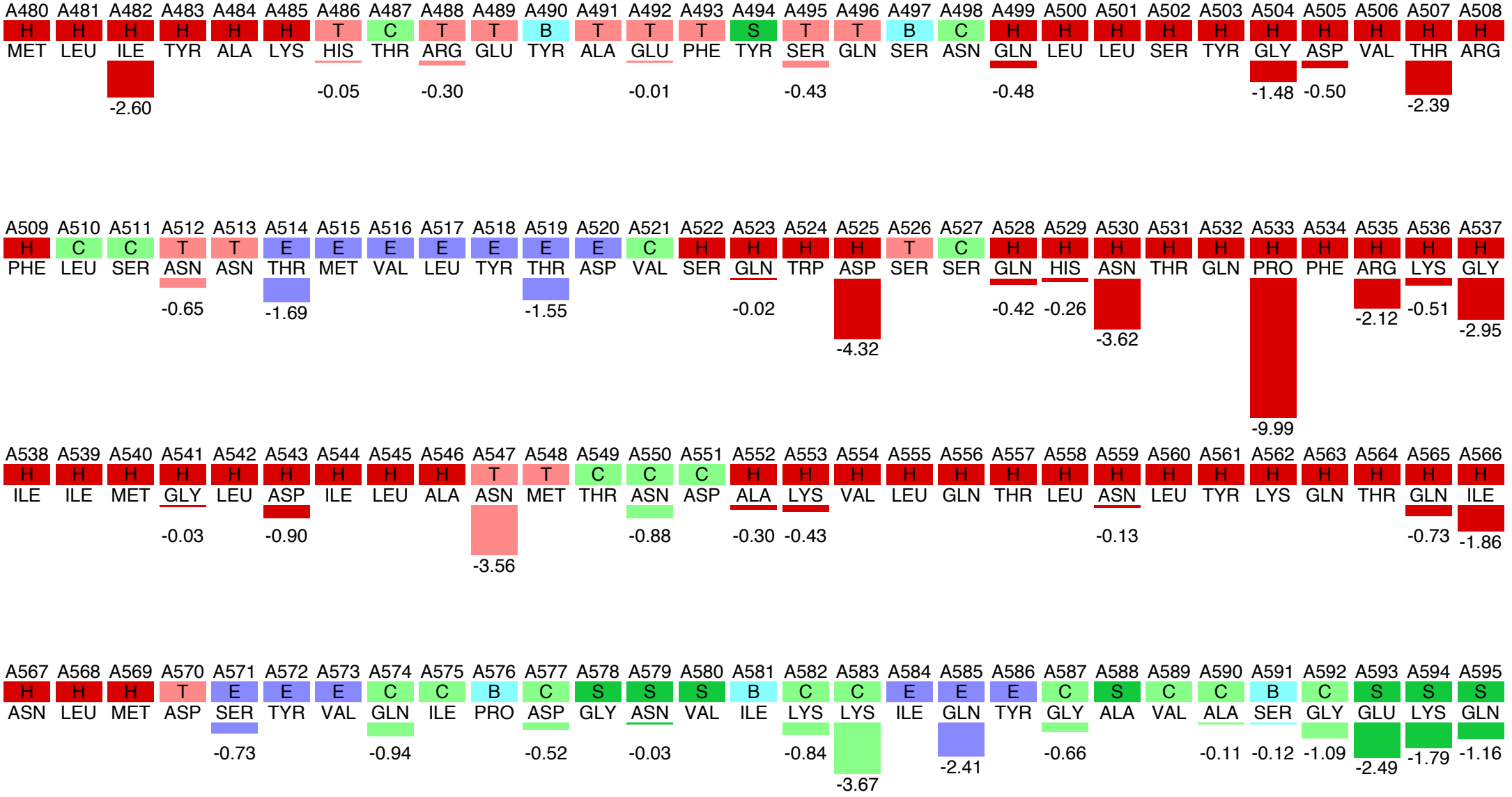
A480 H MET
A481 H LEU
A482 H ILE -2.60
A483 H TYR
A484 H ALA
A485 H LYS
A486 T HIS -0.05
A487 C THR
A488 T ARG -0.30
A489 T GLU
A490 B TYR
A491 T ALA
A492 T GLU -0.01
A493 T PHE
A494 S TYR
A495 T SER -0.43
A496 T GLN
A497 B SER
A498 C ASN
A499 H GLN -0.48
A500 H LEU
A501 H LEU
A502 H SER
A503 H TYR
A504 H GLY -1.48
A505 H ASP -0.50
A506 H VAL
A507 H THR -2.39
A508 H ARG
A509 H PHE
A510 C LEU
A511 C SER
A512 T ASN -0.65
A513 T ASN
A514 E THR -1.69
A515 E MET
A516 E VAL
A517 E LEU
A518 E TYR
A519 E THR -1.55
A520 E ASP
A521 C VAL
A522 H SER
A523 H GLN -0.02
A524 H TRP
A525 H ASP -4.32
A526 T SER
A527 C SER
A528 H GLN -0.42
A529 H HIS -0.26
A530 H ASN -3.62
A531 H THR
A532 H GLN
A533 H PRO -9.99
A534 H PHE
A535 H ARG -2.12
A536 H LYS -0.51
A537 H GLY -2.95
A538 H ILE
A539 H ILE
A540 H MET
A541 H GLY -0.03
A542 H LEU
A543 H ASP -0.90
A544 H ILE
A545 H LEU
A546 H ALA
A547 T ASN -3.56
A548 T MET
A549 C THR
A550 C ASN -0.88
A551 C ASP
A552 H ALA -0.30
A553 H LYS -0.43
A554 H VAL
A555 H LEU
A556 H GLN
A557 H THR
A558 H LEU
A559 H ASN -0.13
A560 H LEU
A561 H TYR
A562 H LYS
A563 H GLN
A564 H THR
A565 H GLN -0.73
A566 H ILE -1.86
A567 H ASN
A568 H LEU
A569 H MET
A570 T ASP
A571 E SER -0.73
A572 E TYR
A573 E VAL
A574 C GLN -0.94
A575 C ILE
A576 B PRO
A577 C ASP -0.52
A578 S GLY
A579 S ASN -0.03
A580 S VAL
A581 B ILE
A582 C LYS -0.84
A583 C LYS -3.67
A584 E ILE
A585 E GLN -2.41
A586 E TYR
A587 C GLY -0.66
A588 S ALA
A589 C VAL
A590 C ALA -0.11
A591 B SER -0.12
A592 C GLY -1.09
A593 S GLU -2.49
A594 S LYS -1.79
A595 S GLN -1.16

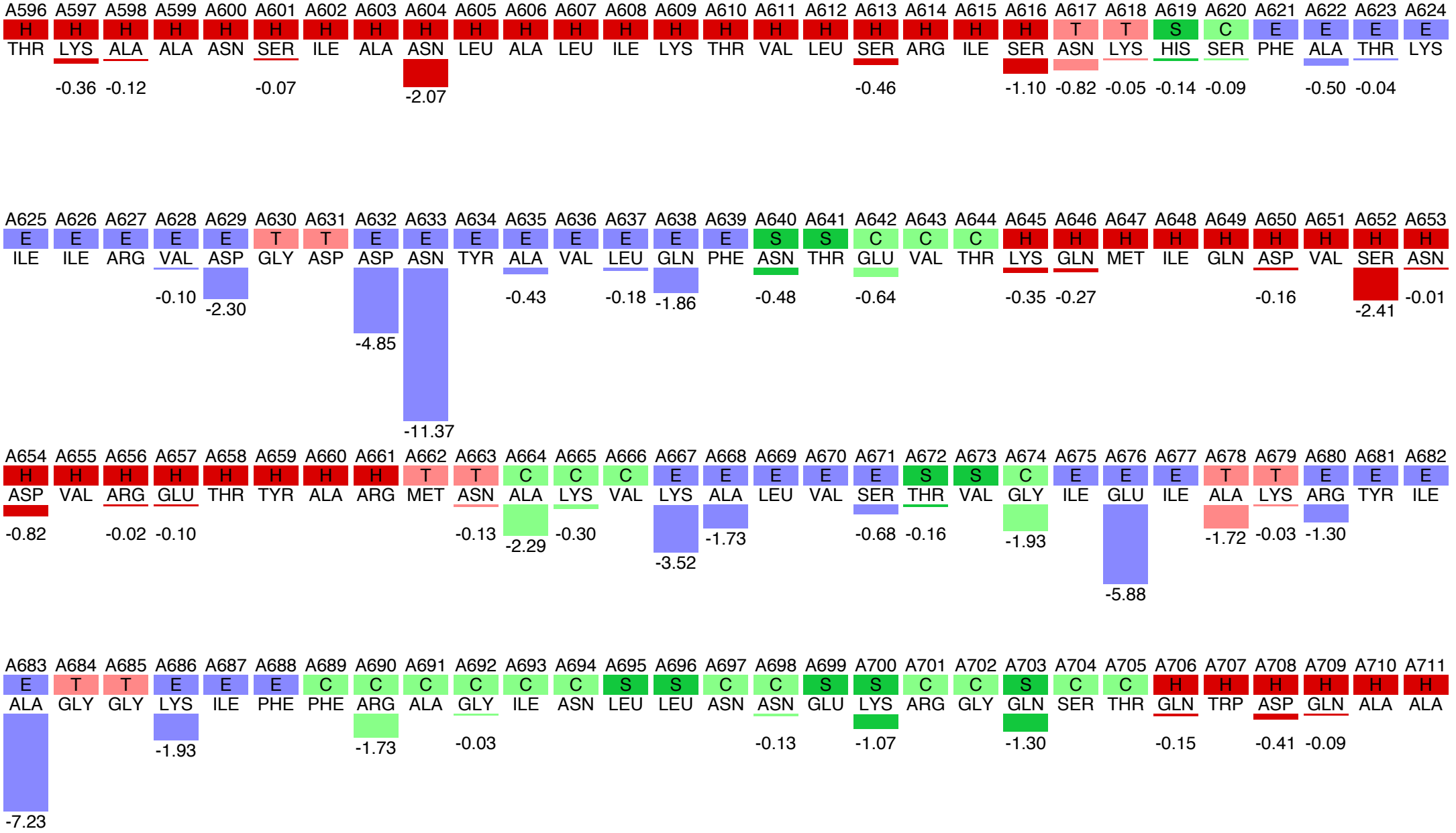
A596 H THR
A597 H LYS -0.36
A598 H ALA -0.12
A599 H ALA
A600 H ASN
A601 H SER -0.07
A602 H ILE
A603 H ALA
A604 H ASN -2.07
A605 H LEU
A606 H ALA
A607 H LEU
A608 H ILE
A609 H LYS
A610 H THR
A611 H VAL
A612 H LEU
A613 H SER -0.46
A614 H ARG
A615 H ILE
A616 H SER -1.10
A617 T ASN -0.82
A618 T LYS -0.05
A619 S HIS -0.14
A620 C SER -0.09
A621 E PHE
A622 E ALA -0.50
A623 E THR -0.04
A624 E LYS
A625 E ILE
A626 E ILE
A627 E ARG
A628 E VAL -0.10
A629 E ASP -2.30
A630 T GLY
A631 T ASP
A632 E ASP -4.85
A633 E ASN -11.37
A634 E TYR
A635 E ALA -0.43
A636 E VAL
A637 E LEU -0.18
A638 E GLN -1.86
A639 E PHE
A640 S ASN -0.48
A641 S THR
A642 C GLU -0.64
A643 C VAL
A644 C THR
A645 H LYS -0.35
A646 H GLN -0.27
A647 H MET
A648 H ILE
A649 H GLN
A650 H ASP -0.16
A651 H VAL
A652 H SER -2.41
A653 H ASN -0.01
A654 H ASP -0.82
A655 H VAL
A656 H ARG -0.02
A657 H GLU -0.10
A658 H THR
A659 H TYR
A660 H ALA
A661 H ARG
A662 T MET
A663 T ASN -0.13
A664 C ALA -2.29
A665 C LYS -0.30
A666 C VAL
A667 E LYS -3.52
A668 E ALA -1.73
A669 E LEU
A670 E VAL
A671 E SER -0.68
A672 S THR -0.16
A673 S VAL
A674 C GLY -1.93
A675 E ILE
A676 E GLU -5.88
A677 E ILE
A678 T ALA -1.72
A679 T LYS -0.03
A680 E ARG -1.30
A681 E TYR
A682 E ILE
A683 E ALA -7.23
A684 T GLY
A685 T GLY
A686 E LYS -1.93
A687 E ILE
A688 E PHE
A689 C PHE
A690 C ARG -1.73
A691 C ALA
A692 C GLY -0.03
A693 C ILE
A694 C ASN
A695 S LEU
A696 S LEU
A697 C ASN
A698 C ASN -0.13
A699 S GLU
A700 S LYS -1.07
A701 C ARG
A702 C GLY
A703 S GLN -1.30
A704 C SER
A705 C THR
A706 H GLN -0.15
A707 H TRP
A708 H ASP -0.41
A709 H GLN -0.09
A710 H ALA
A711 H ALA

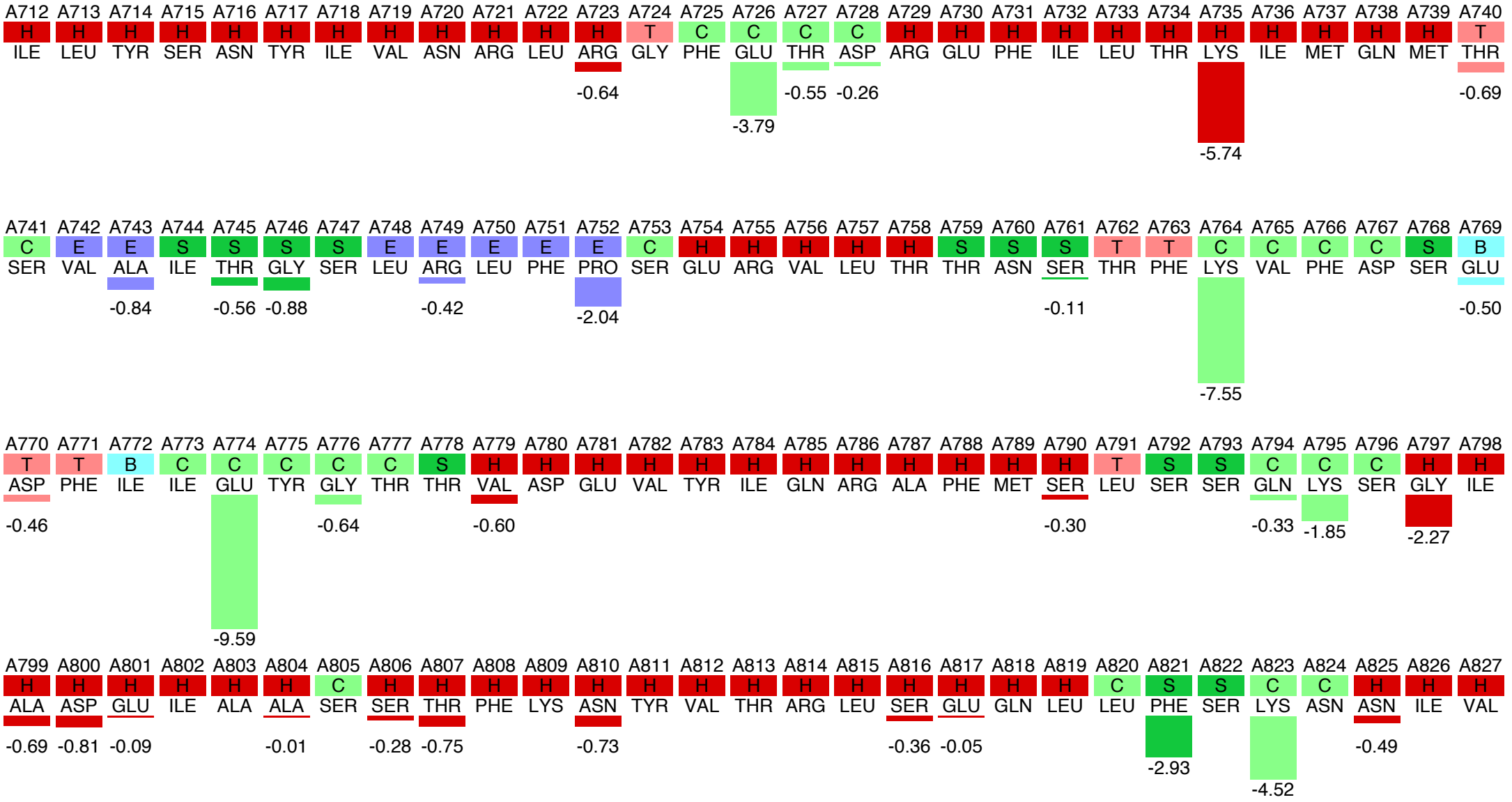
A712 H ILE
A713 H LEU
A714 H TYR
A715 H SER
A716 H ASN
A717 H TYR
A718 H ILE
A719 H VAL
A720 H ASN
A721 H ARG
A722 H LEU
A723 H ARG -0.64
A724 T GLY
A725 C PHE
A726 C GLU -3.79
A727 C THR -0.55
A728 C ASP -0.26
A729 H ARG
A730 H GLU
A731 H PHE
A732 H ILE
A733 H LEU
A734 H THR
A735 H LYS -5.74
A736 H ILE
A737 H MET
A738 H GLN
A739 H MET
A740 T THR -0.69
A741 C SER
A742 E VAL
A743 E ALA -0.84
A744 S ILE
A745 S THR -0.56
A746 S GLY -0.88
A747 S SER
A748 E LEU
A749 E ARG -0.42
A750 E LEU
A751 E PHE
A752 E PRO -2.04
A753 C SER
A754 H GLU
A755 H ARG
A756 H VAL
A757 H LEU
A758 H THR
A759 S THR
A760 S ASN
A761 S SER -0.11
A762 T THR
A763 T PHE
A764 C LYS -7.55
A765 C VAL
A766 C PHE
A767 C ASP
A768 S SER
A769 B GLU -0.50
A770 T ASP -0.46
A771 T PHE
A772 B ILE
A773 C ILE
A774 C GLU -9.59
A775 C TYR
A776 C GLY -0.64
A777 C THR
A778 S THR
A779 H VAL -0.60
A780 H ASP
A781 H GLU
A782 H VAL
A783 H TYR
A784 H ILE
A785 H GLN
A786 H ARG
A787 H ALA
A788 H PHE
A789 H MET
A790 H SER -0.30
A791 T LEU
A792 S SER
A793 S SER
A794 C GLN -0.33
A795 C LYS -1.85
A796 C SER
A797 H GLY -2.27
A798 H ILE
A799 H ALA -0.69
A800 H ASP -0.81
A801 H GLU -0.09
A802 H ILE
A803 H ALA
A804 H ALA -0.01
A805 C SER
A806 H SER -0.28
A807 H THR -0.75
A808 H PHE
A809 H LYS
A810 H ASN -0.73
A811 H TYR
A812 H VAL
A813 H THR
A814 H ARG
A815 H LEU
A816 H SER -0.36
A817 H GLU -0.05
A818 H GLN
A819 H LEU
A820 C LEU
A821 S PHE -2.93
A822 S SER
A823 C LYS -4.52
A824 C ASN
A825 H ASN -0.49
A826 H ILE
A827 H VAL

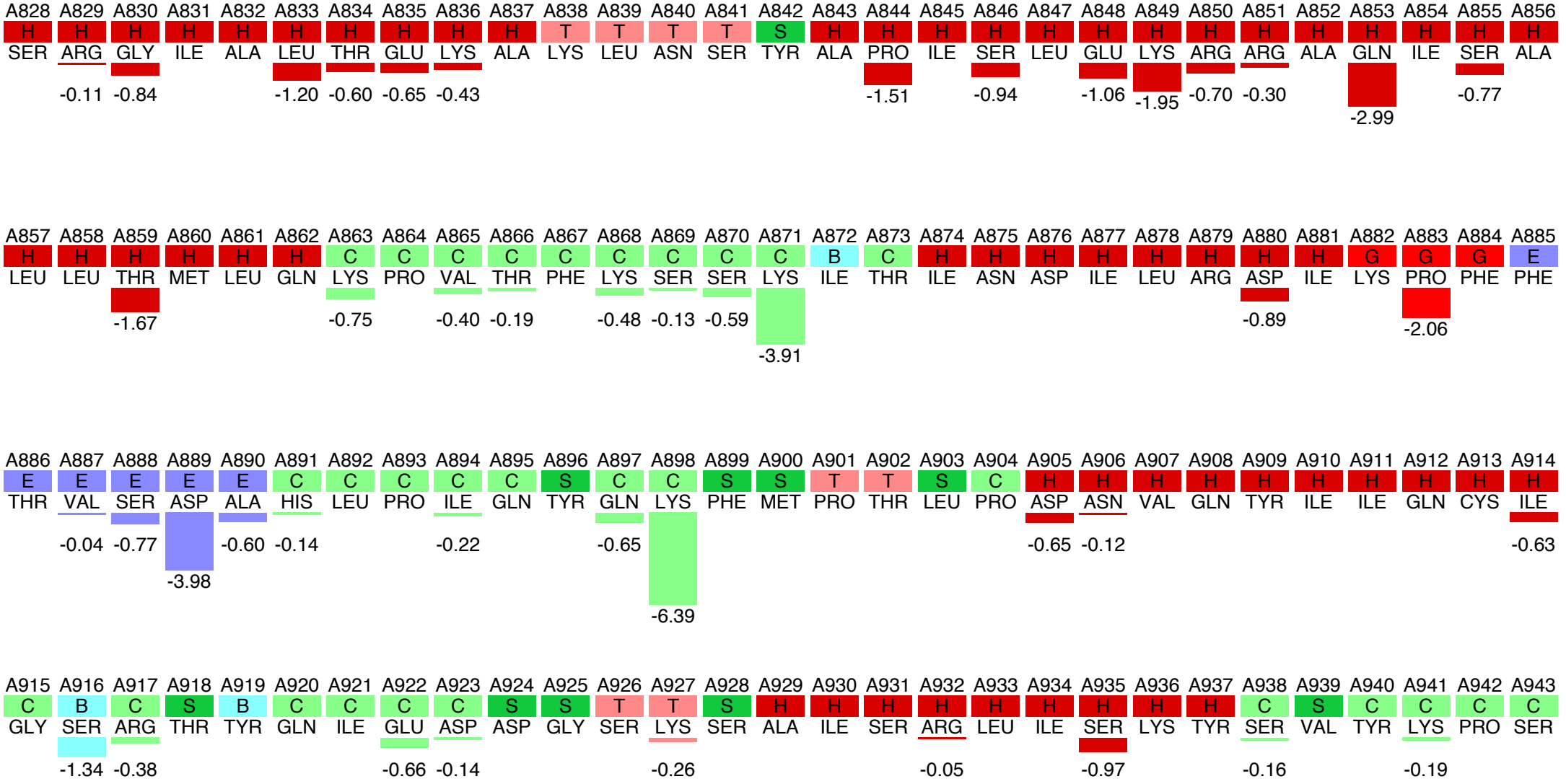
A828 H SER
A829 H ARG -0.11
A830 H GLY -0.84
A831 H ILE
A832 H ALA
A833 H LEU -1.20
A834 H THR -0.60
A835 H GLU -0.65
A836 H LYS -0.43
A837 H ALA
A838 T LYS
A839 T LEU
A840 T ASN
A841 T SER
A842 S TYR
A843 H ALA
A844 H PRO -1.51
A845 H ILE
A846 H SER -0.94
A847 H LEU
A848 H GLU -1.06
A849 H LYS -1.95
A850 H ARG -0.70
A851 H ARG -0.30
A852 H ALA
A853 H GLN -2.99
A854 H ILE
A855 H SER -0.77
A856 H ALA
A857 H LEU
A858 H LEU
A859 H THR -1.67
A860 H MET
A861 H LEU
A862 H GLN
A863 C LYS -0.75
A864 C PRO
A865 C VAL -0.40
A866 C THR -0.19
A867 C PHE
A868 C LYS -0.48
A869 C SER -0.13
A870 C SER -0.59
A871 C LYS -3.91
A872 B ILE
A873 C THR
A874 H ILE
A875 H ASN
A876 H ASP
A877 H ILE
A878 H LEU
A879 H ARG
A880 H ASP -0.89
A881 H ILE
A882 G LYS
A883 G PRO -2.06
A884 G PHE
A885 E PHE
A886 E THR
A887 E VAL -0.04
A888 E SER -0.77
A889 E ASP -3.98
A890 E ALA -0.60
A891 C HIS -0.14
A892 C LEU
A893 C PRO
A894 C ILE -0.22
A895 C GLN
A896 S TYR
A897 C GLN -0.65
A898 C LYS -6.39
A899 S PHE
A900 S MET
A901 T PRO
A902 T THR
A903 S LEU
A904 C PRO
A905 H ASP -0.65
A906 H ASN -0.12
A907 H VAL
A908 H GLN
A909 H TYR
A910 H ILE
A911 H ILE
A912 H GLN
A913 H CYS
A914 H ILE -0.63
A915 C GLY
A916 B SER -1.34
A917 C ARG -0.38
A918 S THR
A919 B TYR
A920 C GLN
A921 C ILE
A922 C GLU -0.66
A923 C ASP -0.14
A924 S ASP
A925 S GLY
A926 T SER
A927 T LYS -0.26
A928 S SER
A929 H ALA
A930 H ILE
A931 H SER
A932 H ARG -0.05
A933 H LEU
A934 H ILE
A935 H SER -0.97
A936 H LYS
A937 H TYR
A938 C SER -0.16
A939 S VAL
A940 C TYR
A941 C LYS -0.19
A942 C PRO
A943 C SER

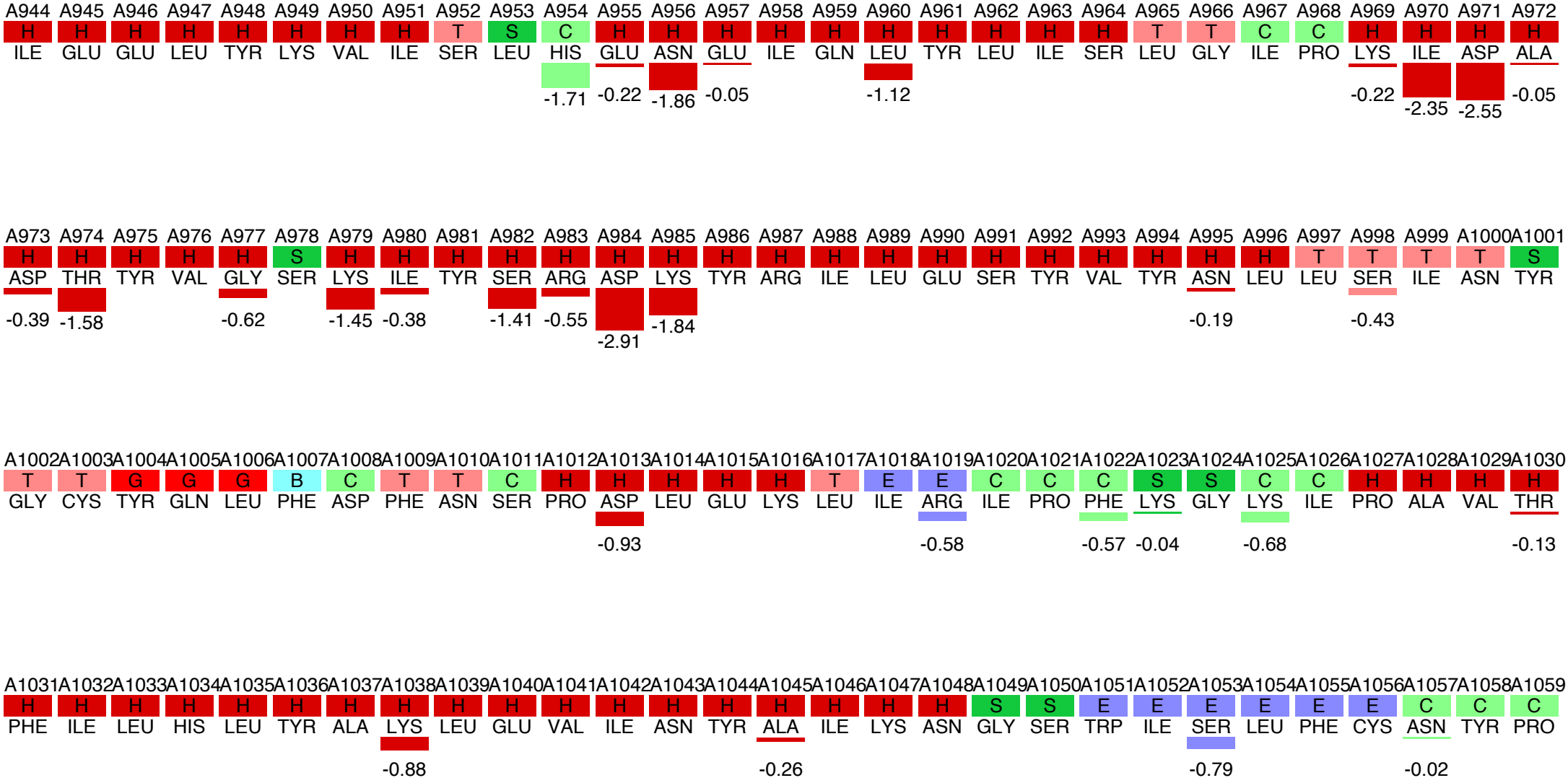
A944 A945 A946 A947 A948 A949 A950 A951 A952 A953 A954 A955 A956 A957 A958 A959 A960 A961 A962 A963 A964 A965 A966 A967 A968 A969 A970 A971 A972
H H H H H H H H T S C H H H H H H H H H H T T C C H H H H
ILE GLU GLU LEU TYR LYS VAL ILE SER LEU HIS GLU ASN GLU ILE GLN LEU TYR LEU ILE SER LEU GLY ILE PRO LYS ILE ASP ALA
-1.71 -0.22 -1.86 -0.05 -1.12 -0.22 -2.35 -2.55 -0.05
A973 A974 A975 A976 A977 A978 A979 A980 A981 A982 A983 A984 A985 A986 A987 A988 A989 A990 A991 A992 A993 A994 A995 A996 A997 A998 A999 A1000 A1001
H H H H H S H H H H H H H H H H H H H H H H H T T T T S
ASP THR TYR VAL GLY SER LYS ILE TYR SER ARG ASP LYS TYR ARG ILE LEU GLU SER TYR VAL TYR ASN LEU LEU SER ILE ASN TYR
-0.39 -1.58 -0.62 -1.45 -0.38 -1.41 -0.55 -2.91 -1.84 -0.19 -0.43
A1002 A1003 A1004 A1005 A1006 A1007 A1008 A1009 A1010 A1011 A1012 A1013 A1014 A1015 A1016 A1017 A1018 A1019 A1020 A1021 A1022 A1023 A1024 A1025 A1026 A1027 A1028 A1029 A1030
T T G G G B C T T C H H H H H T E E C C C S S C C H H H H
GLY CYS TYR GLN LEU PHE ASP PHE ASN SER PRO ASP LEU GLU LYS LEU ILE ARG ILE PRO PHE LYS GLY LYS ILE PRO ALA VAL THR
-0.93 -0.58 -0.57 -0.04 -0.68 -0.13
A1031 A1032 A1033 A1034 A1035 A1036 A1037 A1038 A1039 A1040 A1041 A1042 A1043 A1044 A1045 A1046 A1047 A1048 A1049 A1050 A1051 A1052 A1053 A1054 A1055 A1056 A1057 A1058 A1059
H H H H H H H H H H H H H H H H H H S S E E E E E E C C C
PHE ILE LEU HIS LEU TYR ALA LYS LEU GLU VAL ILE ASN TYR ALA ILE LYS ASN GLY SER TRP ILE SER LEU PHE CYS ASN TYR PRO
-0.88 -0.26 -0.79 -0.02

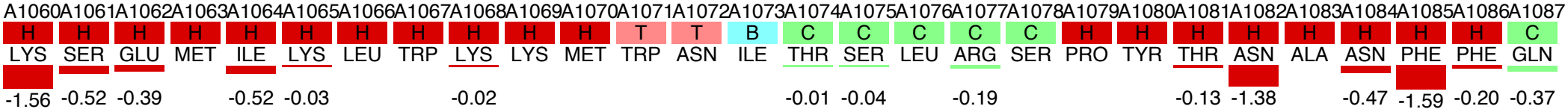
A1060 A1061 A1062 A1063 A1064 A1065 A1066 A1067 A1068 A1069 A1070 A1071 A1072 A1073 A1074 A1075 A1076 A1077 A1078 A1079 A1080 A1081 A1082 A1083 A1084 A1085 A1086 A1087
H H H H H H H H H H H T T B C C C C C H H H H H H H C
LYS SER GLU MET ILE LYS LEU TRP LYS LYS MET TRP ASN ILE THR SER LEU ARG SER PRO TYR THR ASN ALA ASN PHE PHE GLN
-1.56 -0.52 -0.39 -0.52 -0.03 -0.02 -0.01 -0.04 -0.19 -0.13 -1.38 -0.47 -1.59 -0.20 -0.37

APPENDIX C

Manuscript documenting other significant work performed during my Ph.D. training that was not central to my dissertation thesis aims. The purpose of this work was to develop a method rapidly differentiate RV RNA specimens' genotypes between the two major human strains, Wa and DS-1. ***This manuscript is reused with permission from Elsevier.***

Journal of Virological Methods 194 (2013) 197–205

Contents lists available at ScienceDirect

Journal of Virological Methods

journal homepage: www.elsevier.com/locate/jviromet

PCR-based approach to distinguish group A human rotavirus genotype 1 vs. genotype 2 genes

Allison O. McKell[a,c], Joshua C. Nichols[a,b], Sarah M. McDonald[a,b,c,*]

[a] Virginia Tech Carilion Research Institute, Roanoke, VA 24016, USA
[b] Virginia Tech Carilion School of Medicine, Roanoke, VA 24016, USA
[c] Department of Biomedical Sciences and Pathobiology, Virginia-Maryland Regional College of Veterinary Medicine, Blacksburg, VA 24061, USA

Article history:
Received 11 December 2012
Received in revised form 15 August 2013
Accepted 21 August 2013
Available online 4 September 2013

Keywords:
Human rotavirus
Genotyping
RT-PCR/PCR
Viral diversity
Gene reassortment

A B S T R A C T

Group A rotaviruses (RVs) are eleven-segmented, double-stranded RNA viruses and important causes of severe diarrhea in children. A full-genome classification system is readily used to describe the genetic makeup of individual RV strains. In this system, each viral gene is assigned a specific genotype based upon its nucleotide sequence and established percent identity cut-off values. However, a faster and more cost-effective approach to determine RV gene genotypes is to utilize specific oligonucleotide primer sets in RT-PCR/PCR. Such primer sets and PCR-based genotyping methods have already been developed for the VP7-, VP6-, VP4- and NSP4-coding gene segments. In this study, primers were developed for the remaining seven RV gene segments, which encode proteins VP1, VP2, VP3, NSP1, NSP2, NSP3, and NSP5/6. Specifically, primers were designed to distinguish the two most common human RV genotypes (1 vs. 2) for these genes and were validated on several cell culture-adapted human and animal RV strains, as well as on human RVs from clinical fecal specimens. As such, primer sets now exist for all eleven genes of common human RVs, allowing for the identification of reassortant strains with mixed constellations of both genotype 1 and 2 genes using a rapid and economical RT-PCR/PCR method.

1. Introduction

Group A rotaviruses (RVs) are important pathogens that cause acute gastroenteritis in children less than five years of age, leading to severe dehydration and even death (Estes and Kapikian, 2007; Parashar et al., 2009). Current reports indicate that each year over 450,000 preventable fatalities in developing countries are attributable to RVs, and the societal cost of these infections is estimated at upwards of $1 billion annually in the US alone (Payne et al., 2011; Tate et al., 2012). RVs are members of the *Reoviridae* family and exist as non-enveloped, triple-layered icosahedral capsids surrounding an eleven-segmented, double-stranded RNA (dsRNA) genome (Estes and Kapikian, 2007). Each genome (i.e., gene) segment codes for either a single viral structural protein (VP1, VP2, VP3, VP4, VP6, or VP7) or a single viral non-structural protein (NSP1, NSP2, NSP3, NSP4, or NSP5). In some RV strains, gene 11 codes for two non-structural proteins (NSP5 and NSP6) from overlapping open-reading frames. Historically, RVs have been classified based upon the antigenicity of the three major capsid proteins: VP7 (G-serotypes), VP4 (P-serotypes) and VP6 (subgroups) (Fischer and Gentsch, 2004). However, a more recent full-genome classification scheme is now readily used to describe the genetic makeup of individual RV strains (Matthijnssens et al., 2008). In this system, a specific genotype is assigned to each of the eleven viral gene segments based on their nucleotide sequences and established percent identity cut-off values. The nomenclature for the full-genome genotype of a RV strain is now written in the format Gx-P[x]-Ix-Rx-Cx-Mx-Ax-Nx-Tx-Ex-Hx, where each letter corresponds to a single gene encoding a viral protein(s) (i.e., VP7-VP4-VP6-VP1-VP2-VP3-NSP1-NSP2-NSP3-NSP4-NSP5/6) and *x* is a number that corresponds to the gene genotype.

The implementation of this full-genome classification system revealed that, while the G/P-genotypes of human RVs can vary, the non-G/P-genotype genes are usually either all genotype 1 or all genotype 2. For example, of the 333 human RV strains that had been fully sequenced as of December 2012, 312 of them have genotype constellations of either I1-R1-C1-M1-A1-N1-T1-E1-H1 or I2-R2-C2-M2-A2-N2-T2-E2-H2 (Matthijnssens and Van Ranst, 2012). Human RVs with mixed constellations of genotype 1 and 2 genes can be created in the laboratory and have occasionally been isolated from children with gastroenteritis (Matthijnssens and Van Ranst, 2012). However, it is currently hypothesized that such reassortant strains are less fit than those with pure genotype 1 or pure genotype 2 constellations (McDonald et al., 2009, 2011, 2012). To test this hypothesis, resource and time-efficient methods

* Corresponding author at: Virginia Tech Carilion Research Institute, 2 Riverside Circle, Roanoke, VA 24016, USA. Tel.: +1 540 526 2092; fax: +1 540 985 3373.
E-mail address: mcdonaldsa@vtc.vt.edu (S.M. McDonald).

0166-0934/$ – see front matter © 2013 Elsevier B.V. All rights reserved.
http://dx.doi.org/10.1016/j.jviromet.2013.08.025

are needed to differentiate genotype 1 vs. 2 genes of human RVs as part of very large-scale (>1000 specimens) epidemiological surveillance studies. With such methods in-place, investigators can begin to answer important questions related to the diversity of circulating strains and the role of gene reassortment in RV evolution.

One approach that has been used to streamline studies of RV diversity relies on specific oligonucleotide primers to differentiate the common gene genotypes of strains using RT-PCR/multiplex PCR. In this approach, viral RNA is first converted into cDNA and amplified for 10 cycles using RT-PCR and universal primers designed against highly conserved gene regions. The product of this reaction is then re-amplified by PCR in the presence of one of the universal primers as well as two or more genotype-specific primers, which were designed against variable gene regions. The resulting nested genotype-specific amplicons are sufficiently different in size, allowing them to be easily discerned following agarose gel electrophoresis. Such universal and genotype-specific primers have been described for the VP7-coding gene (genotypes G1, G2, G3, G4, G9, and G12) and the VP4-coding gene (genotypes P[4], P[6], and P[8]) (Gouvea et al., 1990; Gentsch et al., 1992; Das et al., 1994; Iturriza-Gómara et al., 2004). Similar approaches and primer sets have since been developed for the VP6-coding gene to differentiate genotype I1 vs. I2/I3 (Lin et al., 2008; Thongprachim et al., 2010). Moreover, for the NSP4-coding gene, primer sets exist to discriminate among genotypes E2, E1, and E3 (Rodrìguez-Dìaz et al., 2008). In the current study, primer sets were developed to distinguish between the two most common genotypes for the other seven non-G/P-type genes encoding: VP1 (R1 vs. R2), VP2 (C1 vs. C2), VP3 (M1 vs. M2), NSP1 (A1 vs. A2), NSP2 (N1 vs. N2), NSP3 (T1 vs. T2), and NSP5/6 (H2 vs. non-H2). The results show that these primers specifically and efficiently recognized the genotype 1 and/or 2 genes of cell-culture adapted and/or primary clinical RV strains by RT-PCR/PCR. Thus, the preliminary full-genome genotypes of most human RVs can now be deduced in a rapid, high-throughput, and cost-effective manner without the requirement for nucleotide sequencing.

2. Materials and methods

2.1. Oligonucleotide primer design

Nucleotide sequence alignments of human RV genotype 1 and 2 genes (encoding VP1, VP2, VP3, NSP1, NSP2, NSP3, NSP4, and NSP5/6) were created using the ClustalX algorithm implemented in Geneious™ Pro (v.5.6.3). Universal forward and reverse primers were designed against highly conserved gene regions. Primers specific for genotype 1 or 2 genes (forward or reverse, depending upon the gene) were designed against regions that were variable between the two genotypes, but conserved within the genotype. GenBank accession numbers of human RV gene sequences used to create the alignments for primer design are shown in Table 1, and primer sequences developed in this study are shown in Table 2. Also shown in Table 2 are the primers developed by Lin et al., and Rodrìguez-Dìaz et al., for the VP6- and NSP4-coding genes, respectively (Lin et al., 2008; Rodrìguez-Dìaz et al., 2008). Primers for G/P-genotyping using RT-PCR/PCR can be found in several published manuscripts (Gouvea et al., 1990; Gentsch et al., 1992; Das et al., 1994; Iturriza-Gómara et al., 2004). Lyophilized primers were generated by Life Technologies (Carlsbad, CA, USA), resuspended in DEPC-treated water to a working concentration of 5–10 pmol/μl, and stored at −20 °C.

2.2. Purification of viral RNA templates

Cell culture-adapted human RVs (strains Wa, DS-1, AU-1, ST3, A64, and L26), the porcine RV strain OSU, and the bovine RV strain UK were generously provided by Dr. John T. Patton (National Institutes of Health). To prepare viral RNA from these strains, approximately 1×10^7 monkey kidney (MA104) cells were infected with trypsin-activated RV as described previously (Arnold et al., 2009). Infections proceeded at 37 °C/5% CO_2 for 3–5 days until the cell monolayer was completely lysed. Total RNA was extracted from the lysate using Trizol® LS (Life Technologies; Carlsbad, CA, USA) as per the manufacturer's protocol. The extracted RNA was concentrated by isopropanol precipitation, resuspended in 25–50 μl of DEPC-treated water, and stored at −20 °C. Viral RNA from RV-positive clinical fecal specimens was a gift from Dr. Carl Kirkwood (Murdoch Childrens Research Institute, Victoria, Australia) and was extracted and G/P-genotyped as described previously (Kirkwood et al., 2011). The specimens were collected from children with RV gastroenteritis in West Australia and/or Victoria during the years of 2009–2012 as part of a routine surveillance program.

2.3. RT-PCR using universal primers for preparation of genotyping templates

To convert viral RNA into cDNA and amplify it for downstream genotyping, one-step RT-PCR was performed using the Super Script® One-Step RT-PCR System with Platinum® *Taq* DNA Polymerase (Life Technologies; Carlsbad, CA, USA). RNA was denatured at 95 °C for 10 min in 50% dimethyl sulfoxide (DMSO) prior to being used as template. Each 25-μl reaction contained 12.5 μl of the Super Script® mix, 0.5 μl enzyme, 0.5 μl universal forward primer, 0.5 μl universal reverse primer, 1.0 μl of the RNA:DMSO mixture, and 10.0 μl DEPC-treated water. The reactions were incubated in a thermocycler at 50 °C for 30 min, 94 °C for 2 min, and then 10 cycles of [94 °C for 30 s; 48 °C for 30 s; 68 °C for 1 min]. A final extension step occurred at 68 °C for 10 min. In some experiments, the universal forward and reverse primers for the VP1-, VP2-, VP3-, NSP1-, NSP2-, NSP3- and NSP5/6-coding genes were combined into a single reaction. More specifically, each 25-μl reaction contained 12.5 μl of the Super Script® mix, 0.5 μl enzyme, 0.5 μl of each universal primer (7.0 μl total), 1.0 μl of the RNA:DMSO mixture, and 4.0 μl DEPC-treated water, with the same cycling parameters described above.

2.4. Genotyping templates using multiplex PCR and specific primers

To determine the genotype of the universal RT-PCR products, multiplex PCR was performed using a nested universal primer and both the genotype 1- and 2-specific primers. Each 25-μl reaction contained 21 μl of the AccuPrime™ *Pfx* Supermix (Life Technologies; Carlsbad, CA), 1.0 μl of the nested universal primer and 1.0 μl each of both genotype-specific primers and 1.0 μl of the RT-PCR (from above). Control reactions containing both universal forward and reverse primers, but lacking the genotype-specific primers were supplemented with 1.0 μl of DEPC-treated water to maintain a consistent reaction volume. The reactions were heated to 94 °C for 2 min in the thermocycler and then underwent 35 cycles of [94 °C for 30 s; 48 °C for 30 s; 68 °C for 1 min], followed by a 10 min final extension step at 68 °C. Reaction products were electrophoresed in 2% agarose-TAE (Tris-acetate-EDTA) gels and visualized by ethidium bromide staining and exposure to ultraviolet light. Gel images were captured using a BioRad ChemiDoc Imaging System. Figures were prepared using Adobe Photoshop (v12.0) and Illustrator (v15.0). To verify the specificity of the amplification, PCR products were excised from the gels, purified using the Qiagen Gel Extraction kit (Qiagen; Gaithersburg, MD, USA), and directly sequenced as described previously (Rippinger et al., 2010).

Table 1
Genotypes and accession numbers for human RV gene sequences used for primer design.

RV strain name*	VP1	VP2	VP3	NSP1	NSP2	NSP3	NSP5/6
RVA/human-tc/USA/**Wa**/1974/G1P[8]	R1-FJ423113	C1-FJ423114	M1-FJ423115	A1-FJ423117	N1-FJ423120	T1-JX406753	H1-FJ423123
RVA/human-tc/USA/**D**/1974/G1P[8]	R1-EF583021	C1-EF583022	M1-EF583023	A1-EF672571	N1-EF672573	T1-EF672572	H1-EF672576
RVA/human-wt/IND/**61060**/2006/G1P[8]	R1-HQ609554	C1-HQ609557	M1-HQ609560	A1-HQ609566	N1-HQ609569	T1-HQ609572	H1-HQ609578
RVA/human-wt/BEL/**BE00036**/2008/G1P[8]	R1-HQ392311	C1-HQ392318	M1-HQ392320	A1-HQ392313	N1-HQ392312	T1-HQ392319	H1-HQ392314
RVA/human-wt/BEL/**BE00029**/2008/G1P[8]	R1-HQ392239	C1-HQ392242	M1-HQ392241	A1-HQ392243	N1-HQ392234	T1-HQ392240	H1-HQ392235
RVA/human-wt/USA/**VU05-06-13**/2006/G1P[8]	R1-JF490578	C1-JF490588	M1-JF490587	A1-JF490586	N1-JF490579	T1-JF490583	H1-JF490580
RVA/human-wt/USA/**VU06-07-1**/2007/G1P[8]	R1-JF490875	C1-JF490885	M1-JF490884	A1-JF490877	N1-JF490876	T1-JF490880	H1-JF490878
RVA/human-tc/USA/**DS-1**/1976/G2P[4]	R2-EF583025	C2-EF583026	M2-EF583027	A2-EF672578	N2-EF672580	T2-EF672579	H2-EF672583
RVA/human-wt/CHN/**TB-Chen**/???/G2P[4]	R2-AY787653	C2-AY787652	M2-AY787654	A2-AY787647	N2-AY787648	T2-AY787649	H2-AY787651
RVA/human-tc/USA/**P**/1974/G3P[8]	R1-EF583037	C1-EF583038	M1-EF583039	A1-EF672599	N1-EF672601	T1-EF672600	H1-EF672604
RVA/human-wt/USA/**DC1563**/1974/G3P[8]	R1-FJ947175	C1-FJ947176	M1-FJ947177	A1-FJ947179	N1-FJ947182	T1-FJ947181	H1-FJ947185
RVA/human-wt/USA/**2008747332**/2008/G3P[8]	R1-HM773689	C1-HM773690	M1-HM773691	A1-HM773693	N1-HM773696	T1-HM773695	H1-HM773699
RVA/human-wt/USA/**2008747336**/2008/G3P[8]	R1-HM773678	C1-HM773679	M1-HM773680	A1-HM773682	N1-HM773685	T1-HM773684	H1-HM773688
RVA/human-tc/GBR/**ST3**/1975/G4P[6]	R1-EF583045	C1-EF583046	M1-EF583047	A1-EF672613	N1-EF672615	T1-EF672614	H1-EF672618
RVA/human-tc/BRA/**IAL28**/1992/G5P[8]	R1-EF583029	C1-EF583030	M1-EF583031	A1-EF672585	N1-EF672587	T1-EF672586	H1-EF672590
RVA/human-tc/USA/**Se584**/1998/G6P[9]	R2-EF583041	C2-EF583042	M2-EF583043	A3-not incl.	N2-EF672608	T1-EF672607	H3-not incl.
RVA/human-wt/COD/**DRC86**/2003/G8P[8]	R2-DQ005125	C2-DQ005124	M2-DQ005123	A2-DQ005119	N2-DQ005118	T2-DQ005117	H2-DQ005115
RVA/human-tc/GBR/**69M**/1980/G8P[10]	R2-EF576937	C2-EF583014	M2-EF576915	A2-EF672557	N2-EF672559	T2-EF672558	H2-EF672562
RVA/human-tc/USA/**Wi61**/1983/G9P[8]	R1-EF583049	C1-EF583050	M1-EF583051	A1-EF672620	N1-EF672622	T1-EF672621	H1-EF672625
RVA/human-tc/UK/**A64**/1987/G10P[14]	R2-EF583017	C2-EF583018	M2-EF503819	A3-not incl.	N2-EF672566	T6-not incl.	H3-not incl.
RVA/human-tc/PHL/**L26**/1987/G12P[4]	R2-EF583033	C2-EF583034	M2-EF583035	A2-EF672592	N1-EF672594	T2-EF672593	H1-EF672597
RVA/human-wt/GER/**GER172-08**/2008/G12P[6]	R1-FJ747625	C1-FJ747626	M1-FJ747627	A1-FJ747631	N1-FJ747632	T1-FJ747633	H1-FJ747635

* Common strain name is highlighted in bold print.

3. Results

3.1. Oligonucleotide primer design

Nucleotide sequence alignments were performed using human RV genotype 1 and 2 genes (encoding VP1, VP2, VP3, NSP1, NSP2, NSP3, and NSP5/6) to identify conserved and variable regions for primer design. The RV gene sequences used in these alignments were (i) from cell-culture adapted human strains as well as from strains found in clinical fecal specimens, (ii) from human strains isolated on different dates from various geographical locations, and (iii) from human strains that exhibit diverse G/P-genotypes (Table 1). The rationale for choosing diverse human RV strains for primer design was to increase the chances that the primers will accurately recognize and discriminate between a broad array of genotype 1 and/or 2 genes in epidemiological studies.

For each gene, two highly conserved regions (≤1 kb apart) were chosen for the design of universal forward and universal reverse primers, which would be expected to amplify both genotype 1 and 2 genes of human RVs in RT-PCRs (Fig. 1 and Table 2). In contrast, gene regions that varied between genotypes 1 and 2, yet that remained highly conserved within each genotype, were identified for the design of specific primers (Fig. 1 and Table 2). The genotype 1- and 2-specific primers were located within the boundaries of the universal primers and were >90 bps apart, allowing the resulting PCR amplicons to be discerned following gel electrophoresis (Fig. 1). For the VP1-, VP2-, VP3- and NSP1-coding genes, the genotype-specific primers were designed as forward primers, to be paired with universal reverse primers in multiplex PCR (Fig. 1 and Table 2). For the NSP2- and NSP3-coding genes, the genotype-specific primers were designed as reverse primers, to be paired with universal forward primers in multiplex PCR (Fig. 1 and Table 2). For the NSP5/6-coding gene, no appropriate variable regions were identified in the alignments for genotype-specific primer design. However, due to an insertion in the 3′ untranslated region (UTR) of the NSP5/6 gene, human RV genotype 2 genes are ~150 bp longer than non-genotype 2 genes (Fig. 1). Therefore, a universal reverse primer was designed against the extreme 3′ terminus, and when paired with an upstream universal forward primer, it would create different sized RT-PCR amplicons from genotype 1 vs. 2 genes (Fig. 1). Specifically, a 537-bp product would be expected for genotype 2 genes, while other human RV genes (including those that are genotype 1) would yield only the smaller, 385-bp amplicon (Fig. 1).

Whenever possible, as allowed by the target sequences, primers were designed to contain ≥29% GC content, to end in either a 3′ G or C, and to avoid self-complementarity. Of the 26 primers designed, 10 of them end in a 3′ G or C, and all are expected to avoid self-complementarity (Table 2). Moreover, of the 14 universal primers designed, 11 of them exhibit GC contents within the optimal range (Table 2). However, universal primers VP1-Ur, VP3-Uf, and NSP1-Ur each have lower than optimal GC contents (17%, 25%, and 28%, respectively) due to fact that the conserved

Table 2
Universal and genotype 1- or 2-specific primers for all nine of the non-G/P-type genes of human RVs.

Protein-coding gene	Primer (name/sequence 5′–3′)	%GC
VP1	**VP1-Uf**/TCA GGA ATA GCT GAT GAA ATT GC	39
	VP1-Ur/AAT AAT TGA TAA CAT CCA TAA TTA	17
	VP1-GT1f/TAC TAT TAA TGA CAT TTT GCG TGA	29
	VP1-GT2f/GCA TAC CAA AAA TAG ATG CTG ATA	33
VP2	**VP2-Uf**/GCT ATT AAA GGC TCA ATG GCG TAC	46
	VP2-Ur/GGA TGT AGA ATT GAT GGA TAA TTG	33
	VP2-GT1f/GAC TTA CCA CAA CAA AAT GAA CG	39
	VP2-GT2f/AGA AGT TGT AAC GGA CAG TCA TGA	42
VP3	**VP3-Uf**/CTA ATC TCA CTA CAC ATA ATA TAT	25
	VP3-Ur/GTA TCC AAT GGA TCC CAC GTC TCA	50
	VP3-GT1f/ATG ATT ATG AGA ATA ACA TAG TTT	21
	VP3-GT2f/AAA TAT AGA AGA TTA TTT ATT ACC A	16
NSP1	**NSP1-Uf**/GTT TGT CAA TGG TGT AGT CAA TAT	33
	NSP1-Ur/TAT GAT TTG ATG TCA CAT AAT TTG G	28
	NSP1-GT1f/CAC GTA ATT GTA GTG AAT TAT CTT C	32
	NSP1-GT2f/TAA TAA GTT TGC AAA CAC AAT TAA A	20
NSP2	**NSP2-Uf**/ATG GCT GAG CTA GCT TGC TTT TGT	46
	NSP2-Ur/CTT CAT CCA TCT TTC TAT CAG TTG	38
	NSP2-GT1r/ACA AGT TCT TTA ACA CAT ACA TC	30
	NSP2-GT2r/CAG CAT ATT TCC ATT TTT ATT ATT AC	23
NSP3	**NSP3-Uf**/CAA GAT GGA GTC TAC TCA GCA GAT	46
	NSP3-Ur/GGT TTT TGA CAG TGT TAG CTT TTA	33
	NSP3-GT1r/TAA AAA TGT TCT GTC ATA ATC TTG A	24
	NSP3-GT2r/TTA TAT ATT TGT AAT TCA TTG ATA	13
NSP5/6	**NSP5/6-Uf**/GCT GGC GTG TCT ATG GAT TCA TCA	50
	NSP5/6-Ur/GGT CAC AAA ACG GGA GTG GGG AGC	63
NSP4*	**NSP4sense**/GGC TTT TAA AAG TTC TGT TCC GAG	42
	NSP4anti/GGT CAC ATC AAG ACC ATT CC	50
	NSP4FW/GGA ATG GCG TAT TTT CC	47
	NSP4-A/TGT TCT TTG TAA CGT GTC	39
	NSP4-B/CTT GCG GTG AAG AGT TCG G	58
VP6**	**VP6-R**/GTC CAA TTC ATN CCT GGT GG	>50
	6EBG.303/AAY GTR TGT ATG GAT GAR ATG	>29
	3END.682c/GTM GTT AAM ACY CTD CGG	>39
	6END.1082c/ATA YTC TTG ACG YAC TGC G	>42

* Rodrìguez-Dìaz et al. (2008).
** Lin et al. (2008).

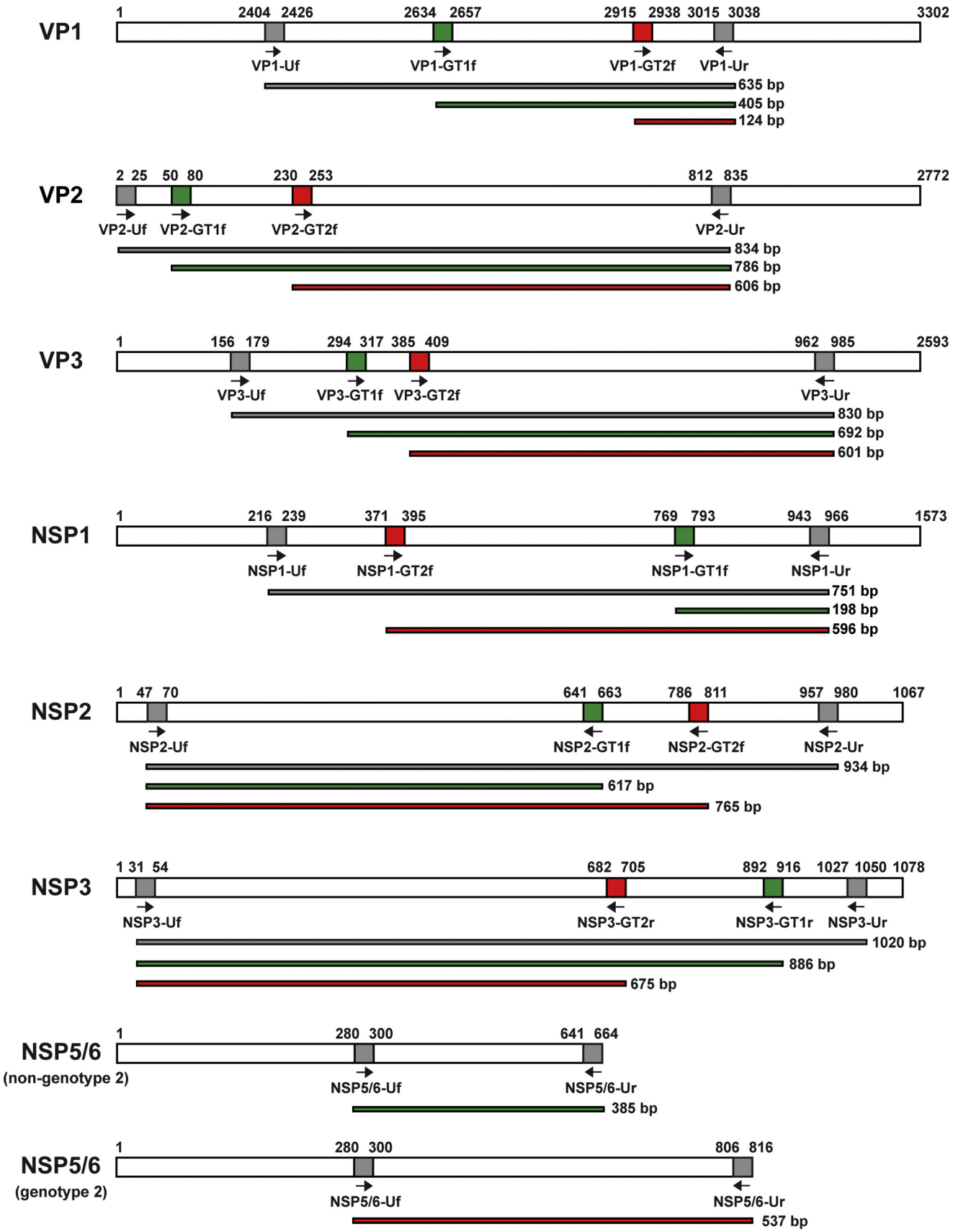

Fig. 1. Cartoon schematics of RV genes encoding VP1, VP2, VP3, NSP1, NSP2, NSP3, and NSP5/6. The figure shows the relative locations of the universal (gray boxes), genotype 1-(green box), and genotype 2-(red box) specific primers for each gene and is not drawn to scale. The nucleotide numbers corresponding to each primer are shown at the top of the schematics and primer orientation (forward or reverse) is indicated with an arrow. All nucleotide numbers are based on that of strain 61060, except for the VP2-coding gene (based upon VU06-07-1) and the genotype 2 NSP5/6-coding gene (based upon TB-Chen). Beneath each schematic are the expected products for PCRs using the different primers. Universal amplicons (gray lines), genotype 1 amplicons (green lines) and genotype 2 amplicons (red lines) are shown with sizes (in bps) listed to the right.

Table 3
Summary of RT-PCR/PCR results with the cell culture-adapted RVs.

	# Genes amplified/# genes tested for each primer set[a]		
RV gene type	Universal primers (RT-PCR)	Genotype 1-specific primers (multiplex PCR)[b,c]	Genotype 2-specific primers (multiplex PCR)[b,c]
Human genotype 1	**14/16**	**11/11**	0/11
Porcine genotype 1	**6/7**	**5/5**	0/5
Human genotype 2	**16/16**	0/15	**15/15**
Bovine genotype 2	**4/4**	0/4	**4/4**
Genotype 3	6/11	1/3	0/3
Genotype 6	0/1	not applicable	not applicable
Genotype 7	**1/1**	**1/1**	0/1

[a] Successful primer-template combinations are shown in bold.
[b] Excludes genes that failed to amplify with universal primers in RT-PCRs.
[c] Excludes the NPS5/6-coding gene, as the strategy for this gene relies on universal primers only.

regions of these genes are very AT-rich (Table 2, Fig. S1, and data not shown). Likewise, 8 of 12 genotype-specific primers exhibit GC contents within the optimal range, but the genotype-specific primers for the VP3- and NSP3-coding genes each have lower than optimal GC contents (16–24%) because the regions with the best inter-genotypic variability are also very AT-rich (Table 2, Fig. S1, and data not shown).

Supplementary material related to this article can be found, in the online version, at http://dx.doi.org/10.1016/j.jviromet.2013.08.025.

3.2. Testing the functionality and specificity of universal and genotype-specific primers

To validate the functionality of the designed primers, RT-PCRs were first performed using RNA templates derived from well-characterized, cell culture-adapted human strains for which full-genome sequences are known. These RVs have purely genotype 1 genes (strains Wa and ST3), purely genotype 2 genes (strain DS-1), or mixed genotype 1 and 2 genes (strain L26) (Fig. 2A) (Heiman et al., 2008; Matthijnssens et al., 2008). To test the extent of primer specificity, RT-PCRs were also performed using RNAs derived from human RVs that contain genotype 3 genes (strains AU-1 and A64), as well as RNA from animal RVs with genotype 1, 2, 3, 6, and/or 7 genes (porcine strain OSU and bovine strain UK) (Fig. 2A) (Heiman et al., 2008; Matthijnssens et al., 2008). In this experiment, RT-PCRs proceeded for 10 cycles, and the amplicons were not detectable following gel electrophoresis (data not shown). A very small amount (1/25 vol) of each universal RT-PCR was used as template in subsequent PCRs containing (i) only the universal primers or (ii) a nested universal primer and both genotype 1- and 2-specific primers. For the NSP5/6-coding gene, just the PCRs with universal primers were performed, since no genotype-specific primers were developed for this segment. The PCR products were electrophoresed in 2% agarose-TAE gels and visualized using ethidium bromide stain (Fig. 2B–H). The sizes of the amplicons, and therefore the putative genotypes of the genes, were determined using molecular weight standards. The bands were also excised from the gels and directly sequenced to confirm their identities (data not shown).

The universal primers efficiently amplified 14 of the 16 tested human RV genotype 1 genes and 16 of the 16 tested human RV genotype 2 genes by RT-PCR (Fig. 2 and Table 3). In fact, of the 32 human RV genotype 1 and 2 genes tested, the only two failures occurred with the universal primers: (i) the VP3-coding gene of strain ST3 and (ii) the NSP1-coding gene of strain Wa (Fig. 2D and E). The universal primers also amplified some of the more divergent RV genes, including: (i) 6 of the 7 tested genotype 1 genes from the porcine RV OSU, (ii) 5 of the five tested of the genotype 2 genes and 1 genotype 7 gene from the bovine strain UK, and (iii) 6 of the 11 genotype 3 genes from human or animal RVs (Fig. 2 and Table 3). As expected, for the NSP5/6-coding gene the larger 537-bp product was seen for the genotype 2 gene of strain DS-1 following universal primer amplification, while all other strains (with non-genotype 2 genes) only showed the smaller 385-bp product (Fig. 2H). A faint 385-bp product was also detected for the NSP5/6-coding gene of DS-1, suggesting that a cryptic or non-specific primer binding site may be present upstream of the 3′ UTR. Testing of additional laboratory strains suggest that this non-specificity is related only to the DS-1 virus, as no other tested genotype 2 gene produced lower molecular weight product (data not shown). Together, these results suggest that the universal primers recognize and amplify many human RV genotype 1 and 2 genes, as well as some non-genotype 1/2 genes and non-human RV genes, by RT-PCR.

For The NSP5/6-gene, the universal primer set was sufficient to genotype the human RV genes by RT-PCR. However, for the other six genes of this study, genotype-type specific primers were needed. Of the 11 human RV genotype 1 templates that were synthesized by the universal primers in RT-PCRs for these genes, all 11 were also correctly amplified by the genotype 1-specific primers in multiplex PCRs (Fig. 2 and Table 3). Likewise, all 15 of the human RV genotype 2 templates that were synthesized by the universal primers in RT-PCRs for these genes, all 15 were also correctly PCR-amplified by the genotype 2-specific primers (Fig. 2 and Table 3). Importantly, in the multiplex PCRs, there was no detectable cross-amplification of human RV genotype 1 genes with the genotype 2-specific primers and vice versa. However, as expected, there were some strain-to-strain differences in robustness of the PCRs. For example, due to intra-genotypic variation, strain L26 showed faint bands corresponding to genotype 2 amplicons for the VP3- and NSP1-coding genes, while strain DS-1 showed brighter bands (Fig. 2D–E, and S1). The genotype 1-specific primers, which were designed to recognize human RV genes, also amplified the porcine RV genotype 1 VP1-, VP2-, NSP1-, NSP2-, and NSP3-coding cDNAs of strain OSU (Fig. 2B, E–G, and Table 3). In a similar manner, the genotype 2-specific primers also recognized the bovine RV genotype 2 VP1-, VP2-, VP3-, and NSP2-coding templates from strain UK (Fig. 2B–D, F, and Table 3). The only non-genotype 1/2 genes that were amplified by the specific primers were the genotype 3 VP1- and VP2-coding genes of AU-1 and the genotype 7 NSP3-coding gene of strain UK (Fig. 2G and Table 3). This result suggests that, although the genotype-specific primers correctly differentiate genotype 1 vs. genotype 2 genes in multiplex PCR, they may not discriminate between human vs. animal genes of the same genotype nor would they differentiate genotype T1 vs. genotype T7.

3.3. Validation of approach with RVs in human fecal specimens

To further validate this PCR-based genotyping approach, viral RNA from 5 G1P[8]-positive and 5 G2P[4]-positive human fecal specimens were tested. In this experiment, the universal primers for the VP1-, VP2-, VP3-, NSP1-, NSP2-, NSP3-, and NSP5/6 genes

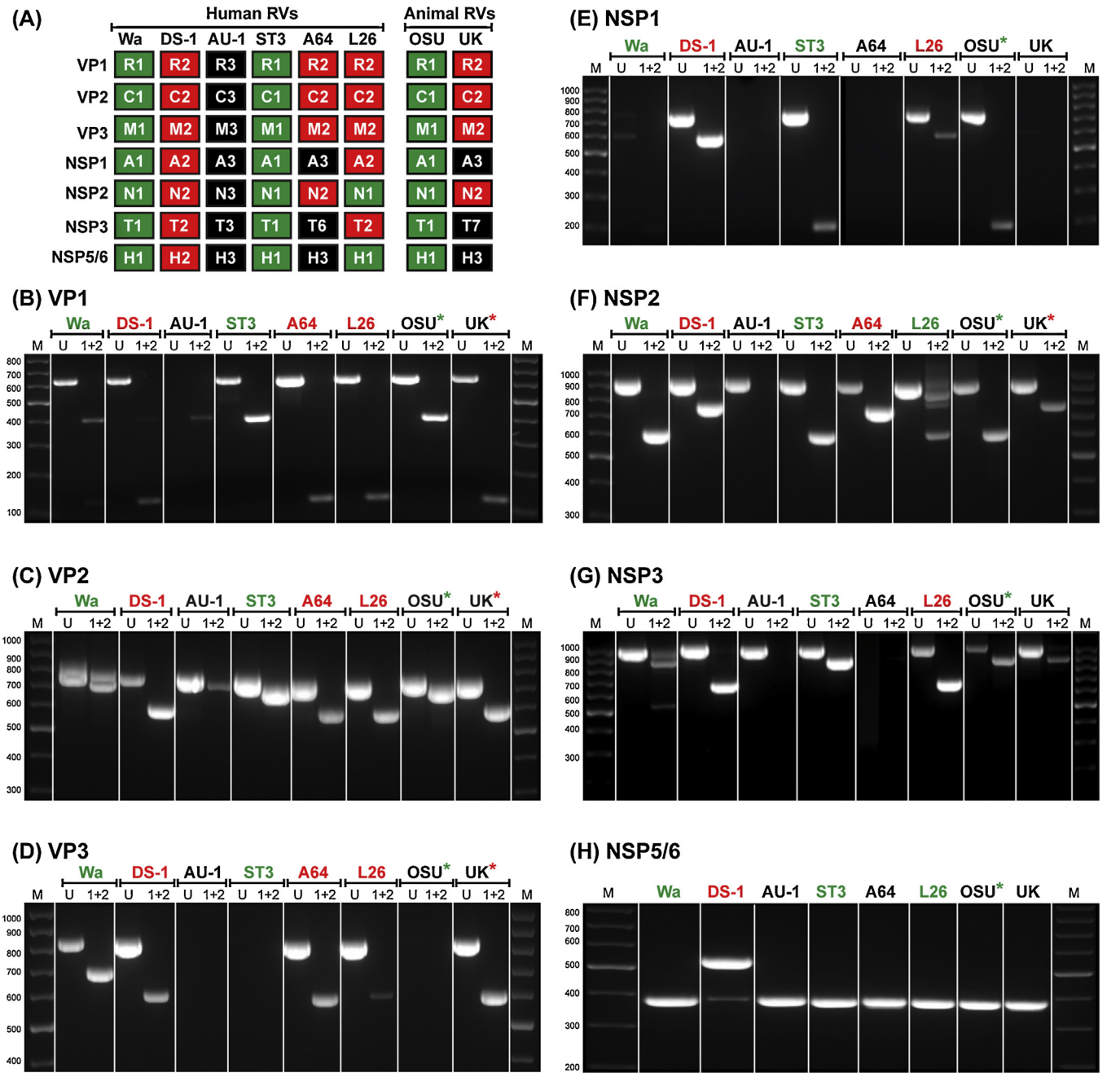

Fig. 2. Functionality and specificity of primers in RT-PCR/PCR using RNA from cell culture-adapted strains. (A) Genotype constellations of cell culture-adapted human or animal RVs. Genotype 1 genes are shown in green, genotype 2 genes are shown in red, and non-genotype 1/2 genes are shown in black. (B)–(H) Results of RT-PCR/PCR. Viral RNAs of various strains were converted to cDNAs and further amplified using universal primers and RT-PCR. These templates were then individually programmed into PCRs containing either the universal forward and reverse primers as a control (U) or a nested universal primer plus both the genotype 1- and 2-specific primers (1+2). Approximately 10 μl of the PCRs were electrophoresed in 2% agarose-TAE gels. A DNA ladder was used as a molecular weight marker and sizes (in bps) are listed to the left of each gel image. Strain names are listed at the top of each gel image. Green print represents human strains with genotype 1 genes, red print represents human strains with genotype 2 genes, and black print represents all other genes. The genotype 1 genes of the porcine RV strain OSU are noted by green asterisks. The genotype 2 genes of the bovine RV strain UK are noted by red asterisks.

were used simultaneously at the RT-PCR step, so as to improve the cost-effectiveness of the genotyping approach. Then, 1.0 μl (1/25 vol) of the RT-PCR was used as template for separate gene-specific PCRs containing (i) only the universal primers (data not shown) or (ii) a nested universal primer and both genotype 1- and 2-specific primers (Fig. 3). Again, for the NSP5/6-coding gene, the universal forward and reverse primers were used. The PCR products were electrophoresed in 2% agarose-TAE gels and visualized using ethidium bromide stain. The sizes of the amplicons, and therefore the putative genotypes of the genes, were determined using molecular weight standards. The bands were also excised from the gels and directly sequenced to confirm their identities (data not shown).

Following multiplex PCR, the G1P[8] RVs showed genotype 1-sized amplicons for the VP1-, VP2- VP3-, NSP1-, NSP2, NSP3-coding genes, and they showed a non-genotype 2-sized amplicon (385 bp) for the NSP5/6-coding gene (Fig. 3 and data not shown). In contrast, the G2P[4] RVs showed genotype 2-sized amplicons for genes encoding VP1, VP2, VP3, NSP1, NSP3 and NSP5/6 genes (Fig. 3 and data not shown). In contrast to what

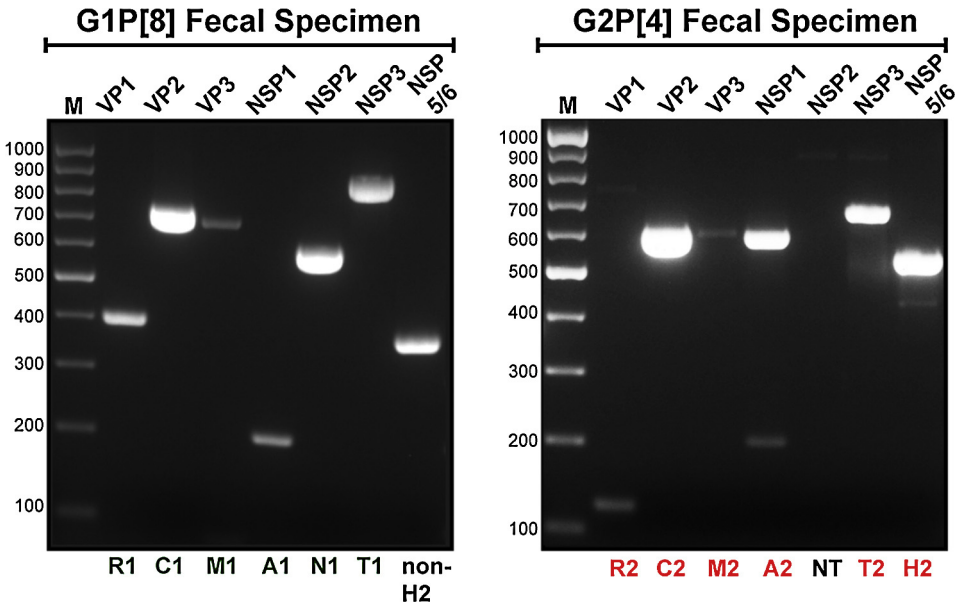

Fig. 3. Optimizing the cost-effectiveness of PCR genotyping and validation of the method with RVs from human fecal specimens. Viral RNA was converted into cDNAs and further amplified using all seven sets of universal primers in a single RT-PCR. These templates were then individually programmed into PCRs containing both the genotype 1- and 2-specific primers. PCRs were electrophoresed in 2% agarose-TAE gels. A DNA ladder was used as a molecular weight marker and sizes (in bps) are listed to the left of each gel image. The deduced genotype of each gene, based on the size of the PCR amplicon, is listed on the bottom of each gel image. Putative genotype 1 genes listed in green and putative genotype 2 genes are listed in red. The genotype 2 NSP2-coding gene was non-typeable (NT) using this combined approach.

was seen for the NSP5/6-coding gene of the cell culture-adapted G2P[4] strain DS-1, those of the clinical specimens only produced a larger 537-bp product following RT-PCR with the universal primers. Unfortunately, the two genotype 2-specific primers for VP3 and NSP2 did not work well when using the combined RT-PCR approach (Fig. 3 and data not shown). This result suggests that single-gene reactions may need to be done or that these particular primers may need further optimization following future field testing. Nonetheless, the cumulative results suggest that the genotype-specific primers recognize and appropriately amplify the genes of RVs in clinical fecal specimens and that combining several primers at the RT-PCR step may be used to reduce the cost of genotyping.

4. Discussion

Ongoing molecular epidemiological studies seek to gain insight into the diversity and evolutionary dynamics of RVs circulating at various geographical locations. RT-PCR/multiplex PCR is regarded as an appropriate high-throughput and cost-effective method for typing human strains in these studies (Fischer and Gentsch, 2004). Usually, the VP7- and VP4-coding genes (and occasionally the VP6- and NSP4-coding genes) of RVs in fecal specimens are assigned genotypes according to their PCR-amplification by specific primer sets (Gouvea et al., 1990; Gentsch et al., 1992; Das et al., 1994; Iturriza-Gómara et al., 2004; Fischer and Gentsch, 2004; Lin et al., 2008; Rodrìguez-Dìaz et al., 2008; Thongprachim et al., 2010). In the current study, the RT-PCR/PCR-based genotyping approach was extended to the remaining seven RV genes (encoding VP1, VP2, VP3, NSP1, NSP2, NSP3, and NSP5/6), allowing for rapid differentiation of genotype 1 vs. genotype 2 genes. The impetus for developing these primers was to gain a more comprehensive understanding of the frequency of human RVs showing mixed genotype constellations (i.e., with both genotype 1 and genotype 2 genes).

Universal forward and reverse primers designed against conserved gene regions were effective at amplifying the vast majority of tested human RV genotype 1 and 2 genes by RT-PCR. The universal primers were also able to amplify some other genes, in addition to human RV genotype 1 or 2 genes. In particular, the universal primers worked well on the genotype 1 and 2 genes of the animal RVs, strains OSU and UK, respectively. The universal primers also amplified C3, N3, T3, H3, and T7 genes from culture-adapted RV strains. Because genotype 3-specific primers have not yet been developed for the VP2-, NSP2-, NSP3- and NSP5/6 genes, the fact that the universal primers recognize them in RT-PCRs may be beneficial to investigators. Indeed, the control RT-PCR reactions for these rare genes could be directly sequenced to determine their genotype. Of the cell culture-adapted human RV strains, only two failures were found: (i) the VP3-coding gene of from strain ST3 (genotype M1) and (ii) the NSP1-coding gene of strain Wa (genotype A1). The universal reverse primers for these genes each show 4 nucleotide mismatches when compared to the sequences of ST3 or Wa, which may explain the lack of RT-PCR products (Fig. S1). Nonetheless, the universal primers for the VP3- and NSP1-coding genes closely match those of other M1 or A1 sequences, and they proved effective on RVs from primary fecal specimens. As such, it is expected that the universal primers for the VP3- and NSP1-coding genes will be useful in epidemiological surveillance studies.

Genotype 1- and 2-specific primers, which were designed against gene regions that varied inter-genotypically but not intra-genotypically, were found to discriminate between human RV genotype 1 vs. 2 templates in multiplex PCRs. Importantly, in the multiplex PCRs, there was no detectable cross-amplification of human RV genotype 1 templates with the genotype 2-specific primers and vice versa. The genotype 1- and 2- specific primers designed here also recognized many of the cognate genotype genes of the animal RV strains OSU and UK. Thus, while human and animal genes sharing the same genotype can often be discerned phylogenetically based upon nucleotide sequences, they would not be differentiated by multiplex PCR with the primers designed in this study (McDonald et al., 2011). Likewise, the genotype 7 NSP3-coding gene of strain UK was recognized by the genotype 1-specific primer; this result is not surprising given that there are only 3 nucleotide mismatches between their sequences (data not shown). Therefore, for the NSP3-coding gene, the current primer sets would not distinguish among human RV genotype 1, porcine RV genotype 1 and bovine RV genotype 7. A similar result was found

for the genotype 3 VP2-coding gene of strain AU-1, which was recognized by the genotype 1 specific primers. However, the primer sets easily discriminate genotype 1-like genes from genotype 2 genes and, thus, will be useful in studies aimed at understanding the prevalence of RVs with mixed genotype 1 and 2 constellations.

Some strain-to-strain differences in robustness of the PCRs were noticed for a few genotype-specific primers. For example, strain L26 showed faint bands corresponding to genotype 2 amplicons for the VP3- and NSP1-coding genes, while other strains (e.g., DS-1) showed brighter bands. Sequence analysis suggests that the weak amplification for L26 gene may reflect very modest intra-genotypic variation at the primer design site (Fig. S1). Indeed, the genotype-specific primers for the VP3-coding gene consistently produced faint bands with the RVs from clinical fecal specimens; conversely, the amplicons for all other genes, including those for the NSP1-coding gene were fairly robust (Fig. 3 and data not shown). It is expected that the primers designed in this study will be functional in discriminating genotype 1 vs. genotype 2 genes of human RVs, but that some may require further optimization following rigorous field testing.

When combined with the previously described primers sets for the VP7-, VP4-, VP6- and NSP4-coding genes, the new primers developed in this study will enable the full-genome genotyping of the most common human RVs using RT-PCR/multiplex PCR (Gouvea et al., 1990; Gentsch et al., 1992; Das et al., 1994; Iturriza-Gómara et al., 2004; Fischer and Gentsch, 2004; Lin et al., 2008; Rodrìguez-Dìaz et al., 2008; Thongprachim et al., 2010).

It is estimated that, using this approach, the genotype constellations of human RVs could be deduced by RT-PCR/PCR for less than $10 USD/specimen, whereas nucleotide sequencing would cost upwards of $150 USD/specimen. Thus, this RT-PCR/multiplex PCR genotyping approach could reasonably be employed to screen fecal specimens for the presence of RVs containing mixed constellations of genotype 1 and 2 genes on a very-large scale (>1000 specimens). Nonetheless, it is important to note that this approach is meant to complement, but not replace, the genetic analysis of human RVs using nucleotide sequencing. PCR-based genotyping should simply be used as a facile and inexpensive way of screening RVs to identify representative strains for downstream nucleotide sequencing. It is recommended that nucleotide sequencing be used to confirm the genotypes of human RVs in cases of non-typeable genes, or whenever evidence of cross-amplification by genotype-specific primers is seen, as this might indicate a co-infected specimen.

Acknowledgements

The authors would like to thank John T. Patton (National Institutes of Health) for providing the cell culture-adpated RV strains and Carl Kirkwood (Murdoch Childrens Research Institute, Victoria, Australia) for providing RNA from clinical fecal specimens. This work was supported by new investigator start-up funding from the Virginia Tech Carilion Research Institute. AOM is also supported by the Graduate Program in Biomedical and Veterinary Sciences through the Virginia-Maryland Regional College of Veterinary Medicine. A financial contribution toward the work by JCN was also provided from the Virginia Tech Carilion School of Medicine.

References

Arnold, M., Patton, J., McDonald, S., 2009. Culturing, storage, and quantification of rotaviruses. In: Curr. Prot. Microbiol. Wiley Interscience/John Wiley & Sons, Inc, 15C.3.1-15C.3.24.

Das, B., Gentsch, J., Cicirello, H., Woods, P., Gupta, A., Ramachandran, M., Kumar, R., Bhan, M., Glass, R., 1994. Characterization of rotavirus strains from newborns in New Delhi, India. J. Clin. Microbiol. 32, 1820–1822.

Estes, M., Kapikian, A., 2007. Rotaviruses and their replication. In: Knipe, D., Howley, P., Griffin, D., Lamb, R., Martin, M., Roizman, B., Straus, S. (Eds.), Fields Virology. , 5th ed. Lippincott, Williams & Wilkins, Philadelphia, pp. 1917–1974.

Fischer, T., Gentsch, J., 2004. Rotavirus typing methods and algorithms. Rev. Med. Virol. 14, 71–82.

Gentsch, J., Glass, R., Woods, P., Gouvea, V., Gorziglia, M., Flores, J., Das, B., Bhan, M., 1992. Identification of Group A rotavirus gene 4 types by polymerase chain reaction. J. Clin. Virol. 30, 1365–1373.

Gouvea, V., Glass, R., Woods, P., Taniguichi, K., Clark, F., Forrester, B., Fang, Z., 1990. Polymerase chain reaction amplification and typing of rotavirus nucleic acid from stool specimens. J. Clin. Virol. 28, 276–282.

Heiman, E., McDonald, S., Barro, M., Taraporewala, Z., Bar-Magen, T., Patton, J., 2008. Group A human rotavirus genomics: evidence that gene constellations are influenced by viral protein interactions. J. Virol. 82, 11106–11116.

Iturriza-Gómara, M., Kang, G., Gray, J., 2004. Rotavirus genotyping: keeping up with an evolving population of human rotaviruses. J. Clin. Virol. 31, 259–265.

Kirkwood, C., Boniface, K., Barnes, G., Bishop, R., 2011. Distribution of rotavirus genotypes after introduction of rotavirus vaccines, Rotarix® and RotaTeq®, into the National Immunization Program of Australia. Pediatr. Infect. Dis. J. 30, S48–S53.

Lin, Y., Kao, C., Chang, S., Taniguchi, K., Hung, P., Lin, H., Huang, L., Huang, H., Yang, J., Lee, A., 2008. Determination of human rotavirus VP6 genogroups I and II by reverse transcription-PCR. J. Clin. Microbiol. 46, 3330–3337.

Matthijnssens, J., Ciarlet, M., Heiman, E., Arijs, I., Delbeke, T., McDonald, S., Palombo, E., Iturriza-Gómara, M., Maes, P., Patton, J., Rahman, M., Van Ranst, M., 2008. Full genome-based classification of rotaviruses reveals a common origin between human Wa-like and porcine rotavirus strains and human DS-1-like and bovine rotavirus strains. J. Virol. 82, 3204–3219.

Matthijnssens, J., Van Ranst, M., 2012. Genotype constellation and evolution of group A rotaviruses infecting humans. Curr. Opin. Virol. 2, 426–437.

McDonald, S., Matthijnssens, J., McAllen, J., Hine, E., Overton, L., Wang, S., Lemey, P., Zeller, M., Spiro, D., Patton, J., 2009. Evolutionary dynamics of human rotaviruses: balancing reassortment with preferred genome constellations. PLoS Path. 5, e10000634.

McDonald, S., Davis, K., McAllen, J., Spiro, D., Patton, J., 2011. Intra-genotypic diversity of archival G4P[8] human rotaviruses from Washington, DC. Infect. Gen. Evol. 11, 1586–1594.

McDonald, S., McKell, A., Rippinger, C., McAllen, J., Akopov, A., Kirkness, E., Payne, D., Edwards, K., Chappell, J., Patton, J., 2012. Diversity and relationships of co-circulating modern human rotaviruses revealed using large-scale comparative genomics. J. Virol. 86, 9148–9162.

Parashar, U., Burton, A., Lanata, C., Boschi-Pinto, C., Shibuya, K., Steele, D., Birmingham, M., Glass, R., 2009. Global mortality associated with rotavirus disease among children in 2004. J. Infect. Dis. 200 (Suppl. 1), S9–S15.

Payne, D., Staat, M., Edwards, K., Szilagyi, P., Weinberg, G., Hall, C., Chappell, J., Curns, A., Wikswo, M., Tate, J., Lopman, B., Parashar, U., 2011. Direct and indirect effects of rotavirus vaccination upon childhood hospitalizations in 3 US Counties, 2006–2009. Clin. Infect. Dis. 53, 245–253.

Rippinger, C., Patton, J., McDonald, S., 2010. Complete genome sequence analysis of candidate human rotavirus vaccine strains RV3 and 116E. Virology 405, 201–213.

Rodrìguez-Dìaz, J., Rubilar-Abreu, E., Spitzner, M., Hedlund, K., Liprandi, F., Svensson, L., 2008. Design of a multiplex nested PCR for genotyping of the NSP4 from group A rotavirus. J. Virol. Methods 149, 240–245.

Tate, J., Burton, A., Boschi-Pinto, C., Steele, A., Duque, J., Parashar, U., 2012. 2008 estimate of worldwide rotavirus-associated mortality in children younger than 5 years before the introduction of universal rotavirus vaccination programmes: a systematic review and meta-analysis. Lancet Infect. Dis. 12, 136–141.

Thongprachim, A., Chaimongkol, N., Khamrin, P., Pantip, C., Mizuguchi, M., Ushijima, H., Maneekarn, N., 2010. A novel multiplex RT-PCR for identification of VP6 subgroups of human and porcine rotaviruses. J. Virol. Methods 168, 191–196.